Wiring up diversity:

subset-specific development of midbrain dopaminergic neurons

Sara Brignani

The research described in this thesis was performed at the Department of Translational Neuroscience, Brain Center Rudolf Magnus, University Medical Center Utrecht, the Netherlands.

Research in this thesis was financially supported by the Netherlands Organization for Scientific Research (ALW- VICI), the People Program (Marie Curie Actions) of the European Union's Seventh Framework Program (FP7) 2007–2013 under REA grant agreement number 289581 (NPlast), the UU Strategic Theme "Dynamics of Youth", and Stichting ParkinsonFonds.

Publication of this thesis was financially supported by the Brain Center Rudolf Magnus.

Cover & layout: Guus Gijben, proefschrift-AIO.nl
Printing: proefschrift-AIO.nl
ISBN: 978-94-92801-52-4

Wiring up diversity:

subset-specific development of midbrain dopaminergic neurons

Bedrading van diversiteit:
subset-specifieke ontwikkeling van dopaminerge neuronen
in de middenhersenen
(met een samenvatting in het Nederlands)

Proefschrift

ter verkrijging van de graad van doctor aan de Universiteit Utrecht op gezag van de rector magnificus, prof. dr. H.R.B.M. Kummeling, ingevolge het besluit van het college voor promoties in het openbaar te verdedigen op vrijdag 5 oktober 2018 des ochtends te 12.45 uur

door

Sara Brignani

geboren op 8 augustus 1986
te Manerbio, Italië

Promotoren: Prof. dr. R.J. Pasterkamp
Prof. dr. J.P.H. Burbach

To Ivano,

who taught me to pay attention to

and to feel wonder for

the beauty of the things in the world

Contents

Chapter 1

General Introduction

Adapted from: Brignani S and Pasterkamp RJ (2017) Neuronal Subset-Specific Migration and Axonal Wiring Mechanisms in the Developing Midbrain Dopamine System. Front. Neuroanat. 11:55.doi: 10.3389/fnana.2017.00055

Preface

The dopamine system of the ventral midbrain (mDA system) can be subdivided into three main nuclei: substantia nigra pars compacta (SNc, A9), ventral tegmental area (VTA, A10), and retrorubral field (RRF, A8). Dopaminergic neurons of the mDA system are characterized by the synthesis and release of the neurotransmitter dopamine, and the expression of tyrosine hydroxylase (TH) and the dopamine transporter (DAT). SNc mDA neurons contribute to the control of voluntary movement and their selective degeneration is a pathological hallmark of Parkinson's disease (Kalia and Lang, 2015). VTA mDA neurons play a role in positive and negative reinforcement, decision making, working memory, and aversion (for a review see (Morales and Margolis, 2017)). Dopamine imbalance in VTA mDA neurons has been implicated in schizophrenia, attention deficit hyperactivity disorder (ADHD), obsessive-compulsive disorder (OCD), addiction, and depression (Chaudhury et al., 2012; Faraone et al., 2005; Milton and Everitt, 2012; Winterer and Weinberger, 2004). Their important physiological functions and implication in human disease has triggered an enormous interest in understanding the development and function of mDA neurons.

It is becoming clear that neurons within the anatomically defined SNc and VTA nuclei are not homogeneous. Rather multiple distinct mDA neuron subsets exist within and across the boundaries of the SNc and VTA. For example, subsets that differ by specific molecular markers, by afferent inputs, and by the brain structures they innervate. To understand how these differences arise, the developmental origin and molecular programs in mDA neuron subsets are studied intensively. It is likely, and in part known, that different mDA neuron subsets express specific molecular cues that allow subset-specific differentiation, migration and axon guidance. This thesis aims at investigating the development of subsets of mDA neurons. New genetic tools to distinguish mDA neuron-clusters in vivo are generated and applied to understand the cellular and molecular mechanisms orchestrating the migration and axon guidance of mDA neuron subtypes.

Neuronal subset-specific migration and axonal wiring mechanisms in the developing midbrain dopamine system

Here, we first summarize and discuss our current knowledge of the neuron subsets present in the mDA system. Then, molecular mechanisms are highlighted that aid mDA neurons in migrating to their final position in the midbrain and that allow the formation of selective patterns of efferent connections. We will focus mainly on studies that show differences in these mechanisms between different subsets of mDA neurons and for which *in vivo* data is available.

1. Neuronal diversity in the mDA system

Identification of mDA neuron subsets

Historically, anatomical and cytological features have been used to subdivide mDA neurons into subsets. According to this approach, SNc can be divided into a ventral and dorsal tier, whereas the VTA includes the parabrachial pigmented nucleus (PBP), the paranigral nucleus (PN), the caudal linear nucleus (CLi), the interfascicular nucleus (IF), and the rostral linear nucleus of the raphe (RLi) (Fu et al., 2012) (Figure 1A, B). Molecular markers exclusively expressed by single mDA subsets have not been identified yet. However, the expression of a few genes is commonly used to molecularly distinguish larger mDA domains. For example, the glycosylated active form of the dopamine transporter (glyco-DAT) and the G-protein-gated inwardly rectifying K+ channel (Grik2) are more abundantly expressed by the SNc and dorso-lateral VTA mDA neurons (Afonso-Oramas et al., 2009; Schein et al., 1998; Thompson et al., 2005), while Calbindin 1 (Calb1) expression is enriched in mDA neurons of the VTA and of the dorsal tier of the SNc (Fu et al., 2012; Di Salvio et al., 2010; Thompson et al., 2005). Within the VTA, the transcription factor Otx2 strongly labels ventro-medial mDA neurons and gradually deceases in the central and dorso-lateral VTA (Simeone et al., 2011).

The development and use of single-cell RNA approaches has recently led to a further subdivision of the SNc and VTA on basis of molecular features (La Manno et al., 2016; Poulin et al., 2014). In one study, mDA neurons were collected at postnatal day 4 (P4) using a dopaminergic neuron-specific Cre-driver mouse line (*Slc6a3-Cre*) crossed with a TdTomato Cre-reporter mouse. qPCR was performed on single mDA neurons to determine expression levels of 96 selected genes. An unbiased coefficient similarity hierarchical clustering analysis allowed to cluster cells in groups on basis of their gene expression profiles. This method identified 2 main cell clusters (Cluster 1 and Cluster 2). On basis of their expression profiles, mDA neurons from Cluster 1 were more similar to SNc neurons, whereas neurons from Cluster 2 had an expression

profile related to VTA neurons. The two clusters were subsequently subdivided in 2 and 4 cell types, respectively (i.e. 1A, B, 2A-D) (Poulin et al., 2014). Another study analyzed P21 mDA neurons, collected using the same genetic strategy as described above, by single-cell RNA sequencing (RNAseq). In this second study, 5 cell types were identified (SNC, VTA1-4) (La Manno et al., 2016). By using a set of marker genes, we compared these 5 cell types with the 6 cell types identified at P4 by Poulin at al. (Figure 2). Interestingly, each of the 5 cell types identified at P21 has a corresponding cell type identified at P4. This suggests that the mDA system can be subdivided in (at least) 5 cellular subsets, each of which is characterized by a specific molecular signature. Moreover, the analysis indicates that these 5 neuronal subsets are already in place at P4. One cluster identified at P4 (2C) does not correspond to a cluster found at P21. This cluster expresses genes shared by all populations of Cluster 2 (e.g., Calb1, Cck, and Slc17a6), but none of the markers that define specific cell types within Cluster 2 (Slc32a1 (2A), Adcyap1 (2B), and Vip (2D)) (Poulin et al., 2014). This group of mDA neurons (2C) might be composed of neurons that are not completely mature at P4, and that acquire an adult phenotype at later stages, becoming part of one of the other subsets of Cluster 2.

Comparison of the dopaminergic subnuclei defined on basis of anatomical features and the location of the 5 subsets described above (SNc/1A, VTA1/1B, VTA2/2B, VTA3/2D, VTA4/2A) shows that cell types 1A and 1B mainly correspond to the ventral and dorsal parts of the SNc, respectively (Figure 1B). In Parkinson's disease, mDA neurons of the ventral tier are known to be particularly vulnerable and in line with this cluster 1A is more selectively affected in a mouse model of Parkinson's disease, as compared to cluster 2B (Poulin et al., 2014). The VTA contains neurons from different clusters (2A, 2B, 2C, and part of 1B) (Figure 1B). Cluster 2B is selectively positive for Grp and is positioned mainly in the PN and IF, which are nuclei with mDA neurons that project their axons to the NAc (La Manno et al., 2016; Poulin et al., 2014). In line with these results, an independent study demonstrated that VTA mDA neurons projecting to the NAc are Grp^+ (Ekstrand et al., 2014). The most caudal VIP^+ cluster (2D) is restricted to the dorsal raphe nucleus (DR) and periaqueductal gray (PAG) (La Manno et al., 2016; Poulin et al., 2014). Immunostaining for Vip, which is expressed by mDA axons, demonstrates that these mDA neurons establish connections with the stria terminalis and the amygdala (Poulin et al., 2014), indicating that molecular profiles are correlated with specific projection patterns. None of the identified cell-types is located in the RRF, even though the *Slc6a3-Cre* mouse line efficiently labels this structure (Bäckman et al., 2006). A possible explanation for this observation is that the RRF may host relatively small cell clusters which are not identified by the currently applied RNAseq and data analysis methods.

One of the studies described above also performed an unbiased analysis based on single-cell RNAseq data obtained from embryonic ventral midbrain tissue (collected from E11.5 to E15.5, and at E18.5). This procedure allowed the identification of a group of mDA precursors (medial neuroblasts, NbM), two immature mDA cell-types (NbDA and DA0), and two clusters of mature mDA neurons (DA1 and DA2)(La Manno et al., 2016). At E18.5, DA2 neurons express Aldh1a1, Sox6, and Calb1*low* which, in the adult brain, label three cell-subsets (1A/SNC, 1B/VTA1, 2B/VTA2). This suggests that DA2 neurons may be a common ancestor of these three groups (Figure 2), whereas DA1 may give rise to 2D/VTA3 and 2A/VTA4 (La Manno et al., 2016). However, it is important to note that according to the study of Poulin at al. the 2B/VTA2 subset belongs to Cluster 2 and therefore it may derive from DA1 rather than DA2. Further work is needed to establish which ancestor (DA1 or DA2) generates the mDA subset 2B/VTA2. Interestingly, previous work has shown that the differentiation of the $Calb1^+/Aldh1a1^+$ mDA neurons (which correspond to the cluster 2B/VTA2) requires the expression of the transcription factor Otx2. The deletion of *Otx2* gene from the midbrain at early developmental time points causes the depletion of the large majority of $Calb1^+$ and $Aldh1a1^+$ mDA neurons of the VTA, with only the mDA neurons of the dorso-lateral VTA ($GIRK2^+$) surviving untill adulthood (Di Giovannantonio et al., 2013).

The identification of mDA neuron subsets, their developmental origin and molecular signatures is important for understanding how subset-specific connectivity is established in the mDA system. For example, defining clusters of mDA precursors, and immature and mature mDA neurons (NbM, NbDA, DA0, DA1, and DA2) from the RNA expression analysis allows the identification of guidance genes expressed by these neuronal populations (Table 1) (La Manno et al., 2016). Members of different guidance cue families (e.g. Semaphorins, Ephrins) can be detected in different clusters. Guidance genes expressed at early developmental time points might play a role in the migration and/or axon guidance of mDA neuron subsets. In the following sections, we discuss what is currently known about the mechanisms that control mDA neuron migration and axon guidance, with a particular emphasis on subset-specific mechanisms.

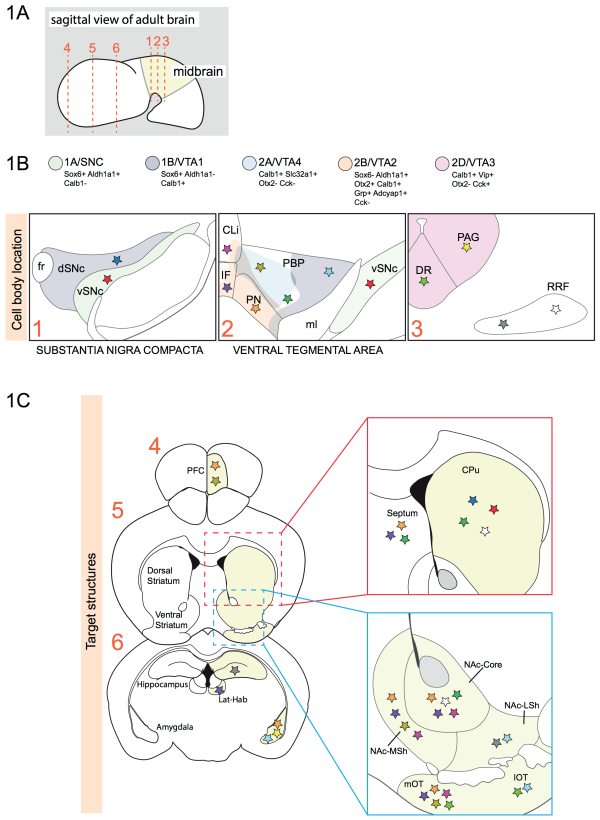

Figure 1.

Projection areas of molecularly defined subsets of dopaminergic neurons in the adult brain.

(A) Sagittal representation of an adult brain. Numbered dotted lines refer to coronal views in (B,C). (B) Overlap of anatomically defined domains (dSNc, vSNc, PBP, PN, CLi, and IF) and mDA neuron clusters identified by specific molecular signatures (1A/SNC, 1B/VTA1, 2A/VTA4, 2B/VTA2, and 2D/VTA3; see Figure 2). Each cluster is defined by a few distinctive molecular markers and by unique colors. Colored stars represent mDA neuron subsets projecting to specific brain structures in Figure 1C. (C) A colored star in C represents the brain region innervated by a specific mDA subset identified by a colored star in B. Stars with the same color represent mDA subsets and their target structures, respectively. (Aransay et al., 2015; Gasbarri et al., 1996; Ikemoto, 2007; Khan et al., 2017; Lammel et al., 2008; Matsuda et al., 2009; Poulin et al., 2014; Stamatakis et al., 2013). vSNc, SNc ventral tier; dSNc, SNc dorsal tier; PBP, parabrachial pigmented nucleus; PN, paranigral nucleus; IF, interfascicular nucleus; CLi, caudal linear nucleus; DR, dorsal raphe nucleus; PAG, periaqueductal gray; RRF, retrorubral field; fr, fasciculus retroflexus; ml, medial lemniculus; mPFC, medial prefrontal cortex; Lat-Hab, lateral habenula; CPu, caudate-putamen; NAc, nucleus accumbens; MSh, medial shell; LSh, lateral shell; mOT, medial olfactory tubercle; lOT, lateral olfactory tubercle.

Table 1

Axon guidance genes expressed by dopaminergic precursors, and by immature and mature mDA.

NbM	NbDA	DA0	DA1	DA2
DCC	*DCC*	*DCC*	*DCC*	*DSCAM*
Draxin	*Draxin*	*Draxin*	*Draxin*	*Sema4D*
Sema6C	*Sema6C*	*Sema3F*		*EphA5*
PlxnB1	*Nrp2*	*Sema5B*		
Nrp2	*EphA5*	*PlxnC1*		
EphA3	*EfnB1*	*EfnB2*		

mRNA expression of axon guidance genes in mDA precursors (medial neuroblasts, NbM), two immature mDA cell-types (NbDA and DA0), and two clusters of mature mDA neurons (DA1 and DA2). These molecules might be involved in migration and/or axon guidance of mDA neuron subsets. Data obtained from Linnarsson's lab webpage (www.linnarssonlab.org/ventralmidbrain). (See Figure 2).

2. Cellular and molecular mechanisms of mDA neuron migration

2.1 Distinct origins and migratory routes of SNc and VTA mDA neurons

In mice, the majority of SNc mDA neurogenesis occurs at E10 and progressively declines, whereas VTA neurogenesis peaks at E11 and persist till later time points (Bayer et al., 1995; Bye et al., 2012). Both SNc and VTA mDA neurons originate from progenitor cells positioned in the floor plate (FP) of the midbrain ventricular zone (VZ). mDA progenitors are divided into two subsets in the medial and the lateral zones of the FP. Around E8.5-E9.5, Sonic hedgehog (Shh) is exclusively expressed by medial mDA progenitors. However, at E11.5 Shh is no longer expressed in the medial zone, but is restricted to the lateral zone (Blaess et al., 2011; Joksimovic et al., 2009). This specific spatiotemporal pattern of Shh expression was recently exploited to perform fate mapping of mDA neurons and revealed that medial progenitors give rise to SNc mDA neurons, while lateral progenitors generate VTA mDA neurons (Blaess et al., 2011; Bodea et al., 2014). This observation was confirmed via immunostaining for Sox6 and Otx2/Nolz1, markers for both progenitors and mature mDA neurons of SNc and VTA, respectively. Sox6^{+}/Otx2*weak*/Nolz1- progenitors are located to the medial zone of the FP and Sox6-/Otx2*strong*/Nolz1^{+} progenitors are confined to the lateral zone (Panman et al., 2014) (Figure 3A).

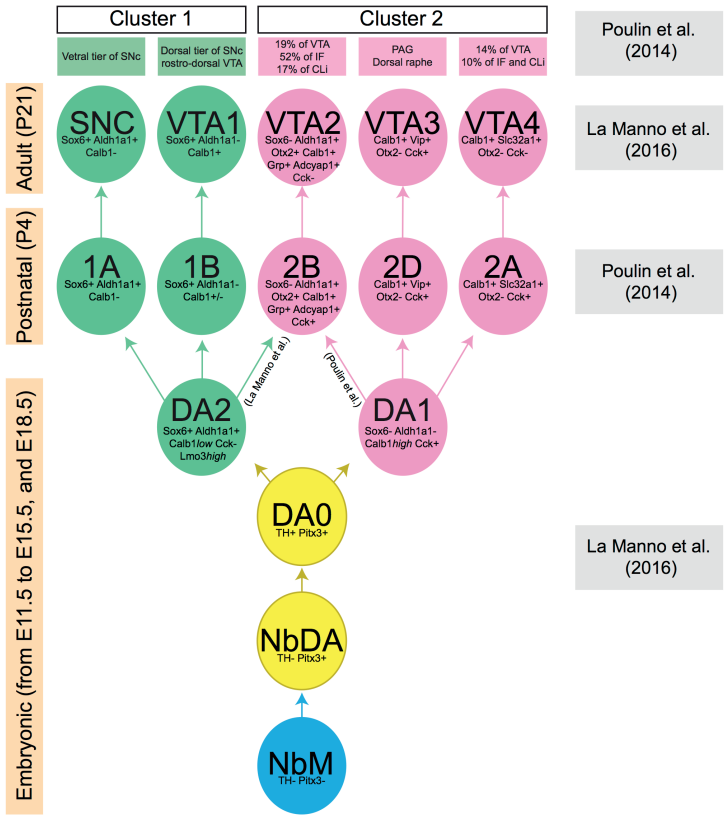

Figure 2

Lineage of mDA neuron subsets obtained by the comparison of two recent publications (La Manno et al., 2016; Poulin et al., 2014).

Each mDA neuron cluster is defined by a few distinctive molecular markers which are indicated in the cluster. Orange boxes at the left indicate the developmental stage at which a specific collection of clusters is present (embryonic, postnatal, and adult phases). Boxes at the right indicate the publication that generated the data at specified time points. The green and pink boxes at the top list the anatomically defined domains in SNc or VTA in which the molecularly-defined mDA clusters are positioned. During embryonic development, a group of mDA precursors (NbM, blue circle) gives rise to two consecutive groups of immature mDA subsets (NbDA and DA0, yellow circles). Then, two clusters of mature mDA neurons (DA1 and DA2, pink and green circles, respectively) originate from DA0. DA1 is the ancestor of all clusters represented in pink circles, whereas DA2 is the ancestor of all clusters represented in green circles. Data are not conclusive on the origin of mDA cluster 2B/VTA2, which may originate from DA1 or DA2. Calb1 is variably expressed by mDA neurons of cluster 1B (indicated in figure as Calb1+/-).

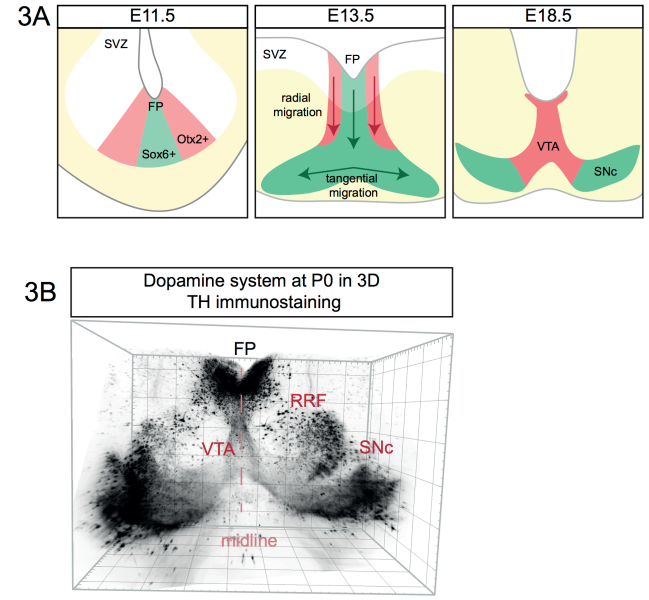

Figure 3

Schematic representation of mDA neuron migration and a 3D reconstruction of the dopamine system at postnatal day (P) 0.

(A) mDA neurons are generated in the subventricular zone (SVZ). SNc mDA progenitors are $Sox6^+$ (green) and are positioned in the medial floor plate (FP). VTA mDA progenitors are $Otx2^+$ (red) and are located in the lateral FP. First, mDA neurons migrate radially aligned along radial glia fibers. Next, only SNc mDA neurons migrate tangentially probably by using contralateral axons as a scaffold. At E18.5 mDA neuron migration is complete. (B) Coronal view of 3D reconstruction of a P0 mouse brain immunostained using an anti-TH antibody (Brignani and Pasterkamp, unpublished data). Tissue was cleared using 3DISCO and imaged using Ultramicroscope lightsheet microscopy. The mDA system extends in three dimensions, with the neurogenic FP positioned caudally to the two wings of SNc.

Following neurogenesis, postmitotic mDA migrate from the FP to their final destination in the marginal zone (MZ). This migratory stage is characterized by two phases. During the first phase SNc and VTA mDA neurons undergo radial migration. Migrating VTA neurons ($Otx2^+$/$Nolz1^+$) originating from lateral progenitors are positioned laterally in the intermediate zone (IZ), while SNc neurons ($Sox6^+$) generated from medial progenitors are located medially in the IZ (Panman et al., 2014) (Figure 3A). Both VTA and SNc neurons show leading and trailing processes that are oriented radially, aligned with the fibers of radial glia-like (RGL) cells (Bodea et al., 2014; Shults et al., 1990). RGL fibers are thought to act as scaffolds for radially migrating mDA neurons, similar to the role of these cells in other regions of the developing nervous system (Marín et al.,

2010). During the second phase of mDA neuron migration, SNc mDA neurons migrate tangentially, which results in their movement from the medial towards the lateral MZ. This ultimately results in the formation of the characteristic wing-like SNc structure observed in the postnatal and adult brain (Figure 3A). It has been proposed that during tangential migration the leading processes of SNc mDA neurons follow tangential fibers, presumably axons originating from neurons positioned in the lateral midbrain (Kawano et al., 1995). The leading and trailing processes of VTA mDA neurons are almost exclusively oriented radially, and not tangentially. Therefore, it is thought that VTA neurons migrate mainly radially (Bodea et al., 2014).

The dopamine system is an extremely complex structure that extends in three dimensions, with the neurogenic FP positioned more medio-caudally than the two wings of the developing SNc, which are protruding towards the rostro-lateral edges of the midbrain (Figure 3B, C). Data on the migration of mDA neurons along the anterior-posterior (A-P) axis is lacking and most of the studies on mDA neuron migration are performed on coronal sections at intermediate A-P levels of the mDA system. As we demonstrate in Chapter 5, the development of the mDA system not only involves radial and tangential migration of mDA neurons but also movement along the A-P axis.

2.2 Guidance molecules involved in radial migration of mDA neurons

Radial migration of postmitotic mDA neurons starts in the FP, continues in the IZ and concludes in the MZ. During this migratory process, postmitotic cells differentiate and become mDA neurons. RGL cells are positioned in the ventricular zone, both in the FP and basal plate (BP), and extend their fibers to the pial surface. Recent work identifies three distinct RGL cell types in the midbrain ventricular zone: RGL1, present in both the FP and BP; RGL2, confined to the BP; and RGL3, restricted to the FP. RGL1 and RGL2 are found from E11.5 to E15.5 during radial migration of mDA neurons. RGL3 is only detected at E15.5 (La Manno et al., 2016). The functional role(s) of these RGL cells in the midbrain remains unknown. However, single-cell RNAseq data of the ventral midbrain shows that several axon guidance genes are expressed by the three types of RGL cells (La Manno et al., 2016) (Table 2). These axon guidance genes may be involved in the development of RGL cell fibers but also in guiding migrating mDA neurons towards the pial surface. Interestingly, while several axon guidance genes are expressed in all three RGL cell types, others are specific to one or two subtypes. Further work is needed to determine the role of the three RGL cell types and of the specific axon guidance molecules they express. However, it is tempting to speculate that specific RGL cells and their associated cues may be responsible for guiding different subsets of mDA neurons.

Table 2

Canonical axon guidance genes expressed in three types of radial glia-like cells.

RGL1	RGL2	RGL3
Slit3	*Sema3B*	*Netrin1*
Sema3B	*Sema5B*	*Slit1*
Sema5B	*Sema6A*	*Slit2*
PlxnB1	*PlxnB1*	*Sema3B*
EphB1	*EphB1*	*Sema5B*
EphA3	*EphA3*	PlxnB1
EfnA4	EphB3	Nrp1
EfnB1	EfnA4	EphA3
	EfnB1	EfnA4
		EfnB1

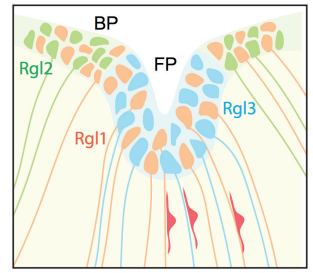

Three populations of radial glia-like cells (RGL) have been identified in the midbrain ventricular zone. RGL extend their processes from the ventricular zone to the pial surface, functioning as scaffolds for the migrating mDA neurons (red in the drawing). RGL1 is positioned in both the floor plate (FP) and the basal plate (BP). RGL2 resides only in the BP, while RGL3 only in the FP. The three RGL populations express common and different guidance genes which are listed in the table. Data was obtained from Linnarsson's lab webpage (www.linnarssonlab.org/ventralmidbrain) and validated using the Allen Brain Atlas database (www.brain-map.org). Red indicates that the mRNA of the gene is detected in the Allen Brain Atlas at E13.5 and E15.5. Green indicates that signals are detected only at E13.5. Gray indicates that mRNA is not detected.

Although the specific RGL cell-derived molecules that regulate radial migration remain to be determined, meninges-derived chemokine signals have recently been shown to direct mDA neurons to the pial surface. Radially migrating mDA neurons express the chemokine receptor Cxcr4 from E10.5 to E14.5. Cxcr4 is a G protein-coupled receptor that is activated by the chemokine Cxcl12, which induces the phosphorylation of its C-terminal domain. Cxcl12 mRNA is expressed by meningeal cells during the period of mDA neuron migration (Bodea et al., 2014; Yang et al., 2013). *In vitro* meningeal explants attract migrating mDA neurons. This effect is blocked by administration of a Cxcr4 antagonist (Yang et al., 2013). Ectopic expression of Cxcl12 in the reticular formation *in vivo* causes mDA neurons to follow an abnormal route away from the midline in the IZ towards the ectopic $Cxcl12^{+}$ cells (Yang et al., 2013). The speed and trajectory of migrating mDA neurons are intact when Cxcr4/Cxcl12 signaling is perturbed *in vitro*, indicating that other aspects of migration are controlled by this chemokine system (Bodea et al., 2014). Analysis of *Cxcr4* and *Cxcl12* KO mouse brains reveals that lack of Cxcr4/Cxcl12 signaling *in vivo* causes an accumulation of mDA neurons in the IZ, in contrast to control conditions where these neurons

reach the MZ (Bodea et al., 2014). Moreover, during the initial stage of radial migration (E11.5), mDA neurons lacking Cxcr4 have processes oriented in both radial and tangential directions, whereas most processes from neurons in wild-type mice show a radial orientation (Yang et al., 2013). At later developmental stages, defects are much milder in *Cxcr4* KO mice and absent in *Cxcl12* KO mice. This observation may hint at compensation of loss of chemokine signaling by other molecular signals (Bodea et al., 2014; Yang et al., 2013).

The cell surface receptor DCC and its ligand Netrin1 also play a role in mDA neuron migration. DCC protein is expressed by mDA neurons during the period of their migration (Xu et al., 2010). The *Netrin1* promoter is active in the ventral midbrain, both in the FP and in TH^+ nuclei (Li et al., 2014). *DCC* and *Netrin1* KO mice show ectopically (dorsally) positioned mDA neurons at P0, when mDA neuron migration has been completed (Li et al., 2014; Xu et al., 2010). Although the migration defects detected in *DCC* and *Netrin1* KO mice are similar, how DCC-Netrin1 signaling controls mDA neuron migration remained unknown. This is one of the topics of this thesis. As shown in Chapter 5, Netrin1 is expressed by RGL cells in the FP and provides guidance to a subset of SNc mDA neurons during their radial migration.

2.3 Guidance molecules involved in tangential migration of mDA neurons

Following their radial migration, SNc mDA neurons migrate tangentially, in part under control of Reelin and its receptors. Reelin controls the correct layering and polarization of different brain areas, such as the cortex and hippocampus (D'Arcangelo, 2014; Förster, 2014). It is a component of the extracellular matrix and signals via two receptors called low density lipoprotein receptor-related protein 8 (Apoer2) and very low density lipoprotein receptor (Vldlr). Binding of reelin to its receptors induces tyrosine phosphorylation of the intracellular signaling protein Dab1.

In the *reeler* mouse, an autosomal-recessive mouse mutant carrying a disrupted reelin gene, the SNc does not extend laterally at intermediate A-P levels and mDA neurons accumulate in the VTA region. At rostral levels, the SNc develops normally and no significant change in the total number of mDA neurons is observed. *Dab1* deficient mice (*yotari* mice) and double KO mice for *Apoer2* and *Vldlr* show similar mDA neuron migration defects (Bodea et al., 2014; Kang et al., 2010; Nishikawa et al., 2003). This suggests that both receptors and Dab1 are mediators of reelin signaling in the midbrain. In line with these observations, both *in vivo* and *in vitro* experiments show that a subset of SNc neurons fails to orient their processes tangentially when reelin signaling is perturbed, while VTA mDA neurons are unaffected (Bodea et al., 2014). Reelin deficiency may alter the guidance scaffolds required for mDA neuron migration, but there is a lack of consensus on this hypothesis. Some studies report that tangential axons are intact in reeler mice at E15.5, whearas other work describes defects in the development of tangential axons in reeler and yotari mice as early as E14.5 (Kang et al., 2010; Nishikawa et al., 2003).

At E13.5, when mDA neurons are migrating both radially and tangentially, reelin mRNA is expressed by the red nucleus and absent from mDA neurons (Bodea et al., 2014). If the red nucleus is the main source of reelin for migrating mDA neurons, lack of red nucleus cells should cause malformation of the SNc. Interestingly, in *Nkx6-1* KO mice the number of cells in the red nucleus is dramatically decreased at E12.5, and at E18.5 only 27% of these neurons remain (Prakash et al., 2009). Nkx6-1 is a transcription factor expressed in the BP by progenitors of red nucleus neurons, but not by mDA progenitors nor by mDA neurons. In *Nkx6-1* KO mice, the dopamine system develops normally, suggesting that reelin expressed by the red nucleus may not be responsible for the correct tangential migration of SNc mDA neurons. Recently, reelin protein was detected in mDA neurons and in the surrounding area at P0, but not at earlier developmental stages (Sharaf et al., 2015). However, at P0 migration of mDA neurons is complete. In contrast, other work detects reelin in the extracellular space surrounding mDA neurons as early as E15.5. It is possible that other cells, such as embryonic striatal neurons which are $reelin^+$ at E15.5, supply the midbrain with reelin through their axonal projections (Nishikawa et al., 2003). In this case, reelin may function as a chemoattractant for tangentially migrating SNc mDA neurons, and lack of reelin could prevent SNc mDA neurons from orienting their processes in the correct direction.

In conclusion, experimental data show that reelin and its receptors are necessary for the correct tangential migration of a subset of SNc mDA neurons. It remains to be determined whether reelin influences SNc mDA neuron movement directly by acting as an attractant guidance cue, or whether it is required for the correct development of the guidance scaffolds used by these neurons for migration.

4. Growth and guidance of mDA axons

4.1 mDA efferent and afferent connections

The mouse mDA system contains around 30.000 neurons and despite its small size it is connected to many brain areas (Figure 1C, 4A). The majority of mDA axons is oriented rostro-ventrally in the diencephalon, and is tightly fasciculated into two ipsilateral axon bundles called the medial forebrain bundles (MFB). The MFBs pass first through the ventral diencephalon and then towards the telencephalon. mDA axons projecting to the habenula do not elongate inside the MFB, but are instead oriented in a rostro-dorsal direction towards the lateral habenula, which resides in the diencephalon, using the fasciculus retroflexus as scaffold. In Chapter 2 of this thesis, we will demonstrate how the specific innervation of the lateral habenula by mDA axons is established. Recent

advances in brain tissue clearing and 3D reconstruction of axonal tracts has further unveiled the complex axon projections that derive from the mDA system (Belle et al., 2014; Renier et al., 2014) (Figure 4A). This approach holds great promise for analyzing the normal development of mDA axon connections and of defects in axon growth and guidance present in KO mouse models.

SNc and VTA mDA neurons target partly distinct areas in the forebrain. The SNc and the dorso-lateral VTA project to the dorsal striatum, forming the mesostriatal pathway. Medial SNc mDA neurons innervate the dorso-medial striatum, while lateral SNc mDA neurons project to the dorso-lateral striatum (Lerner et al., 2015). Within the striatum, each SNc mDA neuron generates extensive axonal arborizations, establishing connections with on average 75.000 striatal neurons, positioned in both the striatal patch and matrix structure (Matsuda et al., 2009), which are two striatal compartments defined by different biochemical markers and different afferent and efferent connections (Gerfen, 1992).

mDA neurons of the VTA mainly project to the prefrontal cortex (PFC), the amygdala, and the ventral striatum, which is subdivided in the medial and lateral olfactory tubercle (mOT and lOT, respectively) and the nucleus accumbens (NAc - core, medial shell, lateral shell), forming the mesocorticolimbic pathway (Ikemoto, 2007; Lammel et al., 2008). VTA mDA neurons projecting to more medial regions of the ventral striatum are distributed medially within the VTA, whereas laterally positioned VTA mDA neurons establish connections with more lateral nuclei (Figure 1C) (Beier et al., 2015; Ikemoto, 2007; Lammel et al., 2008). In contrast to SNc mDA neurons, which have few collaterals outside the striatum, single VTA mDA neurons can have axon collaterals projecting to different brain areas. For example, a mDA neuron in the PBP can innervate both the cortex and the amygdala, while a neuron in the PN can establish connections with the amygdala, the NAc-core, and the septum (Aransay et al., 2015). Other VTA mDA neurons, like those projecting to the lateral habenula, are more selective and do not have axon collaterals (Stamatakis et al., 2013).

SNc and VTA mDA neurons do not only differ with respect to the targets they innervate. Several studies in the past decade have also unveiled striking differences in the afferent inputs of SNc and VTA mDA neurons. For example, ventral striatum mainly innervates VTA mDA neurons, whereas dorsal striatum establishes connections with SNc mDA neurons. Interestingly, in the dorsal striatum, striatal neurons residing in striosomes establish connections preferentially with SNc mDA neurons, while striatal neurons of the matrix show a preference for GABAergic neurons located in the SN reticulata (Gerfen et al. 1987; Fujiyama et al. 2011; Watabe-Uchida et al. 2012). Axonal projections from the NAc to the ventral midbrain mainly target VTA mDA neurons. Furthermore, SNc mDA neurons receive inputs from the somatosensory and motor cortex, subthalamic nucleus, superior colliculus, PAG, and DR (Watabe-Uchida et al., 2012). VTA mDA neurons receive glutamatergic inputs from the medial PFC, pedunculopontine tegmentum, laterodorsal tegmentum nucleus, lateral habenula, PAG, bed nucleus of the stria terminalis, and DR. VTA dopamine neurons receive GABAergic inputs from the rostromedial mesopontine tegmental nucleus, PAG, lateral hypothalamus, ventral pallidum. There are also local glutamate and GABA synapses onto VTA dopamine neurons arising from neurons within the VTA (recently reviewed in (Morales and Margolis, 2017)).

In conclusion, the efferent and afferent connections of SNc and VTA mDA neurons are strikingly distinct. In the following section, we discuss the different stages of mDA axon guidance and the molecules involved. We highlight differences between mDA axonal subsets, cell subtype-specific expression of axon guidance receptors, and the differential response to guidance cues.

4.2 Rostrally oriented axon growth in the midbrain

The first mDA axons appear around E11 and their rostral orientation is determined by the expression of gradients of axon guidance cues along the A-P axis. An important signaling center involved in the generation of these molecular gradients is the midbrain-hindbrain organizer (MHO), which is positioned at the boundary between the caudal midbrain and the rostral hindbrain (Raible and Brand, 2004). Several secreted proteins are expressed by MHO cells, including members of the wingless (Wnt) and the fibroblast growth factor (FGF) families. The secretion of FGF8 by the MHO induces the expression of the axon repellent Semaphorin3F (Sema3F) (Yamauchi et al., 2009). At early developmental time points, Sema3F inhibits mDA axon outgrowth *in vitro* via its receptor Nrp2, which is expressed by a subset of medially-positioned mDA neurons (Hernández-Montiel et al., 2008; Kolk et al., 2009; Yamauchi et al., 2009). *Nrp2* KO mice display mDA axons aberrantly growing caudally towards the MHO (Yamauchi et al., 2009). A similar phenotype is detected when Nrp2 is conditionally removed from mDA neurons (using TH-Cre mice) (Kolk et al., 2009). Together, these results indicate that Sema3F creates a non-permissive territory in the caudal midbrain for early $Nrp2^{+}$ mDA axons (Figure 4B).

Wnts also contribute to the rostral orientation of mdDA axons. Wnt5a is expressed in a caudal-high-to-rostral-low gradient in the midbrain, whereas Wnt7b is expressed in an opposite molecular gradient. mDA neurons express the core planar cell polarity (PCP) components Frizzled3, Celsr3, and Vangl2, necessary for transducing Wnt-mediated signaling. *In vitro*, both SNc and VTA axons are repelled by Wnt5a (Blakely et al., 2013; Fenstermaker et al., 2010) and attracted by Wnt7b (Fenstermaker et al., 2010; Fernando et al., 2014). These effects are mediated by the receptor Frizzled3 (Fenstermaker et al., 2010). In *Frizzled3, Celsr3*, and *Vangl2* KO mice, mDA axons lose their rostral orientation and display aberrant dorsal and caudal projections (Fenstermaker et al., 2010). Conditional deletion of Frizzled3 from mDA neurons (using *DAT-Cre* mice) causes similar defects in mDA axon orientation, with mDA axons

forming a caudal tract that descends into the spinal cord (Hua et al., 2014). Abnormal, but transient, caudal mdDA axon projections are detected in *Wnt5a* KO mice (Fenstermaker et al., 2010). Together, these data show that Wnt-PCP signaling along the A-P axis of the midbrain is required for orienting mDA axons rostrally (Figure 4B).

4.3 Axon fasciculation in the MFB and ipsilateral projections

In the ventral diencephalon, mDA axons form the MFB that traverses the diencephalon towards its targets in the telencephalon (Figure 4A). Axon guidance receptors and cues play a role in the fasciculation of axons within the MFBs and in preventing mDA axons from crossing the midline. During their growth in the diencephalon, mDA neurons express several axon guidance receptors. Previous work has shown that from E12.5 onwards, a subset of mDA axons positioned in the ventral MFB expresses Nrp2. The Nrp2 ligand Sema3F is expressed in several brain regions surrounding the trajectory of the MFB (Kolk et al., 2009; Torigoe et al., 2013; Yamauchi et al., 2009). In *Nrp2* KO mice, the MFB is defasciculated. A similar phenotype is described in *Sema3F* KO mice and in conditional *Nrp2* KO mice in which Nrp2 is removed from mDA neurons (Kolk et al., 2009) (Table 3). These observations together with data showing that Sema3F is a potent axon repellent for $Nrp2^+$ mDA axons *in vitro* (Hernández-Montiel et al., 2008; Kolk et al., 2009; Yamauchi et al., 2009) indicate that Sema3F acts to fasciculate mDA axons *en route* to their distant targets.

The caudal hypothalamus is an important intermediate target for mDA axons. In KO mice lacking Netrin1, DCC, Slit2, Slit1 and Slit2, Robo1 and Robo2, or Nrp2, a subset of mDA axons leaves the MFB at the level of the caudal hypothalamus and turns ventrally to form an abnormal axon bundle that crosses the ventral midline (Bagri et al., 2002; Dugan et al., 2011; Li et al., 2014; Torigoe et al., 2013; Xu et al., 2010) (Figure 4C; Table 3). In *Nrp2* KO mice, the use of a β-galactosidase reporter that is present downstream of the Nrp2 promoter shows that this promoter is active in the ventral part of the MFB and in the aberrantly projecting axons. Since $Nrp2^+$ mDA neurons are normally positioned medially in the mDA system (Kolk et al., 2009; Torigoe et al., 2013; Yamauchi et al., 2009), these results suggest that the abnormal ventral axon projections in *Nrp2* KO mice originate from a subset of mDA neurons, most probably located in the VTA. It remains to be determined whether the aberrant ventral mDA axon bundles detected in the other KO mice also derive from specific mDA neuron subsets. Furthermore, it is unclear whether in these KO mice the abnormal projections form as a result of a lack of expression of axon repellent cues in ventral structures, e.g. such as Slit1, Slit2, and Netrin1, or of defects in other axon bundles that normally function as scaffolds for mDA axons. mDA axons are not the first axons to extend along the A-P axis of the developing brain. For example, at E13 mDA axons in the MFB interact with $GAD65^+$ axons extending along the A-P axis towards the striatum. These axons might be descending fibers coming from the telencephalon and/or from the mammillary bodies of the caudal hypothalamus forming the mammillo-tegmental tract. The *in vivo* ablation of $GAD65^+$ axons induces many mDA axons to turn ventrally into the hypothalamic region (Garcia-Pena et al. 2014). These data strongly suggest that (at least) a subset of mDA axons needs other pre-existing longitudinal axons as scaffolds for guidance to rostral targets.

4.4 Innervation of the striatum

The striatum is a major target of mDA axons. Striatal innervation by mDA axons starts around E13.5 (Figure 4A). *In vitro* both late embryonic and postnatal, but not early embryonic, striatal explants attract mDA axons (Gates et al., 2004). Following their entry into the striatum, mDA axons arborize extensively. Co-culturing mDA neurons with striatal neurons enhances axonal branching. The same effect is observed when culturing mDA neurons with medium conditioned by striatal neurons, indicating that secreted cues are expressed by the striatum to promote mDA branching (Manier et al., 1997). Several axon guidance cues are expressed by the striatum that may play a role in the innervation of mDA axons and the subsequent branching of these axons (Table 3, and reviewed in (Van den Heuvel and Pasterkamp, 2008; Prestoz et al., 2012)). Netrin1 is an interesting candidate as it induces mDA axon attraction (Li et al., 2014), elongation, and branching (Xu et al., 2010) via DCC. Analyses of the effects of Netrin1 on SNc and VTA explants show that effects of mDA axon attraction and elongation are induced at lower Netrin1 concentrations in SNc explants as compared to VTA explants. Interestingly, SNc mDA axons do not respond to high Netrin1 concentrations (Li et al., 2014). *In vivo*, Netrin1 expression is high in the ventro-lateral and low in the dorso-medial striatum. In *Netrin1* KO mice, SNc axons fail to innervate the dorsal striatum and accumulate in the ventral striatum (Li et al., 2014). On basis of these data it was proposed that SNc axons innervate the dorsal striatum attracted by low levels of Netrin1 expression, whereas VTA axons are directed to the ventral striatum attracted by higher Netrin1 concentration. However, in Chapter 4 we provide evidence supporting a different model. Netrin1 may not be required for the topographic guidance of nigrostriatal axons but rather to induce their branching *in vivo*.

The striatum is mainly composed of medium spiny neurons (MSNs), and displays a unique mosaic organization composed of two neuroanatomically and neurochemically distinct compartments called the matrix and patches (or striosomes) (Gerfen, 1992). Patch neurons are generated first and migrate from the lateral ganglionic eminence to the striatal mantle from E11-E12, followed by matrix neurons that start striatal mantle invasion at E13 (van der Kooy and Fishell, 1987; Mason et al., 2005). The two populations are initially intermingled in the striatal mantle, then segregate to form the matrix/patch mosaic at E18. At

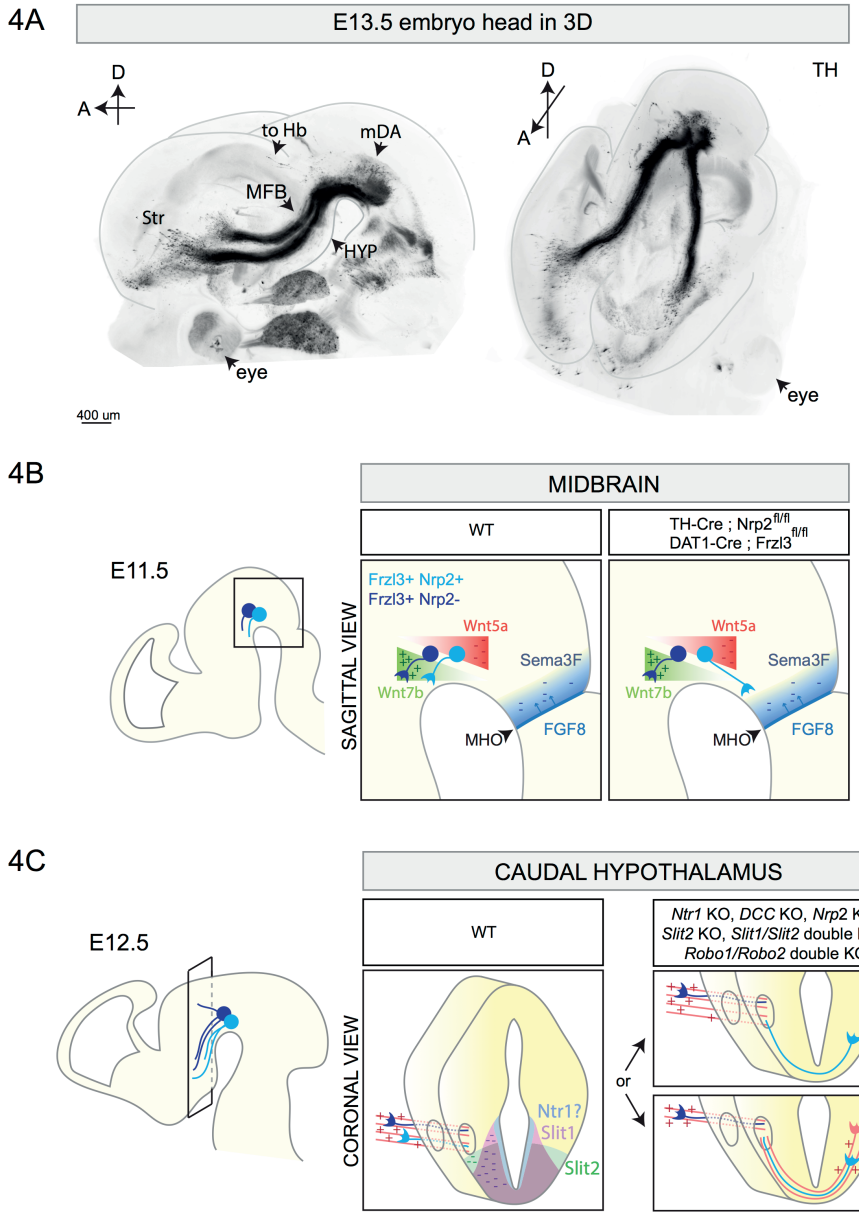

Figure 4

3D reconstruction of the E13.5 mDA system and schematic representations of different stages of mDA axon growth and guidance.

(A) 3D reconstruction of a E13.5 mouse embryo head with a sagittal (left) and horizontal (right) view. The brain is immunostained for TH and cleared using the 3DISCO protocol (Brignani and Pasterkamp, unpublished data). 3D reconstruction shows mDA neurons positioned on top of the midbrain flexure. The majority of mDA axons elongates towards the forebrain forming the MFB. mDA axons projecting to the habenula (to Hb) do not grow in the MFB, but are instead oriented in a rostro-dorsal direction. At E13.5, the first mDA axons reach the striatum (Str). (B) The rostral orientation of mDA axons (represented in blue) in the midbrain is determined by the expression of gradients of guidance cues: Wnt7b acts as attractant (+) for growing mDA axons and shows an increasing caudo-rostral gradient, whereas Wnt5a functions as a repellent (-) and shows a rostro-caudal gradient. mDA axons express the receptor Fzd3 which mediates Wnt signaling. The conditional removal of *Fzd3* from mDA neurons causes the misrouting of a subset of mDA axons towards the caudal midbrain. Moreover, in normal conditions, neurons of the MHO secrete FGF8 which in turn induces the expression of the repellent Sema3F (-). The Sema3F receptor Nrp2 is expressed by a subset of medial mDA neurons. The conditional removal of Nrp2 from mDA neurons causes the caudal misrouting of a subset of mDA axons. (C) The caudal hypothalamus expresses *Netrin1*, *Slit1*, and *Slit2*. mDA axons elongate longitudinally most likely following other pre-existing axons that function as scaffolds (red parallel lines). In *Netrin1* KO, *DCC* KO, *Nrp2* KO, *Slit2* KO, *Slit1/Slit2* double KO, and in *Robo1/Robo2* double KO, a subset of mDA axons exits the MFB, turns ventrally, and crosses the midline growing to the contralateral side of the brain. This phenotype might be a result of lack of expression of repellent guidance cues (Netrin1, Slit1, and Slit2) or of the misrouting of pioneer axons which normally function as a scaffold for mDA axons. MFB, medial forebrain bundles; Str, striatum; HYP, hypothalamus; to Hb, indicates mDA fibers growing towards the habenula; MHO, midbrain-hindbrain organizer.

this age, both patch and matrix MSNs extend their dendrites almost exclusively within their respective compartments (Kawaguchi et al., 1989). The first mDA axons arrive in the developing striatum around E13, and therefore most likely receive guidance from patch MSNs. At this age, mDA innervation is sparse and scattered. From E18 onwards, the entire striatum is innervated, but TH^+ innervation is denser in striatal patches as compared to the matrix. These areas of dense TH^+ innervation are called "dopamine islands', and are detectable until P15, after which striatal innervation of mDA axons becomes more homogeneous (Edley and Herkenham, 1984). Initially it was thought that in adult rat brain most mDA neurons of the ventral SNc were arborizing in patches, while dorsal SNc mDA axons are innervating the matrix compartment (Prensa and Parent, 2001). However, more recently it has been demonstrated that in adult mice both ventral and dorsal SNc mDA neurons innervate both striatal compartments (Matsuda et al., 2009).

Depletion of mDA neurons at early developmental timepoints does not cause changes in striatal patch/matrix organization. This indicates that aggregation of patch MSNs is independent from mDA innervation (Snyder-Keller, 1991). In contrast, the formation of 'dopamine islands' strictly relies on correct striatal development. In *Ctip2* KO mice and *Notch1* KO mice, where patch/matrix organization is lost and patches are not formed, dopaminergic innervation is correct at E15 (before aggregation of patch MSNs occurs), but disorganized and diffuse at P0 without discernable 'dopamine islands' (Arlotta et al., 2008; Mason et al., 2005). These results suggest that patch MSNs express molecular cues that induce the aggregation of a subset of mDA axons to form 'dopamine islands'. Interesting candidates for such a role are Ephs and ephrins. For example, the EphA4 receptor and its ligand ephrinA5 are expressed by matrix and patch MSNs, respectively, and are required for the correct development of striatal compartments (Passante et al., 2008). Other Ephs are also enriched in striatal patches, e.g. EphA7 and EphA8 (Allen Brain Atlas). The precise function of 'dopamine islands' during development remains to be determined, whether their transient appearance is necessary for the development of the postnatal brain, and which guidance molecules induce mDA axons to aggregate in the patch compartment.

4.5 Innervation of the medial prefrontal cortex

VTA mDA axons follow two trajectories to reach the mPFC: 1) a subset of axons exits from the MFB at the point where most mdDA axons enter the striatum and then extends rostrally to move into the PFC just caudal of the olfactory bulb; and 2) another subset of VTA mDA extends through the striatum, crosses the external capsule and innervates the mPFC. Within the mPFC the first mDA axons are detected in the subplate (SP) and the marginal zone (MZ) around E15. At E16.5, the innervation of these regions increases, while the cortical plate (CP) remains devoid of mDA axons. After a waiting period of two days, mDA axons invade the CP from the SP, following a radial path (Kolk et al., 2009) Such a waiting period for mesocortical mDA projections is observed also in human PFC (Verney, 1999).

In vitro mPFC explants release diffusible molecules that induce mDA VTA subset-specific axon outgrowth. From E14 onwards, rostral VTA explants are attracted by mPFC, whereas caudal VTA explants are strongly repelled (Kolk et al., 2009). This observation strongly suggests that rostral VTA mDA neurons, but not caudal VTA mDA neurons, constitute the VTA cell subtype that establish connections with the mPFC. Sema3F is expressed in the CP and exerts an interesting bifunctional guidance effect on rostral VTA explants: at E12.5, Sema3F is a strong repellent, while at E14.5 becomes an attractant. Both effects are mediated by the Nrp2 receptor. Despite the presence of several mDA axonal defects along the trajectory of mDA axons (caudal growth into the midbrain, MFB defasciculation, and hypothalamic innervation), many mDA axons reach the mPFC. Here, chemoattraction mediated by Sema3F and Nrp2 is required to orient mDA axons projections in the CP (Kolk et al., 2009). The bifunctional effect of Sema3F is an important molecular mechanism that allows one molecule to exert distinct effects in different spatio-temporal conditions. As we discussed previously, Sema3F acts first as a repellent for mDA axons in the midbrain, directing them towards the diencephalon. Then, when mDA axons approach the mPFC, Sema3F becomes an attractant to promote the correct innervation of the CP. Although it has been demonstrated that both the attractant and repellent effects of Sema3F are mediated by Nrp2, further work is needed to dissect how a single receptor can transduce two opposite biological effects.

Table 3
Canonical axon guidance genes involved in mDA pathway development.

Axon guidance gene(s)	Species	In vivo observations	*In vitro* observations	Expression data	References
EphrinA/EphA signaling	Mice	Transgenic mice expressing EphA5ecto-Fc show 40-50% less mDA neurons innervating the striatum.			(Sieber et al., 2004)
EphrinA5	Mice[ab], Rats[b]	No developmental defects in mDA system[a]; 10% reduction in the number of mDA neurons innervating the striatum[b].	mDA axon repellent[a]; mDA axon growth promotion via EphA5[b].	mRNA expression in the ventral midbrain dorsally to TH^+ neurons, in the thalamus, and in the striatum[a]; mRNA expression in the dorso-lateral striatum and NAc-shell[b].	[a](Deschamps et al., 2010) [b](Cooper et al., 2009)
EphA5	Mice	14% reduction in the number of mDA neurons innervating the striatum.	mDA axon growth promotion via EphrinA5.	Promoter activity in developing VTA and SNc mDA neurons.	(Cooper et al., 2009)
EphrinB2	Mice		mDA axon growth inhibition of SNc neurons.	mRNA expression in the striatum: higher expression in the ventral striatum from P1 to P7, and almost no difference at E18.	(Yue et al., 1999)
EphB1	Mice	No structural defect in the mDA system[b].		Higher mRNA levels in SNc than VTA mDA neurons from E18 to P7[a]. No promoter activity in mDA neurons, but detected in neurons of the SN reticulata[b].	[a](Yue et al., 1999) [b](Richards et al., 2007)

Table 3
Continued

DCC	Mice[a], Rats[b]	Aberrant migration of a subset of mDA neurons; Abnormal mDA innervation of the ventral striatum; reduced mDA innervation of the cortex, and a subset of mDA axons crosses the midline at the level of the caudal hypothalamus[a].	Function blocking anti-DCC antibody blocks mDA axon elongation and branching induced by Netrin1[a].	Protein expression in both SNc and VTA mDA neurons from E14 to E18[a]. In dissociated E14 mDA neurons, protein expression more abundant in SNc mDA neurons than VTA mDA neurons[b].	[a](Xu et al., 2010) [b](Lin et al., 2005)
Netrin1	Mice[b-d], Rats[a,c], mDA neurons derived from hESC[c]	Aberrant migration of a subset of mDA neurons positioned in the reticular formation, reduced mDA innervation of the dorsal striatum. A subset of mDA axons crosses the midline at the level of the caudal hypothalamus[d].	Promotion of mDA neurite outgrowth[a,c], elongation[b], attraction[c], and branching[b]. SNc mDA axons are attracted when Netrin1 is provided at low concentrations, whereas VTA mDA axons are attracted at higher concentrations[d].	Promotor activity in the entire mDA system from early time points, at the midline in the caudal hypothalamus, high ventro-lateral and low dorso-medial gradient in striatum[d].	[a](Lin et al., 2005) [b](Xu et al., 2010) [c](Cord et al., 2010) [d](Li et al., 2014)
Robo1	Rats[a], Mice[b]	KO mice show a wider MFB, with a subset of mDA axons deviating both ventrally and dorsally[b]. In *Robo1*/*Robo2* double KO mice a subset of mDA axons crosses the midline at the level of the caudal hypothalamus, mDA axons leave the MFB to grow dorsally[b].		Expression in dissociated E14 mDA neurons[a]. Expression in some mDA neurons and by longitudinal fibers in close association with mDA axons of the MFB[b].	[a](Lin et al., 2005) [b](Dugan et al., 2011)
Robo2	Rats[a], Mice[b]	No defects in mDA system development[b].		Expression in dissociated E14 VTA mDA neurons[a]. No expression by mDA neurons, but by longitudinal fibers in dorsal, anterior, and posterior regions of the mDA system[b].	[a](Lin et al., 2005) [b](Dugan et al., 2011)

Table 3
Continued

Slit2	Rats[a,b], Mice[c,d], mDA neurons derived from hESC[b]	A wider MFB, with a subset of mDA axons crossing the midline at the level of the caudal hypothalamus[c,d].	Inhibition of growth and repulsion of mDA axons [a,b,d].	mRNA expression along the ventral midline, in the hypothalamus, and lateral thalamus[d].	[a](Lin et al., 2005) [b](Cord et al., 2010) [c](Dugan et al., 2011) [d](Bagri et al., 2002)
Sema3A	Rats		Promotion of mDA axon growth.		(Hernández-Montiel et al., 2008)
Sema3C	Rats		Promotion of growth and attraction of mDA axons.		(Hernández-Montiel et al., 2008)
Sema3F	Rats[a,c], Mice[a,b]	MFB defasciculation and increase in width, random orientation of mDA axons in the cortical plate[b].	mDA axon repulsion at early time points[a-c], axon attraction at later time points[b].	mRNA expression in the caudal and dorsal midbrain[a,c], and in the cortical plate[b].	[a](Hernández-Montiel et al., 2008) [b](Kolk et al., 2009) [c](Yamauchi et al., 2009)
Nrp2	Mice	Caudal growth of mDA axons[a,b], MFB defasciculation and increase in width[a], a subset of mDA axons crossing the midline in the caudal hypothalamus[a,c], random orientation of mDA axons in the cortical plate[a].	Mediates Sema3F mDA axon repulsion[a].	Promoter activity in medial mDA neurons and in ventral MFB mDA axons[b,c].	[a](Kolk et al., 2009) [b](Yamauchi et al., 2009) [c](Torigoe et al., 2013)
Sema7A	Mice[b], Rats[a]		Reduced axonal arborization of SNc but not VTA mDA neurons[b].	mRNA expression in a mediolateral gradient within the developing striatum[a].	[a](Pasterkamp et al., 2007) [b](Pacelli et al., 2015)

Overview of *in vivo* and *in vitro* experiments reported in literature linking canonical axon guidance genes to different aspects of mDA pathway development. Expression data as reported in literature are shown.

4.6 Subset-specific transcription factors control axon guidance gene expression

As described in this section, during brain development, the expression of different axon guidance receptors allows subsets of mDA axons to respond to specific environmental cues that steer them to the correct target. The expression of different guidance receptors derives from the activation of specific developmental programs that differ between mDA neuron subsets. Many studies have analyzed which transcription factors specifically characterize SNc and VTA mDA neurons, but only a few studies have focused on the expression of axon guidance receptors induced by subset-specific transcription factors. Interesting examples are the transcription factors Otx2 and Sox6, expressed by VTA and SNc mDA neurons, respectively (Panman et al., 2014). *In vitro* overexpression of Otx2 in mDA neurons increases the expression of the guidance receptors Nrp1 and Nrp2, whereas PlxnC1 and EphB3 levels are unaffected. Downregulation of Otx2 causes the opposite effect. This indicates that transcription of Nrp1 and Nrp2 in VTA mDA neurons relies on the subset-specific transcription factor Otx2 (Chung et al., 2010). As we discussed, Nrp2 is an important receptor required during several stages of VTA mDA axon navigation (e.g. mDA axon orientation in the midbrain, fasciculation of the MBF, and mPFC innervation). Sox6 is necessary for EphA5 expression in SNc mDA neurons (Panman et al., 2014). In *Sox6* KO mice, SNc mDA neurons lack EphA5 expression (Panman et al., 2014), which is required for the correct innervation of the striatum (Cooper et al., 2009). However, in contrast to the subset-specific expression of Nrp2, the EphA5 promoter is active in both SNc and VTA mDA neurons (Cooper et al., 2009). This suggests then that the expression of EphA5 in VTA mDA neurons is regulated by another transcription factor. Future studies are needed to further unravel the transcription factor networks that control subset-specific axon guidance cue expression.

Aim and outline of this thesis

This thesis is aimed at unveiling cellular and molecular processes that guide the development of different mDA neuron-subsets by using a combination of cellular, molecular, and genetic approaches. First, we study the development of VTA mDA projections that innervate that lateral habenula. Next, we develop new mouse models to visualize and distinguish different subsets of mDA neurons *in vivo*. We then apply these models in combination with *in vitro* methods to determine the molecular mechanisms that control neuron migration and axon guidance of different subsets of SNc mDA neurons. These experimental studies are presented in the following chapters.

Chapter 2: Subdomain-mediated axon-axon signaling and chemoattraction cooperate to regulate afferent innervation of the lateral habenula. A subset of VTA mDA neurons innervates the lateral habenula. However, how these connections develop is largely unknown. In this chapter, we demonstrate that the habenula determines its own afferent innervation by developing projections that guide VTA mDA axons to the lateral habenula. This mechanism of axon-axon interaction cooperates with the local expression of Netrin1 by the lateral habenula, that allows the entry of mDA axons.

Chapter 3: Pitx3-ITC: a new genetic strategy to study dopaminergic neuron development, function and diversity. In this chapter, we present a new genetic strategy to distinguish mDA neuron subsets *in vivo*, both in embryonic and adult mouse brains. This approach, called Pitx3-ITC, relies on the expression of different fluorescent proteins in distinct subsets of mDA neurons in a single mouse. The characterization of several mouse lines shows that *Pitx3-ITC* mice allow the selective labelling of SNc mDA neurons. In addition, we have generated *Nrp2-FlpO* and *Gucy2C-Cre* mouse lines that, in combination with *Pitx3-ITC* mice, can label single mDA neurons. These mouse lines allow the visualization of dendrites and axonal projections of single mDA neurons *in vivo*.

Chapter 4: Development of dopaminergic axon-subsets and the role of Netrin1 in nigrostriatal axon branching. Here, we study the ontogeny of nigrostriatal and mesocorticolimbic axon projections. To distinguish the two mDA pathways *in vivo*, we use two transgenic mouse models that label SNc and VTA neurons, respectively. In the second part of the chapter, we analyze the role of the axon guidance cue Netrin1 during the development of SNc mDA axons. We demonstrate that Netrin1 induces branching of SNc mDA axons in the dorsal striatum *in vivo*.

Chapter 5: Netrin1 regulates migration of specific subsets of midbrain dopaminergic neurons. In the first part of this chapter, we analyze the migration of SNc mDA neurons in 2D and 3D, and conclude that SNc mDA neurons migrate in three spatial directions: i.e. along the caudo-rostral, medio-lateral, and dorso-ventral axes. Then, we investigate the cellular and molecular mechanisms that control the migration of different SNc mDA neuron subsets. Our study unveils novel mechanisms of mDA neuron migration based on the interaction between different neuronal populations in the midbrain, and between neurons and axons. In addition, we identify Netrin1 as an important regulator of these processes.

This thesis unveils developmental mechanisms that regulate the migration and axon guidance of mDA neuron subsets. These principles may apply not only to the dopamine system of the midbrain, but also to the many other neuron clusters present in the developing brain. In addition, this thesis provides new genetic tools that may be used in future studies to better comprehend the development of the dopamine system.

References

Afonso-Oramas, D., Cruz-Muros, I., de la Rosa, D.Á., Abreu, P., Giráldez, T., Castro-Hernández, J., Salas-Hernández, J., Lanciego, J.L., Rodríguez, M., and González-Hernández, T. (2009). Dopamine transporter glycosylation correlates with the vulnerability of midbrain dopaminergic cells in Parkinson's disease. Neurobiol. Dis. *36*, 494–508.

Aransay, A., Rodríguez-López, C., García-Amado, M., Clascá, F., and Prensa, L. (2015). Long-range projection neurons of the mouse ventral tegmental area: a single-cell axon tracing analysis. Front. Neuroanat. *9*, 59.

Arlotta, P., Molyneaux, B.J., Jabaudon, D., Yoshida, Y., and Macklis, J.D. (2008). Ctip2 controls the differentiation of medium spiny neurons and the establishment of the cellular architecture of the striatum. J. Neurosci. *28*, 622–632.

Bäckman, C.M., Malik, N., Zhang, Y., Shan, L., Grinberg, A., Hoffer, B.J., Westphal, H., and Tomac, A.C. (2006). Characterization of a mouse strain expressing Cre recombinase from the 3′ untranslated region of the dopamine transporter locus. Genesis *44*, 383–390.

Bagri, A., Marín, O., Plump, A.S., Mak, J., Pleasure, S.J., Rubenstein, J.L.R., and Tessier-Lavigne, M. (2002). Slit Proteins Prevent Midline Crossing and Determine the Dorsoventral Position of Major Axonal Pathways in the Mammalian Forebrain. Neuron *33*, 233–248.

Bayer, S.A., Wills, K. V, Triarhou, L.C., and Ghetti, B. (1995). Time of neuron origin and gradients of neurogenesis in midbrain dopaminergic neurons in the mouse. Exp. Brain Res. *105*, 191–199.

Beier, K.T., Steinberg, E.E., DeLoach, K.E., Xie, S., Miyamichi, K., Schwarz, L., Gao, X.J., Kremer, E.J., Malenka, R.C., and Luo, L. (2015). Circuit Architecture of VTA Dopamine Neurons Revealed by Systematic Input-Output Mapping. Cell *162*, 622–634.

Belle, M., Godefroy, D., Dominici, C., Heitz-Marchaland, C., Zelina, P., Hellal, F., Bradke, F., and Chédotal, A. (2014). A Simple Method for 3D Analysis of Immunolabeled Axonal Tracts in a Transparent Nervous System.

Blaess, S., Bodea, G.O., Kabanova, A., Chanet, S., Mugniery, E., Derouiche, A., Stephen, D., and Joyner, A.L. (2011). Temporal-spatial changes in Sonic Hedgehog expression and signaling reveal different potentials of ventral mesencephalic progenitors to populate distinct ventral midbrain nuclei. Neural Dev. *6*, 29.

Blakely, B.D., Bye, C.R., Fernando, C. V, Prasad, A.A., Pasterkamp, R.J., Macheda, M.L., Stacker, S.A., and Parish, C.L. (2013). Ryk, a receptor regulating Wnt5a-mediated neurogenesis and axon morphogenesis of ventral midbrain dopaminergic neurons. Stem Cells Dev. *22*, 2132–2144.

Bodea, G.O., Spille, J.-H., Abe, P., Andersson, A.S., Acker-Palmer, A., Stumm, R., Kubitscheck, U., and Blaess, S. (2014). Reelin and CXCL12 regulate distinct migratory behaviors during the development of the dopaminergic system. Development *141*, 661–673.

Bye, C.R., Thompson, L.H., and Parish, C.L. (2012). Birth dating of midbrain dopamine neurons identifies A9 enriched tissue for transplantation into parkinsonian mice. Exp. Neurol. *236*, 58–68.

Chaudhury, D., Walsh, J.J., Friedman, A.K., Juarez, B., Ku, S.M., Koo, J.W., Ferguson, D., Tsai, H.-C., Pomeranz, L., Christoffel, D.J., et al. (2012). Rapid regulation of depression-related behaviours by control of midbrain dopamine neurons. Nature *493*, 532–536.

Chung, C.Y., Licznerski, P., Alavian, K.N., Simeone, A., Lin, Z., Martin, E., Vance, J., and Isacson, O. (2010). The transcription factor orthodenticle homeobox 2 influences axonal projections and vulnerability of midbrain dopaminergic neurons. Brain *133*, 2022–2031.

Cooper, M.A., Kobayashi, K., and Zhou, R. (2009). Ephrin-A5 regulates the formation of the ascending midbrain dopaminergic pathways. Dev. Neurobiol. *69*, 36–46.

Cord, B.J., Li, J., Works, M., McConnell, S.K., Palmer, T., and Hynes, M.A. (2010). Characterization of axon guidance cue sensitivity of human embryonic stem cell-derived dopaminergic neurons. Mol. Cell. Neurosci. *45*, 324–334.

D'Arcangelo, G. (2014). Reelin in the Years: Controlling Neuronal Migration and Maturation in the Mammalian Brain. Adv. Neurosci. *2014*, 1–19.

Deschamps, C., Morel, M., Janet, T., Page, G., Jaber, M., Gaillard, A., and Prestoz, L. (2010). EphrinA5 protein distribution in the developing mouse brain. BMC Neurosci. *11*, 105.

Dugan, J.P., Stratton, A., Riley, H.P., Farmer, W.T., and Mastick, G.S. (2011). Midbrain dopaminergic axons are guided longitudinally through the diencephalon by Slit/Robo signals. Mol. Cell. Neurosci. *46*, 347–356.

Edley, S.M., and Herkenham, M. (1984). Comparative development of striatal opiate receptors and dopamine revealed by autoradiography and histofluorescence. Brain Res. *305*, 27–42.

Ekstrand, M.I., Nectow, A.R., Knight, Z.A., Latcha, K.N., Pomeranz, L.E., and Friedman, J.M. (2014). Molecular profiling of neurons based on connectivity. Cell *157*, 1230–1242.

Faraone, S. V., Perlis, R.H., Doyle, A.E., Smoller, J.W., Goralnick, J.J., Holmgren, M.A., and Sklar, P. (2005). Molecular Genetics of Attention-Deficit/Hyperactivity Disorder. Biol. Psychiatry *57*, 1313–1323.

Fenstermaker, A.G., Prasad, A.A., Bechara, A., Adolfs, Y., Tissir, F., Goffinet, A., Zou, Y., and Pasterkamp, R.J. (2010). Development/Plasticity/Repair Wnt/Planar Cell Polarity Signaling Controls the Anterior–Posterior Organization of Monoaminergic Axons in the Brainstem.

Fernando, C. V., Kele, J., Bye, C.R., Niclis, J.C., Alsanie, W., Blakely, B.D., Stenman, J., Turner, B.J., and Parish, C.L. (2014). Diverse Roles for Wnt7a in Ventral Midbrain Neurogenesis and Dopaminergic Axon Morphogenesis. Stem Cells Dev. *23*, 1991–2003.

Förster, E. (2014). Reelin, neuronal polarity and process orientation of cortical neurons. Neuroscience *269*, 102–111.

Fu, Y., Yuan, Y., Halliday, G., Rusznák, Z., Watson, C., and Paxinos, G. (2012). A cytoarchitectonic and chemoarchitectonic analysis of the dopamine cell groups in the substantia nigra, ventral tegmental area, and retrorubral field in the mouse. Brain Struct. Funct. *217*, 591–612.

Fujiyama, F., Sohn, J., Nakano, T., Furuta, T., Nakamura, K.C., Matsuda, W., and Kaneko, T. (2011). Exclusive and common targets of neostriatofugal projections of rat striosome neurons: a single neuron-tracing study using a viral vector. Eur. J. Neurosci. *33*, 668–677.

Garcia-Pena, C.M., Kim, M., Frade-PÃ©rez, D., Ã vila-GonzÃ¡lez, D., TÃ©llez, E., Mastick, G.S., Tamariz, E., and Varela-EchavarrÃa, A. (2014). Ascending midbrain dopaminergic axons require descending GAD65 axon fascicles for normal pathfinding. Front. Neuroanat. *8*, 43.

Gasbarri, A., Packard, M.G., Sulli, A., Pacitti, C., Innocenzi, R., and Perciavalle, V. (1996). The projections of the retrorubral field A8 to the hippocampal formation in the rat. Exp. Brain Res. *112*, 244–252.

Gates, M.A., Coupe, V.M., Torres, E.M., Fricker-Gates, R.A., and Dunnett, S.B. (2004). Spatially and temporally restricted chemoattractive and chemorepulsive cues direct the formation of the nigro-striatal circuit. Eur. J. Neurosci. *19*, 831–844.

Gerfen, C.R. (1992). The neostriatal mosaic: multiple levels of compartmental organization. Trends Neurosci. *15*, 133–139.

Gerfen, C.R., Herkenham, M., and Thibault, J. (1987). The neostriatal mosaic: II. Patch- and matrix-directed mesostriatal dopaminergic and non-dopaminergic systems. J. Neurosci. *7*, 3915–3934.

Di Giovannantonio, L.G., Di Salvio, M., Acampora, D., Prakash, N., Wurst, W., and Simeone, A. (2013). Otx2 selectively controls the neurogenesis of specific neuronal subtypes of the ventral tegmental area and compensates En1-dependent neuronal loss and MPTP vulnerability. Dev. Biol. *373*, 176–183.

Hernández-Montiel, H.L., Tamariz, E., Sandoval-Minero, M.T., and Varela-Echavarría, A. (2008). Semaphorins 3A, 3C, and 3F in mesencephalic dopaminergic axon pathfinding. J. Comp. Neurol. *506*, 387–397.

Van den Heuvel, D.M.A., and Pasterkamp, R.J. (2008). Getting connected in the dopamine system. Prog. Neurobiol. *85*, 75–93.

Hua, Z.L., Jeon, S., Caterina, M.J., and Nathans, J. (2014). Frizzled3 is required for the development of multiple axon tracts in the mouse central nervous system. Proc. Natl. Acad. Sci. U. S. A. *111*, E3005-14.

Ikemoto, S. (2007). Dopamine reward circuitry: Two projection systems from the ventral midbrain to the nucleus accumbens–olfactory tubercle complex. Brain Res. Rev. *56*, 27–78.

Joksimovic, M., Anderegg, A., Roy, A., Campochiaro, L., Yun, B., Kittappa, R., McKay, R., and Awatramani, R. (2009). Spatiotemporally separable Shh domains in the midbrain define distinct dopaminergic progenitor pools. Proc. Natl. Acad. Sci. U. S. A. *106*, 19185–19190.

Kalia, L. V, and Lang, A.E. (2015). Parkinson's disease. Lancet *386*, 896–912.

Kang, W.-Y., Kim, S.-S., Cho, S.-K., Kim, S., Suh-Kim, H., Lee, Y.-D., Ballif, B., Arnaud, L., Arthur, W., Guris, D., et al. (2010). Migratory defect of mesencephalic dopaminergic neurons in developing reeler mice. Anat. Cell Biol. *43*, 241.

Kawaguchi, Y., Wilson, C.J., and Emson, P.C. (1989). Intracellular recording of identified neostriatal patch and matrix spiny cells in a slice preparation preserving cortical inputs. J. Neurophysiol. *62*, 1052–1068.

Kawano, H., Ohyama, K., Kawamura, K., and Nagatsu, I. (1995). Migration of dopaminergic neurons in the embryonic mesencephalon of mice. Dev. Brain Res. *86*, 101–113.

Khan, S., Stott, S.R.W., Chabrat, A., Truckenbrodt, A.M., Spencer-Dene, B., Nave, K.-A., Guillemot, F., Levesque, M., and Ang, S.-L. (2017). Survival of a Novel Subset of Midbrain Dopaminergic Neurons Projecting to the Lateral Septum Is Dependent on NeuroD Proteins. J. Neurosci. *37*.

Kolk, S.M., Gunput, R.-A.F., Tran, T.S., van den Heuvel, D.M. a, Prasad, A. a, Hellemons, A.J.C.G.M., Adolfs, Y., Ginty, D.D., Kolodkin, A.L., Burbach, J.P.H., et al. (2009). Semaphorin 3F is a bifunctional guidance cue for dopaminergic axons and controls their fasciculation, channeling, rostral growth, and intracortical targeting. J. Neurosci. *29*, 12542–12557.

van der Kooy, D., and Fishell, G. (1987). Neuronal birthdate underlies the development of striatal compartments. Brain Res. *401*, 155–161.

Lammel, S., Hetzel, A., Häckel, O., Jones, I., Liss, B., and Roeper, J. (2008). Unique properties of mesoprefrontal neurons within a dual mesocorticolimbic dopamine system. Neuron *57*, 760–773.

Lerner, T.N., Shilyansky, C., Davidson, T.J., Evans, K.E., Beier, K.T., Zalocusky, K.A., Crow, A.K., Malenka, R.C., Luo, L., Tomer, R., et al. (2015). Intact-Brain Analyses Reveal Distinct Information Carried by SNc Dopamine Subcircuits. Cell *162*, 635–647.

Li, J., Duarte, T., Kocabas, A., Works, M., McConnell, S.K., and Hynes, M.A. (2014). Evidence for topographic guidance of dopaminergic axons by differential Netrin1 expression in the striatum. Mol. Cell. Neurosci. *61*, 85–96.

Lin, L., Rao, Y., and Isacson, O. (2005). Netrin1 and slit-2 regulate and direct neurite growth of ventral midbrain dopaminergic neurons. Mol. Cell. Neurosci. *28*, 547–555.

Manier, M., Cristina, N., Chatellard-Causse, C., Mouchet, P., Herman, J.P., and Feuerstein, C. (1997). Striatal target-induced axonal branching of dopaminergic mesencephalic neurons in culture via diffusible factors. J. Neurosci. Res. *48*, 358–371.

La Manno, G., Gyllborg, D., Codeluppi, S., Nishimura, K., Salto, C., Zeisel, A., Borm, L.E., Stott, S.R.W., Toledo, E.M., Villaescusa, J.C., et al. (2016). Molecular Diversity of Midbrain Development in Mouse, Human, and Stem Cells. Cell *167*, 566–580.e19.

Marín, O., Valiente, M., Ge, X., and Tsai, L.-H. (2010). Guiding neuronal cell migrations. Cold Spring Harb. Perspect. Biol. *2*, a001834.

Mason, H.A., Rakowiecki, S.M., Raftopoulou, M., Nery, S., Huang, Y., Gridley, T., and Fishell, G. (2005). Notch signaling coordinates the patterning of striatal compartments. Development *132*, 4247–4258.

Matsuda, W., Furuta, T., Nakamura, K.C., Hioki, H., Fujiyama, F., Arai, R., and Kaneko, T. (2009). Single nigrostriatal dopaminergic neurons form widely spread and highly dense axonal arborizations in the neostriatum. J. Neurosci. *29*, 444–453.

Milton, A.L., and Everitt, B.J. (2012). The persistence of maladaptive memory: Addiction, drug memories and anti-relapse treatments. Neurosci. Biobehav. Rev. *36*, 1119–1139.

Morales, M., and Margolis, E.B. (2017). Ventral tegmental area: cellular heterogeneity, connectivity and behaviour. Nat. Rev. Neurosci. *18*, 73–85.

Nishikawa, S., Goto, S., Yamada, K., Hamasaki, T., and Ushio, Y. (2003). Lack of Reelin causes malpositioning of nigral dopaminergic neurons: Evidence from comparison of normal andRelnrl mutant mice. J. Comp. Neurol. *461*, 166–173.

Pacelli, C., Giguère, N., Bourque, M.-J., Lévesque, M., Slack, R.S., and Trudeau, L.-É. (2015). Elevated Mitochondrial Bioenergetics and Axonal Arborization Size Are Key Contributors to the Vulnerability of Dopamine Neurons. Curr. Biol. *25*, 2349–2360.

Panman, L., Papathanou, M., Laguna, A., Oosterveen, T., Volakakis, N., Acampora, D., Kurtsdotter, I., Yoshitake, T., Kehr, J., Joodmardi, E., et al. (2014). Sox6 and Otx2 Control the Specification of Substantia Nigra and Ventral Tegmental Area Dopamine Neurons. Cell Rep. *8*, 1018–1025.

Passante, L., Gaspard, N., Degraeve, M., Frisén, J., Kullander, K., De Maertelaer, V., and Vanderhaeghen, P. (2008). Temporal regulation of ephrin/Eph signalling is required for the spatial patterning of the mammalian striatum. Development *135*, 3281–3290.

Pasterkamp, R.J., Kolk, S.M., Hellemons, A.J., and Kolodkin, A.L. (2007). Expression patterns of semaphorin7A and plexinC1 during rat neural development suggest roles in axon guidance and neuronal migration. BMC Dev. Biol. *7*, 98.

Poulin, J.-F., Zou, J., Drouin-Ouellet, J., Kim, K.-Y.A., Cicchetti, F., and Awatramani, R.B. (2014). Defining Midbrain Dopaminergic Neuron Diversity by Single-Cell Gene Expression Profiling. Cell Rep. *9*, 930–943.

Prakash, N., Puelles, E., Freude, K., Trümbach, D., Omodei, D., Di Salvio, M., Sussel, L., Ericson, J., Sander, M., Simeone, A., et al. (2009). Nkx6-1 controls the identity and fate of red nucleus and oculomotor neurons in the mouse midbrain. Development *136*.

Prensa, L., and Parent, A. (2001). The nigrostriatal pathway in the rat: A single-axon study of the relationship between dorsal and ventral tier nigral neurons and the striosome/matrix striatal compartments. J. Neurosci. *21*, 7247–7260.

Prestoz, L., Jaber, M., and Gaillard, A. (2012). Dopaminergic axon guidance: which makes what? Front. Cell. Neurosci. *6*, 32.

Raible, F., and Brand, M. (2004). Divide et Impera--the midbrain-hindbrain boundary and its organizer. Trends Neurosci. *27*, 727–734.

Renier, N., Wu, Z., Simon, D.J., Yang, J., Ariel, P., and Tessier-Lavigne, M. (2014). iDISCO: A Simple, Rapid Method to Immunolabel Large Tissue Samples for Volume Imaging. Cell *159*, 896–910.

Richards, A.B., Scheel, T.A., Wang, K., Henkemeyer, M., and Kromer, L.F. (2007). EphB1 null mice exhibit neuronal loss in substantia nigra pars reticulata and spontaneous locomotor hyperactivity. Eur. J. Neurosci. *25*, 2619–2628.

Di Salvio, M., Di Giovannantonio, L.G., Acampora, D., Prosperi, R., Omodei, D., Prakash, N., Wurst, W., and Simeone, A. (2010). Otx2 controls neuron subtype identity in ventral tegmental area and antagonizes vulnerability to MPTP. Nat. Neurosci. *13*, 1481–1488.

Schein, J.C., Hunter, D.D., and Roffler-Tarlov, S. (1998). Girk2 Expression in the Ventral Midbrain, Cerebellum, and Olfactory Bulb and Its Relationship to the Murine Mutationweaver. Dev. Biol. *204*, 432–450.

Sharaf, A., Rahhal, B., Spittau, B., and Roussa, E. (2015). Localization of reelin signaling pathway components in murine midbrain and striatum. Cell Tissue Res. *359*, 393–407.

Shults, C.W., Hashimoto, R., Brady, R.M., and Gage, F.H. (1990). Dopaminergic cells align along radial glia in the developing mesencephalon of the rat. Neuroscience *38*, 427–436.

Sieber, B.-A., Kuzmin, A., Canals, J.M., Danielsson, A., Paratcha, G., Arenas, E., Alberch, J., Ögren, S.O., and Ibáñez, C.F. (2004). Disruption of EphA/ephrin-A signaling in the nigrostriatal system reduces dopaminergic innervation and dissociates behavioral responses to amphetamine and cocaine. Mol. Cell. Neurosci. *26*, 418–428.

Simeone, A., Di Salvio, M., Di Giovannantonio, L.G., Acampora, D., Omodei, D., and Tomasetti, C. (2011). The Role of Otx2 in Adult Mesencephalic–Diencephalic Dopaminergic Neurons. Mol. Neurobiol. *43*, 107–113.

Snyder-Keller, A.M. (1991). Development of striatal compartmentalization following pre- or postnatal dopamine depletion. J. Neurosci. *11*, 810–821.

Stamatakis, A.M., Jennings, J.H., Ung, R.L., Blair, G.A., Weinberg, R.J., Neve, R.L., Boyce, F., Mattis, J., Ramakrishnan, C., Deisseroth, K., et al. (2013). A Unique Population of Ventral Tegmental Area Neurons Inhibits the Lateral Habenula to Promote Reward. Neuron *80*, 1039–1053.

Thompson, L., Barraud, P., Andersson, E., Kirik, D., and Björklund, A. (2005). Identification of dopaminergic neurons of nigral and ventral tegmental area subtypes in grafts of fetal ventral mesencephalon based on cell morphology, protein expression, and efferent projections. J. Neurosci. *25*, 6467–6477.

Torigoe, M., Yamauchi, K., Tamada, A., Matsuda, I., Aiba, A., Castellani, V., and Murakami, F. (2013). Role of neuropilin-2 in the ipsilateral growth of midbrain dopaminergic axons. Eur. J. Neurosci. *37*, 1573–1583.

Verney, C. (1999). Distribution of the catecholaminergic neurons in the central nervous system of human embryos and fetuses. Microsc. Res. Tech. *46*, 24–47.

Watabe-Uchida, M., Zhu, L., Ogawa, S.K., Vamanrao, A., and Uchida, N. (2012). Whole-brain mapping of direct inputs to midbrain dopamine neurons. Neuron *74*, 858–873.

Winterer, G., and Weinberger, D.R. (2004). Genes, dopamine and cortical signal-to-noise ratio in schizophrenia. Trends Neurosci. *27*, 683–690.

Xu, B., Goldman, J.S., Rymar, V.V., Forget, C., Lo, P.S., Bull, S.J., Vereker, E., Barker, P.A., Trudeau, L.E., Sadikot, A.F., et al. (2010). Critical Roles for the Netrin Receptor Deleted in Colorectal Cancer in Dopaminergic Neuronal Precursor Migration, Axon Guidance, and Axon Arborization. Neuroscience *169*, 932–949.

Yamauchi, K., Mizushima, S., Tamada, A., Yamamoto, N., Takashima, S., and Murakami, F. (2009). FGF8 Signaling Regulates Growth of Midbrain Dopaminergic Axons by Inducing Semaphorin 3F. J. Neurosci. *29*.

Yang, S., Edman, L.C., Sánchez-Alcañiz, J.A., Fritz, N., Bonilla, S., Hecht, J., Uhlén, P., Pleasure, S.J., Villaescusa, J.C., Marín, O., et al. (2013). Cxcl12/Cxcr4 signaling controls the migration and process orientation of A9-A10 dopaminergic neurons. Development *140*, 4554–4564.

Yue, Y., Widmer, D.A.J., Halladay, A.K., Cerretti, D.P., Wagner, G.C., Dreyer, J.-L., and Zhou, R. (1999). Specification of Distinct Dopaminergic Neural Pathways: Roles of the Eph Family Receptor EphB1 and Ligand Ephrin-B2. J. Neurosci.

Chapter 2

Subdomain-Mediated Axon-Axon Signaling and Chemoattraction Cooperate to Regulate Afferent Innervation of the Lateral Habenula

Ewoud R. E. Schmidt[1], Sara Brignani[1], Youri Adolfs[1], Suzanne Lemstra[1], Jeroen Demmers[2], Marina Vidaki[3], Amber-Lee S. Donahoo[4], Kersti Lillevälli[5], Eero Vasar[5], Linda J. Richards[4], Domna Karagogeos[3], Sharon M. Kolk[1,6] and R. Jeroen Pasterkamp[1#]

[1] Department of Translational Neuroscience, Brain Center Rudolf Magnus, University Medical Center Utrecht, 3584 CG, Utrecht, the Netherlands

[2] Proteomics Centre and Department of Cell Biology, Erasmus University Medical Centre, Rotterdam 3015 GE, The Netherlands

[3] Department of of Basic Science, Faculty of Medicine, University of Crete and Institute of Molecular Biology and Biotechnology, FoRTH, Heraklion, Greece 71110

[4] The University of Queensland, Queensland Brain Institute and The School of Biomedical Sciences, Brisbane, Queensland, 4067, Australia

[5] Department of Physiology, Institute of Biomedicine and Translational Medicine, University of Tartu, Ravila 19, 50411 Tartu, Estonia

[6] Present address: Department of Molecular Animal Physiology, Donders Institute for Brain, Cognitive and Behaviour, Radboud University Nijmegen, Nijmegen, the Netherlands

Neuron, 83 (2) pp. 372-387.

Abstract

A dominant feature of neural circuitry is the organization of neuronal projections and synapses into specific brain nuclei or laminae. Lamina-specific connectivity is controlled by the selective expression of extracellular guidance and adhesion molecules in the target field. However, how (sub)nucleus-specific connections are established and whether axon-derived cues contribute to subdomain targeting is largely unknown. Here we demonstrate that the lateral subnucleus of the habenula (lHb) determines its own afferent innervation by sending out efferent projections that express the cell adhesion molecule LAMP to reciprocally collect, sort and guide dopaminergic afferents to the lHb – a phenomenon we term subdomain-mediated axon-axon signaling. This process of reciprocal axon-axon interactions cooperates with lHb-specific chemoattraction mediated by Netrin1, which controls axon target entry, to ensure specific innervation of the lHb. We propose that cooperation between pre-target reciprocal axon-axon signaling and subdomain-restricted instructive cues provides a highly precise and general mechanism to establish subdomain-specific neural circuitry.

Introduction

The formation of precise connections between afferent axons and their partner neurons is essential for the assembly of functional neural circuits. The organization of the nervous system in two main anatomical units, i.e. brain nuclei and laminated structures, facilitates this process by spatially grouping synaptic partners and enabling subdomain-restricted expression of instructive cues. Despite the important role of these organizing principles, our understanding of the cellular and molecular basis of lamina- or subnucleus-specific circuit development is still limited.

Our current knowledge of subdomain-specific axon targeting mainly derives from work on laminated structures and recent studies have uncovered different molecular strategies that control lamina-specific targeting independent of neural acitvity. This work shows that initially target-derived membrane-associated or secreted guidance cues function to direct axon projections to or exclude them from specific layers. Subsequently, combinatorial expression of cell adhesion molecules facilitates the formation of contacts between matched pre- and postsynaptic neurons (Baier, 2013; Huberman et al., 2010; Robles and Baier, 2012; Sanes and Yamagata, 2009; Williams et al., 2010). Similar to laminated structures, brain nuclei are often subdivided into smaller subdomains comprising small clusters of related neurons (e.g. (Aizawa et al., 2012; Molnár et al., 2012)). A striking example of a brain nucleus in which subdomain-specific connectivity coordinates complex physiological functions is the habenula. The habenula receives afferent inputs from many forebrain regions, mediates reward-related behavior and is linked to psychiatric disease (Li et al., 2011, 2013, Matsumoto and Hikosaka, 2007, 2009). It comprises two main subdomains, the medial habenula (mHb) and lateral habenula (lHb). The mHb primarily projects axons to the interpeduncular nucleus, while the lHb can directly innervate monoaminergic nuclei, including dopaminergic neurons (Bianco and Wilson, 2009; Hikosaka et al., 2008). The lHb is the only subdomain that receives reciprocal dopaminergic innervation (Gruber et al., 2007), which acts as a feedback loop to inhibit lHb activity (Kowski et al., 2009; Shen et al., 2012; Stamatakis et al., 2013). However, our understanding of how subdomain-specific innervation patterns in the habenula and other brain nuclei are established is limited.

During development, axons do not only rely on molecular gradients presented in the surrounding environment for guidance (Pasterkamp and Kolodkin, 2013), but also on signals provided by other axons. Axon-axon signaling serves critical roles in nervous system wiring, but the underlying mechanisms are incompletely understood. Furthermore, our current understanding of axon-axon interactions mainly derives from studies on axon types extending alongside as part of the

same bundle (Grueber and Sagasti, 2010; Imai and Sakano, 2011; Luo and Flanagan, 2007; Tessier-Lavigne and Goodman, 1996; Wang and Marquardt, 2013). In contrast, molecular mechanisms that drive instructive interactions between reciprocially projecting axons, e.g. those between the habenula and dopamine system, and the contribution of such interactions to neural circuit assembly remain largely unresolved (Deck et al., 2012). This is surprising as reciprocal connections function as important feedback and feedforward loops in many neural circuits.

Here, we show that the habenula integrates different, previously uncharacterized cellular and molecular mechanisms to control its subdomain-specific innervation by dopaminergic axons. Our observations unveil a novel role for axon-axon signaling by showing that a specific subdomain, the lHb, sends out molecularly labeled efferent projections in a larger axon bundle to collect, sort and guide its own reciprocal afferent projections in a subdomain-restricted manner. This process of subdomain-mediated axon-axon signaling cooperates with lHb-specific chemoattraction to control the specific innervation of the lHb by dopaminergic afferents. Together, our findings identify conceptually novel axonal wiring principles in the habenula that may also apply more generally to other brain nuclei or laminated structures.

Results

The habenula receives subdomain-restricted afferent inputs, including those from dopaminergic neurons in the ventral tegmental area (VTA) (Fig. 1A) (Gruber et al., 2007; Phillipson and Griffith, 1980). However, despite the important physiological role of these dopaminergic afferents (Stamatakis et al., 2013), how dopaminergic innervation of the habenula is established is unknown. To determine how dopaminergic afferents specifically innervate the lHb, we first characterized their ontogeny using immunohistochemistry for tyrosine hydroxylase (TH), the rate-limiting enzyme in dopamine synthesis. TH-positive axons started to project towards the habenula around E12.5 and arrived at this structure by E13.5. At E16.5, TH-positive axons had entered the lHb, but not the mHb, and two days later, at E18.5, this innervation was further increased (Fig. 1B, C; data not shown). Thus, during development dopaminergic axons selectively innervate the lHb without expanding into the mHb.

1. Netrin1 is a Subnucleus-specific Attractant for Dopaminergic Axons

How is the selective innervation of the lHb achieved? To address this question, we searched for molecular differences between the mHb and lHb by using laser capture microdissection in combination with mass spectrometry (Fig. S1A). This analysis identified 2880 unique proteins and revealed differential expression of several classes of proteins with established roles in neural circuit development, e.g. axon guidance and cell adhesion molecules (Table S1). A few of the identified proteins were shown previously to display lHb- or mHb-specific patterns of expression, confirming the specificity of the microdissection procedure (Quina et al., 2009). Analysis of the expression of several of the candidates revealed subdomain-specific expression for *Netrin1* and *DCC* in the habenula. *DCC* strongly labeled the mHb at E16.5, while *Netrin1* expression was confined to the lHb (Fig. 1D)(Quina et al., 2009). Netrin1 is a chemoattractant for dopaminergic axons via its DCC receptor, which has been detected throughout the embryonic and adult dopaminergic system (Cord et al., 2010; Lin et al., 2005; Manitt et al., 2013; Osborne et al., 2005; Xu et al., 2010). Indeed, immunohistochemistry showed DCC expression in dopaminergic afferents of the lHb, both at E16.5 (Fig. S1B) and in the adult (Osborne et al., 2005).

The expression of DCC on dopaminergic axons *en route* to the lHb and *Netrin1* in the lHb suggested that this ligand-receptor pair may regulate the dopaminergic innervation of this subnucleus. To test this model, we first performed explant co-culture assays by combining VTA and lHb explants. Axons emanating from VTA explants preferentially extended towards lHb explants and this effect was blocked by the addition of DCC function blocking antibodies, but not IgG control antibodies (P/D ratio 1.39 ± 0.12 for control (n = 16), 1.34 ± 0.09 for control IgG (n = 12) and 1.01 ± 0.06 for anti-DCC (n = 10); $P < 0.05$; Fig. S1C). Analysis of the trajectories of individual dopaminergic axons emerging parallel to the lHb explants (Fig. S1D)(Bagnard et al., 1998; Pasterkamp et al., 2003), confirmed the ability of lHb to reorient dopaminergic VTA axons in a DCC-dependent manner *in vitro* (Fig. S1E). To establish that Netrin1 can indeed attract dopaminergic axons projecting to the habenula, we developed an organotypic culture assay that recapitulates the *in vivo* development of the habenular system (Fig. S2A) and positioned Netrin1-expressing cells or control cells adjacent to the presumptive trajectory of the dopaminergic projections in E12.5 hemisections. Whereas the normal trajectory of dopaminergic axons towards the habenula was not affected by control cells, dopaminergic axons extending in the vicinity of Netrin1-expressing cells were reoriented towards these cells (16.7 % for control; 85.7% for Netrin1, n = 6 and n = 7 for control and Netrin1; $P < 0.05$; Fig. 1E, G). To remove DCC from dopaminergic axons, *DCC* conditional

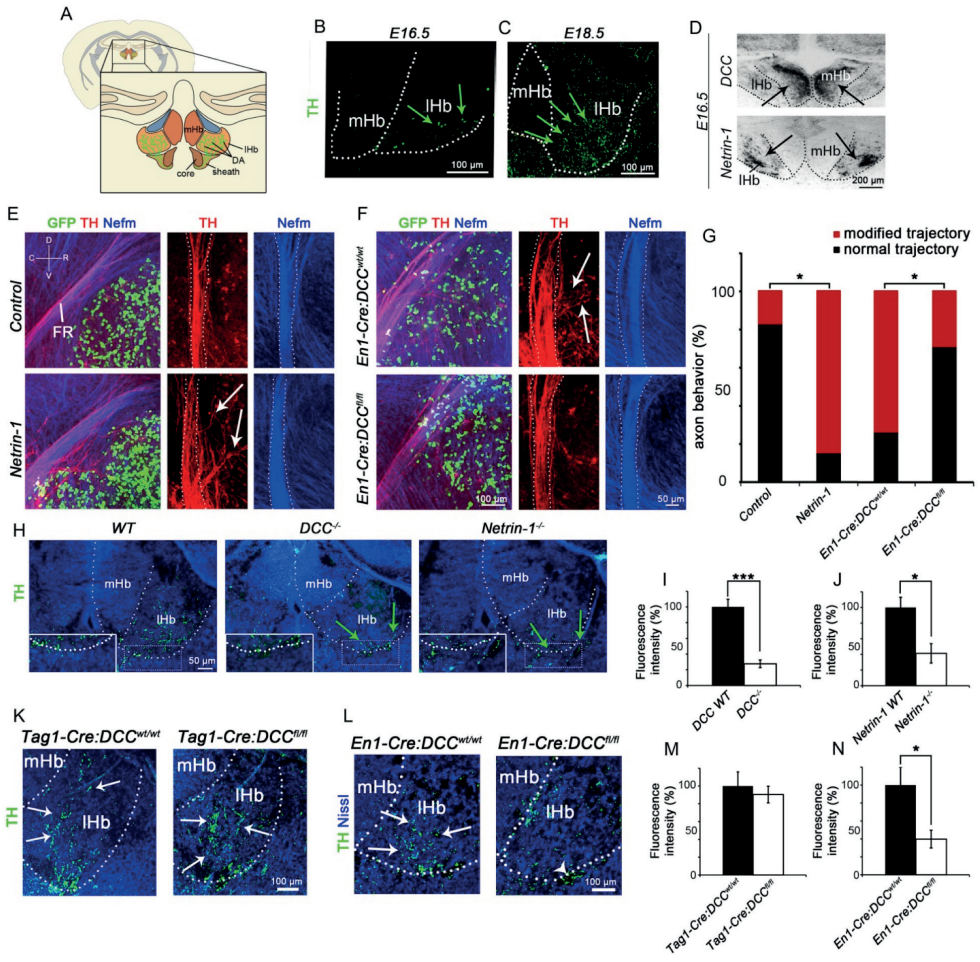

Figure 1

Netrin1 is a Subnucleus-Specific Attractant for Dopaminergic Axons

(A) Schematic of a coronal section of the mouse brain depicting the medial habenula (mHb), lateral habenula (lHb) and the fasciculus retroflexus (FR). The FR is the major output bundle of the habenula. Dopaminergic (DA) innervation of the habenula is restricted to the lHb. (B, C) Immunohistochemistry for tyrosine hydroxylase (TH) on coronal sections of the embryonic habenula. Green arrows indicate TH-positive axons. (D) *In situ* hybridization for *DCC* and *Netrin1* in coronal sections of the habenula. Black arrows point to prominent expression of *DCC* in the mHb and of *Netrin1* in the lHb. (E, F) E12.5 organotypic slices were cultured for 3 days *in vitro* (DIV) and subjected to immunohistochemistry for GFP, TH and neurofilament medium polypeptide (Nefm). Placing Netrin1 expressing cell aggregates adjacent to the presumptive FR reorients DA axons towards the aggregate (white arrows). This effect is not observed in cultures from *En1-Cre:DCC$^{fl/fl}$* mice in which DCC is absent from DA neurons (F). C, caudal; D, dorsal; R, rostral; V, ventral. (G) Quantification indicating the percentage of cultures with a normal or modified trajectory of dopaminergic projections. *$P < 0.05$. (H) Immunohistochemistry for tyrosine hydroxylase (TH) in coronal sections of the E18.5 habenula of wild-type (WT), *DCC$^{-/-}$* or *Netrin1$^{-/-}$* mice. Insets show a higher magnification of the boxed areas showing the ventral border of the lateral habenula (lHb). Green arrows point to aberrant accumulation of dopaminergic axons. (I, J) Quantification of the dopaminergic innervation of the lHb in *DCC$^{-/-}$* (I) and *Netrin1$^{-/-}$* (J) mice. * $P < 0.05$, *** $P < 0.001$. Error bars indicate S.E.M.. (K, L) Immunohistochemistry for TH in coronal sections of E18.5 *Tag1-Cre:DCC$^{wt/wt}$* and *Tag1-Cre:DCC$^{fl/fl}$* mice (K) or *En1-Cre:DCC$^{wt/wt}$* and *En1-Cre:DCC$^{fl/fl}$* mice (L). White arrows indicate dopaminergic axons in the lHb. Arrowhead in L indicates accumulation of dopaminergic axons at the ventral border of the lHb. (M, N) Quantification of the dopaminergic innervation of the lHb in *Tag1-Cre:DCC* (M) and *En1-Cre:DCC* (N) conditional knockout mice. Innervation is not affected in *Tag1-Cre:DCC$^{fl/f}$* mice, but is dramatically reduced in *En1-Cre:DCC$^{fl/fl}$* mice. * $P < 0.05$. Error bars indicate S.E.M.. See also Figure S1, S2 and Table S1.

mutants (Krimpenfort et al., 2012) were crossed with *Engrailed*(*En1*)*-Cre* mice, which drive Cre recombinase expression in the early embryonic midbrain but not in the habenula (Fig. S2B-E)(Kimmel et al., 2000). We tested several other Cre-lines with reported expression in dopaminergic neurons (e.g. *Pitx3-Cre*, *DAT-Cre*), but none of these lines induced recombination at sufficiently early stages of development (data not shown). In cultures derived from *En1-Cre:DCC*$^{fl/fl}$ embryos, Netrin1 cells could no longer significantly alter the normal linear trajectory of dopaminergic axons (73.3% for *En1-Cre:DCC*$^{wt/wt}$; 28.5% for *En1-Cre:DCC*$^{fl/fl}$, n = 15 and n = 7 for *En1-Cre:DCC*$^{wt/wt}$ and *En1-Cre:DCC*$^{fl/fl}$; $P < 0.05$; Fig. 1F, G). Together, these data show that Netrin1 secreted by the lHb acts as an attractant for DCC-expressing dopaminergic VTA axons.

2. Netrin1 Controls Dopaminergic Axon Target Entry in the lHb

To examine whether DCC and Netrin1 are required *in vivo* for subdomain-specific innervation of the lHb, dopaminergic targeting of the lHb was analyzed in *DCC*$^{-/-}$ and *Netrin1*$^{-/-}$ mice at E18.5, when dopaminergic fibers occupy most of the lHb (Fig. 1C). Genetic ablation of *DCC* resulted in an almost complete loss of lHb innervation (27.7% ± 4.8% of control, n = 4 for control and *DCC*$^{-/-}$; $P < 0.001$; Fig. 1H, I) and TH-positive axons were found to accumulate at the ventral border of the lHb in *DCC*$^{-/-}$ mice instead of entering this structure (Fig. 1H, insets). *Netrin1*$^{-/-}$ mice displayed similar phenotypes, although some innervation of the lHb was observed, most likely because this mouse mutant is a hypomorph displaying residual Netrin1 expression (41.3% ± 12.3% of control, n = 3 and n = 4 for control and *Netrin1*$^{-/-}$, respectively; $P < 0.05$; Fig. 1H, J) (Serafini et al., 1996). To determine whether lack of dopaminergic innervation of the lHb in *DCC*$^{-/-}$ mice is due to removal of DCC from habenular or dopaminergic axons, we next genetically ablated *DCC* in the habenula or in the dopaminergic midbrain. To remove DCC from the habenula, a bacterial artificial chromosome (BAC) mouse was generated expressing Cre recombinase under the control of *Tag-1* promotor sequences. Tag1 is a marker of the habenula and *Tag-1-Cre:ROSA26-eYFP* mice revealed robust recombination in the habenula but not in dopaminergic neurons (Fig. S3A). Crossing *Tag1-Cre* mice with *DCC*$^{fl/fl}$ mice resulted in loss of DCC expression in mHb neurons and axons but did not change the number of dopaminergic axons in the lHb (90.4% ± 9.4% of control, n = 3; n.s.; Fig. 1K, M). In contrast, loss of DCC in midbrain dopamine neurons in *En1-Cre:DCC*$^{fl/fl}$ mice caused reduced innervation of the lHb (39.7% ± 9.9% of control, n = 3; $P < 0.05$; Fig. 1L, N). This reduction was somewhat less severe in *En1-Cre:DCC*$^{fl/fl}$ mice as compared to *DCC* full knockout mice, presumably because En1 levels vary among dopaminergic neurons (Veenvliet et al., 2013). Nevertheless, the majority of dopaminergic axons accumulated at the border of the lHb in *En1-Cre:DCC*$^{fl/fl}$ mice and did not enter the lHb (Fig. 1L). Finally, we directed siRNAs targeting *Netrin1* to the habenula at E12.5 before dopaminergic afferents reach this structure using *ex vivo* electroporation (Fig. S3C). Electroporation with Netrin1 siRNAs induced a significant decrease in the dopaminergic innervation of the lHb (Fig. S3D-F). This effect was evident despite our observation that only a subset of habenular neurons is targeted by the *ex vivo* electroporation procedure. Collectively, these data show that Netrin1 expressed in the lHb instructs dopaminergic axons expressing DCC to enter the lHb (Fig. S3G).

3. Reciprocal Axon-Axon Interactions Guide Dopaminergic Afferents to the lHb

Although dopaminergic axons did reach the lHb in *DCC*$^{-/-}$ and *Netrin1*$^{-/-}$ mice, we observed that their organization in the fasciculus retroflexus (FR) was severely disrupted. The FR is the major output bundle of the habenula in which efferent habenular axons are intermingled with specific afferent projections. Habenular efferents display a characteristic segregated distribution in the FR, with axons from the mHb projecting in the core of the bundle and lHb axons forming a sheath around this core (Fig. 2A) (Bianco and Wilson, 2009). To analyze this organization in relation to dopaminergic afferents in *DCC*$^{-/-}$ and *Netrin1*$^{-/-}$ mice, we identified and applied new markers for mHb and lHb axons: Robo3 and Neurofilament medium polypeptide (Nefm), respectively (Fig. S4A). In E18.5 wild-type mice, TH-positive axons were restricted to the Nefm-postive sheath region and absent from the Robo3-positive core (Fig. 2B; Fig. S4A). In contrast, in *DCC*$^{-/-}$ and *Netrin1*$^{-/-}$ mice thick bundles of TH-positive axons traversed the entire width of the FR (Fig. 2B). The mutant FR consisted mainly of Nefm-positive axons, while only few Robo3-positive axons were detected. Instead an aberrant population of Robo3-positive mHb axons was detected at the dorsal roof of the habenula (Fig. S4B). These results together with the ability of Netrin1 to attract habenular axons *in vitro*, and DCC and *Netrin1* expression in the FR core and ventral midbrain, respectively (Funato et al., 2000), suggest that Netrin1 and DCC are required for the guidance of mHb axons to the midbrain. Interestingly, TH-positive axons in the FR in *DCC*$^{-/-}$ and *Netrin1*$^{-/-}$ mice were restricted to regions occupied by Nefm-positive lHb axons, resembling their close association in the sheath region of wild-type mice. Furthermore, the overall number of TH-positive axons reaching the lHb in mutant mice was comparable to control (not shown). Ablation of DCC in the habenula in *Tag1-Cre:DCC*$^{fl/fl}$ mice induced similar phenotypes, namely, intermingling of the TH and lHb axons throughout the width of the FR and a dorsal redirection of many Robo3-positive

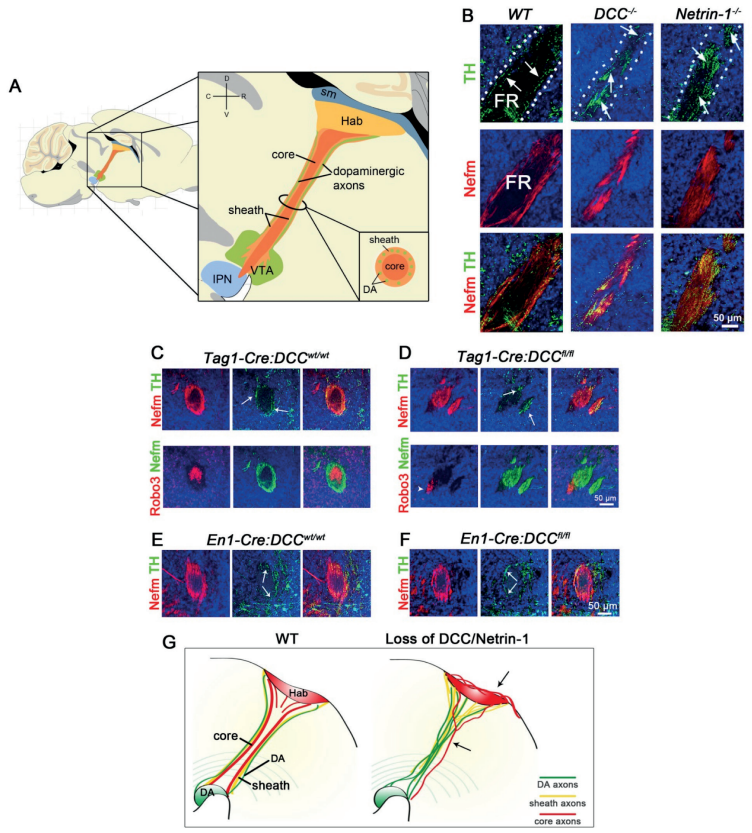

Figure 2

Abnormal Organization of the FR in *DCC* and *Netrin1* Knockout Mice.

(A) Schematic of a sagittal section of the mouse brain showing the segregated organization of habenular (Hab) and dopaminergic axons in the fasciculus retroflexus (FR). Axons from medial habenula (mHb) neurons run in the core of the FR, while lateral habenula (lHb) and dopaminergic (DA) axons are closely associated in the sheath of the FR. IPN, interpeduncular nucleus; sm, stria medullaris; VTA, ventral tegmental area. (B) Double-immunohistochemistry for tyrosine hydroxylase (TH) and neurofilament medium polypeptide (Nefm) on sagittal sections. In E18.5 *DCC* and *Netrin1* knockout mice, thick bundles of TH-positive axons and Nefm-positive habenular axons intermingle throughout the entire FR (arrows), contrasting their normal lateral distribution in the FR in wild-type (WT, arrows) mice. (C, D) Immunohistochemistry for Robo3, Nefm and TH on coronal sections of the FR of E18.5 *Tag1-Cre:DCC* conditional knockout mice. The organization of the FR is severly disrupted in *Tag1-Cre:DCC*$^{fl/fl}$ mice: TH-positive axons intermingle with lHb axons throughout the FR (arrow), while a small number of Robo3-positive mHb axons is situated outside of the sheath (arrowhead). (E, F) Immunohistochemistry for Nefm and TH on coronal sections of the FR of E18.5 *En1-Cre:DCC* conditional knockout mice. (G) Schematic representation of the disrupted organization of the FR following loss of Netrin1 or DCC. Misrouted core axons are observed at the dorsal roof of the habenula and closely associated lHb and dopaminergic axons occupy the entire FR (arrows). See also Figure S3 and S4.

mHb axons (Fig. 2C, D; Fig. S4C). In contrast, loss of DCC in dopaminergic axons in *En1-Cre:DCC*$^{fl/fl}$ mice did not affect the organization of the FR (Fig. 2E, F). Together, these data suggest that dopaminergic axons utilize lHb efferents to reach the lHb (Fig. 2G). This latter hypothesis is in line with our observation that during development habenular axons first extend to the ventral midbrain following which dopaminergic axons reciprocally project to the habenula along the developing FR (Fig. S5).

To evaluate a model in which dopaminergic axons use lHb efferents to reach the lHb and to study whether such dependency would be uni- or bidirectional, we performed *in vivo* genetic ablation studies. DTA mice, which conditionally express subunit A of the diphtheria toxin, were crossed with *Tag1-Cre* mice to ablate the habenula. *Tag1-Cre:DTA* embryos displayed a loss of the habenula and the FR, whereas dopaminergic neurons in the VTA were unaffected (Fig. S6A-E). No dopaminergic projections extended to the habenula in *Tag1-Cre:DTA* mice, while other dopaminergic pathways in the brain were intact (Fig. 3A, S6C). Thus, dopaminergic axons require the habenula and/or the FR for guidance towards the lHb. To assess whether, the converse, lHb axons depending on dopaminergic neurons or axons for guidance to the midbrain, is true, the region of the midbrain containing dopaminergic neurons was ablated by crossing *En1-cre* and *DTA* mice. Although *En1-cre:DTA* embryos showed complete loss of midbrain dopaminergic neurons and their axons, the projection and organization of mHb and lHb neurons and axons was intact (Fig. 3B, S6F, G).

Together these data reveal that dopaminergic axons are dependent on either long-distance instructive cues from the habenula, or short-range cues on lHb axons in the sheath, for long-distance guidance to the lHb. To investigate these two possibilities, we placed a blocking membrane at the ventral border of the habenula in E12.5 mouse brain hemisections and cultured them for three days. The membrane contains pores that allow the diffusion of secreted molecules but block the growth of axons (López-Bendito et al., 2006). In cultures without membrane insertion, a clear FR had formed with both mHb and lHb axons extending into the midbrain, as visualized by Robo3 and Nefm immunohistochemistry in combination with TH staining (Fig. 3C). In contrast, insertion of blocking membranes prevented the extension of the FR to the midbrain (Fig. 3D, E). In addition, the number of dopaminergic axons growing to the habenula was dramatically reduced (Bin 1, 26.4% ± 6.3% of control; Bin 2, 44.4% ± 9.3% for control and 5.3% ± 1.4% for blocked, n = 7 and n = 10 slices for control and blocked; $P < 0.001$; Fig. 3C-F), and no dopaminergic axons were detected directly at the habenula (Bin 3, 39.1% ± 2.8% for control and 1.9% ± 0.4% for blocked; $P < 0.001$; Fig. 3C-F). Thus, our expression, genetic and cell culture data show that dopaminergic axons depend on short-range cues on lHb axons for guidance towards the lHb (Fig. 3G). This suggests that the lHb sends out efferent projections to collect and guide its own afferent projections.

4. Subdomain-specific Axon Guidance and Cell Adhesion Molecule Expression in the FR

Although our data show that dopaminergic projections rely on lHb axons for guidance towards the habenula, how this interaction is mediated at the molecular level is not known. To identify the underlying molecular mechanism, laser capture microdissection experiments were performed on the embryonic FR in combination with mass spectrometry analysis to identify subdomain-specific proteins in the FR at the time of dopaminergic axon pathfinding (Fig. 4A). Since axon guidance proteins and adhesion molecules are likely candidates for mediating axon-axon interactions, these proteins were selected from the mass spectrometry data and subjected to immunohistochemical analysis (Table S2 and Fig. 4B-D). Immunohistochemistry on transverse sections of the FR showed that these selected proteins can be grouped on basis of their subdomain localization within the FR. Candidates were either localized to the entire FR (Fig. 4B), the core (Fig. 4C) or the sheath domain (Fig. 4D). These results reveal subdomain-specific expression of various axon guidance and cell adhesion molecules in the developing FR, uncovering a molecular code that could underlie various aspects of FR organization, including the segregation of different axonal populations and their guidance towards specific subdomains.

5. Axon-derived LAMP Guides Dopaminergic Axons to the lHb

Two FR proteins identified by mass spectrometry (Table S2) displayed sheath-specific expression; close homologue of L1 (CHL1) and limbic-system associated protein (LAMP) (Fig. 4D). Given their selective expression and reported role in cell adhesion and neurite outgrowth (Hillenbrand et al., 1999; Zhukareva and Levitt, 1995), we next assessed whether CHL1 or LAMP mediated interactions between lHb and dopaminergic axons. CHL1 is a type I transmembrane protein, while LAMP is tethered to the membrane via a glycosylphosphatidylinositol (GPI) anchor. We exploited these differences in membrane presentation by using the enzyme phosphatidylinositol-specific phospholipase C (PI-PLC) in combination with hemisection cultures. PI-PLC will remove GPI-linked proteins, such as LAMP, but leaves transmembrane proteins, such as CHL1, intact (Fig. 5A). Treatment with PI-PLC did not affect the initial growth of TH-positive axons towards the habenula, indicating that this enzymatic treatment does not have a deleterious effect on axon growth (Bin 1, 102.9% ± 16.23% of control, n = 11 for both control and PI-PLC; $P = 0.896$; Fig. 5B, C). Despite this initial growth towards the habenula, dopaminergic axons did not reach this

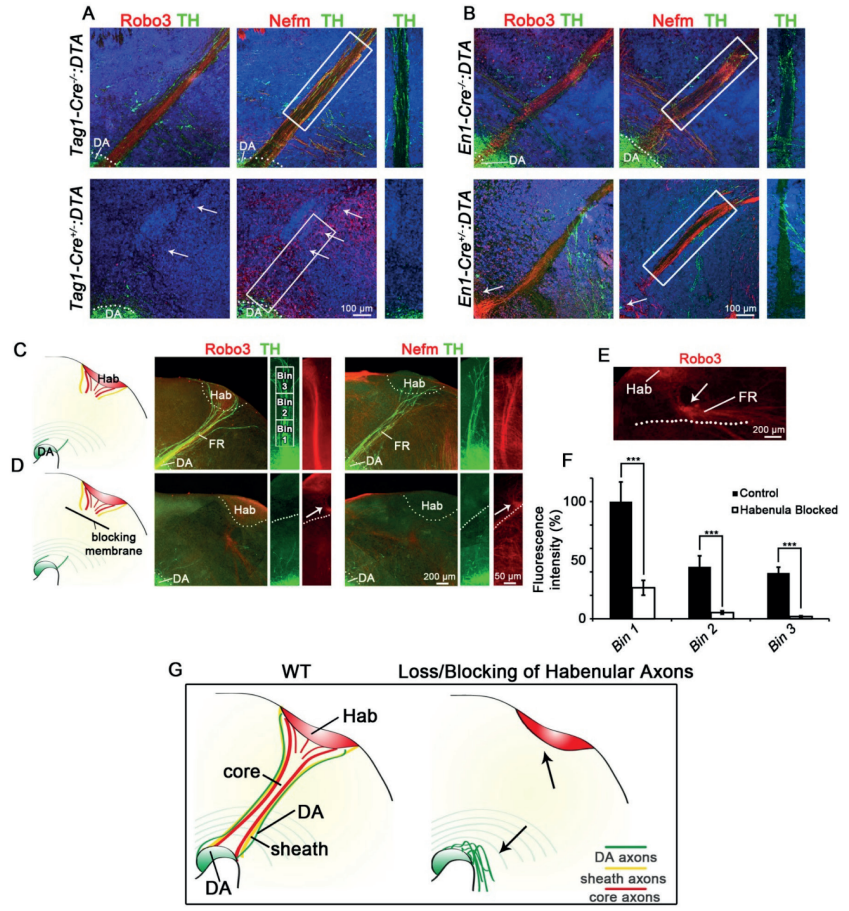

Figure 3

Lateral Habenula Axons Serve as a Scaffold for Dopaminergic Afferents Targeting this Subnucleus.

(A, B) Immunohistochemistry for neurofilament medium polypeptide (Nefm), Robo3 and/or tyrosine hydroxylase (TH) on sagittal sections of E18.5 *Tag1-Cre:DTA* and *En1-Cre:DTA* mice. The fasciculus retroflexus (FR) is absent in *Tag1-Cre*$^{+/-}$*:DTA* mice (A, white arrows) and TH-positive dopaminergic (DA) axons fail to project to the habenula (A). In *En1-Cre*$^{+/-}$*:DTA* mice midbrain DA neurons are absent (white arrows), but the FR is intact (B). Boxed areas are shown at a higher magnification at the right. (C-E) E12.5 organotypic slices were cultured for 3 days *in vitro* (DIV) and subjected to immunohistochemistry for Robo3, TH and Nefm. Insertion of blocking membranes (dotted lines) redirects habenular axons (white arrows, magnification in E) and prevents growth of DA axons towards the habenula (D). Squares in C show bins used for quantification shown in F. (F) Growth of DA axons was quantified using the bins shown in C. All bins were normalized to Bin 1 of the control condition. *** $P < 0.001$. Error bars indicate S.E.M.. (G) Schematic representation of the effect of Hab and FR ablation or of insertion of blocking membranes on dopaminergic axon growth towards the Hab. See also Figure S5 and S6.

brain region following PI-PLC treatment but, rather, stalled or detached from the FR halfway along their normal trajectory (Bin 2, 82.8% ± 12.2% for control and 45% ± 7.8% for PI-PLC; $P < 0.05$; Bin 3, 63.1% ± 7.4% for control and 15% ± 2.3% for PI-PLC; $P < 0.001$; Fig. 5B, C). PI-PLC treatment did not alter the growth of habenular axons in the FR, as visualized by Nefm immunohistochemistry (Fig. 5B).

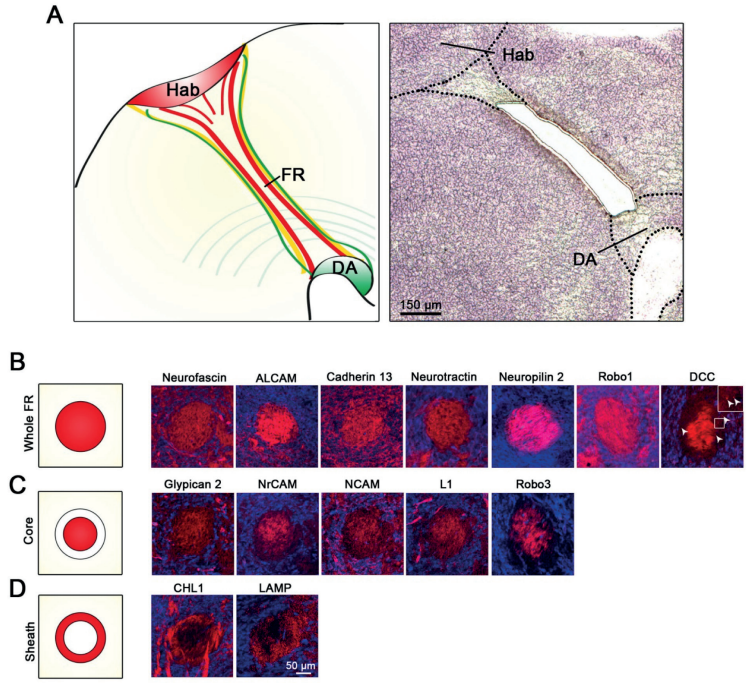

Figure 4

Laser Capture Microdissection of the Fasiculus Retroflexus Reveals Subdomain-Specific Expression of Axon Guidance and Cell Adhesion Molecules.

(A) Laser capture microdissection was performed on the fasciculus retroflexus (FR) in E16.5 sagittal mouse brain sections. Hab, habenula; DA, dopamine neuron pool. (B-D) Immunohistochemistry on coronal sections of the FR using antibodies against different axon guidance and cell adhesion molecules. Proteins identified by mass spectrometry on FR samples display three modes of expression: throughout the FR (B), restricted to the core region of the FR (C), or specific to the sheath (D). Inset in B shows a magnification of the indicated boxed area. DCC-positive axons (white arrowheads) are located in the sheath of the FR. See also Table S2.

To confirm that the impaired growth of TH-positive axons towards the habenula following PI-PLC application resulted from the cleavage of LAMP, LAMP function blocking antibodies were applied to the hemisection cultures (Fig. 5D). In line with the effect of PI-PLC treatment (Fig. 5A-C), TH-positive axon growth

towards the habenula was reduced, with many axons running off the FR in the presence of anti-LAMP antibodies (Bin 1, 70.4% ± 4.3% of control, n = 15 and n = 17 for control and anti-LAMP; $P < 0.001$; Bin 2, 61.9% ± 4.9% for control and 35.1% ± 4.3% for anti-LAMP; $P < 0.001$; Bin 3, 48.3% ± 3.32% for control and 23.3% ± 3% for anti-LAMP; $P < 0.001$; Fig. 5E, F). Application of PI-PLC induced a greater reduction of TH-positive axons as compared to anti-LAMP antibody application. This could reflect an inability of the antibody to block all LAMP, perhaps due to limited tissue penetration, or a role for additional GPI-linked proteins in the development of dopaminergic projections to the lHb. Anti-LAMP antibody treatment did not alter the growth of habenular axons in the FR (Fig. 5E).

LAMP is a member of the IgLON family, which includes proteins that promote or inhibit cell adhesion and axon growth of specific neuronal populations (Gil et al., 2002; Keller et al., 1989; Zhukareva and Levitt, 1995). Therefore, we hypothesized that LAMP on lHb axons serves as an adhesive and growth promoting substrate for dopaminergic axons. To test this idea, dopaminergic explant cultures were grown on coverslips coated with control or LAMP substrate. In line with the PI-PLC and antibody blocking experiments, TH-positive axon growth was increased on LAMP as compared to control protein (116.1% ± 3.24% of control, n = 310 and n = 320 for control and LAMP; $P < 0.001$; Fig 7A, B). To examine whether LAMP is not only a growth-promoting but also instructive cue for dopaminergic axons, we cultured VTA explants on alternating stripes of control and LAMP protein or on control stripes only. Control stripes had no effect on dopaminergic axons extending from the explants. In contrast, dopaminergic axons displayed a clear preference for LAMP stripes when provided with a choice between control and LAMP substrate (157% ± 18.8% of control, n = 52 for LAMP and control; $P < 0.05$; Fig. 6C, D). Together, these experiments show that LAMP serves as a growth-promoting and instructive cue for dopaminergic VTA axons.

To confirm the specificity of the antibody experiments and to establish that LAMP expressed by lHb axons, rather than other structures in the vicinity of the FR, guides dopaminergic axons, we directed siRNAs to the habenula during early stages of dopaminergic pathfinding using *ex vivo* electroporation. siRNAs were introduced at E12.5 or E13.5 followed by immunohistochemical assessment of the trajectories of habenular and dopaminergic axons three days later. Electroporation with scrambled control siRNAs did not visibly alter the growth or trajectory of habenular or dopaminergic axons. In contrast, LAMP knockdown induced a significant decrease in the outgrowth of TH-positive axons towards the habenula, causing a marked reduction in the dopaminergic innervation of this nucleus (Bin 3, 82.6% ± 7.5% for control (n = 13) and 52% ± 8.5% (n = 8) for si-LAMP; $P < 0.05$; Fig 6G-I, S7A, B). Furthermore, similar to our observations following PI-PLC treatment and antibody application, many TH-positive axons detached from the FR halfway along their trajectory towards

the habenula (Fig. 6H). LAMP knockdown did not visibly alter the growth of habenular axons in the FR, as visualized by Nefm immunohistochemistry (Fig. 6G, H).

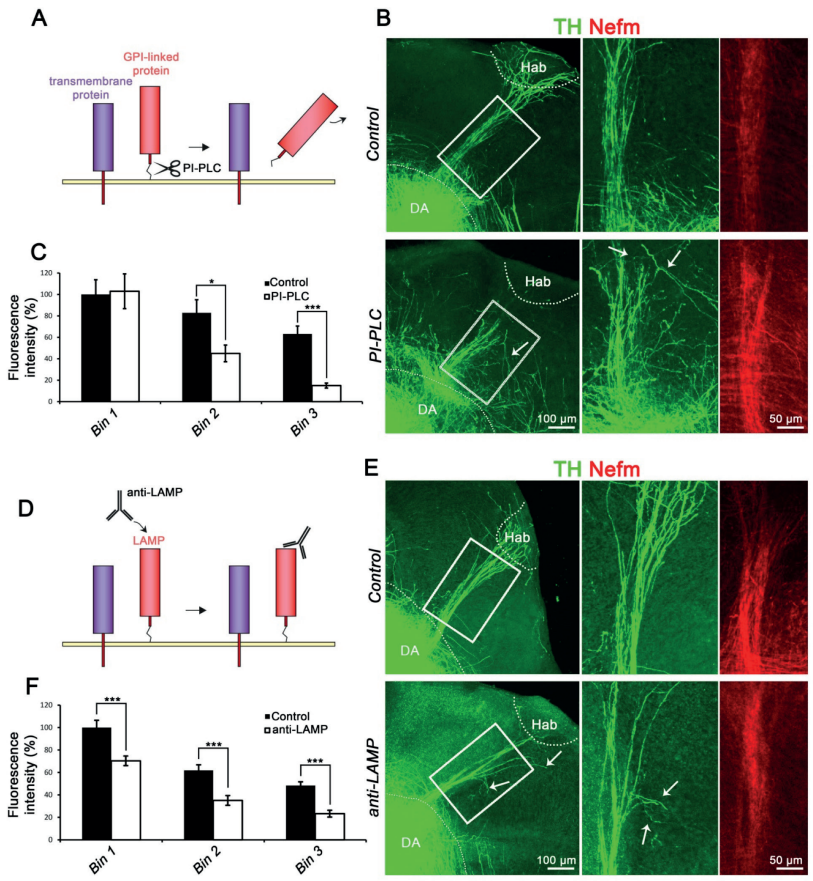

Figure 5

The GPI-linked Cell Adhesion Molecule LAMP Mediates Guidance of Dopaminergic Axons to the Habenula.

(A, D) Schematics showing the PI-PLC or function blocking antibody treatments to specifically remove glycophosphatidylinositol (GPI)-anchored molecules (A) or block limbic system associated protein (LAMP) (D). (B, E) Immunohistochemistry for tyrosine hydroxylase (TH) and neurofilament medium polypeptide (Nefm) on E12.5 organotypic slice cultures treated with PI-PLC or anti-LAMP antibodies and cultured for 3 days *in vitro*. Boxed areas are shown at higher magnification in two right panels. White arrows indicate stalled or detached axons. DA, dopaminergic; Hab, habenula. (C, F) Quantification of PI-PLC or antibody treated cultures using bins as shown in Fig. 3C. * $P < 0.05$, *** $P < 0.001$. Error bars indicate S.E.M..

To show that LAMP not only guides dopaminergic afferents to the lHb but also has an instructive role in the targeting dopaminergic axons specifcally towards the lHb, we ectopically expressed LAMP in the mHb or in a region adjacent to the lHb and FR using *ex vivo* electroporation. Co-electroporation of LAMP and GFP expression vectors confirmed the presence of LAMP protein in electroporated neurons and axons (Fig. S7C). LAMP or control expression vectors were electroporated at E13.5 and dopaminergic innervation of the FR and habenula was assessed three days later using immunohistochemistry. As expected, in experiments targeting the habenula many GFP-positive neurons were present in the mHb and extended axons into the core of the FR. Interestingly, TH-positive axons from the sheath region often crossed over to nearby GFP/LAMP-positive axons in the core but never to axons expressing GFP only (Fig. 7A). This effect was also reflected at the level of the mHb. Robo3 was used to identify the mHb, which was devoid of dopaminergic axons after electroporation of GFP (Fig. 7B). In contrast, overexpression of GFP and LAMP induced aberrant dopaminergic innervation of the mHb (321,4% ± 70,8% of control, n = 11 for and n = 14 for control and LAMP, respectively; $P < 0.05$; Fig. 7B, C). Although only a small subset of mHb neurons was targeted by the *ex vivo* electroporation procedure, several dopaminergic axons were found to abnormally innervate the mHb along GFP-positive axons and continue along the cell bodies and processes of LAMP-expressing neurons in the mHb (Fig. 7B). Ectopic expression of LAMP adjacent to the lHb or the FR had no effect on the trajectory of TH-positive or habenular axons. TH-positive axons followed the FR into the lHb but did not extend into adjacent regions of ectopic LAMP expression (n = 4; Fig. 7D). Thus, LAMP functions on lHb axons to direct dopaminergic axons to the lHb. Finally, to examine whether LAMP is required *in vivo* for the innervation of the lHb by dopaminergic afferents, *LAMP*$^{-/-}$ embryos were analyzed (Innos et al., 2011). In line with the antibody blocking and siRNA-induced knockdown experiments (Fig. 5D-E, 6G-I), genetic ablation of *LAMP* caused a marked reduction in the dopaminergic innervation of the lHb at E18.5 (Fig. 7E, F, n = 4 WT and *LAMP*$^{-/-}$). Furthermore, many TH-positive axons detached from the FR in *LAMP*$^{-/-}$ embryos and invaded the region immediately surrounding this bundle, resembling the detachment of dopaminergic axons observed following manipulation of LAMP *ex vivo* (Fig. 7E, G). The ability of a subset of dopaminergic axons to innervate the lHb in the absence of LAMP may reflect compensation by other proteins. No defects in the trajectories of habenular efferents were observed in *LAMP*$^{-/-}$ embryos (Fig. 7G). Together these results show that LAMP expressed on lHb axons in the sheath of the FR serves as a molecular scaffold for dopaminergic axons, guiding these axons to a specific subdomain of the habenula, the lHb (Fig. 7H, I). These data indicate that pre-target reciprocal axon-axon signaling can contribute to subdomain-specific axon targeting and provide insight into the function of the poorly characterized IgCAM LAMP.

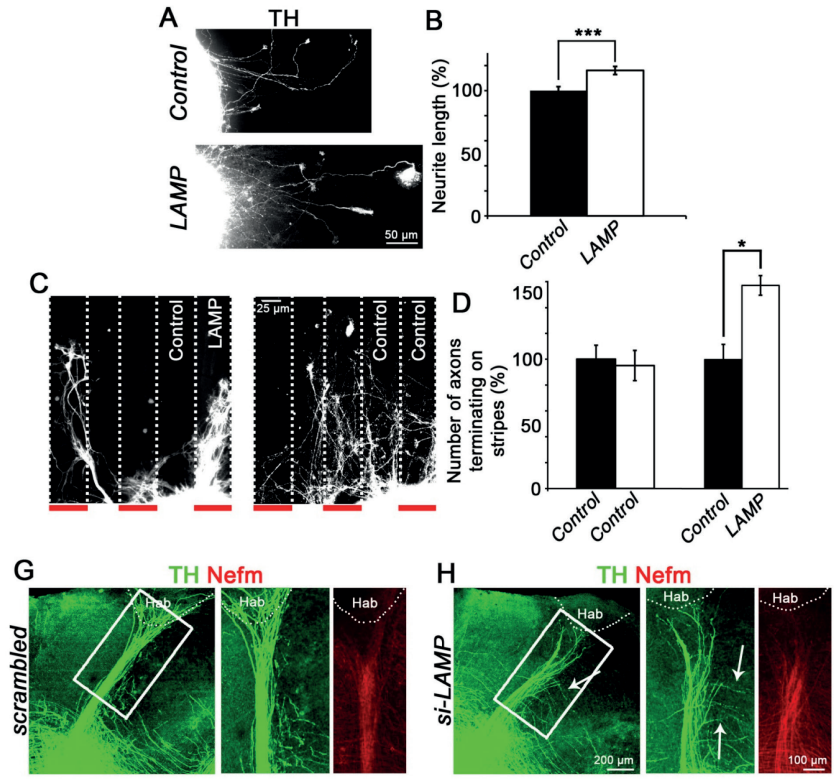

Figure 6

LAMP Mediates Growth of Dopaminergic Afferents Towards the Habenula.

(A, B) Explants of the E14.5 ventral tegmental area (VTA) were grown on control or limbic system-associated protein (LAMP) substrate and subjected to immunocytochemistry for tyrosine hydroxylase (TH) (A). The length of TH-positive axons is increased on LAMP as compared to control substrate (B). *** $P < 0.001$. Error bars denote S.E.M.. (C, D) Explants of the E14.5 VTA were grown on alternating control and LAMP stripes or on control stripes only, and subjected to immunohistochemistry for TH (C). Axons show a preference for growth on LAMP stripes over control stripes (D). * $P < 0.05$. Error bars denote S.E.M.. (G, H) Immunohistochemistry for TH and neurofilament medium polypeptide (Nefm) following electroporation of the habenula with scrambled (G) or *LAMP* (H) siRNAs. White arrows indicate detached axons. (I) Quantification of fluorescence intensty using bins as shown in Fig. 3C. * $P < 0.05$. Error bars denote S.E.M.. See also Figure S7.

Discussion

Numerous brain nuclei are distinguishable in the vertebrate nervous system and often these structures are further subdivided on a functional basis into smaller subdomains. Although clustering of neurons into (sub)nuclei facilitates the generation of highly specific patterns of synaptic connectivity, how brain nuclei are formed and innervated remains poorly understood. Here we show that reciprocal axon-axon interactions cooperate with subnucleus-restricted chemoattractive mechanisms to coordinate the dopaminergic innervation of the lateral subnucleus of the habenula (lHb). We demonstrate that the lHb determines its own pattern of afferent innervation by sending out LAMP-positive efferent projections that reciprocally guide dopaminergic afferents to the lHb. At the lHb, the secreted attractant Netrin1 is required for the entry of dopaminergic afferents into this subnucleus (Fig. 8). Together, our findings identify pre-target axon-axon signaling mediated by axonal cues derived from the target as a novel mechanism to wire reciprocally connected brain regions in a subdomain-specific manner.

Reciprocal Axon-Axon Signaling Guides Dopaminergic Afferents

Although the guidance of axons by chemotropic cues in their environment has been well established (Pasterkamp and Kolodkin, 2013), less is known about the role of axon-derived cues. It is clear, however, that axon-axon interactions are used to establish complex neural circuits (Grueber and Sagasti, 2010; Imai and Sakano, 2011; Luo and Flanagan, 2007; Tessier-Lavigne and Goodman, 1996; Wang and Marquardt, 2013). Our knowledge of these interactions mainly derives from studies on interactions between different sub-groups of axons within afferent bundles. For example, Eph-ephrin signaling between sensory and motor axons in the periphery mediates their segregation and guidance, while axon-derived semaphorins and their receptors mediate pre-target sorting of olfactory sensory axons (Gallarda et al., 2008; Imai et al., 2009; Joo et al., 2013; Lattemann et al., 2007; Wang et al., 2011). How interactions between reciprocally projecting axon types are controlled or contribute to circuit assembly is poorly understood.

The habenula is an excellent system for studying axon-axon signaling. Neurons in the lHb and mHb give rise to well-characterized, anatomically segregated efferent projections in a large axon bundle, the FR. In addition, during early development many habenular afferents make a binary choice between the lHb and mHb, providing a sensitive assay for studies on axon target selection and innervation. Finally, the habenular system not only contains efferent and afferent axon types that run alongside, but it also harbors reciprocal connections (Fig. 2A) (Bianco and Wilson, 2009). Here, we exploited these characteristics to reveal a requirement for reciprocal axon-axon signaling in the development

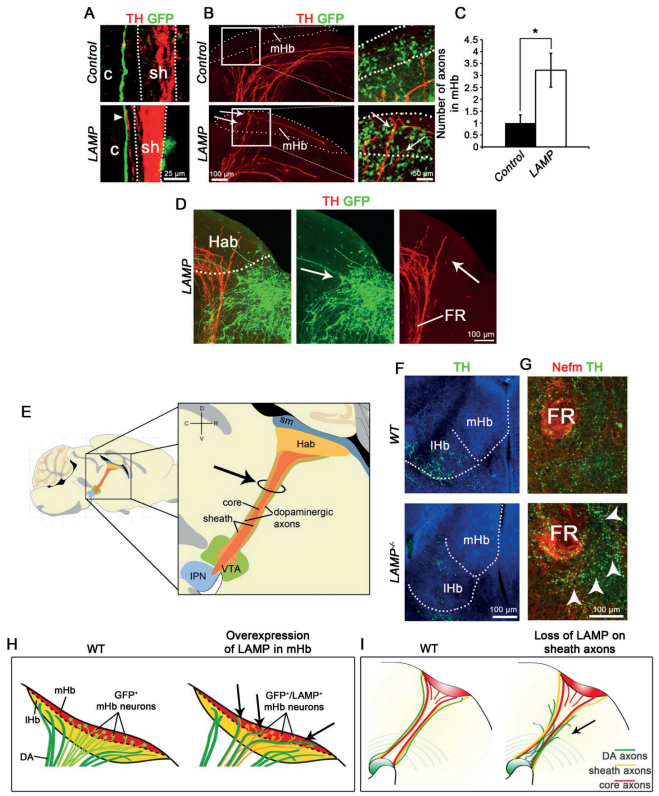

Figure 7

LAMP is Required on lHb Axons to Establish Subdomain-Restricted Innervation of the Habenula by Dopaminergic Afferents

(A, B) Immunohistochemistry for tyrosine hydroxylase (TH) and GFP on slice cultures 3 days after electroporation. Dotted lines in A indicate sheath region and arrowhead points to a TH-positive axon crossing over from the sheath region to a GFP/limbic system-associated membrane (LAMP)-positive core axon. c, core; sh, sheath. Dotted line in B indicates the medial habenula (mHb) as determined by immunohistochemistry for Robo3. Boxed area is shown at higher magnification at the right. Arrows indicate TH-positive axons extending along GFP/LAMP-expressing cell bodies and processes in the mHb. (C) Quantification of the number of dopaminergic axons innervating the mHb. * $P < 0.05$. Error bars denote S.E.M.. (D) Immunohistochemistry for TH and GFP on slice cultures 3 days after electroporation. Dotted line in D indicates the habenula (Hab). Ectopic expression of LAMP adjacent to the habenula does not induce misrouting of TH-positive axons. FR, fasciculus retroflexus. (E) Schematic of a sagittal section of the mouse brain showing the segregated organization of habenular (Hab) and dopaminergic axons in the FR. Black arrow indicates the position of the coronal section in G. IPN, interpeduncular nucleus; sm, stria medullaris; VTA, ventral tegmental area. (F, G) Immunohistochemistry for TH and neurofilament medium polypeptide (Nefm) on coronal sections of the habenula and FR of E18.5 wild-type (WT) or LAMP$^{-/-}$ mice. Loss of LAMP results in a reduction of dopaminergic innervation of the lHb (F). In addition, rather than extending in the FR sheath, many TH-positive axons traverse the region surrounding the FR in LAMP$^{-/-}$ mice (G, arrowheads). (H, I) Schematics summarizing the effects of ectopic LAMP expression in the mHb and LAMP knockdown or knockout on dopaminergic axon guidance towards the habenula and on subdomain targeting in the habenula. See also Figure S7.

of subdomain-specific dopaminergic connections. Remarkably, our data show that the lHb determines its own pattern of afferent innervation by sending out molecularly labeled efferents in a larger axon bundle that collect, sort and guide afferents and specifically deliver them to the lHb, a phenomenon we term subdomain-mediated axon-axon signaling (Fig. 8). Multiple lines of evidence support this model. First, expression data localize dopaminergic axons in the FR sheath intermingled with reciprocally projecting lHb axons. Second, dopaminergic axon targeting of the lHb is largely intact in *Tag1-Cre:DCC$^{fl/fl}$* mice in which the FR is almost exclusively composed of lHb axons. Third, blockage of habenular axon growth *in vitro* and genetic ablation of the habenula and the FR *in vivo* prevents dopaminergic innervation of the lHb. Fourth, neutralization, knockdown or knockout of the lHb-specific cue LAMP prevents dopaminergic innervation of the lHb. Finally, ectopic LAMP expression in mHb neurons and their axons erroneously redirects dopaminergic afferents to the mHb.

One of the best-studied examples of reciprocal axon-axon interactions is the interdependency of thalamocortical and corticothalamic axons (Molnár et al., 2012). During development, thalamocortical axons traverse the subpallium and are then used by corticothalamic afferents for reciprocal guidance through this intermediate target (Deck et al., 2013). However, whether these reciprocal axon-axon interactions also contribute to the subdomain-specific innervation of the cortex or thalamus and which axonal cues mediate these interactions is unknown. Our data show that reciprocal axon-axon interactions not only provide a scaffold for guidance, but also function to direct afferent projections to specific subdomains within the target. Further, our study provides an example of a protein that can mediate such reciprocal axon-axon interactions, LAMP. LAMP is an instructive cue for dopaminergic axons and is expressed in dopaminergic neurons that project afferents to the habenula (Gruber et al., 2007) (Fig. 7A-D, S7D). This, together with the fact that the adhesive effects of LAMP are attributed to homophilic interactions (Zhukareva and Levitt, 1995) supports a model in which homophilic LAMP interactions guide dopaminergic axons (Fig. 8). Notably, LAMP is also expressed in reciprocally connected parts of the thalamus and cortex and *in vitro* it regulates the growth and guidance of the axonal projections connecting these structures (Mann et al., 1998). Further studies are needed to determine whether LAMP mediates interactions between thalamocortical and corticothalamic axons, or other reciprocal connections in the brain, analogous to its role in the habenular system.

Axon-Axon Signaling Regulates Subdomain-Specific Axon Targeting

The ordered distribution of different axon types in large axon tracts is a pervasive anatomical feature of neural circuits and underlies the generation of precise synaptic connections (Wang and Marquardt, 2013). Efferent projections

from the mHb and lHb are segregated in the core and sheath regions of the FR, respectively. Although the molecular basis of this segregation is unknown, our findings show that lHb axon-derived LAMP localizes dopaminergic afferents to the FR sheath. In addition, misexpression of LAMP in the mHb and core axons aberrantly redirects dopaminergic afferents to the mHb revealing that LAMP-positive lHb axons not only guide dopaminergic afferents but also dictate their subdomain targeting. Our current understanding of the molecular basis of subdomain-specific axon targeting mainly derives from studies on laminar structures such as the hippocampus and the visual system. This work shows that target-derived guidance cues first direct axons toward or away from specific

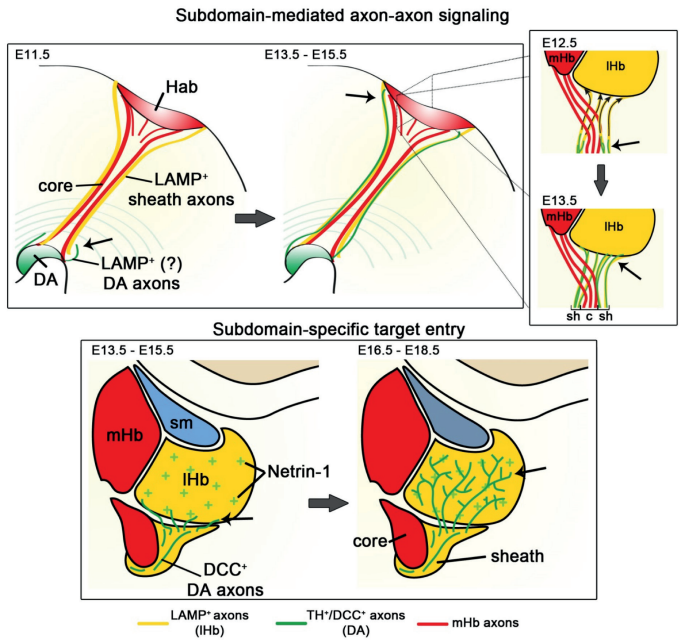

Figure 8

Subdomain-Specific Innervation of the Habenula Requires Cooperation Between Reciprocal Axon-Axon Signaling and Subnucleus-Restricted Chemoattraction.

In our model, the lateral subnucleus of the habenula (lHb) sends out efferent projections that selectively express the cell adhesion molecule limbic system-associated membrane protein (LAMP) to reciprocally guide afferent dopaminergic (DA) axons over a long distance and deliver these axons specifically to the border of the lHb, a process we refer to as subdomain-mediated axon-axon signaling. Upon arrival at the lHb, subdomain-restricted expression of the secreted attractant Netrin1 is required for the entry of DCC-expressing dopaminergic afferents into this subnucleus. These findings reveal the first subnucleus-specific axonal targeting mechanisms and highlight novel axonal wiring principles that are likely to also apply to subdomain-specific wiring events in other reciprocally connected neural systems. See text for more details. c, core; Hab, habenula; mHb, medial habenula; lHb, lateral habenula; sh, sheath; sm, stria medullaris.

laminae followed by the combinatorial expression of cell adhesion molecules, which facilitates the formation of (sub)lamina-specific synaptic contacts (Baier, 2013; Huberman et al., 2010; Robles and Baier, 2012; Sanes and Yamagata, 2009; Williams et al., 2010). Our data show that subdomain-mediated axon-axon signaling provides an additional strategy to regulate subdomain-specific circuit assembly that relies on axon-axon interactions rather than on cues expressed in the target. Previous studies have implicated axon-axon signaling in different aspects of target selection, innervation and mapping (Imai et al., 2009; Lattemann et al., 2007; Mizumoto and Shen, 2013; Schwabe et al., 2013; Sweeney et al., 2007; Takeuchi et al., 2010). Our findings are, however, conceptually distinct from these previous reports: we find that molecular interactions between reciprocal efferent and afferent axons target dopaminergic afferents to the lHb, rather than signaling between afferent projections heading for the same target. Thus, while previous work has shown pretarget axon-axon signaling independent from the target, our work now identifies a role for axonally expressed cues generated by neurons in the target in the subdomain-specific guidance of afferent axons.

Netrin1 is a Subdomain-Specific Cue Regulating Subnuclear Axon Target Entry

Although one might predict that dopaminergic axons would simply follow LAMP-positive axons into the lHb to meet their synaptic targets, our data identify a requirement for Netrin1 in the entry of dopaminergic afferents into this subnucleus (Fig. 8). In the absence of Netrin1, or its receptor DCC, dopaminergic axons accumulate at their normal entry site of the lHb. Our data show that Netrin1 secreted by the lHb serves as an attractant for DCC-expressing dopaminergic axons *en route* to the lHb. Analysis of conditional and full *DCC* and *Netrin1* mutant mice suggests that *in vivo* Netrin1 most likely functions as a short-range attractant, since axons arrive at the lHb in the absence of Netrin1-DCC signaling but accumulate at its ventral border. This idea is in line with recent work on short-range attractive effects of Netrin-B during the lamina-specific targeting of R8 retinal axons in the medulla of the *Drosophila* optic lobe. Here, Netrin-B is released in the R8 axon-recipient layer M3 of the retina by afferent axonal projections and subsequently captured by neuron-associated Frazzled, the fly homologue of DCC. This results in a short-range Netrin-B signal that attracts ingrowing R8 axons into layer M3 (Timofeev et al., 2012). Our data extend these findings by showing that Netrin1 mediates the entry of dopaminergic afferents into a specific subnucleus in vertebrate species. This indicates that Netrins play conserved roles in the subdomain-specific innervation of both laminated structures and brain nuclei and identifies a novel role for these cues distinct from previously reported functions in for example axon guidance, topographic sorting and synaptogenesis ((Bielle et al., 2011;

Goldman et al., 2013; Lai Wing Sun et al., 2011; Manitt et al., 2011; Poon et al., 2008; Powell et al., 2008) and references therein).

Our work further shows that at least two distinct mechanisms are needed to control the dopaminergic innervaton of the lHb. A possible explanation for this cooperation between axon-axon signaling and chemoattraction is that lHb axons act to deliver dopaminergic axons specifically at the lHb following which Netrin1 uncouples these axons. This would allow other (non-)axonal molecular signals within the lHb to guide dopaminergic axons to their partner neurons. Further studies will be needed to dissect the mechanistic details of Netrin1-mediated axon target entry.

Despite its important physiological functions and its implication in disorders such as major depressive disorder (MDD) (Hikosaka, 2010), the mechanisms underlying habenular circuit development in mammals remain largely unknown (Chen et al., 2000; Funato et al., 2000; Giger et al., 2000; Kantor et al., 2004). Our study reveals mechanisms that enable the generation of highly specific patterns of afferent innervation of the habenula. These principles may not only apply to dopaminergic axons but also to the many other afferent projections targeting the habenula (Bianco and Wilson, 2009). Together, our work provides tools and a conceptual framework for the further dissection of habenular circuit assembly. More generally, our findings unveil an unexpected cooperation between subdomain-mediated axon-axon signaling and subnucleus-restricted chemoattraction in subdomain-specific axon targeting. Analogous combinatorial targeting strategies could be widely used because many brain nuclei and layered structures in the nervous system display subdomain-specific patterns of guidance cue expression and are interconnected with their afferent target regions though reciprocal axon projections.

Matherials and methods

Mouse lines.

Animal use and care was in accordance with local institutional guidelines. Generation of transgenic mice and all other mouse lines used in this study are described in the Supplemental Experimental Procedures.

Immunohistochemistry and *in situ* hybridization.

Nonradioactive *in situ* hybridization and immunohistochemistry were performed as described previously (Kolk et al., 2009; Pasterkamp et al., 2007). Average fluorescence intensity was measured using the histogram function in Adobe Photoshop. Background was determined in areas without staining and subtracted from images after which mean signal intensity was determined. See Supplemental Experimental Procedures for more details on reagents and protocols.

Laser capture microdissection.

Laser capture microdissection was performed using a PALM laser microscope system (Zeiss). Samples were subjected to SDS-PAGE and were sent for mass spectrometry analysis. See Supplemental Experimental Procedures for a more detailed description.

Explant and organotypic slice cultures.

Three dimensional collagen matrix assays were performed as described previously (Schmidt et al., 2012). See Supplemental Experimental Procedures for a detailed description of the antibody prepration, coating and quantification. For organotypic slice cultures, E12.5 mouse brains were dissected to produce two sagittal hemisections. Following three days in culture, hemisections were fixed in 4% PFA and stained using appropriate antibodies. See Supplemental Experimental Procedures for more detailed description of the culture conditions, immunohistochemistry and quantification.

Ex vivo electroporation.

To test siRNA knockdown efficiency, HEK 293 cells were plated onto poly-D-lysine coated coverslips. siRNAs (ON-TARGET plus SMARTpool; Dharmacon) were transfected using Lipofectamine 2000 (Invitrogen) according to manufacturer's protocol. For electroporation, mouse embryos were collected at E12.5 or E13.5 and the third ventricle was injected with siRNA (25 µM) and DNA (1 µg/µl). After electroporation hemisections were cultured as described above for the organotypic slice cultures. See Supplemental Experimental Procedures for more details.

Quantification and statistics methods.
Statistical analyses were performed using IBM SPSS Statistics by Student's t-test or chi-square test (for hemisection-aggregate assays). All experiments were repeated at least 3 times. All data were expressed as means ± S.E.M. and significance was defined as $P < 0.05$.

Acknowledgements

We thank members of the Pasterkamp laboratory for assistance and discussions and Alex Kolodkin and Gulermina Lopez-Bendito for reading the manuscript. We thank Marc Tessier-Lavigne, Anton Berns, Cecilia Flores, Wolfgang Wurst, Alain Chedotal, Meng Li and Marten Smidt for providing mouse lines. We would like to thank Nicoletta Kessaris for advice on BAC technology and Seiji Miyata and Helen Cooper for sharing reagents. We thank Jerre van Veluw for technical assistance on the laser capture microdissection. Anti-Tag1 and anti-LAMP anitbodies were obtained from the Developmental Studies Hybridoma Bank. This study is supported by grants from the Netherlands Organization for Scientific Research (TopTalent; to E.R.E.S.), Stichting Parkinson Fonds, the Netherlands Organization for Health Research and Development (VIDI, ZonMW-TOP), the European Union (mdDANeurodev, FP7/2007-2011, Grant 222999), and the People Programme (Marie Curie Actions) of the European Union's Seventh Framework Programme FP7/2007-2013/ under REA grant agreement n° [289581] (NPlast) (to R.J.P.). This study was partly performed within the framework of Dutch Top Institute Pharma Project T5-207 (to R.J.P.). This work was partly supported by project grants (631466 and1043045) from the National Health and Medical Research Council, Australia (NHMRC). LJR was supported by an NHMRC Principal Research fellowship, A-L S.D was supported by an Australian Post-graduate Award scholarship and a top-up scholarship from the Queensland Brain Institute, and E.V. by an Institutional investigation grant (IUT20-41) from the Estonian Research Council.

References

Aizawa, H., Kobayashi, M., Tanaka, S., Fukai, T., and Okamoto, H. (2012). Molecular characterization of the subnuclei in rat habenula. J. Comp. Neurol. *520*, 4051–4066.

Bagnard, D., Lohrum, M., Uziel, D., Püschel, A.W., and Bolz, J. (1998). Semaphorins act as attractive and repulsive guidance signals during the development of cortical projections. Development *125*, 5043–5053.

Baier, H. (2013). Synaptic laminae in the visual system: molecular mechanisms forming layers of perception. Annu. Rev. Cell Dev. Biol. *29*, 385–416.

Bianco, I.H., and Wilson, S.W. (2009). The habenular nuclei: a conserved asymmetric relay station in the vertebrate brain. Philos. Trans. R. Soc. Lond. B. Biol. Sci. *364*, 1005–1020.

Bielle, F., Marcos-Mondéjar, P., Leyva-Díaz, E., Lokmane, L., Mire, E., Mailhes, C., Keita, M., García, N., Tessier-Lavigne, M., Garel, S., et al. (2011). Emergent growth cone responses to combinations of Slit1 and Netrin 1 in thalamocortical axon topography. Curr. Biol. *21*, 1748–1755.

Chen, H., Bagri, A., Zupicich, J.A., Zou, Y., Stoeckli, E., Pleasure, S.J., Lowenstein, D.H., Skarnes, W.C., Chédotal, A., and Tessier-Lavigne, M. (2000). Neuropilin-2 Regulates the Development of Select Cranial and Sensory Nerves and Hippocampal Mossy Fiber Projections. Neuron *25*, 43–56.

Cord, B.J., Li, J., Works, M., McConnell, S.K., Palmer, T., and Hynes, M.A. (2010). Characterization of axon guidance cue sensitivity of human embryonic stem cell-derived dopaminergic neurons. Mol. Cell. Neurosci. *45*, 324–334.

Deck, M., Lokmane, L., Chauvet, S., Mailhes, C., Keita, M., Niquille, M., Yoshida, M., Yoshida, Y., Lebrand, C., Mann, F., et al. (2013). Pathfinding of Corticothalamic Axons Relies on a Rendezvous with Thalamic Projections. Neuron *77*, 472–484.

Funato, H., Saito-Nakazato, Y., and Takahashi, H. (2000). Axonal growth from the habenular nucleus along the neuromere boundary region of the diencephalon is regulated by semaphorin 3F and Netrin1. Mol. Cell. Neurosci. *16*, 206–220.

Gallarda, B.W., Bonanomi, D., Müller, D., Brown, A., Alaynick, W. a, Andrews, S.E., Lemke, G., Pfaff, S.L., and Marquardt, T. (2008). Segregation of Axial Motor and Sensory Pathways via Heterotypic Trans-Axonal Signaling. Science *320*, 233–236.

Giger, R.J., Cloutier, J.F., Sahay, a, Prinjha, R.K., Levengood, D. V, Moore, S.E., Pickering, S., Simmons, D., Rastan, S., Walsh, F.S., et al. (2000). Neuropilin-2 is required in vivo for selective axon guidance responses to secreted semaphorins. Neuron *25*, 29–41.

Gil, O.D., Zhang, L., Chen, S., Ren, Y.Q., Pimenta, A., Zanazzi, G., Hillman, D., Levitt, P., and Salzer, J.L. (2002). Complementary expression and heterophilic interactions between IgLON family members neurotrimin and LAMP. J. Neurobiol. *51*, 190–204.

Goldman, J.S., Ashour, M. a, Magdesian, M.H., Tritsch, N.X., Harris, S.N., Christofi, N., Chemali, R., Stern, Y.E., Thompson-Steckel, G., Gris, P., et al. (2013). Netrin1 Promotes Excitatory Synaptogenesis between Cortical Neurons by Initiating Synapse Assembly. J. Neurosci. *33*, 17278–17289.

Gruber, C., Kahl, A., Lebenheim, L., Kowski, A., Dittgen, A., and Veh, R.W. (2007). Dopaminergic projections from the VTA substantially contribute to the mesohabenular pathway in the rat. Neurosci. Lett. *427*, 165–170.

Grueber, W., and Sagasti, A. (2010). Self-avoidance and tiling: mechanisms of dendrite and axon spacing. Cold Spring Harb. Perspect. … 1–16.

Hikosaka, O. (2010). The habenula: from stress evasion to value-based decision-making. Nat. Rev. Neurosci. *11*, 503–513.

Hikosaka, O., Sesack, S.R., Lecourtier, L., and Shepard, P.D. (2008). Habenula: crossroad between the basal ganglia and the limbic system. J. Neurosci. *28*, 11825–11829.

Hillenbrand, R., Molthagen, M., Montag, D., and Schachner, M. (1999). The close homologue of the neural adhesion molecule L1 (CHL1): patterns of expression and promotion of neurite outgrowth by heterophilic interactions. Eur. J. Neurosci. *11*, 813–826.

Huberman, A.D., Clandinin, T.R., and Baier, H. (2010). Molecular and cellular mechanisms of lamina-specific axon targeting. Cold Spring Harb. Perspect. Biol. *2*, a001743.

Imai, T., and Sakano, H. (2011). Axon-axon interactions in neuronal circuit assembly: lessons from olfactory map formation. Eur. J. Neurosci. *34*, 1647–1654.

Imai, T., Yamazaki, T., Kobayakawa, R., Kobayakawa, K., Abe, T., Suzuki, M., and Sakano, H. (2009). Pre-target axon sorting establishes the neural map topography. Science *325*, 585–590.

Innos, J., Philips, M., Leidmaa, E., Heinla, I., Raud, S., Reemann, P., Plaas, M., Nurk, K., Kurrikoff, K., Matto, V., et al. (2011). Lower anxiety and a decrease in agonistic behaviour in Lsamp-deficient mice. Behav. Brain Res. *217*, 21–31.

Joo, W.J., Sweeney, L.B., Liang, L., and Luo, L. (2013). Linking cell fate, trajectory choice, and target selection: genetic analysis of Sema-2b in olfactory axon targeting. Neuron *78*, 673–686.

Kantor, D.B., Chivatakarn, O., Peer, K.L., Oster, S.F., Inatani, M., Hansen, M.J., Flanagan, J.G., Yamaguchi, Y., Sretavan, D.W., Giger, R.J., et al. (2004). Semaphorin 5A is a bifunctional axon guidance cue regulated by heparan and chondroitin sulfate proteoglycans. Neuron *44*, 961–975.

Keller, F., Rimvall, K., Barbe, M.F., and Levitt, P. (1989). A membrane glycoprotein associated with the limbic system mediates the formation of the septo-hippocampal pathway in vitro. Neuron *3*, 551–561.

Kimmel, R.A., Turnbull, D.H., Blanquet, V., Wurst, W., Loomis, C.A., and Joyner, A.L. (2000). Two lineage boundaries coordinate vertebrate apical ectodermal ridge formation. Genes Dev. 1377–1389.

Kolk, S.M., Gunput, R.-A.F., Tran, T.S., van den Heuvel, D.M. a, Prasad, A. a, Hellemons, A.J.C.G.M., Adolfs, Y., Ginty, D.D., Kolodkin, A.L., Burbach, J.P.H., et al. (2009). Semaphorin 3F is a bifunctional guidance cue for dopaminergic axons and controls their fasciculation, channeling, rostral growth, and intracortical targeting. J. Neurosci. *29*, 12542–12557.

Kowski, a B., Veh, R.W., and Weiss, T. (2009). Dopaminergic activation excites rat lateral habenular neurons in vivo. Neuroscience *161*, 1154–1165.

Krimpenfort, P., Song, J.-Y., Proost, N., Zevenhoven, J., Jonkers, J., and Berns, A. (2012). Deleted in colorectal carcinoma suppresses metastasis in p53-deficient mammary tumours. Nature *482*, 538–541.

Lai Wing Sun, K., Correia, J.P., and Kennedy, T.E. (2011). Netrins: versatile extracellular cues with diverse functions. Development *138*, 2153–2169.

Lattemann, M., Zierau, A., Schulte, C., Seidl, S., Kuhlmann, B., and Hummel, T. (2007). Semaphorin-1a controls receptor neuron-specific axonal convergence in the primary olfactory center of Drosophila. Neuron *53*, 169–184.

Li, B., Piriz, J., Mirrione, M., Chung, C., Proulx, C.D., Schulz, D., Henn, F., and Malinow, R. (2011). Synaptic potentiation onto habenula neurons in the learned helplessness model of depression. Nature *470*, 535–539.

Li, K., Zhou, T., Liao, L., Yang, Z., Wong, C., Henn, F., Malinow, R., Yates, J.R., and Hu, H. (2013). βCaMKII in lateral habenula mediates core symptoms of depression. Science *341*, 1016–1020.

Lin, L., Rao, Y., and Isacson, O. (2005). Netrin1 and slit-2 regulate and direct neurite growth of ventral midbrain dopaminergic neurons. Mol. Cell. Neurosci. *28*, 547–555.

López-Bendito, G., Cautinat, A., Sánchez, J.A., Bielle, F., Flames, N., Garratt, A.N., Talmage, D. a, Role, L.W., Charnay, P., Marín, O., et al. (2006). Tangential neuronal migration controls axon guidance: a role for neuregulin-1 in thalamocortical axon navigation. Cell *125*, 127–142.

Luo, L., and Flanagan, J.G. (2007). Development of continuous and discrete neural maps. Neuron *56*, 284–300.

Manitt, C., Mimee, A., Eng, C., Pokinko, M., Stroh, T., Cooper, H.M., Kolb, B., and Flores, C. (2011). The netrin receptor DCC is required in the pubertal organization of mesocortical dopamine circuitry. J. Neurosci. *31*, 8381–8394.

Manitt, C., Eng, C., Pokinko, M., Ryan, R.T., Torres-Berrío, A., Lopez, J.P., Yogendran, S. V, Daubaras, M.J.J., Grant, A., Schmidt, E.R.E., et al. (2013). dcc orchestrates the development of the prefrontal cortex during adolescence and is altered in psychiatric patients. Transl. Psychiatry *3*, e338.

Mann, F., Zhukareva, V., Pimenta, a, Levitt, P., and Bolz, J. (1998). Membrane-associated molecules guide limbic and nonlimbic thalamocortical projections. J. Neurosci. *18*, 9409–9419.

Matsumoto, M., and Hikosaka, O. (2007). Lateral habenula as a source of negative reward signals in dopamine neurons. Nature *447*, 1111–1115.

Matsumoto, M., and Hikosaka, O. (2009). Representation of negative motivational value in the primate lateral habenula. Nat. Neurosci. *12*, 77–84.

Mizumoto, K., and Shen, K. (2013). Interaxonal interaction defines tiled presynaptic innervation in C. elegans. Neuron *77*, 655–666.

Molnár, Z., Garel, S., López-Bendito, G., Maness, P., and Price, D.J. (2012). Mechanisms controlling the guidance of thalamocortical axons through the embryonic forebrain. Eur. J. Neurosci. *35*, 1573–1585.

Osborne, P.B., Halliday, G.M., Cooper, H.M., and Keast, J.R. (2005). Localization of immunoreactivity for Deleted in Colorectal Cancer (DCC), the receptor for the guidance factor Netrin1, in ventral tier dopamine projection pathways in adult rodents. Neuroscience *131*, 671–681.

Pasterkamp, R.J., and Kolodkin, A.L. (2013). SnapShot: Axon Guidance. Cell *153*, 494–494.e2.

Pasterkamp, R.J., Peschon, J.J., Spriggs, M.K., and Kolodkin, A.L. (2003). Semaphorin 7A promotes axon outgrowth through integrins and MAPKs. Nature *424*, 398–405.

Pasterkamp, R.J., Kolk, S.M., Hellemons, A.J., and Kolodkin, A.L. (2007). Expression patterns of semaphorin7A and plexinC1 during rat neural development suggest roles in axon guidance and neuronal migration. BMC Dev. Biol. *7*, 98.

Phillipson, O.T., and Griffith, a C. (1980). The neurones of origin for the mesohabenular dopamine pathway. Brain Res. *197*, 213–218.

Poon, V.Y., Klassen, M.P., and Shen, K. (2008). UNC-6/netrin and its receptor UNC-5 locally exclude presynaptic components from dendrites. Nature *455*, 669–673.

Powell, A.W., Sassa, T., Wu, Y., Tessier-Lavigne, M., and Polleux, F. (2008). Topography of thalamic projections requires attractive and repulsive functions of Netrin1 in the ventral telencephalon. PLoS Biol. *6*, e116.

Quina, L. a, Wang, S., Ng, L., and Turner, E.E. (2009). Brn3a and Nurr1 mediate a gene regulatory pathway for habenula development. J. Neurosci. *29*, 14309–14322.

Robles, E., and Baier, H. (2012). Assembly of synaptic laminae by axon guidance molecules. Curr. Opin. Neurobiol. *22*, 799–804.

Sanes, J.R., and Yamagata, M. (2009). Many paths to synaptic specificity. Annu. Rev. Cell Dev. Biol. *25*, 161–195.

Schmidt, E.R.E., Morello, F., and Pasterkamp, R.J. (2012). Dissection and culture of mouse dopaminergic and striatal explants in three-dimensional collagen matrix assays. J. Vis. Exp. 1–5.

Schwabe, T., Neuert, H., and Clandinin, T.R. (2013). A network of cadherin-mediated interactions polarizes growth cones to determine targeting specificity. Cell *154*, 351–364.

Serafini, T., Colamarino, S. a, Leonardo, E.D., Wang, H., Beddington, R., Skarnes, W.C., and Tessier-Lavigne, M. (1996). Netrin1 is required for commissural axon guidance in the developing vertebrate nervous system. Cell *87*, 1001–1014.

Shen, X., Ruan, X., and Zhao, H. (2012). Stimulation of Midbrain Dopaminergic Structures Modifies Firing Rates of Rat Lateral Habenula Neurons. PLoS One *7*, e34323.

Stamatakis, A.M., Jennings, J.H., Ung, R.L., Blair, G.A., Weinberg, R.J., Neve, R.L., Boyce, F., Mattis, J., Ramakrishnan, C., Deisseroth, K., et al. (2013). A Unique Population of Ventral Tegmental Area Neurons Inhibits the Lateral Habenula to Promote Reward. Neuron *80*, 1039–1053.

Sweeney, L.B., Couto, A., Chou, Y.-H., Berdnik, D., Dickson, B.J., Luo, L., and Komiyama, T. (2007). Temporal target restriction of olfactory receptor neurons by Semaphorin-1a/PlexinA-mediated axon-axon interactions. Neuron *53*, 185–200.

Takeuchi, H., Inokuchi, K., Aoki, M., Suto, F., Tsuboi, A., Matsuda, I., Suzuki, M., Aiba, A., Serizawa, S., Yoshihara, Y., et al. (2010). Sequential arrival and graded secretion of Sema3F by olfactory neuron axons specify map topography at the bulb. Cell *141*, 1056–1067.

Tessier-Lavigne, M., and Goodman, C.S. (1996). The molecular biology of axon guidance. Science *274*, 1123–1133.

Timofeev, K., Joly, W., Hadjieconomou, D., and Salecker, I. (2012). Localized netrins act as positional cues to control layer-specific targeting of photoreceptor axons in Drosophila. Neuron *75*, 80–93.

Veenvliet, J. V., Alves, M.T.M., Kouwenhoven, W.M., Oerthel, L. Von, Lim, J.L., Linden, A.J.A. Van Der, Koerkamp, M.J. a. G., Holstege, F.C.P., Smidt, M.P., dos Santos, M.T.M. a., et al. (2013). Specification of dopaminergic subsets involves interplay of En1 and Pitx3. Development *140*, 4116–4116.

Wang, L., and Marquardt, T. (2013). What axons tell each other: axon–axon signaling in nerve and circuit assembly. Curr. Opin. Neurobiol. *23*, 974–982.

Wang, L., Klein, R., Zheng, B., and Marquardt, T. (2011). Anatomical coupling of sensory and motor nerve trajectory via axon tracking. Neuron *71*, 263–277.

Williams, M.E., de Wit, J., and Ghosh, A. (2010). Molecular mechanisms of synaptic specificity in developing neural circuits. Neuron *68*, 9–18.

Xu, B., Goldman, J.S., Rymar, V.V., Forget, C., Lo, P.S., Bull, S.J., Vereker, E., Barker, P.A., Trudeau, L.E., Sadikot, A.F., et al. (2010). Critical Roles for the Netrin Receptor Deleted in Colorectal Cancer in Dopaminergic Neuronal Precursor Migration, Axon Guidance, and Axon Arborization. Neuroscience *169*, 932–949.

Zhukareva, V., and Levitt, P. (1995). The limbic system-associated membrane protein (LAMP) selectively mediates interactions with specific central neuron populations. Development *121*, 1161–1172.

Supplemental information

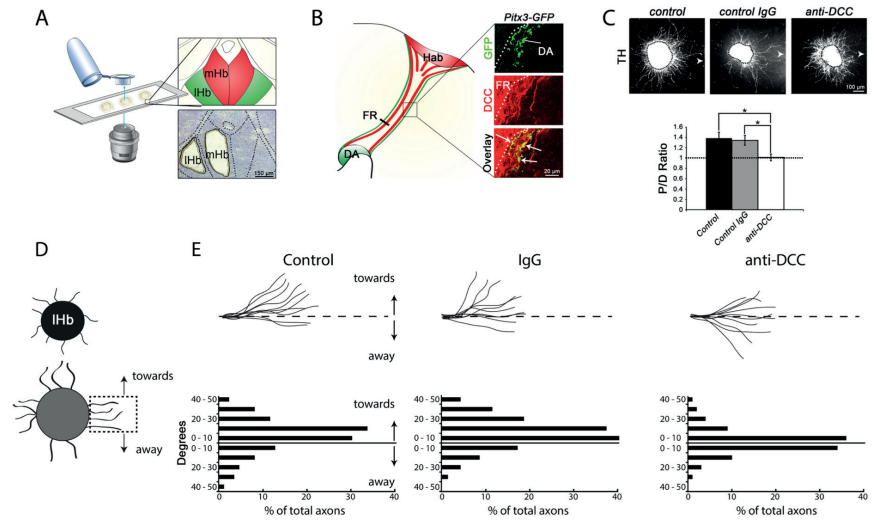

Figure S1

Netrin1 is an Attractant for Dopaminergic Axons of the Ventral Tegmental Area (VTA), Related to Figure 1

(A) Laser capture microdissection was performed on the medial habenula (mHb) or lateral habenula (lHb) in E16.5 mouse brain sections. (B) Schematic of a sagittal section of the mouse brain depicting the habenula (Hab), dopaminergic midbrain (DA) and fasciculus retroflexus (FR). To confirm that deleted in corectal cancer (DCC) protein is expressed on dopaminergic axons growing towards the lHb, we performed immunohistochemistry for DCC in Pitx3-GFP mice, because of an inability to combine DCC and tyrosine hydroxylase (TH) antibodies for double immunostaining on embryonic axons. In Pitx3-GFP mice, midbrain dopamine neurons and their axons express GFP (Zhao et al., 2004). Immunohistochemistry for DCC and GFP on Pitx3-GFP mouse brain sections reveals expression of DCC on GFP-positive dopaminergic axons in the FR (arrows). Dashed line indicates border between core and sheath region. (C) Immunocytochemistry for TH on collagen matrix assays combining E14.5 ventral tegmental area (VTA) and lHb explants in the absence of antibody (control) or in the presence of IgG control or anti-DCC function blocking antibodies. Arrowheads indicate position of adjacent lHb explants. Quantifications show the average proximal/distal (P/D) ratio for control, control IgG and anti-DCC conditions. * $P < 0.05$. Error bars indicate S.E.M.. (D, E) Changes in the orientation of TH-positive axons growing parallel to the adjacent lHb explants in co-cultures as shown in C were analyzed (D). (E) On top are camera lucida drawings of representative axons for each condition. Histograms depict how many degrees axons deviate from a straight course. Quantification shows turning of dopaminergic axons towards the lHb in the control and IgG conditions, but not in the presence of function-blocking anti-DCC antibodies.

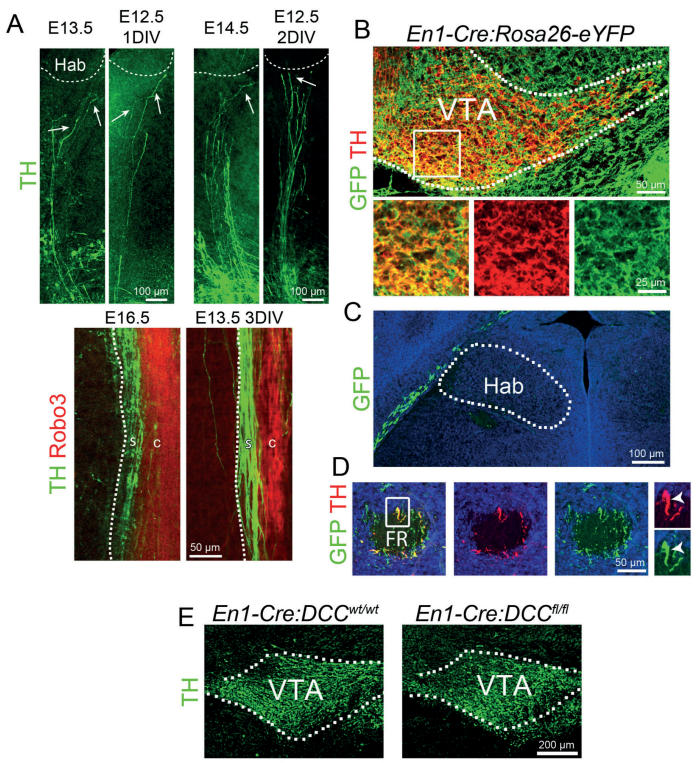

Figure S2

Characterization of the *Ex Vivo* Hemisection Culture System and of *En1-Cre* Mice, Related to Figure 1

(A) Comparison of acute (left panels) and cultured hemisections (right panels) stained for tyrosine hydroxylase (TH) and Robo3. The growth and development of dopaminergic afferents towards the habenula is similar *ex* and *in vivo* (Hab, arrows). Segregation between the core (c) and sheath (s) compartments of the fasciculus retroflexus (FR) is maintained *ex vivo*. DIV, days *in vitro*. (B-D) Immunohistochemistry on coronal sections of E13.5 *En1-Cre:Rosa26-eYFP* mice. GFP is expressed by TH-positive neurons in the ventral tegmental area (VTA) (B, dotted lines). Boxed area is shown at higher magnification in lower panels. (C) No expression of GFP is observed in the habenula of *En1-Cre:Rosa26-eYFP* mice (dotted line). (D) TH-positive axons in the FR express GFP^+. Boxed area is shown at higher magnification in panels on the right. Arrowheads indicate $GFP^+;TH^+$ axons. (E) Immunohistochemistry for TH on coronal sections of *En1-Cre:DCC*$^{fl/fl}$ mice. No change in the organization of dopaminergic neurons in the VTA is observed in *En1-Cre:DCC*$^{fl/fl}$ mice, as compared to *En1-Cre:DCC*$^{wt/wt}$ littermate controls.

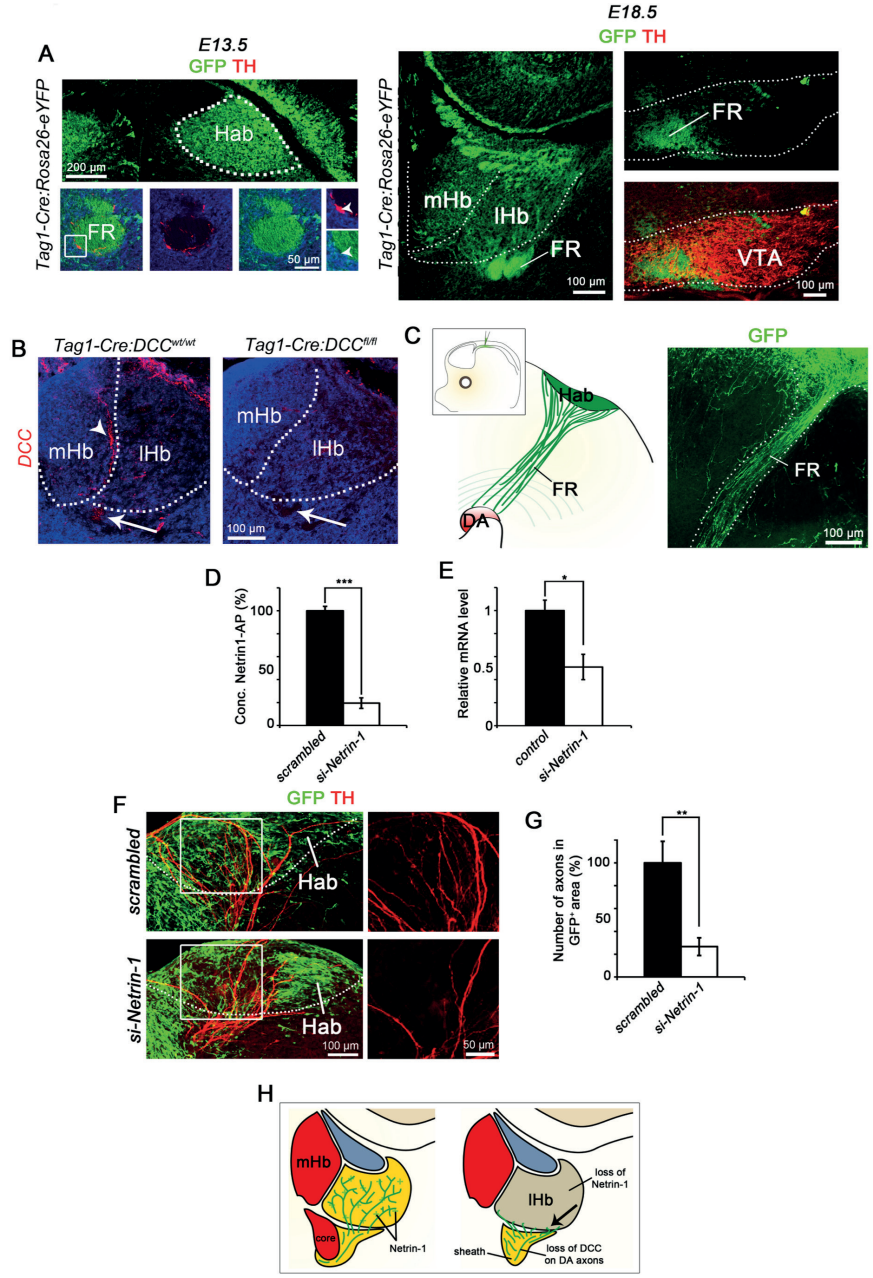

Figure S3

Characterization of Tag1-Cre Mice and siRNA-mediated Knockdown of *Netrin1* in the Habenula by Ex Vivo Electroporation, Related to Figure 2.

(A) Immunohistochemistry for GFP and tyrosine hydroxylase (TH) on coronal sections of E13.5 and E16.5 *Tag1-Cre:Rosa26-eYFP* mice. GFP is expressed in the habenula (Hab) and in the fasciculus retroflexus (FR), but not in dopaminergic neurons in the ventral tegmental area (VTA) and TH-positive axons in the FR (arrowheads). Boxed area is shown at higher magnification in panels on the right. Arrowheads indicate TH^{+};GFP^{-} axon. mHb, medial habenula; lHb, lateral habenula. (B) Immunohistochemistry for DCC on coronal sections of the habenula of *Tag1-Cre:DCC* mice. Axons from the mHb forming the core of the FR (white arrows) no longer stain for DCC in the mHb (arrowhead) and FR (arrow) in *Tag1-Cre:DCC$^{fl/fl}$* mice. (C) Schematic showing the injection site used for *ex vivo* electroporation of GFP and siRNAs. Electroporation of GFP into the habenula results in expression in both the habenula as well as in axons projecting into the FR, but not in the ventral midbrain containing dopaminergic neurons (not shown). DA, dopamine neuron pool. (D-G) siRNAs targeting *Netrin1* induce efficient knockdown of Netrin1 protein expression as measured by the concentration of Netrin1-AP in the tissue culture medium of transfected 293 cells (**D**). (**E**) Quantitative PCR on E14-15 cerebral cortex slices electroporated with scrambled control or *Netrin1* siRNAs and cultured for 3 days. *Netrin1* siRNAs significantly downregulate *Netrin1* expression in neuronal tissue following *ex vivo* electroporation. (**F**) Immunohistochemistry for TH and GFP following electroporation with scrambled or *Netrin1* siRNAs. Boxed areas are shown at higher magnification at the right. (**G**) Knockdown of Netrin1 results in significantly reduced innervation of the habenula by dopaminergic afferents. * $P < 0.05$, ** $P < 0.01$, *** $P < 0.001$. Error bars denote S.E.M.. (**H**) Schematic representation of the defects in dopaminergic innervation of the lHb observed following loss of DCC or Netrin1. Dopaminergic axons fail to enter the lHb and accumulate at the ventral border of this subnucleus (arrow).

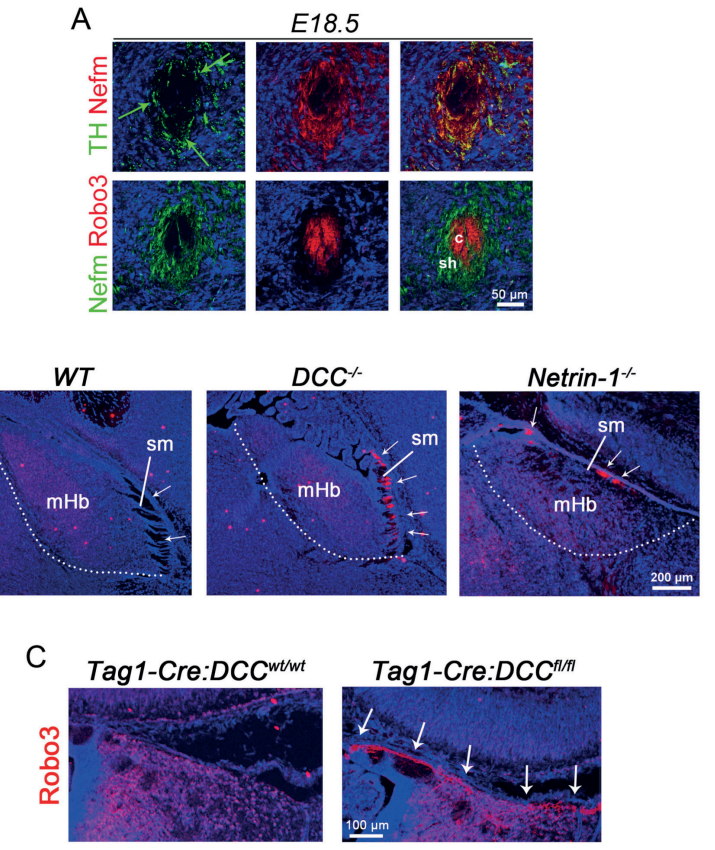

Figure S4

Markers Allow for Specific Visualization of the Core and Sheath Domains of the Fasciculus Retroflexus (FR), Related to Figure 2

(A) Immunohistochemistry for tyrosine hydroxylase (TH), neurofilament medium polypeptide (Nefm) and/or Robo3 on coronal sections of the FR. Nefm is specific for the sheath and shows that dopaminergic axons (green arrows) are confined to this subdomain of the FR. The core is stained by Robo3. Double staining of Robo3 and Nefm reveals the complete segregation of the core and sheath domains. (B, C) Immunohistochemistry for Robo3 in the habenula. In *DCC$^{-/-}$* and *Netrin1$^{-/-}$* mice (B) and in *Tag1-Cre:DCC$^{fl/fl}$* mice (C) Robo3-positive axons are found at the dorsal roof of the habenula (arrows). c, core; mHb, medial habenula; sh, sheath; sm, stria medullaris.

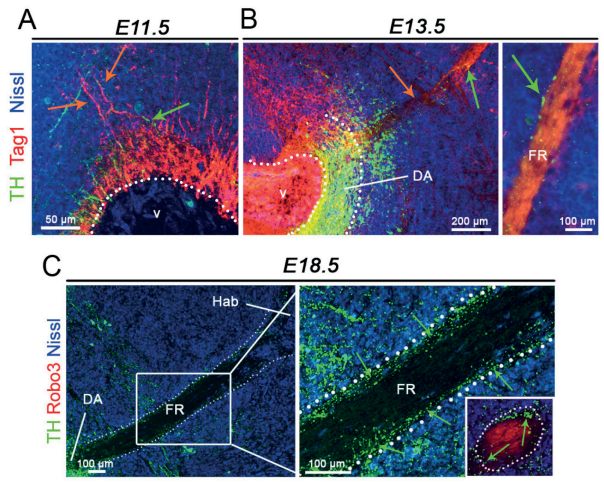

Figure S5

Development of Reciprocal Habenular and Dopaminergic Projections, Related to Figure 3

(A-C) Immunohistochemistry for tyrosine hydroxylase (TH), Tag1 and/or Robo3 on sagittal sections of the fasciculus retroflexus (FR). At E11.5, Tag1-positive axons from the habenula arrive at the dopaminergic midbrain (red arrows). Dopaminergic neurons extend axons but these do not yet progress towards the habenula (green arrow) (A). At E13.5, a bundle of fasciculated axons from the habenula (red arrow) extends into the dopaminergic midbrain. A few dopaminergic axons (green arrow) grow along this bundle and are restricted to the outer part of the FR (B). At E18.5, dopaminergic axons (green arrows) are restricted to the outer part of the FR (C). Inset shows a coronal cross section of the FR. DA, dopamine neuron pool; Hab, habenula; v, ventricle.

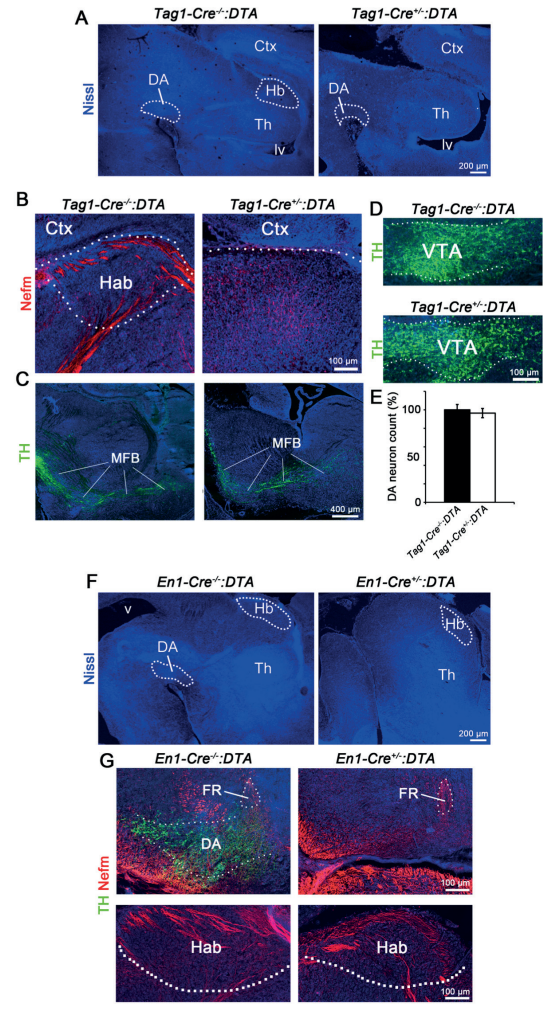

Figure S6

Characterization of *Tag1-Cre:DTA* and *En1-Cre:DTA* mice. Related to Figure 3

(A, F) Nissl stained sagittal sections of E16.5 *Tag1-Cre:DTA* and *En1-Cre:DTA* mice reveal ablation of habenular or dopaminergic neurons in the midbrain in *Tag1-Cre$^{+/-}$:DTA* mice (A) and *En1-Cre$^{+/-}$:DTA* mice (F), respectively. Ctx, cortex; DA, dopamine neuron pool. Hb, habenula; lv, lateral ventricle; Th, thalamus; v, third ventricle. (B-E) Immunohistochemistry for tyrosine hydroxylase (TH) and neurofilament medium polypeptide (Nefm) on sections of *Tag1-Cre:DTA* mice. The habenula is ablated in *Tag1- Cre$^{+/-}$:DTA* mice (B) but dopaminergic neurons in the ventral tegmental area (VTA) (D) and dopaminergic projections running through the medial forebrain bundle (MFB; C) are intact. No changes were observed in the number of TH-positive neurons in the VTA of *Tag1-Cre$^{+/-}$:DTA* mice as compared to *Tag1-Cre$^{+/-}$:DTA* littermate controls (E). Error bars denote S.E.M.. (G) Immunohistochemistry for TH and Nefm on sections of *En1-Cre:DTA* mice. Dopaminergic neurons are ablated in *En1-Cre$^{+/-}$:DTA* mice, while the Nefm^{+} habenula and FR are present.

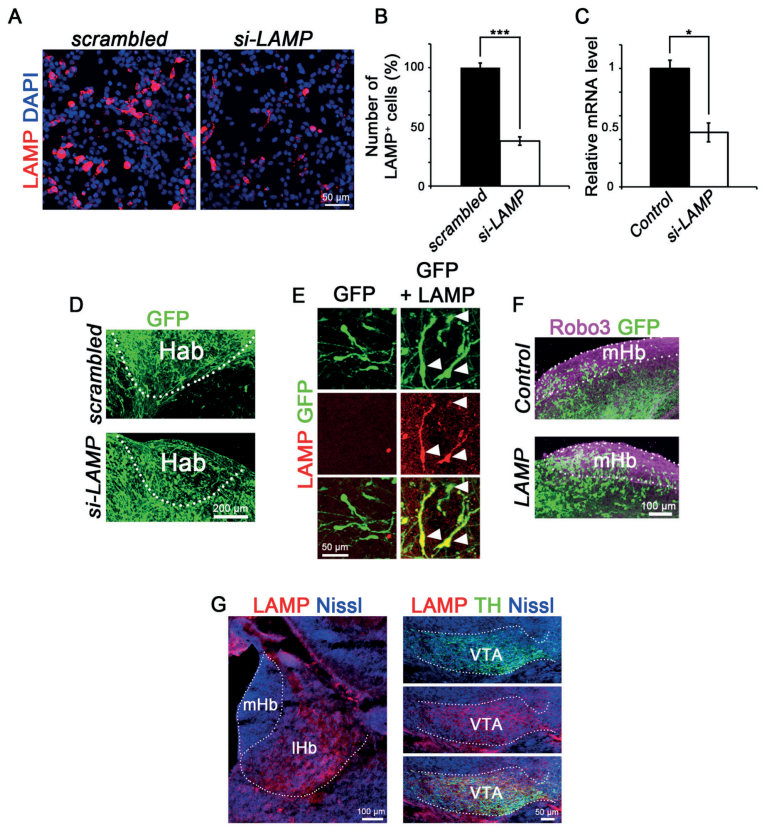

Figure S7

LAMP Protein is Expressed in the Lateral Habenula (lHb) and Ventral Tegmental Area (VTA), Related to Figure 6 and 7

(A, B) HEK293 cells transfected with a limbic-system associated membrane protein (LAMP) expression vector show robust LAMP expression. Subsequent transfection of siRNAs directed against *LAMP* (*si-LAMP*) but not of scrambled control siRNAs induces efficient knock-down of LAMP. *** $P < 0.001$. Error bars denote S.E.M.. (C) Quantitative PCR on E14-15 cerebral cortex slices electroporated with scrambled control or *LAMP* siRNAs and cultured for 3 days. *LAMP* siRNAs significantly downregulate *LAMP* expression in neuronal tissue following *ex vivo* electroporation. (D) Representative example showing immunohistochemistry for GFP following electroporation of the habenula with a GFP expression vector in combination with scrambled or *LAMP* targeted siRNAs. (E) Immunohistochemistry for LAMP and GFP following electroporation with a GFP or a combination of LAMP and GFP expression vectors. Electroporation of the LAMP expression vector induces ectopic expression of LAMP protein. Arrowheads indicate GFP-positive cells expressing ectopic LAMP in the medial habenula (mHb). (F) Immunohistochemistry for Robo3 and GFP following electroporation of the habenula with a GFP or a combination of LAMP and GFP expression vectors. (G) Immunohistochemistry for LAMP and/or tyrosine hydroxylase (TH) on coronal sections. At E18.5, LAMP is specifically expressed in the lHb and in dopaminergic neurons in the VTA. lHb, lateral habenula.

Table S1

Related to Figure 1

	Symbol (Entrez)	Protein
mHb	ALCAM	Activated leukocyte cell adhesion molecule
	Amigo2	Adhesion molecule with Ig like domain 2
	Cntn2	Contactin-2
	Crk	Adapter molecule crk
	DCC	Deleted in colorectal carcinoma
	Nrp2	Neuropilin 2
	Plxnb2	Plexin-B2
lHb	Gap43	Neuromodulin
	Gpc2	Glypican-2
	NCAM1	Neural cell adhesion molecule 1
	Nefm	Neurofilament medium polypeptide
	Nlgn2	Neuroligin-2
	Nlgn3	Neuroligin-3
	NrCAM	Neuronal cell adhesion molecule

List of cell adhesion and axon guidance molecules detected or enriched in either the mHb or lHb.

Table S2

Related to Figure 4

	Symbol (Entrez)	Protein
Whole FR	ALCAM	Activated leukocyte cell adhesion molecule
	Cdh13	Cadherin 13
	Negr1	Neuronal growth regulator 1
	Nfasc	Neurofascin
	Nrp2	Neuropilin 2
	Robo1	Roundabout homolog 1 (Drosophila)
Core	DCC	Deleted in colorectal carcinoma
	Gpc2	Glypican 2 (cerebroglycan)
	L1CAM	L1 cell adhesion molecule
	NCAM1	Neural cell adhesion molecule 1
	NrCAM	Neuron-glia-CAM-related cell adhesion molecule
	Robo3	Roundabout homolog 3 (Drosophila)
Sheath	CHL1	Cell adhesion molecule with homology to L1CAM
	LAMP	Limbic system-associated membrane protein

List of cell adhesion and axon guidance molecules detected in the FR. Expression and localization was confirmed by immunohistochemistry, as shown in main Figure 5.

Supplemental experimental procedures

Mouse lines. All animal use and care were in accordance with institutional guidelines. The morning on which a vaginal plug was detected was considered embryonic day 0.5 (E0.5). C57BL/6 mice were obtained from Charles River. *DTA* and *Rosa26-eYFP* mice were from the Jackson Lab. *En1-Cre* mice were a kind gift of Wolfgang Wurst (Helmholtz Zentrum München) and kindly provided by Alain Chédotal (INSERM). *Pitx3-GFP* mice were a kind gift of Meng Li (MRC Clinical Science Center) and kindly provided by Marten Smidt (University of Amsterdam). *LAMP* knockout mice were as described (Innos et al., 2011). *DCC* conditional mutant mice were a kind gift of Anton Berns (Netherlands Cancer Institute) and kindly provided by Cecilia Flores (McGill University). *DCC*$^{-/-}$ (Fazeli et al., 1997) and *Netrin1* hypomorph mice (Serafini et al., 1996) were originally obtained from the laboratory of Marc Tessier-Lavigne (Rockefeller University) and then bred at the University of Queensland under the approval of the University of Queensland Animal Ethics Committee and according to the Australian Code of Practice for the Care and Use of Animals for Scientific Purposes. *DCC* and *Netrin1* knockout mice were backcrossed for over 10 generations onto a C57Bl/6 background.

Generation of *Tag1-Cre* mice. The *Tag1*(Tg)Cre line was generated using BAC technology (Bacterial Artificial Chromosome) as described previously (Fogarty et al., 2007; Kessaris et al., 2006; Lee et al., 2001). Briefly, 3 clones containing the entire murine *Tag1* gene and upstream and downstream genomic sequences were selected from a BAC library (Ensemble CytoView). In parallel, a plasmid was constructed containing a transgene that included Cre- recombinase flanked by sequences homologous to sequences upstream (9565-9796 bp) and downstream (9861-10159) of exon 2 of the *Tag1* gene that contains the ATG. A polyA-frt- kanamycin-frt cassette was also included in the vector. The appropriate BAC clone and the plasmid were introduced into EL250 cells, colonies were tested for homologous recombination (by which exon 2 sequences were replaced by Cre-recombinase) using restriction digestion and Southern blotting with a probe for the 5' homology region of the *Tag1* gene. Finally, the recombined transgene was isolated and generation of transgenic mice by pronuclear injection of the modified BAC was as described previously (Kessaris et al., 2006). Mice were genotyped using primers to detect a 550bp Cre fragment (5'- TGAGTGCTTTAGCTCTACAGC-3' and 5'-GACACAGCATTGGAGTCAGA-3'). To examine the spatiotemporal patterns of Cre recombination in *Tag1-Cre* and *En1-Cre* mice, *Tag1-Cre* and *En1-Cre* mice were crossed with *Rosa26-eYFP* mice, in which a *YFP* cDNA is preceded by a lox-STOP-lox cassette (Srinivas et al., 2001).

Immunohistochemistry. After cervical dislocation, brains were fixed in 4% paraformaldehyde (PFA) in PBS after which they were cryoprotected in 30% sucrose in PBS. Cryostat sections were cut at 16-18 µm, mounted on Superfrost Plus slides (Thermo Fisher Scientific), air-dried, and stored at -20^{O}C. Sections were blocked with 1% BSA in PBS containing 0.4% Triton X-100 for 30 min at room temperature (RT). Subsequent incubation with primary antibodies in blocking buffer was done overnight at 4^{o}C. Sections were washed extensively in PBS and incubated with secondary antibodies conjugated to Alexa Fluor-488, 555 and 680 from appropriate species. After several washes in PBS, sections were counterstained with fluorescent Nissl (Neurotrace; Invitrogen; 1:500), washed in PBS and mounted in FluorSave reagent (Merck Millipore). Staining was visualized on a Zeiss Axioskop A1 epifluorescent microscope or by confocal laser-scanning microscopy (Olympus FV1000). Average fluorescence intensity was measured using the histogram function in Adobe Photoshop. Background was determined in areas without staining and subtracted from images after which the mean signal intensity was measured. Primary antibodies used were mouse anti-Nefm (DHDB, clone 2H3; 1:30), rabbit anti-TH (Millipore; 1:1000), goat anti- Robo3 (R&D Systems; 1:50), mouse anti-Tag1 (DSHB; 1:50), chicken anti-GFP (Abcam; 1:500), rabbit anti-DCC (a kind gift from Dr. Helen M. Cooper (Queensland Brain Institute; 1:500; #2473 and #2744), goat anti-Neurofascin (Santa Cruz; 1:50), goat anti-ALCAM (R&D Systems, 1:50), anti-Cadherin 13 (Santa-Cruz, 1:50), goat anti-Neurotractin (Santa Cruz; 1:50), goat anti-Robo1 (R&D Systems; 1:50), goat anti-Glypican 2 (R&D Systems, 1:50), rabbit anti-NrCAM (Abcam, 1:50), mouse anti-NCAM (R&D Systems, 1:50), goat anti-L1 (R&D Systems, 1:100), goat anti-CHL1 (R&D Systems, 1:100), mouse anti-LAMP (DSHB; 1:50), goat anti-Neuropilin-2 (R&D Systems, 1:100).

Laser capture microdissection. Fresh frozen sections of E16.5 mouse brains were sagittally cut (16 µm) and mounted on MembraneSlides 1.0 PEN (Zeiss). Sections were dried within the cryostat chamber to prevent protein degradation and were stored at -80^{o}C until use. Before the laser dissection procedure, sections were incubated in ice-cold 70% ethanol for 2 min and stained for 1 min with 1% (w/v) cresyl violet in 50% ethanol. Next, sections were washed briefly in ice-cold 70% ethanol and 100% ethanol and subsequently air-dried. Laser capture microdissection was performed on a PALM laser microscope system (Zeiss). Dissected tissue was collected in lysis buffer (20 mM Tris pH7.5, 15 0mM NaCl, 10% glycerol, 1% NP-40) containing protease inhibitor cocktail (Complete; Roche). After the procedure, LDS sample buffer (NuPAGE) and 2-mercaptoethanol was added and samples were stored at -80^{o}C. Samples were subjected to SDS-PAGE and stained using GelCode Blue Stain reagent (Thermo Scientific). Gels were sent for mass spectrometry analysis at the Erasmus Proteomics Center (Rotterdam).

RNA *in situ* hybridization. cDNA was made from whole mouse brain RNA using a one-step RT-PCR kit (Qiagen), according to manufacturer's protocol and using the following primers: *DCC,* 5'-CCCAGTCCAAGGTTACAGATTG-3' and 5'-GGAGGTGTCCAACTCATGATG-3'; *Netrin1*, 5'-GATGTGCCAAA-GGCTACCAG-3' and 5'-TTCTTGCACTTGCCCTTCTTC-3';. cDNA was cloned into pGEM-T Easy (Promega) and transcribed using either SP6 or T7 RNA polymerase (Roche) and digoxigenin-labeled nucleotide mix (Roche) to produce digoxigenin- labeled cRNA probes. Brain sections were from prepared on a cryostat from brains frozen on dry-ice. Sections were cut at 16 µm and stored at -80^{O}C. After hybdrization of probes, digoxigenin was detected using anti-digoxigenin FAB fragments conjugated to alkaline phosphatase (Roche; 1:3000) and stained with NBT/BCIP (Roche). Sections were counterstained with fluorescent Nissl (Neurotrace; Invitrogen; 1:500), mounted using FluorSave reagent and visualized on a Zeiss Axioscope A1.

Explant cultures. E14.5 mouse embryos were collected in ice-cold L15. Appropriate brain regions were dissected in L15 with 5% FCS and explants were cut to a diameter of approximately 350 µm. For co-cultures, explants were placed together in a collagen gel at a distance of approximately 300 µm and were cultured in Neurobasal containing HEPES, B27, β-mercaptoethanol, glutamine and penicillin/streptomycin (Schmidt et al., 2012). For blocking experiments, sodium azide was removed from IgG control (Millipore) and anti-DCC blocking antibodies (Calbiochem) using Slide-A-Lyzer 10K dialysis cassettes (Thermo Scientific). Antibodies were added at a final concentration of 10 µg/ml. After 72 h in culture, explants were fixed in 4% PFA and stained using appropriate antibodies. Quantification of co-cultures was done by measuring the 20 longest neurites in both the proximal and distal quadrants of the culture. Average values of the proximal/distal (P/D) ratio were determined for each explant (Schmidt et al., 2012). To determine whether lHb explants exert chemotropic effects on dopaminergic VTA axons, the trajectories of individual axons emerging parallel to the lHb explants were analyzed. For each experimental condition, 10 individual axons were randomly selected and analyzed per explant. Using Openlab software (Improvision) the angle between the initial (near the explant) and final trajectory (at the axon tip) of each axon was determined (Bagnard et al., 1998; Pasterkamp et al., 2003). For growth on LAMP substrate, coverslips were coated with either poly-D-lysine (PDL) for control or PDL and 10 µg/mL of recombinant mouse LAMP (Sino Biological). Average axon length was determined after 72 h in culture.

Organotypic slice cultures. For organotypic slice culture experiments, E12.5 mouse brains were dissected and cut along the midline to produce two sagittal hemisections. Brain slices were cultured on Millicell cell culture inserts (PTFE, 0.4 µm, Millipore) for three days in 1.6 ml slice culture medium consisting of Basal Medium Eagle (Sigma) and supplemented with cHBSS, glucose, glutamine and penicillin/streptomycin, as described previously (Polleux and Ghosh, 2002). For testing the effect of Netrin1 on the trajectory of dopaminergic axons towards the habenula, 293 cells were transfected with expression vectors for 1) GFP and empty vector (for control) or 2) for GFP and Netrin1-AP. One day after transfection, cells were trypsinized and centrifuged. Aggregates were produced by resuspending cells in tissue culture medium and collagen (6:1) and placing 10 µl droplets onto an inverted lid of 30 mm cell culture dishes for > 1 hr (Schmidt et al., 2012). Cell aggregates were cut to an appropriate size and placed in close vicinity to the developing fasciculus retroflexus onto hemisections. For blocking of axon outgrowth, membrane blocking filters (Nuclepore Track- Etched 8 µm, Whatman) were cut to a size roughly covering the complete ventral side of the habenula and were placed at 0 days *in vitro* (DIV) where they remained for the entire culture period. For removal of GPI-linked proteins, PI-PLC (Sigma) was dissolved according to manufacturer's protocol and added at 0, 1 and 2 DIV to a final concentration of 1 U/ml. Control slices were incubated with the same volume of vehicle. Blocking experiments were performed by adding LAMP function-blocking antibodies (R&D Systems) to a final concentration of 30 µg/ml at 0, 1 and 2 DIV. After 3 DIV slices were fixed in 4% PFA for 1 h and washed in PBS. Slices were blocked in PBS-T (PBS containing 1% Triton-X100) and 10% fetal calf serum (FCS) for 3 h at RT. Slices were stained with primary antibodies overnight in blocking buffer at 4^{o}C and subsequently washed 6 times for 1 h in PBS-T with 1% FCS at RT. Next, slices were incubated with secondary antibodies overnight at 4^{o}C after which they were washed several times in PBS, mounted on microscope slides with ProLong Gold antifade reagent (Invitrogen), and visualized using an Olympus FV1000 confocal laser- scanning microscope. For quantification of axon reorientation in hemsection-aggregate assays, slices were categorized as having a 'normal trajectory' when <5 axons were reoriented towards the cell aggregate. Slices where > 5 axons were reoriented towards the aggregate were categorized as showing a 'modified trajectory'. For quantification of axon growth, three bins of equal size were drawn along the axon bundle and average fluorescence intensity in each bin was determined, as described above (see Fig. 3C).

Stripe assay. The modified stripe assay was performed as described (Knöll et al., 2007). Briefly, alternating stripes (PDL or LAMP (10 µg/ml)) were applied to coverslips pre-treated with PDL. Dopaminergic explants were dissected as described (Schmidt et al., 2012). Approximately 10 explants were seeded on the middle of each coverslip and were cultured for 3 days. Explants were fixed with

4% PFA and 8% sucrose and immunostained with the appropriate antibodies. For quantification, the number of neurites terminating on control or LAMP stripes were counted for each explant (Evans et al., 2007).

siRNA-mediated knockdown. HEK293 cells were plated onto PDL-coated coverslips. For transfection, 1.75 µl of Lipofectamine 2000 was diluted in 25 µl Opti-MEM (Gibco). Separately, 15 pmol siRNA together with 0.5 µg of DNA encoding LAMP (LAMP-pIRES- hrGFP-1a) (Hashimoto et al., 2009) or Netrin1 (Netrin1-AP) was added to 25 µl Opti-MEM. Both Opti-MEM dilutions were mixed and allowed to incubate for 10 min after which they were directly added to each well. For LAMP knockdown, cells were fixed after 72 h in 4% PFA, briefly washed in PBS, and incubated for 30 min in blocking buffer containing 1% BSA in PBS and 0.4% Triton X-100. Cells were incubated with appropriate primary antibodies in blocking buffer overnight at 4°C. Cells were washed in PBS and incubated for 1 h with appropriate secondary antibodies at RT. After washing in PBS, nuclei were counterstained with DAPI (Sigma) after which the coverslips were mounted in Prolong Gold antifade reagent (Invitrogen). For Netrin1 knockdown, growth medium of transfected cells was collected after 72 h and alkaline phosphatase activity was measured.

***Ex vivo* electroporation.** Mouse embryos were collected at E12.5 and the third ventricle was injected, as described (Quina et al., 2009), with siRNA (25 µM) and/or DNA (GFP or LAMP-pIRES-hrGFP-1a; 1 µg/µl) diluted in 0.05% Fast Green Dye (Sigma) using a PLI-100 Pico-injector (Harvard Apparatus). Brains were electroporated using an ECM 830 Electro- Square-Porator (Harvard Apparatus) set to three unipolar pulses at 30 V (100-ms interval and length) and using gold-plated Genepaddles (Fisher Scientific). Brains were dissected and prepared for slice culture assay as described above. Slices were grown for 3 DIV after which they were fixed, stained and visualized on a confocal laser-scanning microscope (Olympus FV1000). For LAMP knockdown experiments, axon growth in each electroporated slice was quantified by drawing three bins of equal size along the axon bundle and subsequently determining average fluorescence intensity in each bin, as described above. LAMP overexpression experiments were quantified by counting the number of TH-positive axons that inappropriately innervated the mHb, as determined by double immunohistochemistry for TH and Robo3. Only those slices were considered where a sufficient amount of GFP-positive cells was found in the habenula and where no abnormal growth of Robo3-positive axons was observed. For Netrin1 knockdown experiments, the number of axons terminating in GFP-positive areas of the habenula were quantified. To determine the efficiency of Netrin1 or LAMP knockdown following *ex vivo* electroporation, a a mix of siRNAs and GFP DNA was injected in the lateral ventricles of E14-E15 mouse brains and directed to the cerebral cortex. Brains were dissected and prepared for slice culture assay as described above. Slices were grown for 3 DIV following which the region of the slice containing GFP-positive cells was microdissected. Tissue from several different embryos was pooled and RNA was prepared using the RNeasy Mini kit (Qiagen). One-step real time reverse transcription-polymerase chain reaction (qPCR) was performed as described previously (Chakrabarty et al., 2012) with the following primers: *Netrin1* 5'-TTGCAAAGCCTGTGATTGCC-3', 5'-TAGCCTTTGGCACATCGGTT-3', *LAMP* 5'- CAGCGTGGATTTTAACCGAGGC-3', 5'- TGATGCCAGAGCGG-TTCAACCA-3'. Each sample was normalized to the house keeping gene *TATA binding protein* (*Tbp*). The Ct values used were the means of triplicates and three independent experiments were performed. Mean values were determined from independent samples for *Netrin1* siRNA, *LAMP* siRNA, and scrambled control siRNAs. Values for *Netrin1* and *LAMP* knockdown were presented as normalized to scrambled control.

Supplemental references

Chakrabarty, K., Von Oerthel, L., Hellemons, A.J., Clotman, F., Espana, A., Groot Koerkamp, M., Holstege F.C.P., Pasterkamp, R.J., and Smidt, M.P. (2012). Genome wide expression profiling of the mesodiencephalic region identifies novel factors involved in early and late dopaminergic development. Biology Open *1*, 693-704.

Evans, A.R., Euteneuer, S., Chavez, E., Mullen, L.M., Hui, E.E., Bhatia, S.N., and Ryan, A.F. (2007). Laminin and fibronectin modulate inner ear spiral ganglion neurite outgrowth in an in vitro alternate choice assay. Dev. Neurobiol. 67, 1721-1730.

Fazeli, A., Dickinson, S., Hermiston, M., Tighe, R., Steen, R., Small, C., Stoeckli, E., Keino-Masu, K., Masu, M., Rayburn, H., et al. (1997). Phenotype of mice lacking functional Deleted in colorectal cancer (Dcc) gene. Nature *386*, 796–804.

Fogarty, M., Grist, M., Gelman, D., Marín, O., Pachnis, V., and Kessaris, N. (2007). Spatial genetic patterning of the embryonic neuroepithelium generates GABAergic interneuron diversity in the adult cortex. J. Neurosci. *27*, 10935–10946.

Hashimoto, T., Maekawa, S., and Miyata, S. (2009). IgLON cell adhesion molecules regulate synaptogenesis in hippocampal neurons. Cell Biochem. Funct. *27*, 496–498.

Kessaris, N., Fogarty, M., Iannarelli, P., Grist, M., Wegner, M., and Richardson, W.D. (2006). Competing waves of oligodendrocytes in the forebrain and postnatal elimination of an embryonic lineage. Nat. Neurosci. *9*, 173–179.

Knöll, B., Weinl, C., Nordheim, A., and Bonhoeffer, F. (2007). Stripe assay to examine axonal guidance and cell migration. Nat. Protoc. *2*, 1216–1224.

Lee, E.C., Yu, D., Martinez de Velasco, J., Tessarollo, L., Swing, D. a, Court, D.L., Jenkins, N. a, and Copeland, N.G. (2001). A highly efficient Escherichia coli-based chromosome engineering system adapted for recombinogenic targeting and subcloning of BAC DNA. Genomics *73*, 56–65.

Polleux, F., and Ghosh, A. (2002). The Slice Overlay Assay: A Versatile Tool to Study the Influence of Extracellular Signals on Neuronal Development. Sci. Signal. *2002*, pl9–pl9.

Quina, L. A, Wang, S., Ng, L., and Turner, E.E. (2009). Brn3a and Nurr1 mediate a gene regulatory pathway for habenula development. J. Neurosci. *29*, 14309–14322.

Schmidt, E.R.E., Morello, F., and Pasterkamp, R.J. (2012). Dissection and culture of mouse dopaminergic and striatal explants in three-dimensional collagen matrix assays. J. Vis. Exp. 1–5.

Srinivas, S., Watanabe, T., Lin, C.S., William, C.M., Tanabe, Y., Jessell, T.M., and Costantini, F. (2001). Cre reporter strains produced by targeted insertion of EYFP and ECFP into the ROSA26 locus. BMC Dev. Biol. *1*, 4.

Zhao, S., Maxwell, S., Jimenez-Beristain, A., Vives, J., Kuehner, E., Zhao, J., O'Brien, C., de Felipe, C., Semina, E., and Li, M. (2004). Generation of embryonic stem cells and transgenic mice expressing green fluorescence protein in midbrain dopaminergic neurons. Eur. J. Neurosci. *19*, 1133-1140.

Chapter 3

Pitx3-ITC: a new genetic strategy to study dopaminergic neuron development, function and diversity

Sara Brignani, Ewoud E. Schmidt, Divya A. Raj, Erik Schild, Anna A. De Ruiter, R. Jeroen Pasterkamp
Department of Translational Neuroscience, Brain Center Rudolf Magnus, University Medical Center Utrecht, University of Utrecht, Utrecht, The Netherlands

Abstract

Midbrain dopaminergic neurons (mDA neurons) are involved in the control of voluntary movements, regulation of emotions and reward, and are associated with multiple psychiatric and neurodegenerative disorders (e.g. schizophrenia and Parkinson's disease). Although all mDA neurons synthesize and release the same neurotransmitter dopamine, they are molecularly and functionally highly heterogeneous. Increasing evidence begins to show that different mDA neuron subsets have specific molecular signatures which, during dopamine system development, are responsible for the correct formation of their afferent and efferent connections. To distinguish and visualize different mDA neuron subsets and their projections *in vivo*, and to identify subset-specific developmental programs, we designed a genetic strategy called Pitx3-ITC. This strategy relies on the expression of different fluorescent proteins (Citrine, TdTomato, infrared fluorescent protein (IFP)) in different subsets of mDA neurons in a single mouse. Characterization of several BAC transgenic mouse lines shows that Pitx3-ITC allows the labeling of SNc mDA neurons. In addition, when using these lines in intersectional approaches, single SNc and VTA mDA neurons can be labeled as well as their dendritic and axonal projections in the midbrain but also at the level of synaptic targets. The Pitx3-ITC strategy offers the unique possibility to differentially label mDA neuron subsets and to visualize mDA neurons at the single-cell level providing a novel tool to unveil the molecular mechanisms underlying different aspects of mDA system function and development.

Introduction

Dopamine neurons of the midbrain (mDA neurons) are grossly divided in three distinct anatomical nuclei called substantia nigra compacta (SNc), ventral tegmental area (VTA), and retro rubral field (RRF). Although they all synthesize and release the same neurotransmitter, dopamine, differences between these neuronal populations are prominent: SNc, VTA, and RRF mDA neurons express different molecular markers, project to distinct brain areas and receive different afferent connections, have specific functional roles, and are involved in different neurological disorders. In particular, SNc mDA neurons innervate the dorsal striatum, forming the nigrostriatal pathway (Ikemoto, 2007; Lerner et al., 2015; Matsuda et al., 2009), and receive afferent connections from for example the dorsal striatum, the somatosensory and motor cortex, the subthalamic nucleus, and the superior colliculus (Fujiyama et al., 2011; Gerfen et al., 1987; Watabe-Uchida et al., 2012). In addition, SNc mDA neurons contribute to the control of voluntary movements, and degenerate in Parkinson's disease (PD). In contrast to VTA mDA neurons, which largely survive in PD (Kalia and Lang, 2015). On the other hand, VTA mDA neurons establish connections with the ventral striatum, the prefrontal cortex, the amygdala, the habenula, and the septum (Ikemoto, 2007; Lammel et al., 2008). Afferent connections of VTA mDA neurons derive for example from the ventral striatum, the medial prefrontal cortex, the lateral habenula, and many other brain regions (Morales and Margolis, 2017). Because of the complex neural network these neurons establish, VTA mDA neurons play a functional role in several aspects of behavior: e.g. in positive and negative reinforcement, decision making, working memory, and aversion.

To comprehend how differences between mDA neuron subsets arise, efforts are needed to understand the molecular and cellular mechanisms that underlie their development. Research focused on studying the development of mDA neuron subsets *in vivo* is limited by the lack of genetic tools suitable for identifying and labeling different mDA subtypes, which would allow to distinguish mDA subsets from each other and from other neurons in the brain. With such genetic tools, mDA neuron subsets could be visualized together with their efferent projections. These cells could be isolated from the brain and separated from other subsets or neuron types. This would allow for determining subset-specific expression profiles and selective knock-out or overexpression of gene candidates *in vitro* and *in vivo*.

Targeting a specific neuronal population *in vivo* requires the identification of at least one gene expressed in the selected neuronal group and not in others. The promoter of this gene could be used to induce the expression of a fluorescent reporter or of a Cre or Flp recombinase. For the dopamine system of the midbrain, no genes have been identified that are selective for single mDA neuron subtypes, and it is therefore unfeasible to use single promoters to target mDA

neuron subsets. To overcome this limitation, we designed a new genetic strategy to differentially label mDA neuron subtypes by the use of the simultaneous activity of multiple promoters. We developed three transgenic mouse lines called *Pitx3-ITC*, *Gucy2C-iCre*, and *Nrp2-FlpO*, to induce the expression of Cre-dependent and Flp-dependent reporter genes in mDA neuron subsets. With our new approach, we are now able to label SNc mDA neurons and their axonal projections within the dorsal striatum. Moreover, in our attempt to generate subset-specific Cre and Flp mouse lines, we developed new transgenic lines which sparsely label SNc mDA neurons, allowing the visualization of dendrites and axons at the single neuron level.

Results

1. Genetic strategy for subset-specific labelling of mDA neurons

To label and visualize mDA neuron subsets, we developed a new genetic approach which relies on a DNA construct called 'ITC' (from *I*FP – Td*T*omato – *C*itrine) (Figure 1A). ITC contains three genes encoding for three different fluorescent proteins: Infrared Fluorescent Protein (IFP), TdTomato, and Citrine. A unique stop cassette at the end of each gene prevents the expression of the following gene, so that each neuron can express only one of the three fluorescent proteins. Two *loxP* sites flank the IFP gene and two *frt* sites flank IFP-TdTomato. This genetic strategy allows: (1) the expression of IFP in all cells where the ITC promoter is active; (2) a Cre-mediated recombination of *loxP* sites, the consequent excision of IFP and the expression of TdTomato under the control of the ITC promoter; (3) a Flp-mediated recombination of *frt* sites resulting in the excision of both IFP and TdTomato genes, and the expression of Citrine (Figure 1A).

To evaluate the correct functioning of ITC, it was inserted into a construct downstream the human CMV promoter, and then transfected into HEK 293 cells. As expected, transfected cells were IFP^{+} but $TdTomato^{-}$ and $Citrine^{-}$ (Figure 1B). Co-transfection of ITC and improved Cre (iCre) resulted in the exclusive expression of TdTomato (Figure 1C); while cells co-transfected with ITC and FlpO showed only expression of Citrine (Figure 1D). Co-transfection of iCre and FlpO together with ITC induced exclusive expression of Citrine (Figure 1E), because of excision of both IFP and TdTomato. These results demonstrate that ITC works efficiently and selectively.

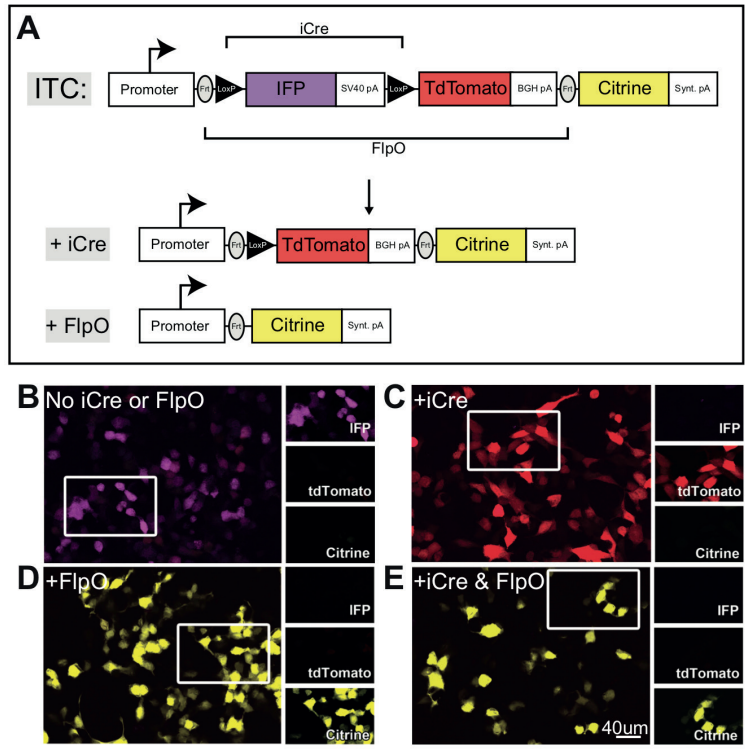

Figure 1

(A) Schematic representation of the Pitx3-ITC BAC construct. In absence of iCre or FlpO recombinases, IFP is expressed. Recombination of *loxP* sites by iCre results in removal of the IFP gene and expression of TdTomato. Expression of Citrine can be induced by recombination of the *frt* sites mediated by FlpO or FlpE. (B) HEK 293 cells transfected with CMV-ITC expressing IFP, but not TdTomato or Citrine. (C) Co-transfection with iCre induces the exclusive expression of TdTomato, while co-transfection with FlpO induces Citrine expression (D). (E) Combined expression of ITC, iCre and FlpO results in expression of Citrine. On the right, separate channels are shown.

2. Selection of promoters to label mDA neuron subsets *in vivo*

Our new genetic approach for labelling different mDA neuron subsets requires the selection of cell-subset specific promoters. The ITC promoter restricts the expression of the fluorescent reporters to a specific neuronal population, such as the entire dopamine system of the midbrain, while Cre and Flp promoters allow labelling of smaller cell-subsets belonging to the same neuronal population, such as for example SNc and VTA mDA neurons (Figure 2A). Because the ITC promoter restricts ITC expression to a specific brain region, the two promoters that drive Cre and Flp may be active also outside this region, since their activity will not activate ITC expression here.

To regulate ITC expression *in vivo*, we selected the *Pitx3* promoter. It has been described that, endogenously, Pitx3 is a transcription factor expressed by all mDA neurons. Its expression starts from embryonic day (E) 11.5, a very early developmental stage which corresponds to the terminal differentiation of mDA neurons, and continues throughout life (Smidt et al., 1997; Veenvliet and Smidt, 2014). We therefore selected the *Pitx3* promoter to restrict ITC expression to mDA neurons *in vivo* from early developmental time points until adulthood (Figure 2A).

A few Cre mouse lines have been generated to target VTA neurons, such as *Otx2-Cre* and *CCK-Cre* mice (Fossat et al., 2006; Taniguchi et al., 2011). Although these can be used together with the *Pitx3-ITC* mouse line to specifically label VTA mDA neurons, Cre mouse lines to target SNc mDA neurons were lacking. Furthermore, Flp mouse lines are rare. In order to be more flexible in choosing which mDA subset to label *in vivo*, we generated a new Cre mouse line to target SNc mDA neurons, and a new Flp mouse line to label VTA mDA neurons. To identify selective promoters to drive Cre or Flp expression, we searched the Allen Brain Atlas (www.brain-map.org). This atlas enabled us to visualize the mRNA expression pattern of genes of interest in the adult brain, and to generate a list of genes which are selectively expressed in SNc or VTA regions. To assess whether these genes were expressed and selective for SNc or VTA also at early developmental time points, their expression pattern was analyzed by *in-situ* hybridization at E13.5 and E16.5. In parallel tissue sections, *in-situ* hybridization for *Pitx3* was performed to delineate the entire dopamine system. These experiments identified Neuropilin-2 (*Nrp2*) and Guanylate cyclase 2C (*Gucy2C*) as markers for VTA and SNc areas, respectively (Figure 2B). *Nrp2* was detected in the medial dopamine system at both time points, as previously reported in other studies (Kolk et al., 2009; Torigoe et al., 2013; Yamauchi et al., 2009). *Gucy2C* expression was confined to the lateral dopamine system at E13.5 and E16.5.

In conclusion, we selected specific promoters for driving the expression of ITC into mDA neurons (*Pitx3*) and the expression of Cre and Flp into subsets of mDA neurons (*Nrp2* and *Gucy2c*) (Figure 2A).

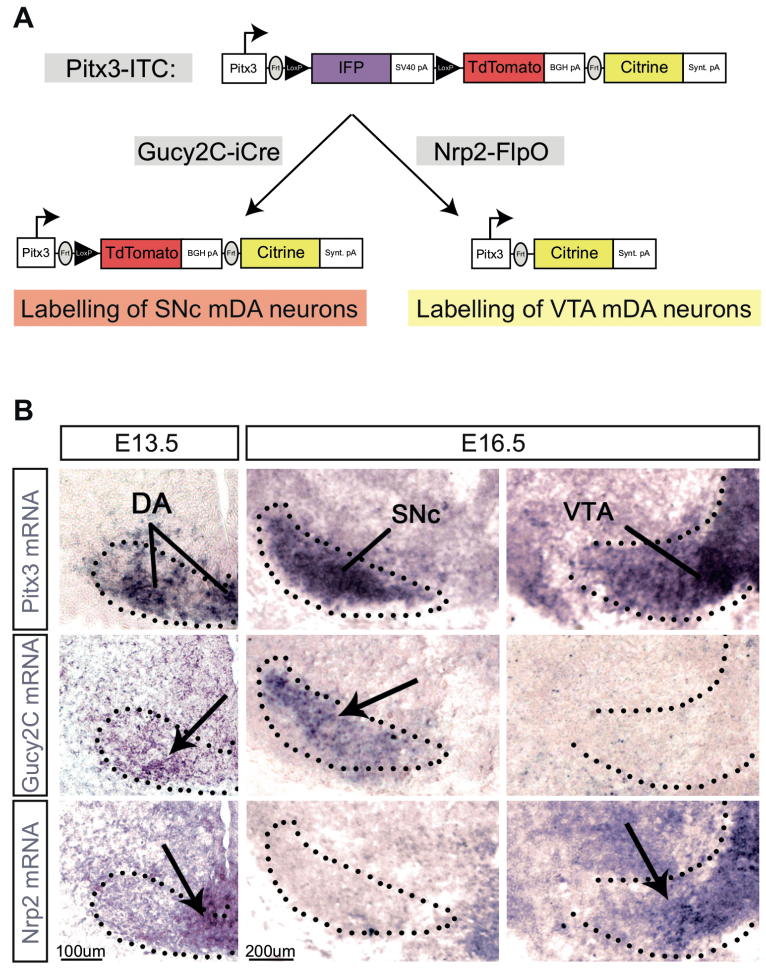

Figure 2

(A) Genetic strategy to induce the expression of different fluorescent proteins in distinct mDA neuron subsets by the use of multiple promoters *in vivo*. The *Pitx3* promoter restricts ITC expression to mDA neurons from early developmental stages. Specific Cre and Flp mouse lines induce different Pitx3-ITC rearrangements in specific mDA neuron subsets. In this way, TdTomato, Citrine, and IFP are expressed by different mDA neuron populations. (B) *In situ* hybridization for *Pitx3*, *Gucy2C*, and *Nrp2* on coronal midbrain sections from E13.5 and E16.5 wild type brains. The midline is on the right. *Pitx3* is expressed by the entire mDA system from early developmental stages. *Gucy2C* expression is selective for SNc mDA neurons, while *Nrp2* is enriched in VTA mDA neurons.

3. Characterization of *Pitx3-ITC* transgenic mice

3.1 *In vivo* Cre/Flp-dependent labelling of mDA neurons

Four *Pitx3-ITC* founder mouse lines (Founder 1-4) were generated using a BAC transgenic approach (Gong et al., 2002), and ITC expression patterns were evaluated in all four mouse lines. As expected, TdTomato and Citrine were not detected *in vivo* by immunohistochemistry. Unexpectedly, IFP expression was also not detected (data not shown). To detect IFP expression *in vitro* and *in vivo*, two different promoters were used, i.e. *CMV* and *Pitx3* respectively. Therefore, IFP expression levels may be lower *in vivo* as compared to in HEK 293 cells and for this reason not detectable. Unfortunately, no anti-IFP antibodies are available and we rely on endogenous signals for detection. In addition, IFP requires the incorporation of biliverdin as a chromophore. Although biliverdin is endogenously expressed in mice and spontaneously incorporated by IFP, intravenous injection of biliverdin may increase IFP fluorescence intensity up to five times (Shu et al., 2009). However, intravenous injection of biliverdin in adult *Pitx3-ITC* mice did not allow us to detect IFP signals (data not shown).

To assess whether TdTomato expression could be induced in Cre^+ mDA neurons and Citrine expression in Flp^+ mDA neurons, we crossed *Pitx3-ITC* mice from Founder 2 with *EIIa-Cre* (Lakso et al., 1996) or *ACTB-FlpE* mice (Rodríguez et al., 2000), respectively. Both *EIIa-Cre* and *ACTB-FlpE* mouse lines ubiquitously express Cre or FlpE at early stages of development, inducing the excision of *loxP*-flanked or *frt*-flanked genes in every cell of the mouse body. PCR was performed on genomic DNA extracted from *Pitx3-ITC:ABCT-FlpE* mice and confirmed that FlpE completely removed *IFP* (Figure 3A). Since FlpE and Cre rearrange ITC in all neurons of the CNS, inter crossing *EIIa-Cre* and *ACTB-FlpE* mice with *Pitx3-ITC* mice should result in expression of Citrine and TdTomato, respectively, by all $Pitx3^+$ mDA neurons (Figure 3B-C). To identify mDA neurons by immunohistochemistry, tyrosine hydroxylase (TH) was used as marker. Immunohistochemical analysis for Citrine on *Pitx3-ITC:ACTB-FlpE* adult brains showed that Citrine is not expressed by all mDA neurons, but in contrast is expressed by a subset of neurons confined to the lateral mDA system (Figure 3B). In particular, $Citrine^+$ mDA neurons appeared enriched in the ventral part of the SNc (vSNc) (Figure 3B). A similar expression pattern was observed for TdTomato in *Pitx3-ITC:EIIa-Cre* mouse tissue (Figure 3C). Because similar expression patterns were observed for TdTomato and Citrine, subsequent analyses of *Pitx3-ITC* mice were performed using *Pitx3-ITC:ACTB-FlpE* mice and by detecting Citrine protein. Citrine signals were higher as compared to TdTomato following immunostaining.

It has been described in literature that SNc and VTA mDA neurons partly innervate distinct areas of the striatum: SNc mDA neurons mainly project into

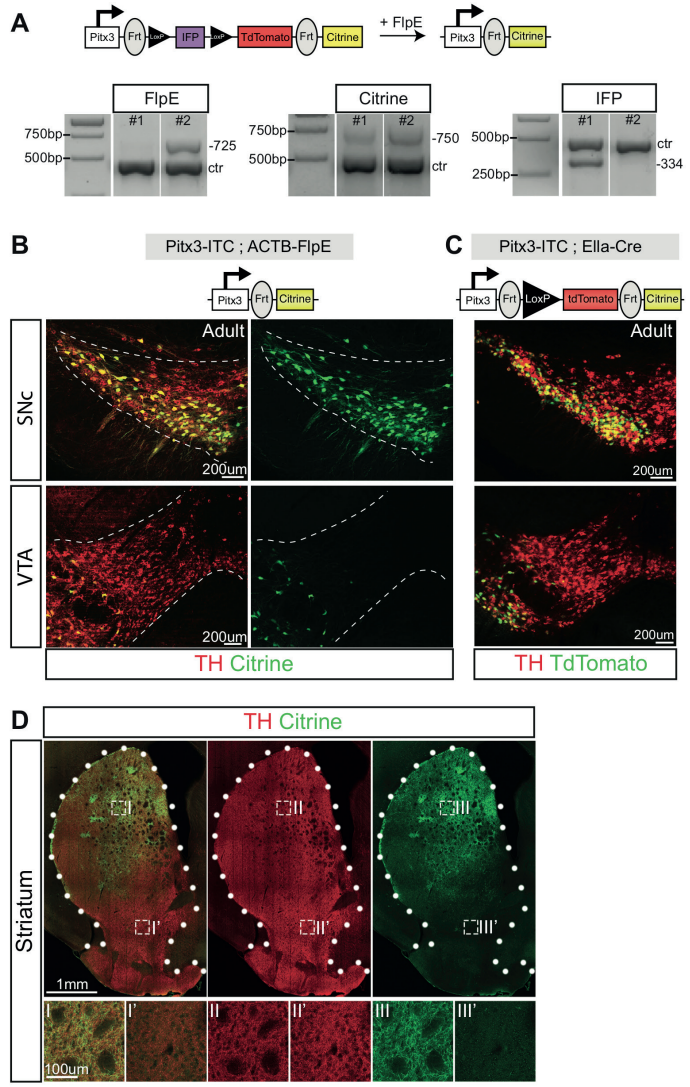

Figure 3

(A) PCR performed on genomic DNA from *Pitx3-ITC:ABCT-FlpE* mice. In absence of FlpE recombinase, both *IFP* and *Citrine* genes are present in the genome (left columns). The ubiquitous expression of FlpE determines the removal of the *IFP* gene, while the *Citrine* gene, located downstream the two *frt* sites, remains in place (right columns). (B-C) Expression of FlpE or Cre in the germline results in the recombination of the *frt* or *loxP* sites in every cell of the brain, and in Pitx3-driven expression of Citrine (B) or TdTomato (C). Immunohistochemistry on coronal sections of adult mouse midbrain. Dopaminergic neurons are identified by TH. $Citrine^+$ or $TdTomato^+$ neurons are confined almost exclusively to lateral regions of the mDA system. (D) Selective visualization of nigrostriatal fibers in the adult dorsal striatum. Immunohistochemistry on a representative coronal section from the middle striatum. All dopaminergic axons are visualized by TH immunostaining.

the dorsal striatum, while VTA mDA neurons innervate the ventral striatum (Ikemoto, 2007; Lammel et al., 2008). In line with this, the adult striatum of *Pitx3-ITC:ACTB-FlpE* mice showed dopaminergic Citrine$^+$ axons confined to the dorsal striatum, whereas the ventral striatum was almost totally devoid of Citrine$^+$ fibers (Figure 3D). These data support the results observed in the midbrain, indicating that *Pitx3-ITC:ACTB-FlpE* enables the visualization of a specific mDA neuron subset.

Outside the midbrain, we could detect Citrine$^+$ but TH$^-$ neurons in two other brain areas, the posterior midbrain and the cortex (Figure 4), while the rest of the brain was devoid of Citrine$^+$ cells. To understand whether Citrine$^+$/TH$^-$ neurons could interfere with studies focused on the dopamine system both during brain development and adulthood, these two neuronal populations were further characterized. The first population resides at the ventral edge of the inferior colliculus from very early developmental stages (E12.5) till adulthood. Citrine$^+$ axons from this region travelled first towards the ventral midline of the midbrain, and then they turned towards the spinal cord (Figure 4A). This means that these axons do not intermingle with developing SNc mDA axons running towards the forebrain. The second population of sparse Citrine$^+$/TH$^-$ neurons was positioned into layers Vb and VIa of the anterior cortex (motor cortex, anterior cingulate area, prelimbic area, infralimbic area) (Figure 4B). These cortical Citrine$^+$/TH$^-$ neurons and axons appear at P10, a postnatal time point during which the dopamine system is highly developed. In addition, most of these Citrine$^+$ neurons were CTIP$^+$ (Figure 4B), a marker for corticospinal motor neurons and corticotectal neurons of layer V and corticothalamic neurons of layer VI (Arlotta et al., 2005). This indicates that cortical Citrine$^+$ neurons do not innervate the striatum and do not intermingle with Citrine$^+$/TH$^+$ SNc mDA axons. Interestingly, these two Citrine$^+$/TH$^-$ neuronal populations were previously detected in another mouse model called *Pitx3-Cre*, which expresses Cre under the control of the *Pitx3* promoter (Smidt et al., 2012). The similarities between the two mouse models suggest that *Pitx3* may not be expressed exclusively by mDA neurons, but also in two other brain areas outside the midbrain. For our next experiments, we focused on Citrine$^+$/TH$^+$ neurons, which are localized only in the midbrain.

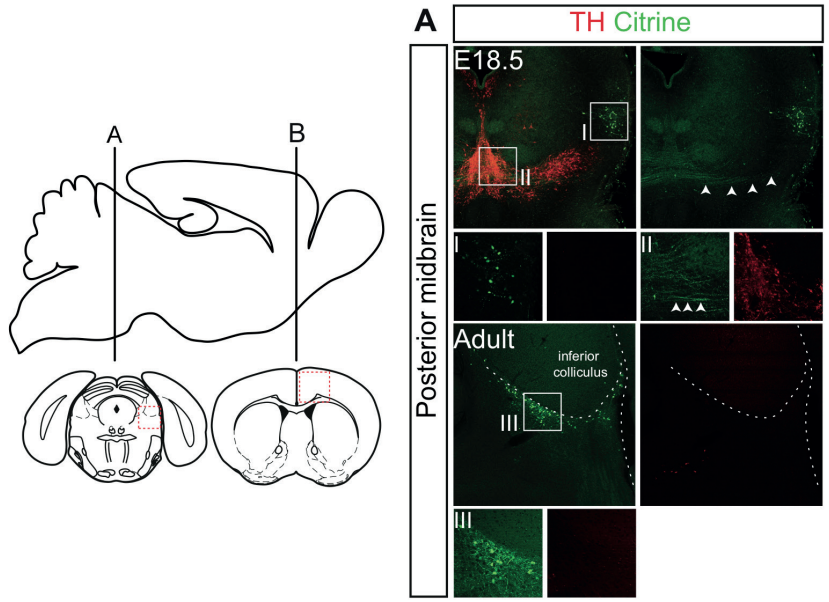

Figure 4

Citrine expression outside the mDA system in *Pitx3-ITC:ABCT-FlpE* mice. (A) Citrine$^+$/TH$^-$ neurons are detected in the posterior midbrain at the ventral edge of the inferior colliculus. These neurons are visible from very early developmental stages (E12.5) till adulthood. Citrine$^+$ axons from the inferior colliculus travel first towards the ventral midline of the midbrain (white arrows), and then they turn towards the spinal cord. (B) From P10 till adulthood, Citrine$^+$/TH$^-$ neurons are present into layers Vb and VIa of the anterior cortex. Most of these Citrine$^+$ neurons are CTIP$^+$, a marker for corticospinal motor neurons and corticotectal neurons of layer V and corticothalamic neurons of layer VI.

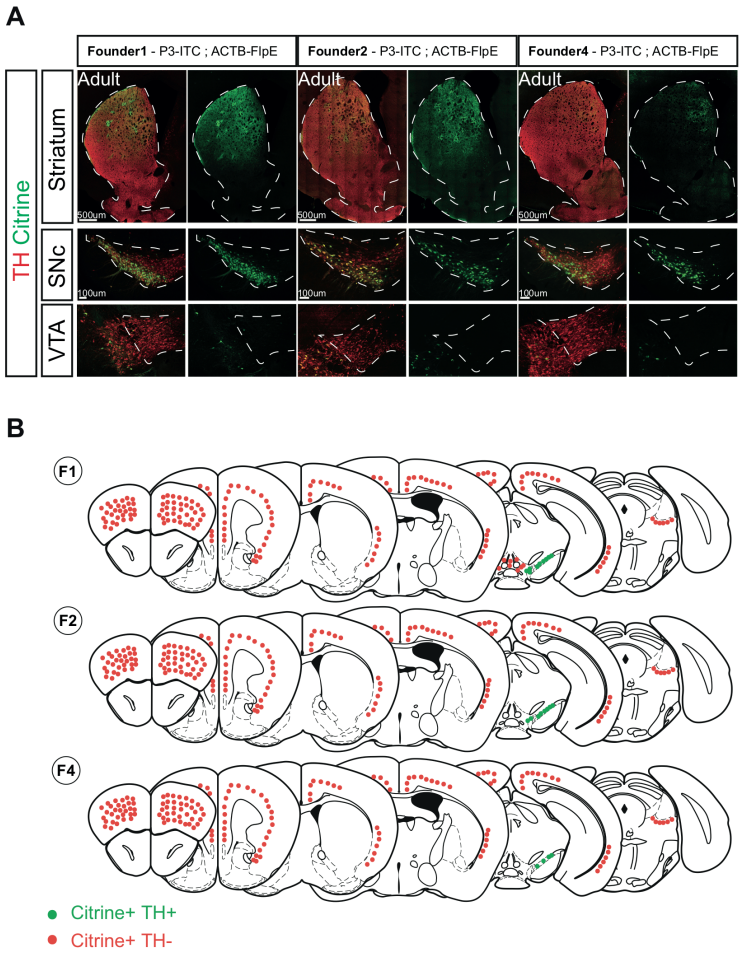

Figure 5

Comparison of Citrine expression patterns in three different *Pitx3-ITC* founder mouse lines. (A) Comparable coronal sections from the middle striatum (top row), SNc (middle row), and VTA (bottom row) from adult brains. The mDA system is delineated using TH immunostaining. In all three founders, Citrine$^+$ neurons are located in the SNc, and nigrostriatal axons are visible in the dorsal striatum. (B) Schematic representation of Citrine$^+$/TH$^+$ (green) and Citrine$^+$/TH$^-$ (red) neurons detected in the three founders (F1, F2, and F4).

Next, we analyzed and compared the four different *Pitx3-ITC* founder mouse lines. The analysis was performed by crossing the founders with *ACTB-FlpE* mice and by analyzing by immunohistochemistry the position of all Citrine$^+$/TH$^+$ and Citrine$^+$/TH$^-$ neurons (Figure 5A, B). Founder 3 did not show any Citrine$^+$ neurons, but the other three *Pitx3-ITC* mouse lines displayed a comparable distribution of Citrine$^+$ neurons. Surprisingly, all three lines labeled a subset of mDA neurons in the SNc, while almost no positive neurons were detected in VTA (Figure 4A). Although the distribution of Citrine$^+$ neurons in the midbrain was very similar between different founders, we detected a few differences. Founder 4 labeled the smallest number of mDA neurons in the midbrain, and showed the most restricted area of dopaminergic striatal innervation. Founder 1 labeled a large number of mDA neurons, in addition to a group of TH$^-$ neurons positioned in the posterior hypothalamic nucleus, located between the two wing-like structures formed by SNc neurons. Founder 2 labelled the highest number TH$^+$ neurons. In line with these observations, dopaminergic Citrine$^+$ fibers innervated the dorsal striatum in all three founders (Figure 5A). Outside the midbrain, Citrine$^+$/TH$^-$ neurons were detected in the posterior midbrain and in the cortex in all three founders. For subsequent analyses, we focused on Founder 2, which labeled a large number of mDA neurons, without labelling of TH$^-$ neurons in the midbrain.

In conclusion, the new genetic strategy Pitx3-ITC allows the visualization of a subset of mDA neurons positioned in the SNc by inducing Cre-dependent TdTomato or Flp-dependent Citrine expression.

3.2 Pitx3-ITC labels SNc mDA neurons

To specifically define the neuron subset labeled in *Pitx3-ITC* mice, we determined by co-immunohistochemistry the number of neurons which co-express TH and Citrine, to establish whether all Citrine$^+$ neurons are dopaminergic. The quantification performed on adult midbrain tissue confirmed that all Citrine$^+$ neurons are TH$^+$, meaning that Pitx3-ITC only labels dopaminergic neurons (Figure 6A, C). We then evaluated the co-localization of Citrine with Sox6 and Otx2, markers for SNc and VTA mDA neurons, respectively (Panman et al., 2014). Quantification of these data demonstrates that 86% of Citrine$^+$ neurons are Sox6$^+$, while 2,9% are Otx2$^+$, showing that the large majority of neurons labeled in adult *Pitx3-ITC* mice are SNc mDA neurons (Figure 6A, C). Next, we assessed Citrine co-localization with TH, Sox6, and Otx2 at E18.5, to evaluate whether Pitx3-ITC labels the same neuronal subset during midbrain development. At E18.5, 98% of Citrine$^+$ neurons express TH, 91% are Sox6$^+$, and 4,1% are Otx2$^+$ (Figure 6B, C). These results demonstrate that *Pitx3-ITC:ACTB-FlpE* mice selectively label SNc mDA neurons *in vivo*.

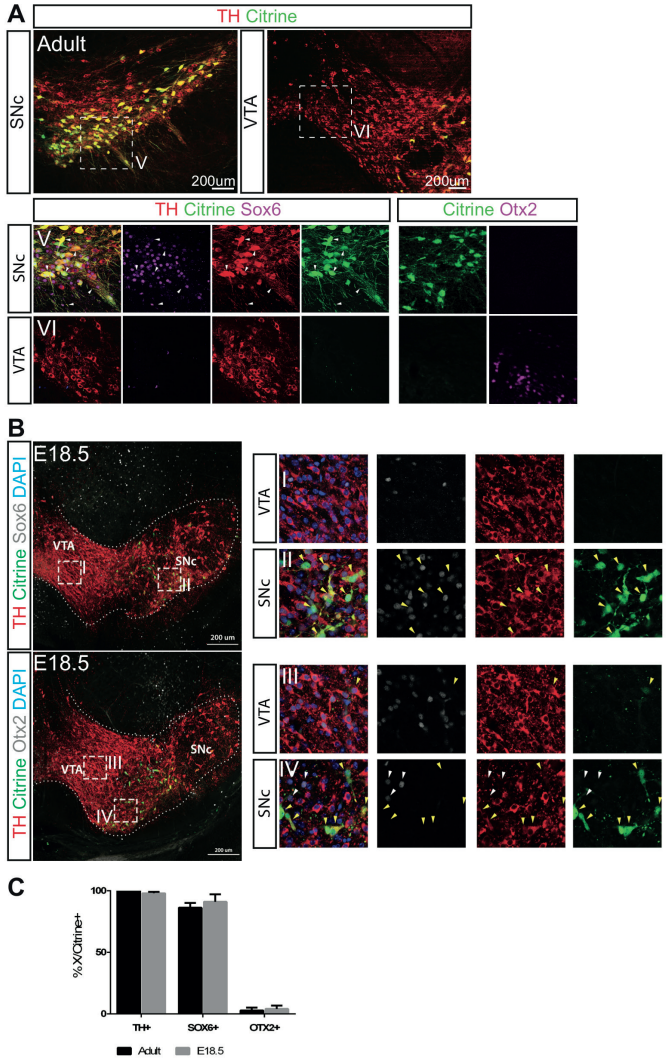

Figure 6

Immunohistochemistry for Citrine, TH, Sox6, and Otx2 on midbrain coronal sections from adult and E18.5 *Pitx3-ITC:ABCT-FlpE* mice. (A-B) Citrine$^+$ neurons co-localize with TH staining, confirming their dopaminergic nature. SNc mDA neurons are identified by the SNc-specific transcription factor Sox6. Staining for the VTA-specific transcription factor Otx2 does not label Citrine$^+$ neurons. (C) Quantification of co-localization of Citrine and TH, Sox6 or Otx2 in adult and E18.5 embryonic brains. Data are shown as percentages of the Citrine$^+$ neurons, from 3 different animals. Mean ± SD.

4. Characterization of *Gucy2C-iCre* and *Nrp2-FlpO* transgenic mice

4.1 Gucy2C-iCre sparsely labels neurons in the ventral midbrain

Five *Gucy2C-iCre* founder mouse lines were generated by BAC transgenesis (Gong et al., 2002) and characterized. In order to determine the expression pattern of iCre in the brain of all five founders, these mice were crossed with a Cre reporter mouse line called 'R26-stop-EYFP' (Srinivas et al., 2001). This mouse line has a EYFP transgene located downstream a *loxP*-flanked STOP sequence. In every neuron expressing iCre, the STOP sequence is excised and EYFP expression is activated (Figure 7A). Analyses were performed in adult brains by co-immunohistochemistry for EYFP and TH. Two *Gucy2C-iCre* founder lines did not show EYFP$^+$ neurons in any brain region, whereas the other three lines (F1, F10, and F13) displayed similar iCre expression patterns with a few differences. In contrast to our expectations, the midbrain of *Gucy2C-iCre* mice did not show broad labelling of SNc neurons. Instead both the SN and VTA displayed very sparse EYFP labelling of TH$^+$ and TH$^-$ neurons (Figure 7A). Outside the midbrain, EYFP labelling differed in different founders (Suppl. Figure 1). For example, sparse EYFP labelling was found in the striatum and in the posterior hypothalamic nucleus in founder 10 or in the septum in founder 13. Next, we crossed *Gucy2C-iCre* and *Pitx3-ITC* mice, and assessed the location of TdTomato$^+$ neurons. As expected, sparse labelling of TdTomato$^+$/TH$^+$ neurons was confined to the SNc, while no TdTomato$^+$/TH$^+$ neurons were detected in the VTA (Figure 7B). Other parts of the brain were devoid of TdTomato$^+$/TH$^-$ neurons (data not shown). Unfortunately, due to relatively low TdTomato expression, we could not clearly visualize dendritic and axonal projections of single SNc mDA neurons. Together, these data show that the combined activity of *Pitx3* and *Gucy2C* promoters successfully allows the selective visualization of a very small subset of SNc mDA neurons.

4.2 Nrp2-FlpO allows labelling of single SNc mDA neurons

Four *Nrp2-FlpO* founder mouse lines were generated using the same BAC transgenic approach applied for generating *Gucy2C-iCre* mice (Gong 2002). To characterize and compare FlpO expression in the four founder mouse lines, we crossed each *Nrp2-FlpO* with a Flp-dependent EGFP reporter mouse line (called $R26^{ZG}$) originally obtained from another mouse line called $R26^{NZG}$ (Yamamoto et al., 2009). This reporter line has a *EGFP* gene downstream an *frt*-flanked *LacZ* gene. In all neurons expressing FlpO, *LacZ* is excised and, as a result, EGFP is expressed (Figure 8A). EGFP expression pattern was then assessed by immunohistochemistry in adult brains (Figure 8B-G). Three out of

four founder mouse lines showed EGFP$^+$ neurons in the brain. In the midbrain, sparse labelling of TH$^+$ and TH$^-$ neurons was observed, with a higher number of EGFP$^+$ neurons in the VTA as compared to the SNc (Figure 8A, D). All founders displayed EGFP expression outside the midbrain in regions such as the cortex, septum, hypothalamus, and hippocampus (Figure 8E, Suppl. Figure 1). For subsequent experiments, we used the founder (founder 595) which expressed FlpO in the largest number of TH$^+$ neurons in the midbrain, with minimal labeling outside the midbrain.

To continue our analysis, *Nrp2-FlpO* mice were crossed with *Pitx3-ITC* mice to restrict fluorescent reporter expression to mDA neurons (Figure 8H). In the midbrain, in all neurons expressing FlpO, IFP and TdTomato genes are removed and Citrine is expressed under the control of the *Pitx3* promoter. As expected, *Nrp2-FlpO:Pitx3-ITC* mice showed sparse Citrine expression only in mDA neurons of the SNc (Figure 8I-K). Outside the midbrain, only a few Citrine$^+$/TH$^-$ neurons were detected in the cortex (data not shown), while other regions of the brain were devoid of Citrine expression (Figure 8I). Combining *Pitx3-ITC* and *Nrp2-Flp* mice allows for the selective labeling of a small population of mDA in the SNc (compare Figure 8E to Figure 8I). Although the *Nrp2-FlpO* mouse line was originally developed to target VTA neurons, it may be used instead for labeling single SNc mDA neurons, after crossing with *Pitx3-ITC*. Moreover, since the labelling is very sparse and Citrine expression levels are high, the *Nrp2-FlpO:Pitx3-ITC* mouse model enables visualization of dendritic and axonal projections of single SNc mDA neurons (Figure 9). The morphology of developing and adult mDA dendrites can be reconstructed *in vivo* and used to study dopaminergic dendrite development, or to visualize morphological alterations in pathological conditions. Within the dorsal striatum, we could observe the presence of extensive Citrine$^+$ axonal arborizations or bushes (Figure 9B). The number of these structures is comparable to the number of the Citrine$^+$ mDA neurons found in the midbrain (n=1 brain), indicating that each Citrine$^+$ axonal arborization is the branching product of a single Citrine$^+$ SNc mDA neuron. Indeed, it has been described that each SNc mDA neuron generates extensive axonal arborizations *in vivo*, establishing connections with on average 75.000 striatal neurons (Matsuda et al., 2009).

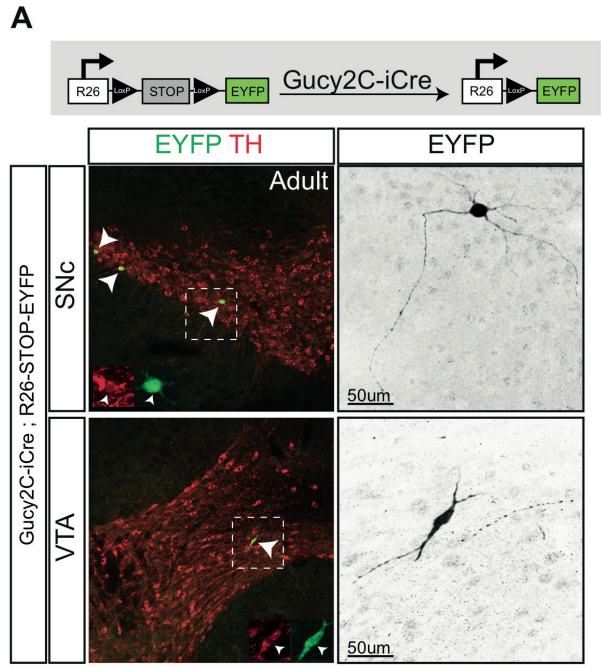

Figure 7

Characterization of *Gucy2C-iCre* mice. (A) *Gucy2C-iCre* mice are crossed with EYFP reporter mice (*R26-STOP-EYFP*). EYFP is expressed by all iCre$^+$ neurons. Both SNc and VTA display very sparse EYFP labelling of TH$^+$ and TH$^-$ neurons. (B) *Gucy2C-iCre* mice are crossed with *Pitx3-ITC* mice. Sparse labelling of TdTomato$^+$/TH$^+$ neurons is confined to SNc, while no TdTomato$^+$/TH$^+$ neurons are present in the VTA.

Discussion

Pitx3-ITC labelling of SNc mDA neurons

To further dissect the molecular and cellular mechanisms which underlie the heterogeneous properties of mDA neurons, we developed a new genetic tool called Pitx3-ITC. Mouse lines are available to target mDA cell subtypes, for example the *Cck-Cre* and the *Otx2-Cre* lines (Fossat et al., 2006; Taniguchi et al., 2011). However, these lines are selective for VTA mDA neuron subsets, and in addition to VTA label many other (non-dopaminergic) neurons outside the midbrain. This hampers selective visualization of mDA cell bodies and processes. With the *Pitx3-ITC* mouse line, we can now selectively label SNc mDA neurons both in developing and adult brains. Furthermore, in *Pitx3-ITC* mice SNc mDA axons can be traced from the midbrain to the striatum, where they establish connections with medium spiny neurons. Thus, *Pitx3-ITC* allows to distinguish SNc mDA neurons and axons from other TH$^+$ neurons in the midbrain. This provides unique opportunities for studying their migration and axon guidance throughout development, both in wildtype and knock-out mice. Although two other small, non-dopaminergic neuronal populations are labeled in *Pitx3-ITC* mice, i.e. in the posterior midbrain and the cortex, these do not interfere with the selective labeling of SNc mDA neurons. Both populations are located far from the mDA system and can easily be identified. Furthermore, their axons do not intermingle with SNc mDA axons.

Our analysis of coronal sections of *Pitx3-ITC:ACTB-FlpE* brains shows that Citrine$^+$ mDA neurons are confined to the lateral part of the mDA system. In particular, these neurons appear enriched in the ventral SNc (vSNc) as compared to the dorsal SNc (dSNc) (Figure 3B). Molecular markers specifically expressed only in one of the two populations and not in other mDA subsets have not been identified yet. However, two studies discovered molecular signatures useful to identify different mDA neuron subsets (La Manno et al., 2016; Poulin et al., 2014). In a recent review, we compared the results of these two studies and noticed that together these studies identify five mDA neuron subsets based on molecular properties (Brignani and Pasterkamp, 2017). Two of these mDA neuron clusters correspond to vSNc and dSNc. To determine whether the mDA subset labeled in *Pitx3-ITC:ACTB-FlpE* mice is mainly composed of vSNc mDA neurons, Citrine$^+$ mDA neurons should be analyzed further and compared with mDA neuron clusters identified by (La Manno et al., 2016; Poulin et al., 2014). First, Citrine$^+$ mDA neurons can be sorted by FACS from the midbrain of *Pitx3-ITC:ACTB-FlpE* mice. Followed by qPCR for a set of selected genes, which could be for example: (1) *Sox6*, a marker for all SNc mDA neurons; (2) *Calbindin 1* (Calb1), expressed by dSNc mDA neurons and by all VTA mDA neurons; (3) *Aldh1a1*, a marker for vSNc mDA neurons and a group of VTA neurons; (4) *Cck* and/or *Otx2*, expressed only by VTA mDA neurons. This analysis will determine

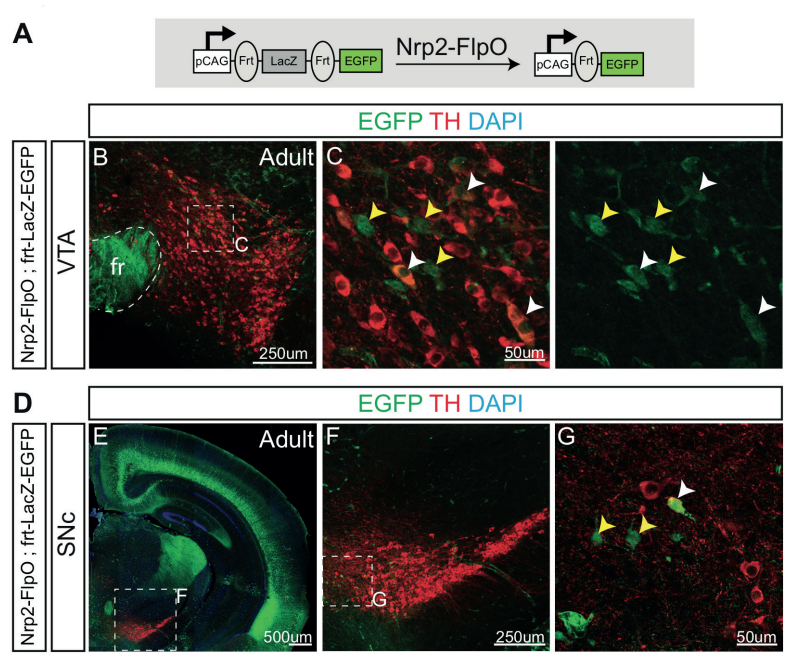

Figure 8

Characterization of *Nrp2-FlpO* mice. (A) *Nrp2-FlpO* mice are crossed with *R26^{ZG}* reporter mice. EGFP is expressed by all FlpO$^+$ neurons. (B-G) In the midbrain, sparse labelling of TH$^+$ and TH$^-$ neurons is observed, with a higher number of EGFP$^+$ neurons in the VTA as compared to the SNc. (E) Outside the midbrain, several brain regions display EGFP$^+$ neurons, such as the cortex and the hippocampus. (H-K) *Nrp2-FlpO* are crossed with *Pitx3-ITC* mice to restrict fluorescent reporter expression to mDA neurons. (J-K) *Nrp2-FlpO:Pitx3-ITC* mice show sparse Citrine expression only in SNc mDA neurons. (I) Almost no Citrine$^+$ neurons are found outside the midbrain.

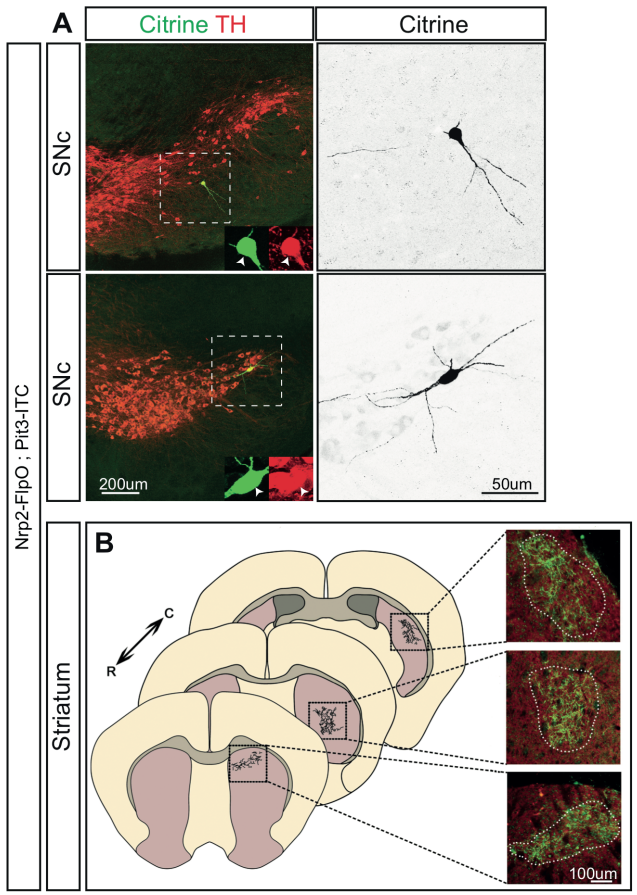

Figure 9

Nrp2-FlpO:Pitx3-ITC brains allow the visualization of dendrites (A) and axons (B) of single SNc mDA neurons. (A) Immunohistochemistry for TH and Citrine on SNc coronal sections. Dendrites of single SNc mDA neurons can be visualized. (B) Schematic representation of axon branches of single SNc mDA neurons in the dorsal striatum along the rostro-caudal axis (R-C). Corresponding coronal brain sections stained for TH and Citrine are shown on the right.

the identity of Citrine$^+$ mDA neurons isolated from *Pitx3-ITC:ACTB-FlpE* mice, to understand whether these neuron have a molecular signature similar to vSNc mDA neurons, or or a more general SNc profile.

Why do the BAC mouse lines not display the expected expression profiles?

Since ITC expression is driven by the *Pitx3* promoter, the entire mDA system should be labeled in *Pitx3-ITC* mice rather than only a subset of SNc mDA neurons. This selective expression is particularly hard to explain if we consider the expression patterns observed in previously published *Pitx3-Cre* and *Pitx3-GFP* mice (Smidt et al., 2012; Zhao et al., 2004). In these mouse lines, both Cre and GFP expression is successfully driven by the *Pitx3* promoter in all mDA neurons, indicating that the activity of this promoter functions as expected *in vivo*. In addition, although it is well known that BAC transgenesis entails a random insertion of the BAC construct into the genome, all three *Pitx3-ITC* founders showed very similar ITC expression patterns, with no labelling of VTA mDA neurons. It is likely that in the three founders, Pitx3-ITC was integrated at different genomic positions and that Pitx3-ITC integration sites are not responsible for lack of VTA labelling. In contrast, the selective nature of the *Pitx3-ITC* line may be caused by intrinsic technical limitations of the BAC transgenesis method or by an error introduced during the generation of the BAC construct. The Pitx3-ITC BAC construct may lack fundamental regulatory elements required to activate the *Pitx3* promoter specifically in VTA mDA neurons. Since both *Pitx3-Cre* and *Pitx3-GFP* mice were generated using a knock-in approach, in these mice all the required regulatory elements are in place to induce the correct activity of *Pitx3* and, in turn, the expression of Cre and GFP in all mDA neurons.

To generate a *Pitx3-ITC* mouse line which expresses ITC in all mDA neurons, we are now developing a new *Pitx3-ITC* mouse line applying a mouse knock-in approach. The new mouse line will be used in combination with mDA subset-specific Cre or Flp mouse lines that are being generated or that are already available. To drive Flp and Cre expression, mDA subset-specific promoters could be used that were identified in previous studies and recently reviewed by us (Brignani and Pasterkamp, 2017; La Manno et al., 2016; Poulin et al., 2014). Good examples are: (1) the promoter of *Grp* or of *Adcyap1*, both markers of a subset of VTA mDA neurons that specifically innervate the nucleus accumbens of the ventral striatum (Ekstrand et al., 2014); (2) the promoter of *Slc32a1* (also known as *Vgat*), active in another small subset of VTA mDA neurons which may project to the lateral habenula (Stamatakis et al., 2013); (3) the *Cck* promoter, which labels all VTA mDA neurons; (4) the *Sox6* promoter, specific for all SNc mDA neurons (Panman et al., 2014). *Grp-Cre*, *Adcyap1-Cre*, *Slc32a1-Cre*, *Cck-Cre* mouse lines are already available (Gerfen et al., 2013; Harris et al., 2014;

Taniguchi et al., 2011), while *Sox6-Cre* are being generated (data not published). We also generated *Nrp2-FlpO* and *Gucy2C-iCre* transgenic mice which, in combination with *Pitx3-ITC*, should have labeled mDA large neuron-subsets. Similar to *Pitx3-ITC* mice, FlpO and iCre mice showed an unexpected selective activity pattern in the midbrain. *Gucy2C-iCre* was designed to target SNc neurons, but *in vivo* labels a few neurons in both VTA and SNc. *Nrp2-FlpO* mice were generated to label VTA neurons, but *in vivo* FlpO is expressed in a few VTA neurons and in a very small number of SNc neurons. To date, the *Gucy2C* promoter has not been used to drive transgene expression *in vivo*, and therefore a comparison of our mouse model with available lines is not possible. The unexpected pattern of iCre expression in *Gucy2C-iCre* mice may be due to the BAC clone selected. In contrast, knock-in mice were generated to express the reporter β-galactosidase under the control of the *Nrp2* promoter (Takashima et al., 2002). In these mice, analysis of β-galactosidase expression pattern showed that Nrp2 labels medial mDA neurons both at E14.5 and at E16.5 (Torigoe et al., 2013), indicating that the activity of the *Nrp2* promoter *in vivo* should properly drive the expression of reporter genes in VTA mDA neurons. As discussed above for *Pitx3-ITC* mice, *Nrp2-FlpO* mice may show more selective expression as compared to knock-in mice because of the lack of fundamental regulatory elements. It is interesting to note that both *Pitx3-ITC* and *Nrp2-FlpO* BAC mouse lines show a more restricted expression pattern as compared to the respective knock-in mouse lines. In particular, in both BAC mouse lines, the abundant transgene expression expected in VTA mDA neurons is absent. It is therefore tempting to speculate that both BAC constructs lack fundamental regulatory elements required to drive gene expression specifically in VTA mDA neurons, while they contain regulatory elements needed for transcription in SNc mDA neurons.

Labelling of single mDA neurons

In the attempt to generate subset-specific Flp and Cre mouse lines to target VTA and SNc mDA neurons (*Nrp2-FlpO* and *Gucy2C-Cre* lines) respectively, we obtained two mouse lines which enable the visualization of single mDA neurons. Although these mouse lines displayed an unexpected selective labeling of mDA neurons, they represent a unique genetic tool. In *Nrp2-FlpO* mice crossed with *Pitx3-ITC* mice single SNc mDA neurons are labeled and both their dendrites and axonal bushes in the dorsal striatum are visible. To label single mDA neurons and their dendritic and axonal structure in adult rats, previous studies performed stereotactic microinjection of anterograde tracers (Matsuda et al., 2009; Prensa and Parent, 2001). These studies analyzed in detail the broad and dense morphology of the axonal bushes of single mDA neurons. Matsuda et al. calculated that a single mDA neuron may establish connections with around 75.000 striatal neurons. In line with these observations, *Nrp2-FlpO:Pitx3-ITC* showed extensive and dense Citrine^{+} axon bushes in the striatum, which most likely are the branching products of single SNc mDA axons. On the other hand, in contrast to previous studies relying tracer injections, our mouse model does not require an invasive procedure in order to label single neurons. This feature makes *Nrp2-FlpO:Pitx3-ITC* mice a new and useful tool to visualize the morphology of single SNc mDA neurons both in adulthood and during brain development. Especially in this latter case in fact, tracer injections would be technically unfeasible. Being able to visualize dendrites and axon bushes of single mDA neurons offers the opportunity to establish how these structures develop, how they may degenerate in disease conditions, and which molecules play a role in these processes. In particular, Parkinson's disease is characterized by a progressive degeneration of the nigrostriatal pathway, and synaptic and axonal alterations appear to precede the loss of neuronal cell bodies in the SNc of human brains (Burke and O'Malley, 2013; Cheng et al., 2010; Kordower et al., 2013). The extent and spatiotemporal development of these pre-symptomatic changes remains largely unknown because of the lack of tools to visualize individual neurons and their connections. *Nrp2-FlpO:Pitx3-ITC* can be applied for studying pre-symptomatic alterations in dopaminergic circuitry caused by mutations in Parkinson's disease genes, and insight into these pre-symptomatic changes will help to further reveal the pathogenic effect of genetic defects associated with Parkinson's disease and to define potential therapeutic windows. In conclusion, together with single-cell specific *Nrp2-FlpO* and *Gugy2C-Cre* mice, the *Pitx3-ITC* mouse line provides new opportunities to unveil the molecular mechanisms required for different aspects of the function and development of specific mDA neuron subsets.

Materials and methods

ITC, iCre, and FlpO DNA vectors

For assembling the ITC construct, Citrine was first cloned into the psiCheck2 vector (Promega) which contains a Synthetic poly(A) sequence. Primers containing an *frt* site were used to clone Citrine and the synthetic poly(A) sequence into pcDNA3.1(Invitrogen). TdTomato with a bGH poly(A) sequence was subsequently cloned upstream of Citrine. IFP with a SV40 poly(A) sequence was cloned upstream TdTomato using primers containing *loxP* and *frt* sites generating ITC. To express iCre and FlpO in HEK 293 cells, CMV-iCre and CMV-FlpO expression vectors were generated by cloning iCre and FlpO into pcDNA3.1.

Cell cultures and transfections

Human embryonic kidney cells (HEK 293) were transfected using Lipofectamine 2000 (Invitrogen) according to manufacturer's protocol. 1.75 µl of Lipofectamine 2000 was diluted in 25 µl Opti-MEM (Gibco). Separately, DNA encoding for ITC, iCre, or FlpO was added to 25 µl Opti-MEM. Both Opti-MEM solutions were mixed and incubated for 10 min, then directly added to each well. After 72 h, cells were fixed in 4% PFA, washed in PBS, and mounted in Prolong Gold antifade reagent (Invitrogen).

BAC recombination and mouse lines

All animal use and care were in accordance with institutional guidelines. Targeting constructs were assembled in pGEM-T Easy (Promega). ITC was flanked by sequences homologous to 458 bp upstream of the Pitx3 ATG start codon in exon 2 and 450 bp downstream of exon 2, FlpO by sequences homologous to 440 bp upstream of the Nrp2 ATG start codon in exon 1 and 447 bp downstream of exon 1, and iCre by sequences homologous to 459 bp upstream of the Gucy2c ATG start codon in exon 1 and 402 bp downstream of exon 1. The resulting cassettes were cloned in the pLD53 shuttle vector (Gong et al., 2002) and used for introducing ITC into Pitx3 BAC clone RP23-125F3 (CHORI), FlpO into Nrp2 BAC clone RP24-238H6 (CHORI) and iCre into Gucy2c BAC clone RP23-93A18 (CHORI).
Recombination was verified by PCR and enzymatic digestion of the recombined BAC clones. To generate transgenic mice, purified DNA was microinjected into fertilized eggs obtained by mating (C57BL/6 X SJL)F1 or C57BL/6 female mice with (C57BL/6 X SJL)F1 male mice. *EIIa-Cre*, *ACTB-FlpE*, *R26-STOP-EYFP*, and $R26^{NZG}$ mouse lines were obtained from The Jaxon Laboratory. $R26^{NZG}$ mouse line was first crossed with *EIIa-Cre* mouse line to remove the PGKNEO cassette and to obtain $R26^{ZG}$ mouse line. $R26^{ZG}$ was then used as Flp-reporter mouse line (Yamamoto et al., 2009).

Mice were genotyped by PCR on genomic DNA using *Taq* DNA polymerase (Qiagen) and the following primers:

Pitx3-ITC – IFP gene (amplicon 334 bp):
5'-CTGACGCCACTGGAGAGATG-3'
5'-TGGTGGCAGACAATCAGTCC-3'

Pitx3-ITC – Citrine gene (amplicon 750 bp):
5'-GAGCGATCGCGCCACCATGGTGAGCAAGGGCGAGGAG-3'
5'-CCGGCGCCGTTTAAACCTTGTACAGCTCGTCCATGCCGAGAGTGATC-3'

ACBT-FlpE (amplicon 725 bp):
5'-CACTGATATTGTAAGTAGTTTGC-3'
5'-CTAGTGCGAAGTAGTGATCAGG-3'

Ella-Cre (amplicon 320 bp):
5'-TTCCCGCAGAACCTGAAGATGTTCG-3'
5'-GGGTGTTATAAGCAATCCCCAGAAATGC-3'

Nrp2-FlpO (amplicon 312 bp):
5'-GCAGGTTCAGCGACATCAAG-3'
5'-GGTAGGGGGCGTTCTTCTTC-3'

Gucy2C-iCre (amplicon 340 bp):
5'-CCCGGGGCCACCATGGT-3'
5'-GACACAGCATTGGAGTCAGA-3'

R26-STOP-EYFP (amplicon 320 bp MUT, 600 bp WT):
5'-AAAGTCGCTCTGAGTTGTTAT-3'
5'-GCGAAGAGTTTGTCCTCAACC-3'
5'-GGAGCGGGAGAAATGGATATG-3'

$R26^{ZG}$ – LacZ gene (amplicon 210 bp):
5'-GGTAAACTGGCTCGGATTAGGG-3'
5'-TTGACTGTAGCGGCTGATGTTG-3'

Injection of biliverdin

Intravenous injections with 250 nmol biliverdin in 10%DMSO was performed in adult *Pitx3-ITC* mice. After one hour, mice were sacrificed and the brains were isolated and cryopreserved at -80°C. Next, 10 µm brain sections we analyzed by confocal laser-scanning microscope (LSM 880, Zeiss).

Immunohistochemistry

Adult mice were transcardially perfused with ice-cold saline followed by 4% PFA. Brains were isolated and post-fixed overnight at 4°C in 4%PFA. Brains were then cryoprotected in 30% sucrose in PBS. Next, they were frozen and cryopreserved at -80°C. 20 µl brain sections were cut on a cryostat. Sections were first blocked with blocking solution (0.4% Tryton X-100, 1% BSA, in PBS) for 1h at RT, followed by incubation with primary antibodies in blocking solution at 4°C overnight. The next day, they were washed in PBS and incubated with secondary antibodies in blocking solution at RT for 1h. Then, they were washed and counterstained with DAPI (4',6'-diamidino-2-phenylindole; 0.1 mg/ml in PBS; Invitrogen). Mounting was performed with FluorSave reagent (Merck Millipore). Staining was visualized on a Zeiss Axioskop A1 epi fluorescent microscope or by confocal laser-scanning microscopy (LSM 880, Zeiss).

Primary Ab.	Species	Company	Catalog Number	Concentration
TH	rabbit	Millipore	AB152	1:1000
TH	sheep	Millipore	AB1542	1:500
GFP	rabbit	Life technologies	A11122	1:500
GFP	chicken	Abcam	ab13970	1:500
Sox6	rabbit	Abcam	ab30455	1:500
Otx2	goat	R&D	AF1979	1:500
TdTomato	rabbit	Rockland	600-401-379	1:500
CTIP2	rat	Abcam	ab18465	1:1000

In situ hybridization

To collect E13.5 and E16.5 embryo brains, timed-pregnant females were sacrificed by means of cervical dislocation. The morning on which a vaginal plug was detected was considered embryonic day 0.5 (E0.5). Embryonic brains were isolated and directly frozen. 16 µm sections were cut on a cryostat, air-dried for 2h and frozen at -80°C. Nonradioactive in situ hybridization was performed according to (Pasterkamp et al., 2007). cDNA was prepared from whole mouse brain RNA using a one-step RT-PCR kit (Qiagen), according to supplied protocol and using the following primers:

Gucy2c:
5'-CATAGGGACCTTTGAGTTGGAG-3'
5'-GTTTGAGACCAGCTTGGGATAC-3'

Nrp2:
5'-AGGACACGAAGTGAGAAGCC-3'
5'-TTGCAGTCGTGTTTCTCGATTTC-3'

Pitx3:
5'-CAGCTTGCACTATGCCCACC-3'
5'-GAATTCCACAGTGAACCAG-3'

cDNA was cloned into pGEM-T Easy (Promega) and transcribed using either SP6 or T7 RNA polymerase (Roche) and digoxigenin-labeled nucleotide mix (Roche) to produce digoxigenin-labeled cRNA probes. Digoxigenin was detected using anti-digoxigenin FAB fragments conjugated to alkaline phosphatase (Roche; 1:5000) and stained with NBT/BCIP (Roche). Sections were mounted using FluorSave reagent and visualized on a Zeiss Axioscope 2.

Acknowledgements

We are very thankful to all the members of the Pasterkamp lab for helpful discussions during the project. We are grateful to Peter Burbach for the critical reading of the manuscript. Special thanks go to Christian van der Meer and Leo Halewijn, who helped with the maintenance of mouse colonies. We thank Rolf Sprengel for sharing the iCre construct and we are grateful to Nathaniel Heintz and Shiaoching Gong for sharing the pLD53 construct and for technical advice on BAC transgenesis. We thank Roger Tsien for sharing the tdTomato, Citrine, and IFP constructs. We are grateful to Roman Giger for his support in coordinating the generation of BAC transgenic mice. We acknowledge Galina Gavrilina, Keith Childs, and Wanda Filipiak for preparation of transgenic mice at the Transgenic Animal Model Core of the University of Michigan's Biomedical Research Core Facilities.

Work on axon guidance and the developing dopamine system was financially supported by the Netherlands Organization for Scientific Research (ALW-VICI), the People Program (Marie Curie Actions) of the European Union's Seventh Framework Program (FP7) 2007–2013 under REA grant agreement number 289581 (NPlast), the UU Strategic Theme "Dynamics of Youth", and Stichting ParkinsonFonds.

References

Arlotta, P., Molyneaux, B.J., Chen, J., Inoue, J., Kominami, R., and Macklis, J.D. (2005). Neuronal subtype-specific genes that control corticospinal motor neuron development in vivo. Neuron *45*, 207–221.

Brignani, S., and Pasterkamp, R.J. (2017). Neuronal Subset-Specific Migration and Axonal Wiring Mechanisms in the Developing Midbrain Dopamine System. Front. Neuroanat. *11*, 55.

Burke, R.E., and O'Malley, K. (2013). Axon degeneration in Parkinson's disease. Exp. Neurol. *246*, 72–83.

Cheng, H.-C., Ulane, C.M., and Burke, R.E. (2010). Clinical progression in Parkinson disease and the neurobiology of axons. Ann. Neurol. *67*, 715–725.

Ekstrand, M.I., Nectow, A.R., Knight, Z.A., Latcha, K.N., Pomeranz, L.E., and Friedman, J.M. (2014). Molecular profiling of neurons based on connectivity. Cell *157*, 1230–1242.

Fossat, N., Chatelain, G., Brun, G., and Lamonerie, T. (2006). Temporal and spatial delineation of mouse Otx2 functions by conditional self-knockout. EMBO Rep. *7*, 824–830.

Fujiyama, F., Sohn, J., Nakano, T., Furuta, T., Nakamura, K.C., Matsuda, W., and Kaneko, T. (2011). Exclusive and common targets of neostriatofugal projections of rat striosome neurons: a single neuron-tracing study using a viral vector. Eur. J. Neurosci. *33*, 668–677.

Gerfen, C.R., Herkenham, M., and Thibault, J. (1987). The neostriatal mosaic: II. Patch- and matrix-directed mesostriatal dopaminergic and non-dopaminergic systems. J. Neurosci. *7*, 3915–3934.

Gerfen, C.R., Paletzki, R., and Heintz, N. (2013). GENSAT BAC Cre-Recombinase Driver Lines to Study the Functional Organization of Cerebral Cortical and Basal Ganglia Circuits. Neuron *80*, 1368–1383.

Gong, S., Yang, X.W., Li, C., and Heintz, N. (2002). Highly efficient modification of bacterial artificial chromosomes (BACs) using novel shuttle vectors containing the R6Kgamma origin of replication. Genome Res. *12*, 1992–1998.

Harris, J.A., Hirokawa, K.E., Sorensen, S.A., Gu, H., Mills, M., Ng, L.L., Bohn, P., Mortrud, M., Ouellette, B., Kidney, J., et al. (2014). Anatomical characterization of Cre driver mice for neural circuit mapping and manipulation. Front. Neural Circuits *8*, 76.

Ikemoto, S. (2007). Dopamine reward circuitry: Two projection systems from the ventral midbrain to the nucleus accumbens–olfactory tubercle complex. Brain Res. Rev. *56*, 27–78.

Kalia, L. V, and Lang, A.E. (2015). Parkinson's disease. Lancet *386*, 896–912.

Kolk, S.M., Gunput, R.-A.F., Tran, T.S., van den Heuvel, D.M.A., Prasad, A.A., Hellemons, A.J.C.G.M., Adolfs, Y., Ginty, D.D., Kolodkin, A.L., Burbach, J.P.H., et al. (2009). Semaphorin 3F Is a Bifunctional Guidance Cue for Dopaminergic Axons and Controls Their Fasciculation, Channeling, Rostral Growth, and Intracortical Targeting. J. Neurosci. *29*.

Kordower, J.H., Olanow, C.W., Dodiya, H.B., Chu, Y., Beach, T.G., Adler, C.H., Halliday, G.M., and Bartus, R.T. (2013). Disease duration and the integrity of the nigrostriatal system in Parkinson's disease. Brain *136*, 2419–2431.

Lakso, M., Pichel, J.G., Gorman, J.R., Sauer, B., Okamoto, Y., Lee, E., Alt, F.W., and Westphal, H. (1996). Efficient in vivo manipulation of mouse genomic sequences at the zygote stage. Proc. Natl. Acad. Sci. U. S. A. *93*, 5860–5865.

Lammel, S., Hetzel, A., Häckel, O., Jones, I., Liss, B., and Roeper, J. (2008). Unique properties of mesoprefrontal neurons within a dual mesocorticolimbic dopamine system. Neuron *57*, 760–773.

Lerner, T.N., Shilyansky, C., Davidson, T.J., Evans, K.E., Beier, K.T., Zalocusky, K.A., Crow, A.K., Malenka, R.C., Luo, L., Tomer, R., et al. (2015). Intact-Brain Analyses Reveal Distinct Information Carried by SNc Dopamine Subcircuits. Cell *162*, 635–647.

La Manno, G., Gyllborg, D., Codeluppi, S., Nishimura, K., Salto, C., Zeisel, A., Borm, L.E., Stott, S.R.W., Toledo, E.M., Villaescusa, J.C., et al. (2016). Molecular Diversity of Midbrain Development in Mouse, Human, and Stem Cells. Cell *167*, 566–580.e19.

Matsuda, W., Furuta, T., Nakamura, K.C., Hioki, H., Fujiyama, F., Arai, R., and Kaneko, T. (2009). Single nigrostriatal dopaminergic neurons form widely spread and highly dense axonal arborizations in the neostriatum. J. Neurosci. *29*, 444–453.

Morales, M., and Margolis, E.B. (2017). Ventral tegmental area: cellular heterogeneity, connectivity and behaviour. Nat. Rev. Neurosci. *18*, 73–85.

Panman, L., Papathanou, M., Laguna, A., Oosterveen, T., Volakakis, N., Acampora, D., Kurtsdotter, I., Yoshitake, T., Kehr, J., Joodmardi, E., et al. (2014). Sox6 and Otx2 Control the Specification of Substantia Nigra and Ventral Tegmental Area Dopamine Neurons. Cell Rep. *8*, 1018–1025.

Pasterkamp, R.J., Kolk, S.M., Hellemons, A.J., and Kolodkin, A.L. (2007). Expression patterns of semaphorin7A and plexinC1 during rat neural development suggest roles in axon guidance and neuronal migration. BMC Dev. Biol. *7*, 98.

Poulin, J.-F., Zou, J., Drouin-Ouellet, J., Kim, K.-Y.A., Cicchetti, F., and Awatramani, R.B. (2014). Defining Midbrain Dopaminergic Neuron Diversity by Single-Cell Gene Expression Profiling. Cell Rep. *9*, 930–943.

Prensa, L., and Parent, A. (2001). The nigrostriatal pathway in the rat: A single-axon study of the relationship between dorsal and ventral tier nigral neurons and the striosome/matrix striatal compartments. J. Neurosci. *21*, 7247–7260.

Rodríguez, C.I., Buchholz, F., Galloway, J., Sequerra, R., Kasper, J., Ayala, R., Stewart, A.F., and Dymecki, S.M. (2000). High-efficiency deleter mice show that FLPe is an alternative to Cre-loxP. Nat. Genet. *25*, 139–140.

Shu, X., Royant, A., Lin, M.Z., Aguilera, T.A., Lev-Ram, V., Steinbach, P.A., and Tsien, R.Y. (2009). Mammalian Expression of Infrared Fluorescent Proteins Engineered from a Bacterial Phytochrome. Science (80-.). *324*, 804–807.

Smidt, M.P., van Schaick, H.S., Lanctôt, C., Tremblay, J.J., Cox, J.J., van der Kleij, A.A., Wolterink, G., Drouin, J., and Burbach, J.P. (1997). A homeodomain gene Ptx3 has highly restricted brain expression in mesencephalic dopaminergic neurons. Proc. Natl. Acad. Sci. U. S. A. *94*, 13305–13310.

Smidt, M.P., von Oerthel, L., Hoekstra, E.J., Schellevis, R.D., and Hoekman, M.F.M. (2012). Spatial and Temporal Lineage Analysis of a Pitx3-Driven Cre-Recombinase Knock-In Mouse Model. PLoS One *7*, e42641.

Srinivas, S., Watanabe, T., Lin, C.S., William, C.M., Tanabe, Y., Jessell, T.M., and Costantini, F. (2001). Cre reporter strains produced by targeted insertion of EYFP and ECFP into the ROSA26 locus. BMC Dev. Biol. *1*, 4.

Stamatakis, A.M., Jennings, J.H., Ung, R.L., Blair, G.A., Weinberg, R.J., Neve, R.L., Boyce, F., Mattis, J., Ramakrishnan, C., Deisseroth, K., et al. (2013). A unique population of ventral tegmental area neurons inhibits the lateral habenula to promote reward. Neuron *80*, 1039–1053.

Takashima, S., Kitakaze, M., Asakura, M., Asanuma, H., Sanada, S., Tashiro, F., Niwa, H., Miyazaki, J., Hirota, S., Kitamura, Y., et al. (2002). Targeting of both mouse neuropilin-1 and neuropilin-2 genes severely impairs developmental yolk sac and embryonic angiogenesis. Proc. Natl. Acad. Sci. *99*, 3657–3662.

Taniguchi, H., He, M., Wu, P., Kim, S., Paik, R., Sugino, K., Kvitsiani, D., Kvitsani, D., Fu, Y., Lu, J., et al. (2011). A resource of Cre driver lines for genetic targeting of GABAergic neurons in cerebral cortex. Neuron *71*, 995–1013.

Torigoe, M., Yamauchi, K., Tamada, A., Matsuda, I., Aiba, A., Castellani, V., and Murakami, F. (2013). Role of neuropilin-2 in the ipsilateral growth of midbrain dopaminergic axons. Eur. J. Neurosci. *37*, 1573–1583.

Veenvliet, J. V., and Smidt, M.P. (2014). Molecular mechanisms of dopaminergic subset specification: fundamental aspects and clinical perspectives. Cell. Mol. Life Sci. *71*, 4703–4727.

Watabe-Uchida, M., Zhu, L., Ogawa, S.K., Vamanrao, A., and Uchida, N. (2012). Whole-brain mapping of direct inputs to midbrain dopamine neurons. Neuron *74*, 858–873.

Yamamoto, M., Shook, N.A., Kanisicak, O., Yamamoto, S., Wosczyna, M.N., Camp, J.R., and Goldhamer, D.J. (2009). A multifunctional reporter mouse line for Cre- and FLP-dependent lineage analysis. Genesis *47*, 107–114.

Yamauchi, K., Mizushima, S., Tamada, A., Yamamoto, N., Takashima, S., and Murakami, F. (2009). FGF8 Signaling Regulates Growth of Midbrain Dopaminergic Axons by Inducing Semaphorin 3F. J. Neurosci. *29*.

Zhao, S., Maxwell, S., Jimenez-Beristain, A., Vives, J., Kuehner, E., Zhao, J., O'Brien, C., de Felipe, C., Semina, E., and Li, M. (2004). Generation of embryonic stem cells and transgenic mice expressing green fluorescence protein in midbrain dopaminergic neurons. Eur. J. Neurosci. *19*, 1133–1140.

Supplemental information

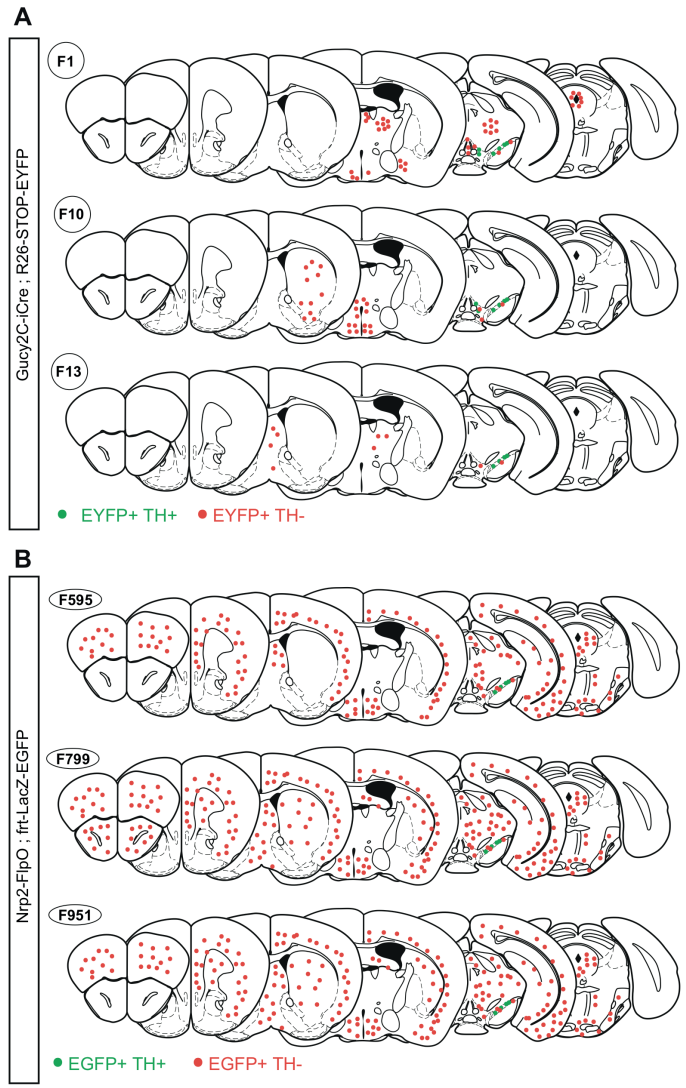

Suppl. Figure 1

characterization of iCre and FlpO expression in *Gucy2C* and *Nrp2-FlpO* founder mouse lines. (A-B) Representation of coronal sections along the anterior-posterior axis. (A) *Gucy2C* founder mice (F1, F10, and F13) are crossed with *R26-STOP-EYFP* mice. The position of $EYFP^+/TH^+$ neurons is represented by green dots, while $EYFP^+/TH^-$ neurons are red dots. (B) *Nrp2-FlpO* founder mice (F595, F799, and F951) are crossed with FlpO reporter mice. $EGFP^+/TH^+$ neurons are green spots, whereas $EGFP^+/TH^-$ neurons are in red.

Chapter 4

Development of dopaminergic axon-subsets and role of Netrin1 in nigrostriatal axon branching

Sara Brignani, Divya A. Raj, Ewoud E. Schmidt, Anna A. de Ruiter, Erik Schild, R. Jeroen Pasterkamp

Department of Translational Neuroscience, Brain Center Rudolf Magnus, University Medical Center Utrecht, Utrecht University, Utrecht, The Netherlands

Abstract

The midbrain dopamine system is involved in the control of cognitive and motor behavior. Midbrain dopamine neurons (mDA) are grossly divided into two anatomically and functionally distinct main subpopulations: substantia nigra pars compacta (SNc) and ventral tegmental area (VTA) neurons. In the adult brain, SNc neurons make precise connections with the dorsal striatum (nigrostriatal projections), while VTA neurons target the ventral striatum and cortex (mesocorticolimbic projections). Both pathways collectively run in the medial forebrain bundle (MFB) towards the forebrain. To distinguish between nigrostriatal and mesocorticolimbic dopaminergic projections during brain development *in vivo*, we used two mouse models labelling SNc and VTA mDA neurons, respectively. These two mouse models show that nigrostriatal and mesocorticolimbic axons are not dispersed throughout the MFB, but rather are segregated in the dorsal and the ventral MFB from early developmental stages. This pre-target segregation of dopaminergic axon-subsets may be important for the correct innervation of the dorsal and ventral striatal domains. In addition, we provide evidence that the axon guidance cue Netrin1 induces branching of SNc mDA axons in the dorsal striatum, rather than functioning as a topographic guidance cue for dopaminergic axons, as suggested by previous studies. Interestingly, the Netrin1-mediated effect on axonal branching does not require cell-autonomous expression of DCC receptor. In conclusion, our genetic approach offers the unique possibility of differentially labeling dopaminergic subsets and visualizing their projections. This allowed us to determine the ontogeny of mDA axon-subsets and to identify molecules involved in their development.

Introduction

The dopamine system of the midbrain consists of a heterogeneous group of dopaminergic neurons (mDA) involved in cognitive and motor functions. Despite sharing the release of the same neurotransmitter dopamine, subsets of mDA neurons receive inputs and establish connections with different brain areas. The lateral mDA nucleus called Substantia nigra compacta (SNc) projects mainly into the dorsal striatum, forming the nigrostriatal pathway (Ikemoto, 2007; Lerner et al., 2015; Matsuda et al., 2009). The medial Ventral Tegmental Area (VTA) innervates several brain regions including the ventral striatum, the prefrontal cortex, the amygdala, and the septum, establishing the mesocorticolimbic pathway, and the lateral habenula via the fasciculus retroflexus (Aransay et al., 2015; Khan et al., 2017; Lammel et al., 2008; Schmidt et al., 2014). The diversity of mDA neuron-subsets is also revealed by their different susceptibility to diseases. SNc mDA neurons are the most affected in Parkinson's disease (Björklund and Dunnett, 2007; Kalia and Lang, 2015), whereas dopamine imbalance in VTA mDA neurons has been implicated in schizophrenia, attention deficit hyperactivity disorder (ADHD), obsessive-compulsive disorder (OCD), addiction, and depression (Chaudhury et al., 2012; Faraone et al., 2005; Milton and Everitt, 2012; Winterer and Weinberger, 2004). To determine the mechanisms that control the formation of such a complex network of mDA connections, insight is needed into how the axons of mDA neuron-subsets wire up during brain development. During development, axons of different mDA neuron-subsets navigate towards specific brain targets following stereotyped routs. Nigrostriatal and mesocorticolimbic mDA axons navigate longitudinally from the midbrain towards the forebrain in a tightly fasciculated ipsilateral axon bundle called medial forebrain bundle (MFB) (reviewed in (Brignani and Pasterkamp, 2017)). According to Hu et al., the development of the nigrostriatal and mesolimbic pathways follows two phases: (1) at early developmental stages both SNc and VTA axons innervate nonspecifically dorsal and ventral striatum, without showing the segregated innervation patterns described in the adult brain; (2) at later stages, the two axonal pathways become segregated through the selective elimination of mis-targeted collaterals (Hu et al., 2004).

Extending mDA axons are tipped by a sensory growth cone. With its highly dynamic behavior and responsiveness to multiple sources of spatial information, the growth cone allows elongating axons to find their intermediate and final targets. Molecules called guidance cues are expressed by the environment along the trajectories of elongating axons and are detected by guidance receptors expressed at the cell membrane of the growth cone. By binding to guidance receptors, guidance cues trigger intracellular signaling cascades inducing cytoskeleton remodeling and subsequent steering of elongating axons. The

specific expression of axon guidance receptors in different mDA cell-subsets may determine how these subsets can differentially respond to guidance cues to ultimately establish connections with specific brain areas.

It has been shown that expression of the axon guidance cue Netrin1 is crucial during several stages of mDA axon development (Cord et al., 2010; Li et al., 2014; Lin et al., 2005; Xu et al., 2010). Netrin1 can act both as a long- and short-range cue, in the latter case by being bound to the extracellular matrix or the cell membrane. Netrin1 receptors include DCC (deleted in colorectal cancer), the DCC paralog Neogenin, four UNC5s (UNC5A-D), and DsCAM (Down syndrome cell adhesion molecule). Netrin1 can function both as a chemoattractant or chemorepellent depending on the guidance receptor expressed by the growth cone. Generally, DCC mediates attraction, whereas repulsion to Netrin1 requires the expression of UNC5 proteins, that may need DCC co-expression (reviewed in (Baker et al., 2006)). Netrin1 mRNA has been detected in cells along the route of elongating mDA axons, such as at the midline of the caudal hypothalamus and in the striatum (Li et al., 2014). In the latter case, Netrin1 expression begins at E13.5 (Morello et al., 2015), when the first mDA axons start invading the striatum, and continues throughout embryonic development (Bonnin et al., 2007; Powell et al., 2008). Interestingly, striatal expression of Netrin1 is not homogeneous, but rather shows a high ventro-lateral and low dorso-medial gradient at E18.5 (Li et al., 2014). *In vitro* experiments demonstrate that Netrin1 promotes mDA axon outgrowth, elongation, attraction, and branching by binding to DCC (Cord et al., 2010; Lin et al., 2005; Xu et al., 2010). In addition, *Netrin1-KO* brains show several defects in mDA axon navigation, guidance, and striatal innervation (Li et al., 2014), that in some cases are also detected in *DCC-KO* brains (Xu et al., 2010). For example, at the level of the caudal hypothalamus, in both *Netrin1-KO* and *DCC-KO* brains a small subset of mDA axons leaves the MFB and is mis-routed towards the midline (Li et al., 2014; Xu et al., 2010). Recently, Li at al. showed that different concentrations of Netrin1 have different effects on SNc or VTA mDA explants *in vitro*. High concentrations of Netrin1 induce VTA mDA axon elongation and attraction, while low concentrations of Netrin1 have the same effects on SNc mDA axons. High Netrin1 concentrations did not affect SNc mDA axons (Li et al., 2014). According to Li at al., *Netrin1-KO* mice show a decrease of mDA innervation in the dorso-medial striatum and an increase in the ventro-lateral striatum. The authors suggest that SNc mDA axons do not innervate the dorso-medial striatum but rather accumulate in the ventro-lateral region (Li et al., 2014). The lack of attraction by low Netrin1 concentrations in the dorso-medial striatum may prevent SNc mDA axons from elongating into the dorso-medial area (Li et al., 2014).

Here, we determine the ontogeny of SNc and VTA mDA axons using BAC transgenic reporter mice. We show that during mDA axon elongation and navigation towards the striatum SNc mDA axons are located in the dorsal MFB, while VTA mDA axons are located ventrally. The two axonal populations remain segregated throughout their journey to the striatum. SNc mDA axons invade the striatum before VTA mDA axons. SNc and VTA mDA axons innervate the dorsal and ventral striatum, respectively, without forming mis-targeted collaterals in non-specific striatal regions. In addition, in the second part of the chapter, we show that Netrin1 does not function as a topographic guidance cue for SNc mDA axons *in vivo*, but rather acts in the striatum as a DCC-independent branching factor for SNc mDA axons.

Results

1. Adult SNc mDA axons occupy the dorsal MFB and innervate the dorsal striatum

To label different mDA cell-subsets and to visualize mDA subset-specific axonal projections *in vivo*, we generated the *Pitx3-ITC:ACTB-FlpE* mouse model (Chapter 3). In this mouse line, expression of Citrine protein is enriched in SNc mDA neurons, which can thereby be distinguished from Citrine-negative VTA mDA neurons both in adult and developing brains (Chapter 3). Citrine expression in SNc mDA neurons allows the selective visualization of their axonal projections, enabling us to distinguish nigrostriatal projections from other TH^+ mDA axons growing in their close proximity (Figure 1A-D). In adult *Pitx3-ITC:ACTB-FlpE* brains, $Citrine^+$ axons were confined to the dorsal part of the striatum at anterior to posterior striatal levels (Figure 1A-C), confirming the results of previous studies reporting that nigrostriatal projections establish connections with the dorsal striatum (Gerfen et al., 1987; Ikemoto, 2007; Lerner et al., 2015). In some striatal sections of adult brains, small axonal patches were detected, where $Citrine^+$ mDA axons were more dense as compared to the surrounding regions (Figure 1A-B). These patches were more often localized in the dorso-lateral striatum, while $Citrine^+$ innervation of the dorso-medial striatum appeared more homogeneous. These structures are called dopamine islands and appear in the dorsal striatum during postnatal development (Edley and Herkenham, 1984; Gerfen, 1992). At early postnatal stages, dopamine islands are characterized by a dense aggregation of TH^+ axons overlapping with a subset of striatal neurons, called striatal patch or striosome neurons (Edley and Herkenham, 1984; Gerfen, 1992). Interestingly, dopamine islands are detectable using the TH marker until P15, after which striatal innervation of mDA axons becomes more homogeneous (Edley and Herkenham, 1984). The observation of $Citrine^+$ dopamine islands in adult *Pitx3-ITC:ACTB-FlpE* brains was therefore unexpected.

Nigrostriatal mDA axons travel over a long distance from the midbrain to the forebrain in order to innervate the dorsal striatum. During their longitudinal journey, they are tightly fasciculated with mesocorticolimbic mDA axons originating from

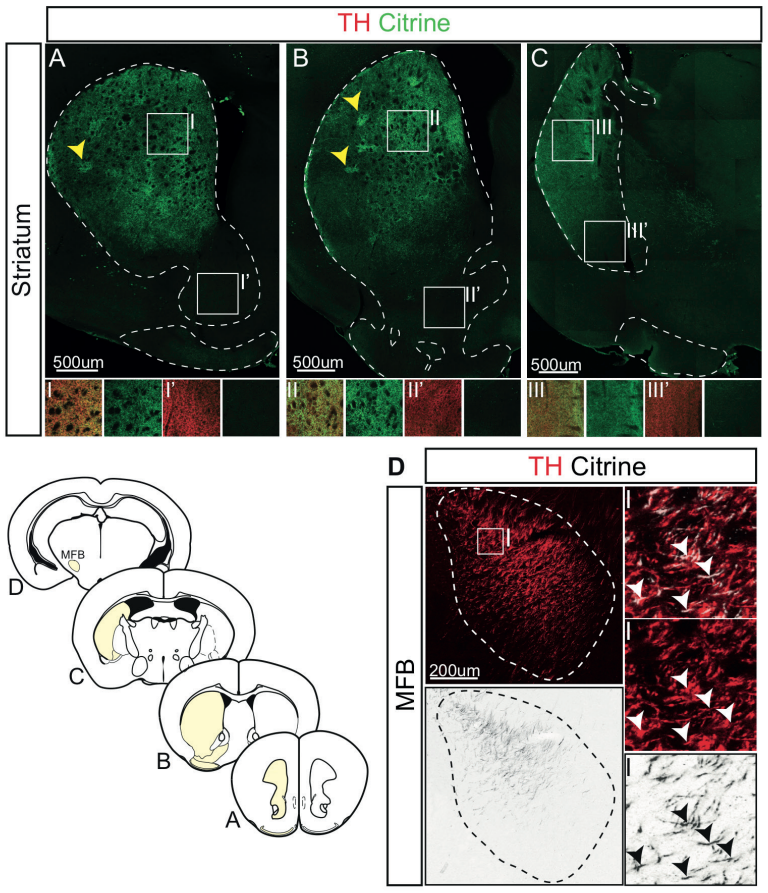

Figure 1

Visualization of nigrostriatal projections in adult brains

Pitx3-ITC:ACTB-FlpE mice allow the selective visualization of SNc mDA axons. (A-C) Immunohistochemistry on three representative coronal sections of the adult striatum. Citrine$^+$ axons innervate the dorsal striatum. Yellow arrows indicate striatal patches formed by Citrine$^+$ SNc mDA axons. (D) Nigrostriatal axons are not dispersed throughout the medial forebrain bundle (MFB), but rather run in the dorsal MFB in adult brains.

VTA mDA neurons forming the MFB (Van den Heuvel and Pasterkamp, 2008; Prestoz et al., 2012). The analysis of coronal sections obtained from the MFB of adult *Pitx3-ITC:ACTB-FlpE* brains revealed that Citrine$^+$ nigrostriatal mDA axons were not dispersed throughout the bundle, but rather segregated dorsally revealing a previously uncharacterized aspect of the organization of the MFB (Figure 1D). Therefore, in the adult brain, nigrostriatal mDA axons show a topographic organization: they occupy the dorsal MFB and innervate the dorsal striatum.

2. Nigrostriatal axons occupy the dorsal MFB during development

We next asked how the dorsal segregation of nigrostriatal projections in the MFB arises, for example whether it appears during early embryonic development, and whether it is the result of an axonal pruning process, as described by Hu et al. (Hu et al., 2004). *Pitx3-ITC:ACTB-FlpE* brains were analyzed at embryonic time points (E14.5, E16.5, and E18.5), when mDA axons are navigating towards the forebrain. At these time points, Citrine$^+$ SNc mDA axons were segregated dorsally in the MFB (Figure 2A). This indicates that the topographic organization of nigrostriatal axons is acquired at early stages of axonal development.

To further study MFB development, hemi-brain organotypic cultures were grown *in vitro* starting at E12.5 and fixed after 2 or 3 days (Figure 2B). This approach allowed us to visualize the entire MFB with its target structure, the striatum, which was delineated by Islet1 immunostaining (dotted lines in Figure 2B). At E12.5, mDA axons were travelling through the diencephalon and mDA axons had not arrived at the striatum yet. Two days later, dorsal mDA axons were innervating the dorsal striatum, whereas the tips of the longest ventral mDA axons only started to enter the striatum. The presence of VTA mDA axons growing towards the habenula in the fasciculus retroflexus indicated that hemi-brain cultures contain medial VTA mDA neurons and axons, and that lack of ventral striatum innervation is not due to the absence of VTA neurons in hemi-brain cultures. After three days *in vitro*, dorsal and ventral mDA axons are innervating the dorsal and the ventral striatum, respectively. Hemi-brain cultures performed with *Pitx3-ITC:ACTB-FlpE* brains confirmed that dorsally-positioned mDA axons in the MFB were Citrine$^+$ SNc mDA axons (Figure 2C). Together, these data show that nigrostriatal axons are segregated in the dorsal MFB from very early stages of MFB development onwards and that SNc mDA axons innervate the striatum before VTA mDA axons.

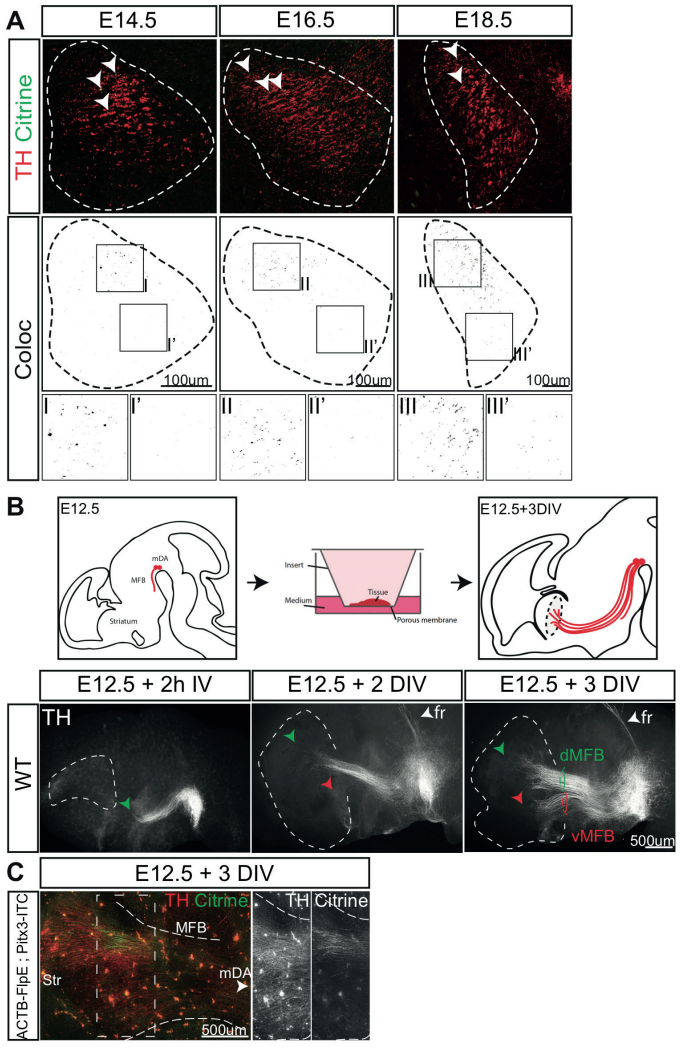

Figure 2

SNc mDA axons are segregated in the dorsal MFB from E14.5 onwards

(A) Immunohistochemistry for TH and Citrine on MFB coronal sections of E14.5, E16.5, and E18.5 *Pitx3-ITC:ACTB-FlpE* brains. Both immunostainings are shown in the top row, while in the bottom row TH/Citrine co-localization spots are displayed. From E14.5 onwards, nigrostriatal axons are segregated in the dorsal MFB. (B) Whole-mount organotypic culture obtained from E12.5 wt embryos and fixed after 2 or 3 days *in vitro* (DIV). At 2 DIV, the first dorsal mDA axons (green arrow) start to innervate the striatum; ventral mDA projections (red arrow) have not entered the striatum yet. One day later (3 DIV), dorsal axons are more deeply innervating the dorsal striatum; ventral axons are entering the ventral striatum. Organotypic cultures reveal a two-phase striatal innervation. (C) Higher magnification of the MFB obtained from E12.5 + 3DIV *Pitx3-ITC:ACTB-FlpE* embryos. Citrine$^+$ axons are visible and located in the dorsal MFB.

3. VTA mDA axons are localized to the ventral MFB

Pitx3-ITC:ACTB-FlpE brains showed the localization of SNc mDA axons in the dorsal MFB, without revealing the position of VTA mDA axons. These axons could be dispersed throughout the bundle and intermingled with SNc mDA axons or be segregated ventrally. In order to visualize VTA mDA axons, we crossed a *CCK-Cre* mouse line with a TdTomato reporter line that expresses TdTomato in all Cre$^+$ cells. *CCK-Cre* mice express Cre recombinase under the control of the CCK promoter (Taniguchi et al., 2011), which is activated mainly in VTA mDA neurons and not in SNc mDA neurons from early embryonic time points on ((La Manno et al., 2016) and reviewed in (Veenvliet and Smidt, 2014)). At E18.5, we could confirm that TdTomato$^+$ neurons were mostly confined to the medial dopamine system, whereas just a few positive neurons were localized in the lateral SNc (Figure 3A). In the VTA, most TdTomato$^+$ neurons co-expressed TH and Otx2, indicating that the majority of TdTomato$^+$ neurons are VTA mDA neurons (Figure 3A). Other areas of the brain showed TdTomato expression, such as the cortex, and several axonal tracts were labeled by TdTomato (data not shown). To distinguish VTA mDA axons from TdTomato$^+$ projections running close to MFB, we analyzed only axons co-expressing TdTomato and TH (Figure 3B). TdTomato$^+$/TH$^+$ VTA mDA axons were segregated in the ventral MFB at all time points analyzed (E14.5, E16.5, and E18.5) (Figure 3B). This indicates that during the elongation phase of their development, VTA mDA axons occupy the ventral MFB in contrast to SNc mDA axons which run dorsally.

4. Nigrostriatal projections innervate the dorsal striatum and reach their target prior to VTA mDA axons *in vivo*

Next we evaluated *in vivo* the spatio-temporal stages of striatal innervation by SNc and VTA mDA axons using *Pitx3-ITC:ACTB-FlpE* and the *CCK-Cre:floxed-stop-TdTomato* mouse models, respectively. Our intention was to establish whether the two axonal populations innervate the dorsal and ventral striatum already at early developmental stages, or whether they innervate the striatum nonspecifically to subsequently undergo selective elimination of mistargeted collaterals only at a later developmental stage, as described by Hu and colleagues (Hu et al., 2004). The analysis performed at E16.5 on comparable coronal sections showed that Citrine$^+$ SNc mDA axons occupy the dorsal striatum whereas TdTomato$^+$/TH$^+$ VTA mDA axons innervate the ventral domain (Figure 4A). The two axonal populations are therefore invading two separate striatal areas already at early developmental stages, only showing minor overlap in the central part of the striatum. Two days later, at E18.5, these two separate regions of dorsal and ventral innervation were very well defined and the

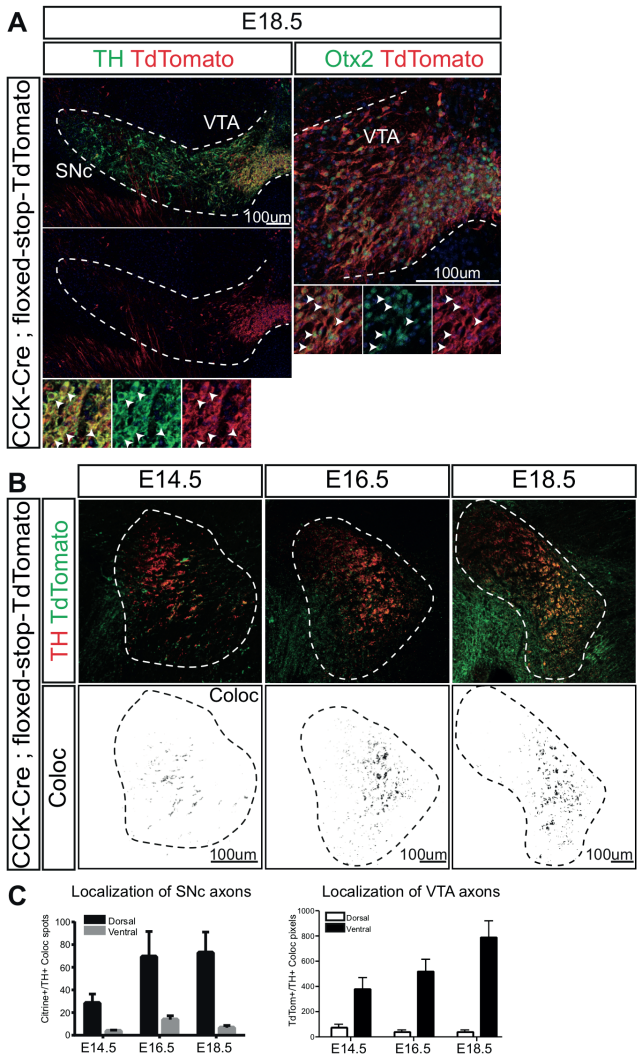

Figure 3

VTA axons are segregated in the ventral MFB

Crossing of *CCK-Cre* knock-in mice and a TdTomato reporter line (*CCK-Cre:floxed-stop-TdTomato*) allows selective labeling of VTA neurons and projections. (A) TdTomato expression is mainly confined to VTA mDA neurons (left). In the VTA, almost all TdTomato$^+$ cells colocalize with Otx2, a marker of VTA neurons (right). (B) Immunohistochemistry for TH and TdTomato on MFB coronal sections. In the top row, both immunostainings are shown. TH/TdTomato colocalization is shown in the bottom row. VTA mDA axons are confined to the ventral MFB during brain development. (C) Quantification of nigrostriatal (left) and mesocorticolimbic (right) projections in the dorsal and ventral MFB. (Left) Citrine/TH co-localizing spots in the ventral and dorsal MFB were counted using the Imaris software. (Right) TdTomato/TH co-localizing pixels were quantified by Fiji (ImageJ). Graphs show the Mean ± S.E.M from three independent experiments.

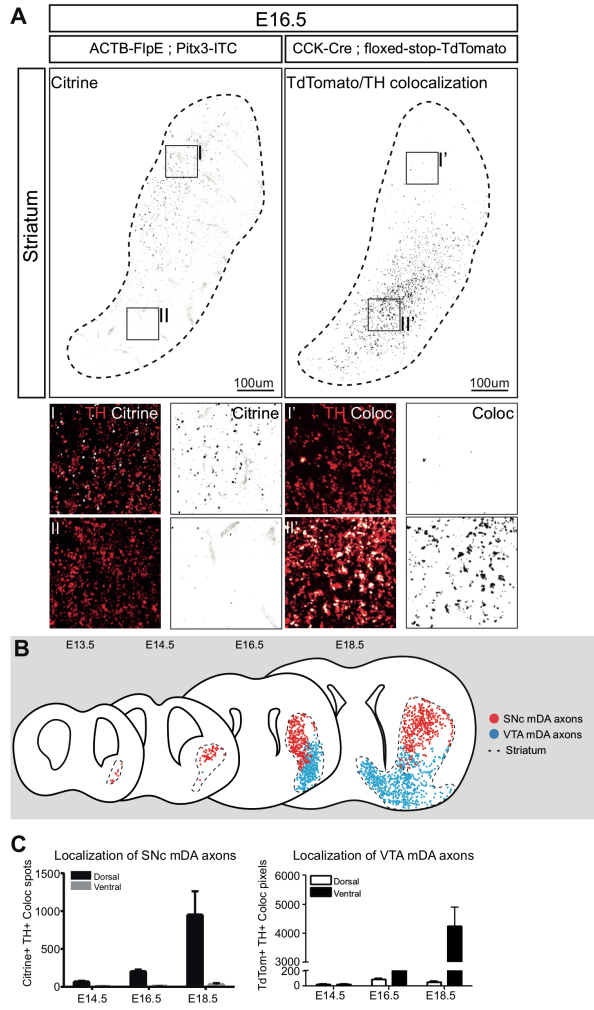

Figure 4

Nigrostriatal projections innervate the dorsal striatum and reach their target prior to VTA axons *in vivo*

(A) Visualization of SNc and VTA mDA axons in the striatum at E16.5 using *Pitx3-ITC:ACTB-FlpE* and *CCK-Cre:floxed-stop-TdTom* mice, respectively. Striatal edges are defined by TH immonostaining. VTA mDA axons are showed as TH/TdTomato co-localized spots. At E16.5, TH$^+$ axons innervate the entire striatum, whereas Citrine$^+$ axons are localized exclusively to the dorsal area. At the same stage, VTA projections are mainly confined to the ventral striatum. (B) Schematic representations of immunostainings on brain sections at different ages. Citrine$^+$ axons arrive at the target earlier than VTA projections. When VTA projections innervate the target, SNc and VTA axons are mainly confined in two distinct areas. (C) Quantification of SNc and VTA mDA axon innervation in the striatum. (Left) Citrine/TH co-localizing spots are quantified using Imaris software. (Right) TdTomato/TH co-localizing pixels are counted by Fiji (ImageJ). Graphs show the Mean ± S.E.M from three independent experiments.

number of both dorsal and ventral axons increased (Figure 4B-C). Furthermore, as already observed *in vitro* using hemi-brain cultures (Figure 2B), SNc mDA axons innervated the striatum prior to VTA mDA axons *in vivo* (Figure 4B). At E13.5, when TH^+ projections start to invade the striatum, only $Citrine^+$ SNc mDA axons were detected, while a small number of VTA mDA axons started to appear in the ventral striatum only a day later at E14.5 (Figure 4B). In conclusion, these data show that SNc and VTA axons innervate their respective targets, the dorsal and ventral striatal compartments, already at the initial stages of striatal innervation. Moreover, SNc axons begin striatal innervation before VTA axons.

5. Netrin1 is not required for the topographic guidance of nigrostriatal axons but rather induces their branching *in vivo*

To identify candidate molecules that may play a role in the segregation of nigrostriatal and mesocorticolimbic projections in the MFB and in the correct innervation of the striatum, we analyzed literature for axon guidance proteins described to be involved in mDA axon development (Brignani and Pasterkamp, 2017). When mDA axons are innervating the striatum, the axon guidance cue Netrin1 shows a specific pattern of expression: Netrin1 mRNA is highly expressed in the ventro-lateral striatum and lower levels are detected in the dorso-medial region (Bonnin et al., 2007; Morello et al., 2015; Powell et al., 2008). In addition, it has been recently reported that a Netrin1 striatal gradient may function as a topographic guidance cue for growing mDA axons. SNc mDA axons are attracted by low levels of Netrin1 in the dorso-medial striatum, whereas VTA mDA axons are attracted by high Netrin1 levels in the ventro-lateral region (Li et al., 2014). We could confirm this Netrin1 expression gradient in the striatum both at E16.5 and E18.5 by *in situ* hybridization (Figure 5). Moreover, using *ACTB-FlpE:Pitx3-ITC* brain sections, we showed that the majority of $Citrine^+$ SNc mDA axons where located in the region of the striatum where Netrin1 mRNA expression is low (Figure 5).

To assess whether Netrin1 is required for the correct development of SNc mDA axons, and whether lack of Netrin1 causes SNc axonal mis-targeting, *ACTB-FlpE:Pitx3-ITC* and *Netrin1-KO* mice were crossed (Yung et al., 2015). In the resulting mice, we can visualize SNc mDA axons in a *Netrin1-KO* background. Immunohistochemical analysis on coronal sections of E18.5 embryos showed that lack of Netrin1 does not cause an accumulation of $Citrine^+$ SNc axons in the ventro-lateral striatum, as shown previously by Li et al. In contrast, the innervation pattern of SNc mDA axons in the *Netrin1-KO* brain was similar to that observed in control mice. However, the overall structure of the striatum was altered, as shown by immunostaining of CTIP2, a marker of striatal neurons (Figure 6A). We noted that the level of SNc mDA axon innervation was strongly reduced in *Netrin1-KO* as compared to control mice. This qualitative observation was confirmed by quantification of all SNc mDA axons in the striatum (Figure 6B). This decrease was not caused by a decrease of $Citrine^+$ SNc mDA neurons (Figure 6C). Therefore, we asked whether decreased striatal innervation was caused by the mis-routing of nigrostriatal projections *en route* to the striatum. To test this hypothesis, the trajectories of $Citrine^+$ SNc mDA axons were analyzed in *ACBT-FlpE:Pitx3-ITC:Netrin1-KO* brains. However, no mis-routed $Citrine^+$ axons were detected. This indicates that all nigrostriatal projections reach the striatum in the absence of Netrin1. In the MFB, SNc mDA axons were correctly segregated in the dorsal MFB (Figure 6D) and were not decreased in number (Figure 6B). At the level of the caudal hypothalamus, aberrant TH^+ axonal projections were identified in *Netrin1-KO* brains that leave the MFB running towards the midline. Interestingly, these mis-routed axons were Citrine negative, indicating that they are most likely VTA mDA axons (Figure 6D). Together, these data indicate that SNc mDA axons reach the striatum in *Netrin1-KO* mice. The observed decrease in striatal innervation in *Netrin1-KO* brains may be due to the stalling of SNc mDA axons when entering the striatum. To assess this hypothesis, we checked whether striatal innervation is altered at E13.5 when, according to our observations, the first group of pioneer SNc mDA axons enters the striatum. Analysis of TH^+ axons revealed that at E13.5 striatal innervation was similar in *Netrin1-KO* and control mice. Thus, nigrostriatal axons are able to invade the striatum in the absence of Netrin1 (Figure 7).

Our data suggest that Netrin1 does not function as a topographic guidance cue for SNc mDA axons in the dorsal striatum. However, lack of Netrin1 induced a strong overall decrease in nigrostriatal innervation, which was not associated with axonal mis-routing or with failure to innervate the striatum. This suggests that the reduced striatal innervation observed at E18.5 in *Netrin1-KO* brains is caused by a reduction of SNc mDA axon branching. These observations are in agreement with earlier *in vitro* data showing that soluble Netrin1 induces branching of dissociated mDA neurons.

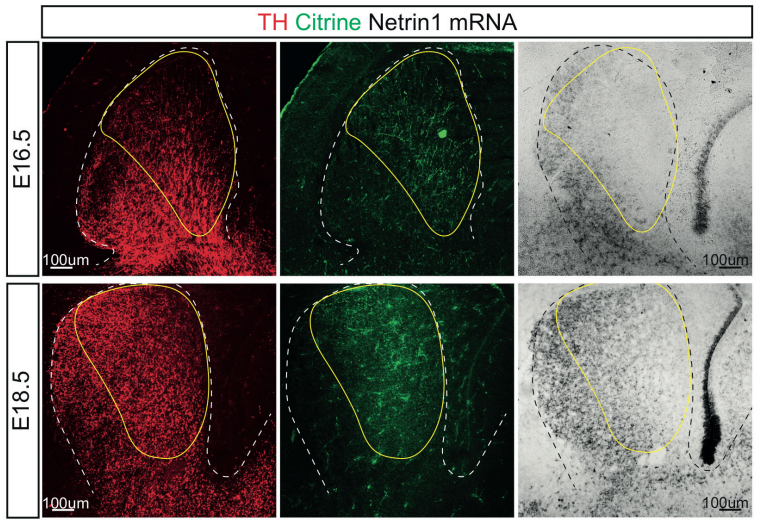

Figure 5

Netrin1 mRNA gradient in the striatum during brain development

(Left) Immunohistochemistry for TH and Citrine in the striatum of E16.5 and E18.5 *Pitx3-ITC:ACTB-FlpE* mice. (Right) *In situ* hybridization to detect Netrin1 mRNA in the striatum. Netrin1 mRNA is higher in the ventro-lateral compared to the dorso-medial striatum. The majority of Citrine^{+} axons is segregated in the striatal regions where Netrin1 expression is lower.

6. No cell-autonomous function for DCC in SNc mDA axon elongation, guidance or branching

DCC is an axon guidance receptor that can mediate Netrin1 signaling (Baker et al., 2006). It has been shown that DCC protein is expressed by all mDA neurons during dopamine system development both at E14.5 and E18.5, (Xu et al., 2010). *In vitro* experiments showed that Netrin1 induces mDA axon branching by activating DCC (Xu et al., 2010). In addition, *DCC-KO* mice display profound changes in mDA axon circuitry, including abnormal innervation of the ventral striatum, reduced innervation of the cerebral cortex, and an aberrant mDA commissure at the level of the caudal hypothalamus (Xu et al., 2010). These defects are also observed in *Netrin1-KO* brains (Xu et al., 2010). Therefore, we decided to investigate whether DCC expression is required for the correct wiring of SNc mDA axons, with a particular interest in understanding if DCC is necessary for nigrostriatal axon branching induced by Netrin1 in the striatum.

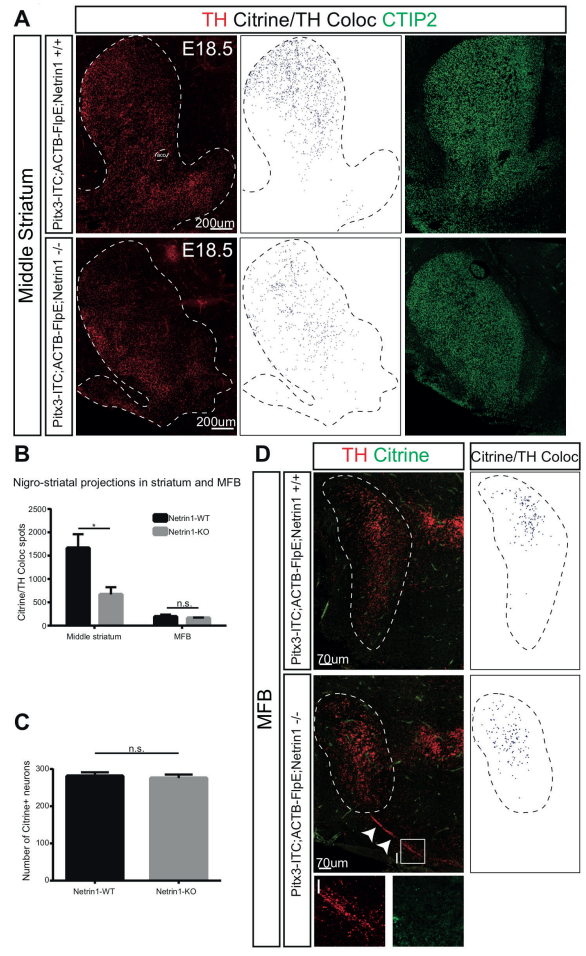

Figure 6

Nigrostriatal projection defects in *Netrin1-KO* brains

(A) Immunohistochemistry on coronal sections of the middle striatum in E18.5 *Pitx3-ITC:ACTB-FlpE:Netrin1-KO* brains. TH^{+} axons innervating the striatum are shown on the left. (Middle) TH/Citrine colocalizing axons in control (top) and *Netrin1-KO* brains (bottom). The structure of the striatum is determined using the CTIP2 marker (right). Although the structure of the striatum is altered, SNc mDA axons innervate the dorsal striatum both in control and KO conditions. However, the amount of SNc mDA axon innervation is decreased as shown in the middle panel and quantified in (B). (B) Citrine/TH colocalizing axons are quantified both in the striatum and in the MFB. The amount and position of nigrostriatal projections in the MFB are not altered in absence of Netrin1 (B and D). The aberrant TH^{+} axon bundle that leaves the MFB to turn towards the midline is not formed by SNc mDA axons (D). (C) The number of Citrine^{+} SNc mDA neurons is not altered in *Netrin1-KO* brains compared to controls. All graphs show Mean ± S.E.M from three independent experiments. Data were tested for significance by Student's *t*-test. *p<0.05

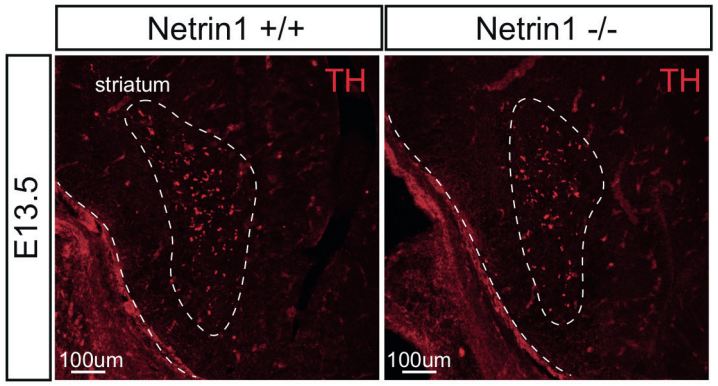

Figure 7

mDA axons innervate the striatum at early developmental stages in *Netrin1-KO* brains

Immunohistochemistry for TH on E13.5 striatal coronal sections in control and *Netrin1-KO* brains. In absence of Netrin1 expression, mDA axons invade the striatum similarly to control brains.

In situ hybridization was used to determine whether DCC was expressed by mDA neurons at early developmental time points. We could detect DCC mRNA at E14.5 and E16.5 both in the medial and lateral dopamine system (Figure 8A). In particular, at E14.5 the entire dopamine system appeared DCC^{+}, with an enrichment in the ventro-medial area. Two days later, at E16.5, the expression of DCC mRNA was higher in the ventro-lateral SNc and in the ventral VTA. To check for DCC protein expression, we performed immunohistochemistry using the anti-DCC antibody published by (Xu et al., 2010). Antibody specificity was confirmed on *DCC-KO* coronal sections (Figure 8B). DCC protein expression was found to co-localize with TH on elongating axons of the MFB at E14.5 (Figure 8C). It is important to notice that DCC protein was also expressed by TH-negative axons which grow longitudinally and in close proximity of mDA axons (Figure 8C).

To determine whether DCC expression is cell-autonomously required by SNc mDA axons during their development, we generated DCC conditional KO (cKO) mice by crossing *Pitx3-Cre* mice (Smidt et al., 2012) with *DCC$^{fl/fl}$* mice (Manitt et al., 2013). In *Pitx3-Cre:DCC$^{fl/fl}$* mice, Cre is expressed by all mDA neurons from E13.5 onwards, thereby inducing DCC ablation from elongating mDA axons. The specific lack of DCC expression by *Pitx3-Cre:DCC$^{fl/fl}$* mDA axons was confirmed by immunohistochemistry on coronal sections of the MFB. DCC was not detected in TH^{+} axons, whereas longitudinal projections running close to mDA axons were DCC^{+} (Figure 8D). Next, *Pitx3-Cre:DCC$^{fl/fl}$:Pitx3-ITC* mice

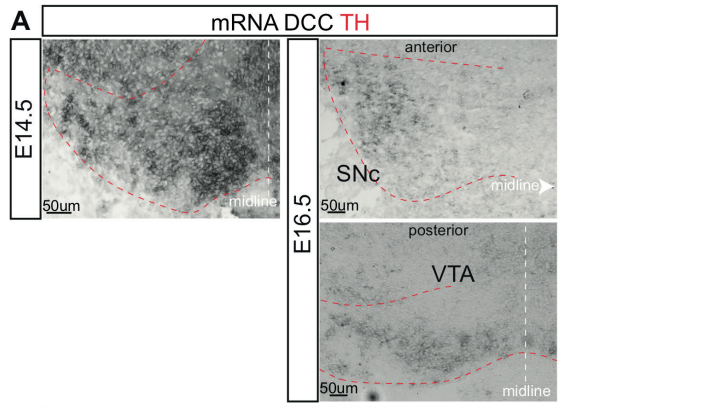

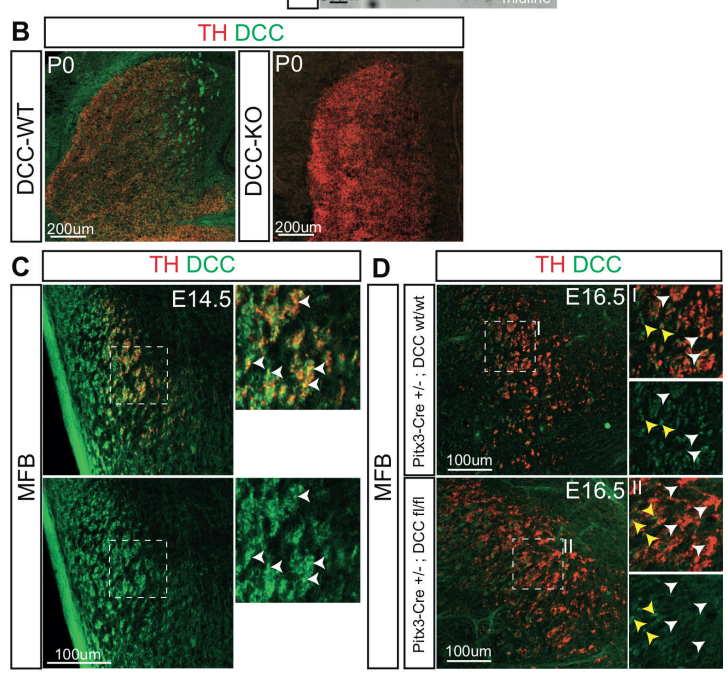

Figure 8

DCC expression during mDA system development

(A) *In situ* hybridization for DCC on E14.5 and E16.5 coronal sections. TH immunohistochemistry was performed on the same sections to delineate the dopamine system (red dotted lines). DCC mRNA is expressed by mDA neurons during mDA axon development. (B) Immunohistochemistry for TH and DCC on control and *DCC-KO* coronal sections to test the specificity of the DCC antibody. On *DCC-KO* sections, no DCC immunostaining is detected. (C) Immunohistochemistry for TH and DCC on MFB coronal sections at E14.5. All mDA axons are DCC positive, as shown by high mag images (right). Longitudinal DCC^{+} axons run next to and intermingled with mDA axons. (D) TH and DCC immunostaining on E16.5 *Pitx3-Cre:DCC$^{fl/fl}$* and control sections. mDA axons in *Pitx3-Cre:DCC$^{fl/fl}$* brains do not show DCC immunostaining.

were generated to conditionally remove DCC from mDA neurons and, at the same time, visualize nigrostriatal axons (Figure 9A). A qualitative analysis of the striatum revealed that both the distribution and the number of SNc mDA axons was not altered in absence of DCC (Figure 9A). This suggests that DCC expression is not cell-autonomously required in nigrostriatal axons to mediate Netrin1-induced branching.

Next, we analyzed the distribution of SNc mDA axons in the MFB. Previous studies have reported that, similar to the aberrant phenotype observed in *Netrin1-KO* mice (Figure 6), a subset of mDA axons leaves the MFB in the caudal hypothalamus of *DCC-KO* brains to navigate towards the midline (Xu et al., 2010). This phenotype could not be detected in *Pitx3-Cre:DCC$^{fl/fl}$:Pitx3-ITC*, meaning that DCC expression is not cell-autonomously required for mDA axon navigation at the level of the caudal hypothalamus (Figure 9B). In addition, SNc mDA axons were segregated normally in the dorsal MFB in *Pitx3-Cre:DCC$^{fl/fl}$:Pitx3-ITC* mice (Figure 9B). This suggests that many of the reported defects in mDA axon development described in *DCC-KO* brains are not caused by cell-autonomous effects of DCC.

Discussion

Development of nigrostriatal and mesolimbic pathways

In this study, the embryonic ontogeny of mDA axon subsets was examined to better understand how the complex network of mDA connections is established during development. Two transgenic mouse lines were used that specifically label SNc and VTA mDA neurons from early stages of dopamine system development. *Pitx3-ITC:ACBT-FlpE* mice allowed us to visualize SNc mDA axons (nigrostriatal projections), whereas in *CCK-Cre:floxed-stop-TdTomato* mice VTA mDA axons (mesocorticolimbic projections) are labeled. Our data show that during development, rather than being dispersed throughout the MFB, nigrostriatal projections are located in the dorsal MFB, while VTA mDA axons occupy a complementary domain in the ventral region (Figure 10A). Increasing evidence indicates that axon-axon interactions and topographical organization of axon tracts is very important during the wiring of the nervous system (Wang and Marquardt, 2013). These mechanisms have not been described for the mDA system yet, but may be of crucial importance during the formation of subset-specific connectivity. SNc and VTA axon segregation may function as a sorting mechanism: the position of an axon within the MFB may be directly related to its final mapping in the striatum. In line with this idea, dorsal nigrostriatal axons innervate dorsal striatal regions, whereas mesolimbic axons establish connections with the ventral striatum. Changes in the segregation of SNc and VTA axons in the MFB may lead to an aberrant innervation of the striatum.

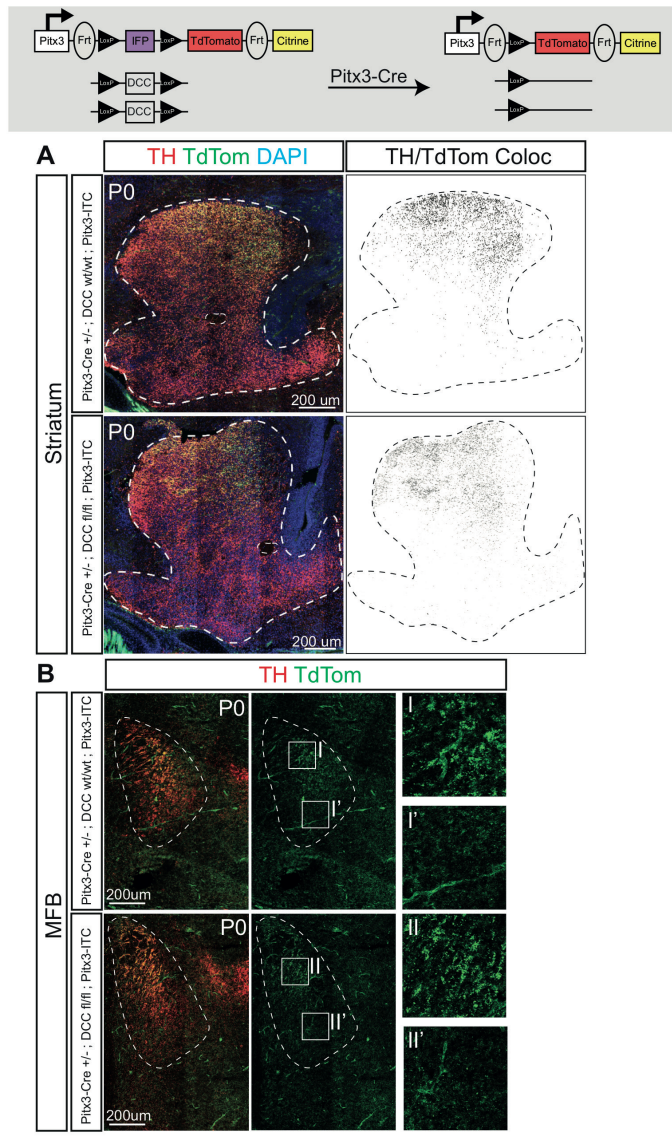

Figure 9

DCC does not play a cell-autonomous role in the SNc mDA axon development

Pitx3-ITC:DCC$^{fl/fl}$ mice were crossed with *Pitx3-Cre* to generate *DCC* conditional KO mice with TdTomato^{+} nigrostriatal axons. (A) Innervation patterns of TdTomato^{+} SNc mDA axons in the striatum of control and DCC conditional KO brains. The absence of DCC expression does not alter SNc mDA axon distribution. (B) Localization of TdTomato^{+} SNc mDA axons in coronal section of the MFB. In DCC conditional KO brains, nigrostriatal projections are segregated in the dorsal striatum similarly to control brains. In addition, the MFB does not show developmental defects in the caudal hypothalamus. Two mouse brains were analyzed for each condition.

In addition, we show that SNc mDA axons start striatal invasion before VTA mDA axons. This suggests that SNc axon outgrowth and navigation towards the striatum may start before that of VTA mDA axons. This hypothesis is in accordance with mDA cell-subset birth dating: the majority of SNc mDA neurons is born around E10.5, whereas neurogenesis of VTA mDA neurons is delayed and peaks around E11.5 (Bayer et al., 1995; Bye et al., 2012). SNc mDA axons are therefore most likely generated prior to VTA mDA axons and may provide a scaffold for elongating mesolimbic projections which are tracking them towards the striatum (Figure 10A). Further molecular analyses are required to determine whether and if so which axon guidance molecules guide VTA mDA axons along the trajectory of SNc mDA projections.

SNc and VTA mDA axons innervate specific striatal compartments from early developmental stages

In contrast to previous work, our data show that SNc and VTA mDA axons innervate the dorsal and ventral striatum, respectively, without developing prominent non-specific collaterals in the other compartment (Figure 10A). A small overlap of SNc and VTA axons was only detected in the central part of the striatum. A previous study by Hu et al. showed that during development, mDA axons from the SNc and the VTA initially project nonspecifically to both the dorsolateral and the ventromedial striatum. According to this study, specificity of the axon pathways develops during late embryogenesis when SNc axons begin to target only the dorsolateral striatum, and axons from the VTA project mainly to the ventromedial striatum. These results were obtained by injection of different retrograde tracers into the dorsal and ventral embryonic striatum to determine into which striatal compartment SNc or VTA mDA neurons (or both) were projecting. At E15.5, mDA neurons were detected that were positive for both tracers, indicating that both SNc and VTA neurons innervate the entire striatum. In contrast, at P0, SNc neurons were labelled only by tracers injected in the dorsal stratum, while VTA neurons were labelled exclusively by tracers injected in the ventral striatum. A possible explanation for these seemingly disparate results is that, at E15.5, injection of retrograde tracers may target a large part of the striatum instead of specific compartments.

As discussed in Chapter 3 of this thesis, the majority of SNc neurons labelled in the *Pitx3-ITC* mouse model are located in the ventral SNc tier (vSNc), while fewer Citrine^{+} neurons are positioned in the dorsal SNc tier (dSNc). It is important to consider, however, that dSNc and vSNc mDA neurons form two distinct mDA neuron-subsets. In Parkinson's disease, for example, vSNc mDA neurons are known to be particularly vulnerable as compared to dSNc mDA neurons (Damier et al., 1999; Fearnley and Lees, 1991; Huddleston et al., 2017). In addition, vSNc and dSNc mDA neurons occupy different anatomical regions in the ventral midbrain, and it has been recently demonstrated that they have

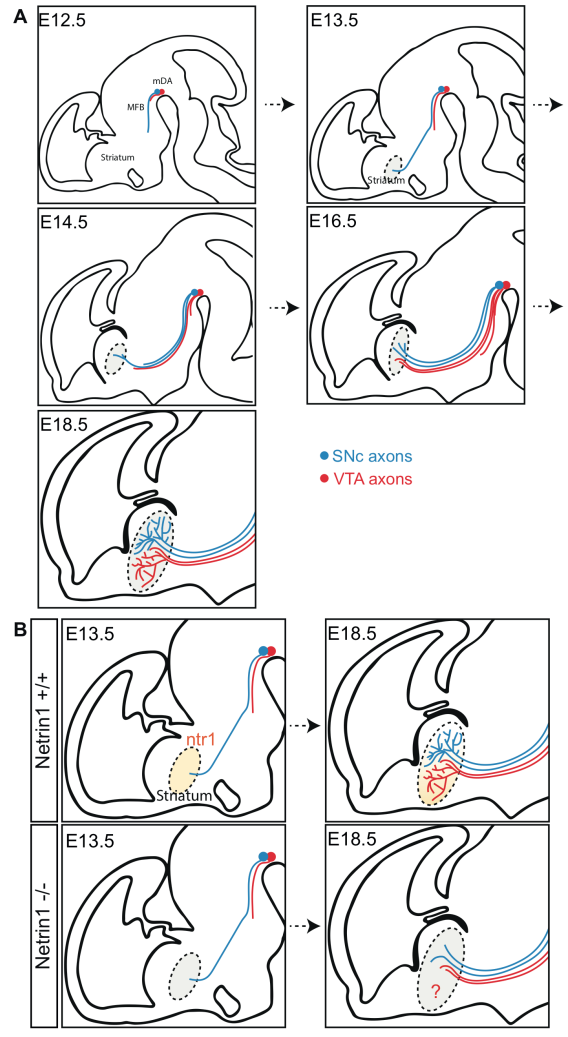

Figure 10

Development of nigrostriatal and mesolimbic projections and role of Netrin1 in nigrostriatal axon branching in the striatum

(A) In our model, SNc mDA axons (blue) are the first mDA axons to grow towards the forebrain at early developmental stages. VTA mDA axons (red) follow SNc mDA axons and occupy the ventral MFB. SNc mDA axons invade the striatum before VTA mDA axons. SNc and VTA mDA axons innervate their respective targets, the dorsal and ventral striatal compartments, already at the initial stages of striatal innervation. (B) Netrin1 expressed in the striatum induces SNc mDA axon branching (top row). In absence of Netrin1 expression, SNc mDA axons invade the striatum normally. However, lack of Netrin1 causes a strong reduction of dorsal striatum innervation (bottom row). It remains to understand the behavior of VTA mDA axons in *Netrin1-KO* brains (question mark in the schematics).

different molecular signatures (La Manno et al., 2016; Poulin et al., 2014). It would be therefore important to understand differences and similarities of vSNc and dSNc mDA axon development, how they navigate towards the striatum, and whether they show specific striatal innervation patterns. To determine the ontogeny of dSNc efferent projections, the development of another mouse model to visualize these axons is needed.

mDA axon navigation through the caudal hypothalamus

The caudal hypothalamus is an important intermediate target for elongating mDA axons. In several KO mouse models lacking axon guidance genes (*Netrin1, DCC, Slit2, Slit1* and *Slit2, Robo1* and *Robo2,* or *Nrp2*), a subset of mDA axons leaves the MFB at the level of the caudal hypothalamus and turns ventrally forming an aberrant bundle that crosses the midline (Bagri et al., 2002; Dugan et al., 2011; Li et al., 2014; Torigoe et al., 2013; Xu et al., 2010). We confirmed these observations in *Pitx3-ITC:ACTB-FlpE:Netrin1-KO* brains, detecting the same aberrant TH^+ axon bundle in the caudal hypothalamus (Figure 6). Although *DCC-KO* brains display the same aberrant phenotype (Xu et al., 2010), the conditional removal of DCC at E13.5 from all mDA neurons does not cause any alteration of mDA axon development (Figure 9). There are several explanations for these results: (1) although mDA axons are DCC^+ during development, DCC is not cell-autonomously required by mDA axons to navigate through the hypothalamus. In this case, the formation of the aberrant TH^+ bundle in *DCC-KO* brains may be the consequence of the mis-routing of other axon bundles that normally function as scaffolds for mDA axons. (2) The conditional removal of DCC from mDA axons at E13.5 occurs too late. DCC protein accumulated at the growth cone of developing mDA axons may function even after the removal of the *DCC* gene and allows mDA axons to normally cross the caudal hypothalamus. To understand whether this hypothesis is true, the *DCC* gene should be conditionally ablated at earlier developmental stages. (3) Another Netrin1 receptor functionally compensates lack of DCC activity. This is probably the most unlikely hypothesis. If other receptors functionally compensate lack of DCC in conditional KO brains, the same receptors would most likely functionally compensate also in *DCC-KO* conditions. This means that *DCC-KO* brains would not display mDA axon defects in the hypothalamus, but this is not the case. To assess this last hypothesis, it is necessary to conditionally remove DCC and other Netrin1 receptors from mDA neurons.

Although lack of Netrin1 causes the formation of an aberrant TH^+ axon bundle in the caudal hypothalamus, nigrostriatal projections do not display any developmental defect in this brain region in *Pitx3-ITC:ACTB-FlpE:Netrin1-KO* brains (Figure 6). This indicates that the aberrant TH^+ axon bundle is most likely composed of VTA mDA axons. To confirm this hypothesis, *CCK-Cre:floxed-stop-TdTomato;Netrin1-KO* mice should be generated and analyzed. TdTomato expression in VTA mDA axons would reveal whether the aberrant TH^+ axon bundle in the caudal hypothalamus is exclusively formed by VTA mDA axons. Interestingly, in *Nrp2* KO mice, the use of the β-galactosidase reporter downstream the *Nrp2* promoter shows that β-galactosidase$^+$ axons are located in the ventral MFB and in the aberrantly projecting axons (Torigoe et al., 2013). Since $Nrp2^+$ mDA neurons are normally positioned in the medial mDA system (Kolk et al., 2009), these results indicate that the aberrant projections in the *Nrp2* KO mice most likely originate from VTA mDA neurons. Together, these data show that lack of Nrp2 or Netrin1 causes similar aberrant phenotypes in the caudal hypothalamus with VTA mDA axons crossing the midline. Although acting through different pathways, both Nrp2 and Netrin1 are crucial for the correct development of VTA mDA axons. It remains to be established whether in these KO mice the abnormal VTA projections form as a result of a lack of expression of repellent cues from the midline, or of defects in other axon bundles that normally act as scaffolds for VTA axons.

Netrin1 induces nigrostriatal axon branching in the dorsal striatum

In the second part of this chapter, we analyzed the functional role of the axon guidance cue Netrin1 in the growth and guidance of nigrostriatal axons. Our results strongly suggest that the expression of Netrin1 in the developing striatum is required for the correct branching of nigrostriatal axons in the dorsal striatal compartment, in line with previous results showing that Netrin1 induces mDA axon branching *in vitro* (Xu et al., 2010). In *Netrin1-KO* brains, the innervation of the dorsal striatum mediated by nigrostriatal axons is strongly decreased. Lack of Netrin1 does not cause SNc mDA axon mis-routing or defects in striatal entry (Figure 10B). However, our conclusions are in contrast with a recent study supporting a different model of nigrostriatal axon development and a different functional role of Netrin1 (Li et al., 2014). This study argues that the *in vivo* gradient of Netrin1 in the striatum induces attraction of SNc and VTA mDA axons in a different manner: low levels of Netrin1 in the dorso-medial striatum attract SNc mDA axons, whereas high levels in the ventro-lateral striatum attract VTA mDA axons (Li et al., 2014). In line with this, their data suggest that in *Netrin1-KO* mice SNc mDA axons do not innervate the dorso-medial striatum but rather accumulate in the ventro-lateral region (Li et al., 2014). Our analyses of *Pitx3-ITC:ACTB-FlpE:Netrin1-KO* mice, in which nigrostriatal axons are labeled in a *Netrin1* KO context, did not reveal an accumulation of SNc axons in the ventral striatum as suggested by Li et al. Although a strong decrease of nigrostriatal innervation was detected in the dorsal striatum, the overall striatal innervation pattern of SNc axons was preserved in the absence of Netrin1 expression. The accumulation of TH^+ axons into the ventral striatum reported by Li et al., which was not quantified and not analyzed in the present

study, may be due to an increase of VTA mDA axon innervation or branching. To test this hypothesis, *CCK-Cre:floxed-stop-TdTomato:Netrin1-KO* mice may be generated. These mice would allow VTA mDA axon visualization in brains lacking Netrin1 expression, and the analysis at the level of the striatum would reveal whether VTA mDA axon branching is increased in absence of Netrin1.

Netrin1-mediated SNc mDA axon branching does not require cell-autonomous expression of DCC

Our data indicate that Netrin1 induces SNc mDA axon branching in the dorsal striatum *in vivo*. Surprisingly, Netrin1-mediated axon branching does not require the cell-autonomous expression of DCC. In *Pitx3-Cre:DCC$^{fl/fl}$* mice, where DCC expression has been removed from embryonic mDA neurons, dopaminergic innervation of the dorsal striatum appears similar to control. Although our data do not implicate DCC in Netrin1-mediated branching of nigrostriatal axons, other Netrin1 receptors may be responsible for this process, such as UNCs, Neogenin, or DsCAM. However, not much is known about their expression in mDA neurons and their functional role(s) in nigrostriatal axons. At E18.5, UNC5A and UNC5C receptors are not expressed by SNc mDA neurons *in vivo*, while their expression increases in adult brains (Xu et al., 2010). UNC5A and UNC5C are therefore not involved in nigrostriatal axon branching that occurs during late embryonic and early postnatal stages. Neogenin mRNA is expressed by both SNc and VTA mDA neurons during embryonic development (van den Heuvel et al., 2013), however, its function in SNc mDA axons remains to be determined. The mRNA of DsCAM, that has been recently identified as a novel Netrin1 receptor (Ly et al., 2008), has been detected by single cell RNA-seq to be enriched in developing SNc mDA neurons as compared to VTA mDA neurons (La Manno et al., 2016). Similar to Neogenin, it has to be assessed whether DsCAM is important for Netrin1-induced nigrostriatal branching. Further studies are needed to determine which receptor(s) transduces Netrin1 signaling responsible for nigrostriatal axon branching in the dorsal striatum.

Conclusions

Despite its fundamental physiological functions and involvement in disorders such as Parkinson's disease, the cellular and molecular mechanisms important for the development of mDA axon-subsets remain mostly unknown (Brignani and Pasterkamp, 2017; Van den Heuvel and Pasterkamp, 2008; Prestoz et al., 2012). Our study shows how nigrostriatal and mesolimbic mDA axon-subsets assemble in space and time, enabling the formation of highly specific patterns of efferent connections in the dorsal and ventral striatum. During their navigation towards the striatum, SNc mDA axons are segregated in the dorsal MFB, while VTA mDA axons are segregated ventrally. Nigrostriatal axons invade the striatum prior to mesolimbic mDA axons. Furthermore, SNc and VTA mDA axons innervate the dorsal and ventral striatum, respectively, without developing mis-targeted axon collaterals in non-specific striatal compartments. Further, our findings demonstrate that absence of Netrin1 in the striatum leads to a prominent decrease of nigrostriatal axon branching *in vivo*. This observation strongly indicates that Netrin1 is necessary for the correct dopaminergic innervation of the dorsal striatum. Finally, we provide evidence that Netrin1-mediated SNc axon branching is DCC independent.

Materials and methods

Mouse lines

All animal use and care were in accordance with institutional guidelines. The morning on which a vaginal plug was detected was considered embryonic day 0.5 (E0.5). *Pitx3-ITC* mice were generated by us and described in Chapter 3 of this thesis. *ACTB-FlpE* (Rodríguez et al., 2000) and *CCK-Cre* (Taniguchi et al., 2011) mice were obtained from The Jackson Laboratories. *Pitx3-Cre* mice were a kind gift of Marten Smidt (University of Amsterdam) (Smidt et al., 2012). *DCC$^{fl/fl}$* mice were kindly provided by Cecilia Flores (McGill University) (Manitt et al., 2013). *DCC-KO* mice were obtained by crossing *DCC$^{fl/fl}$* and *EIIa-Cre* mice (Lakso et al., 1996). *Netrin1-KO* mice were kindly provided by Lisa Goodrich (Harvard Medical School) (Yung et al., 2015).

Immunohistochemistry

Adult mice were transcardially perfused with ice-cold saline followed by 4% PFA, brains were isolated and post-fixed overnight at 4^{o}C in 4%PFA. Brains were then cryoprotected in 30% sucrose in PBS. Next, they were frozen and cryopreserved at -80^{o}C. 20 µl brain sections were prepared at the cryostat. Sections were first blocked with blocking solution (0.4% Tryton X-100, 1% BSA, in PBS) for 1h at RT, next they were incubated with primary antibodies in blocking solution at 4^{o}C overnight. The next day, they were washed in PBS and incubated with secondary antibodies in blocking solution at RT for 1h. Then, they were washed and counterstained with DAPI (4',6'-diamidino-2-phenylindole; 0.1 mg/ml in PBS; Invitrogen). Mounting was performed with FluorSave reagent (Merck Millipore). Staining was visualized on a Zeiss Axioskop A1 epi fluorescent microscope or by confocal laser-scanning microscopy (LSM 880, Zeiss). For the analyses of axon localization in *Pitx3-ITC:ACTB-FlpE* and in *Pitx3-ITC:ACTB-Flp:Netrin1-KO* mice, Imaris software was used to determine TH/Citrine co-localization in the MFB and stratum. Then, Imaris was used to calculate the number of co-localizing spots in the ventral and dorsal

compartments. To evaluate the axon position in *CCk-Cre:floxed-stop-TdTomato* mice, Fiji (ImageJ) was used to determine TH/TdTomato co-localization in the MFB and striatum, and to calculate the number of co-localizing pixels in the ventral and dorsal regions. All the analyses were performed on three independent samples, if not otherwise specified in the figures, and representative images are shown. Statistical evaluations were done in GraphPad Prism 7.

Primary Ab.	Species	Company	Catalog Number	Concentration
TH	rabbit	Millipore	AB152	1:1000
TH	sheep	Millipore	AB1542	1:500
GFP	rabbit	Life technologies	A11122	1:500
GFP	chicken	Abcam	ab13970	1:500
Otx2	goat	R&D	AF1979	1:500
TdTomato	rabbit	Rockland	600-401-379	1:500
DCC	goat	Santa Cruz	Sc-6535	1:500
Islet1	mouse	DSHB	40.3A4	1:200

In situ hybridization

To collect E12.5, E14.5, E16.5, and E18.5 embryo brains, timed-pregnant females were killed by means of cervical dislocation. Embryonic brains were isolated and directly frozen. 16 µm sections were cut on a cryostat, air-dried for 2h and frozen at -80°C. Nonradioactive in situ hybridization was performed according to (Pasterkamp et al., 2007). cDNA was made from whole mouse brain RNA using a one-step RT-PCR kit (Qiagen), according to supplied protocol and using the following primers:

DCC:
5'- CCCAGTCCAAGGTTACAGATTG -3'
5'- GGAGGTGTCCAACTCATGATG -3'

Netrin1:
5'- GATGTGCCAAAGGCTACCAG-3'
5'- TTCTTGCACTTGCCCTTCTTC-3'

cDNA was cloned into pGEM-T Easy (Promega) and transcribed using either SP6 or T7 RNA polymerase (Roche) and digoxigenin-labeled nucleotide mix (Roche) to produce digoxigenin-labeled cRNA probes. Digoxigenin was detected using anti-digoxigenin FAB fragments conjugated to alkaline phosphatase (Roche; 1:5000) and stained with NBT/BCIP (Roche). Sections were mounted using FluorSave reagent and visualized on a Zeiss Axioscope 2. Representative images are shown.

Hemi-brain organotypic cultures

E12.5 embryos were isolated from pregnant wild-type or *Pitx3-ITC:ACTB-FlpE* mice. Brains were isolated and placed in ice-cold dissection medium. Brains were cut in two hemi-brains along the midline. Meninges, brainstem and cortex were removed. Hemi-brains were placed (midline down) on culture inserts (Falcon), with culture medium (70% v/v Basal Eagle Medium, 26% v/v cHBSS, 20mM D-glucose, 1mM L-glutamine, penicillin/streptomycin), and cultured at 37°C and 5% CO_2 for 2 or 3 days. Hemi-brains were fixed in 4% paraformaldehyde, and incubated with antibodies against TH, Islet1, and GFP in blocking buffer (3% BSA and 0.1% Triton-X-100 in PBS), ON 4°C. After PBS washes, the hemi-brains were stained with Alexa-conjugated secondary antibodies (ON, 4°C), washed, and mounted on microscope glasses. Images were taken with a Zeiss Axioskop 2. At least 3 cultures from different litters were used to compare results. Representative images are shown.

Acknowledgements

We thank all the members of the Pasterkamp laboratory for discussions and suggestions, and Peter Burbach for the critical reading of the manuscript. Special thanks to Christian van der Meer and Leo Halewijn, who helped with the maintenance of mouse colonies. We are grateful to Marten Smidt, Cecilia Flores, and Lisa Goodrich for providing us with mouse lines.
Work on axon guidance and the developing dopamine system was financially supported by the Netherlands Organization for Scientific Research (ALW-VICI), the People Program (Marie Curie Actions) of the European Union's Seventh Framework Program (FP7) 2007–2013 under REA grant agreement number 289581 (NPlast), the UU Strategic Theme "Dynamics of Youth", and Stichting ParkinsonFonds.

References

Aransay, A., Rodríguez-López, C., García-Amado, M., Clascá, F., and Prensa, L. (2015). Long-range projection neurons of the mouse ventral tegmental area: a single-cell axon tracing analysis. Front. Neuroanat. *9*, 59.

Bagri, A., Marín, O., Plump, A.S., Mak, J., Pleasure, S.J., Rubenstein, J.L.R., and Tessier-Lavigne, M. (2002). Slit Proteins Prevent Midline Crossing and Determine the Dorsoventral Position of Major Axonal Pathways in the Mammalian Forebrain. Neuron *33*, 233–248.

Baker, K.A., Moore, S.W., Jarjour, A.A., and Kennedy, T.E. (2006). When a diffusible axon guidance cue stops diffusing: roles for netrins in adhesion and morphogenesis. Curr. Opin. Neurobiol. *16*, 529–534.

Bayer, S.A., Wills, K. V, Triarhou, L.C., and Ghetti, B. (1995). Time of neuron origin and gradients of neurogenesis in midbrain dopaminergic neurons in the mouse. Exp. Brain Res. *105*, 191–199.

Björklund, A., and Dunnett, S.B. (2007). Dopamine neuron systems in the brain: an update. Trends Neurosci. *30*, 194–202.

Bonnin, A., Torii, M., Wang, L., Rakic, P., and Levitt, P. (2007). Serotonin modulates the response of embryonic thalamocortical axons to Netrin1. Nat. Neurosci. *10*, 588–597.

Brignani, S., and Pasterkamp, R.J. (2017). Neuronal Subset-Specific Migration and Axonal Wiring Mechanisms in the Developing Midbrain Dopamine System. Front. Neuroanat. *11*, 55.

Bye, C.R., Thompson, L.H., and Parish, C.L. (2012). Birth dating of midbrain dopamine neurons identifies A9 enriched tissue for transplantation into parkinsonian mice. Exp. Neurol. *236*, 58–68.

Chaudhury, D., Walsh, J.J., Friedman, A.K., Juarez, B., Ku, S.M., Koo, J.W., Ferguson, D., Tsai, H.-C., Pomeranz, L., Christoffel, D.J., et al. (2012). Rapid regulation of depression-related behaviours by control of midbrain dopamine neurons. Nature *493*, 532–536.

Cord, B.J., Li, J., Works, M., McConnell, S.K., Palmer, T., and Hynes, M.A. (2010). Characterization of axon guidance cue sensitivity of human embryonic stem cell-derived dopaminergic neurons. Mol. Cell. Neurosci. *45*, 324–334.

Damier, P., Hirsch, E.C., Agid, Y., and Graybiel, A.M. (1999). The substantia nigra of the human brain. II. Patterns of loss of dopamine-containing neurons in Parkinson's disease. Brain *122 (Pt 8)*, 1437–1448.

Dugan, J.P., Stratton, A., Riley, H.P., Farmer, W.T., and Mastick, G.S. (2011). Midbrain dopaminergic axons are guided longitudinally through the diencephalon by Slit/Robo signals. Mol. Cell. Neurosci. *46*, 347–356.

Edley, S.M., and Herkenham, M. (1984). Comparative development of striatal opiate receptors and dopamine revealed by autoradiography and histofluorescence. Brain Res. *305*, 27–42.

Faraone, S. V., Perlis, R.H., Doyle, A.E., Smoller, J.W., Goralnick, J.J., Holmgren, M.A., and Sklar, P. (2005). Molecular Genetics of Attention-Deficit/Hyperactivity Disorder. Biol. Psychiatry *57*, 1313–1323.

Fearnley, J.M., and Lees, A.J. (1991). Ageing and Parkinson's disease: substantia nigra regional selectivity. Brain *114 (Pt 5)*, 2283–2301.

Gerfen, C.R. (1992). The neostriatal mosaic: multiple levels of compartmental organization. Trends Neurosci. *15*, 133–139.

Gerfen, C.R., Herkenham, M., and Thibault, J. (1987). The neostriatal mosaic: II. Patch- and matrix-directed mesostriatal dopaminergic and non-dopaminergic systems. J. Neurosci. *7*, 3915–3934.

van den Heuvel, D.M.A., Hellemons, A.J.C.G.M., and Pasterkamp, R.J. (2013). Spatiotemporal expression of repulsive guidance molecules (RGMs) and their receptor neogenin in the mouse brain. PLoS One *8*, e55828.

Van den Heuvel, D.M.A., and Pasterkamp, R.J. (2008). Getting connected in the dopamine system. Prog. Neurobiol. *85*, 75–93.

Hu, Z., Cooper, M., Crockett, D.P., and Zhou, R. (2004). Differentiation of the midbrain dopaminergic pathways during mouse development. J. Comp. Neurol. *476*, 301–311.

Huddleston, D.E., Langley, J., Sedlacik, J., Boelmans, K., Factor, S.A., and Hu, X.P. (2017). *In vivo* detection of lateral-ventral tier nigral degeneration in Parkinson's disease. Hum. Brain Mapp. *38*, 2627–2634.

Ikemoto, S. (2007). Dopamine reward circuitry: Two projection systems from the ventral midbrain to the nucleus accumbens–olfactory tubercle complex. Brain Res. Rev. *56*, 27–78.

Kalia, L. V, and Lang, A.E. (2015). Parkinson's disease. Lancet *386*, 896–912.

Khan, S., Stott, S.R.W., Chabrat, A., Truckenbrodt, A.M., Spencer-Dene, B., Nave, K.-A., Guillemot, F., Levesque, M., and Ang, S.-L. (2017). Survival of a Novel Subset of Midbrain Dopaminergic Neurons Projecting to the Lateral Septum Is Dependent on NeuroD Proteins. J. Neurosci. *37*.

Kolk, S.M., Gunput, R.-A.F., Tran, T.S., van den Heuvel, D.M.A., Prasad, A.A., Hellemons, A.J.C.G.M., Adolfs, Y., Ginty, D.D., Kolodkin, A.L., Burbach, J.P.H., et al. (2009). Semaphorin 3F Is a Bifunctional Guidance Cue for Dopaminergic Axons and Controls Their Fasciculation, Channeling, Rostral Growth, and Intracortical Targeting. J. Neurosci. *29*.

Lakso, M., Pichel, J.G., Gorman, J.R., Sauer, B., Okamoto, Y., Lee, E., Alt, F.W., and Westphal, H. (1996). Efficient in vivo manipulation of mouse genomic sequences at the zygote stage. Proc. Natl. Acad. Sci. U. S. A. *93*, 5860–5865.

Lammel, S., Hetzel, A., Häckel, O., Jones, I., Liss, B., and Roeper, J. (2008). Unique properties of mesoprefrontal neurons within a dual mesocorticolimbic dopamine system. Neuron *57*, 760–773.

Lerner, T.N., Shilyansky, C., Davidson, T.J., Evans, K.E., Beier, K.T., Zalocusky, K.A., Crow, A.K., Malenka, R.C., Luo, L., Tomer, R., et al. (2015). Intact-Brain Analyses Reveal Distinct Information Carried by SNc Dopamine Subcircuits. Cell *162*, 635–647.

Li, J., Duarte, T., Kocabas, A., Works, M., McConnell, S.K., and Hynes, M.A. (2014). Evidence for topographic guidance of dopaminergic axons by differential Netrin1 expression in the striatum. Mol. Cell. Neurosci. *61*, 85–96.

Lin, L., Rao, Y., and Isacson, O. (2005). Netrin1 and slit-2 regulate and direct neurite growth of ventral midbrain dopaminergic neurons. Mol. Cell. Neurosci. *28*, 547–555.

Ly, A., Nikolaev, A., Suresh, G., Zheng, Y., Tessier-Lavigne, M., and Stein, E. (2008). DSCAM Is a Netrin Receptor that Collaborates with DCC in Mediating Turning Responses to Netrin1. Cell *133*, 1241–1254.

Manitt, C., Mimee, A., Eng, C., Pokinko, M., Stroh, T., Cooper, H.M., Kolb, B., and Flores, C. (2011). The netrin receptor DCC is required in the pubertal organization of mesocortical dopamine circuitry. J. Neurosci. *31*, 8381–8394.

Manitt, C., Eng, C., Pokinko, M., Ryan, R.T., Torres-Berrío, A., Lopez, J.P., Yogendran, S. V, Daubaras, M.J.J., Grant, A., Schmidt, E.R.E., et al. (2013). dcc orchestrates the development of the prefrontal cortex during adolescence and is altered in psychiatric patients. Transl. Psychiatry *3*, e338.

La Manno, G., Gyllborg, D., Codeluppi, S., Nishimura, K., Salto, C., Zeisel, A., Borm, L.E., Stott, S.R.W., Toledo, E.M., Villaescusa, J.C., et al. (2016). Molecular Diversity of Midbrain Development in Mouse, Human, and Stem Cells. Cell *167*, 566–580.e19.

Matsuda, W., Furuta, T., Nakamura, K.C., Hioki, H., Fujiyama, F., Arai, R., and Kaneko, T. (2009). Single nigrostriatal dopaminergic neurons form widely spread and highly dense axonal arborizations in the neostriatum. J. Neurosci. *29*, 444–453.

Milton, A.L., and Everitt, B.J. (2012). The persistence of maladaptive memory: Addiction, drug memories and anti-relapse treatments. Neurosci. Biobehav. Rev. *36*, 1119–1139.

Morello, F., Prasad, A.A., Rehberg, K., Vieira de Sá, R., Antón-Bolaños, N., Leyva-Diaz, E., Adolfs, Y., Tissir, F., López-Bendito, G., and Pasterkamp, R.J. (2015). Frizzled3 Controls Axonal Polarity and Intermediate Target Entry during Striatal Pathway Development. J. Neurosci. *35*, 14205–14219.

Pasterkamp, R.J., Kolk, S.M., Hellemons, A.J., and Kolodkin, A.L. (2007). Expression patterns of semaphorin7A and plexinC1 during rat neural development suggest roles in axon guidance and neuronal migration. BMC Dev. Biol. *7*, 98.

Poulin, J.-F., Zou, J., Drouin-Ouellet, J., Kim, K.-Y.A., Cicchetti, F., and Awatramani, R.B. (2014). Defining Midbrain Dopaminergic Neuron Diversity by Single-Cell Gene Expression Profiling. Cell Rep. *9*, 930–943.

Powell, A.W., Sassa, T., Wu, Y., Tessier-Lavigne, M., and Polleux, F. (2008). Topography of thalamic projections requires attractive and repulsive functions of Netrin1 in the ventral telencephalon. PLoS Biol. *6*, e116.

Prestoz, L., Jaber, M., and Gaillard, A. (2012). Dopaminergic axon guidance: which makes what? Front. Cell. Neurosci. *6*, 32.

Reynolds, L.M., Pokinko, M., Torres-Berrío, A., Cuesta, S., Lambert, L.C., Del Cid Pellitero, E., Wodzinski, M., Manitt, C., Krimpenfort, P., Kolb, B., et al. (2018). DCC Receptors Drive Prefrontal Cortex Maturation by Determining Dopamine Axon Targeting in Adolescence. Biol. Psychiatry *83*, 181–192.

Rodríguez, C.I., Buchholz, F., Galloway, J., Sequerra, R., Kasper, J., Ayala, R., Stewart, A.F., and Dymecki, S.M. (2000). High-efficiency deleter mice show that FLPe is an alternative to Cre-loxP. Nat. Genet. *25*, 139–140.

Schmidt, E., Brignani, S., Adolfs, Y., Lemstra, S., Demmers, J., Vidaki, M., Donahoo, A.-L.S., Lilleväli, K., Vasar, E., Richards, L.J., et al. (2014). Subdomain-mediated axon-axon signaling and chemoattraction cooperate to regulate afferent innervation of the lateral habenula. Neuron *83*, 372–387.

Smidt, M.P., von Oerthel, L., Hoekstra, E.J., Schellevis, R.D., and Hoekman, M.F.M. (2012). Spatial and Temporal Lineage Analysis of a Pitx3-Driven Cre-Recombinase Knock-In Mouse Model. PLoS One *7*, e42641.

Taniguchi, H., He, M., Wu, P., Kim, S., Paik, R., Sugino, K., Kvitsiani, D., Kvitsani, D., Fu, Y., Lu, J., et al. (2011). A resource of Cre driver lines for genetic targeting of GABAergic neurons in cerebral cortex. Neuron *71*, 995–1013.

Torigoe, M., Yamauchi, K., Tamada, A., Matsuda, I., Aiba, A., Castellani, V., and Murakami, F. (2013). Role of neuropilin-2 in the ipsilateral growth of midbrain dopaminergic axons. Eur. J. Neurosci. *37*, 1573–1583.

Veenvliet, J. V., and Smidt, M.P. (2014). Molecular mechanisms of dopaminergic subset specification: fundamental aspects and clinical perspectives. Cell. Mol. Life Sci. *71*, 4703–4727.

Wang, L., and Marquardt, T. (2013). What axons tell each other: axon–axon signaling in nerve and circuit assembly. Curr. Opin. Neurobiol. *23*, 974–982.

Winterer, G., and Weinberger, D.R. (2004). Genes, dopamine and cortical signal-to-noise ratio in schizophrenia. Trends Neurosci. *27*, 683–690.

Xu, B., Goldman, J.S., Rymar, V.V., Forget, C., Lo, P.S., Bull, S.J., Vereker, E., Barker, P.A., Trudeau, L.E., Sadikot, A.F., et al. (2010). Critical Roles for the Netrin Receptor Deleted in Colorectal Cancer in Dopaminergic Neuronal Precursor Migration, Axon Guidance, and Axon Arborization. Neuroscience *169*, 932–949.

Yung, A.R., Nishitani, A.M., and Goodrich, L. V (2015). Phenotypic analysis of mice completely lacking netrin 1. Development *142*, 3686–3691.

Chapter 5

Netrin1 regulates migration of specific subsets of midbrain dopaminergic neurons

Sara Brignani[1], Divya A. Raj[1], Youri Adolfs[1],
Anna A. de Ruiter[1], Erik Schild[1], Juan A. Moreno-Bravo[2],
A. Chédotal[2], R. Jeroen Pasterkamp[1]

[1] Department of Translational Neuroscience, Brain Center Rudolf Magnus, University Medical Center Utrecht, Utrecht University, Utrecht, The Netherlands

[2] Sorbonne Universités, UPMC Université Paris 06, INSERM, CNRS, Institut de la Vision, 75012 Paris

Abstract

Neuron migration during brain development is an extremely important process that determines the final position of neurons, their afferent and efferent connections, and therefore the functions of circuits they are part of. Although neuron migration has been extensively studied in layered brain structures, like the cerebral cortex, migration of neurons into brain nuclei remains poorly understood. The aim of this study is to delineate the migratory behavior of different dopaminergic neuron-subsets in relation to the migration of neighboring GABAergic neurons, and to discover guidance cues that regulate this process. We identify two distinct substantia nigra compacta neuron-subsets that rely on two different mechanisms for their migration. In addition, we demonstrate that Netrin1 is functionally involved during the migration of both substantia nigra compacta neuron-subsets. Netrin1 expressed by radial glia fibers guide the radial migration of one specific SNc mDA neuron-subset via the DCC receptor. Netrin1^{+} longitudinal axons elongating across the ventral midbrain may guide SNr GABAergic neurons into the anterior midbrain where they generate the anterior SNr. The migration of SNr GABAergic neurons in the ventro-lateral side of the SNc determines the formation of the SNc wing-like structure. Our study unveils cellular and molecular mechanisms of midbrain neuron migration based on the interaction between different neuronal populations and between neurons and axons. These processes guide the development of both dopaminergic neuron-subsets and neuronal nuclei positioned in adjacent territories.

Introduction

The development of brain architecture requires the execution of sophisticated biological processes that are precisely regulated in space and time. New neurons arise from the proliferative epithelium (ventricular zone) surrounding the ventricular space of the neural tube, followed by migration along pre-determined routes to their final destination. Here, they integrate into the developing neural network by generating dendritic and axonal processes that extend towards and establish new connections with other elements of the network. The migration of newborn neurons is therefore an essential process of the development of the nervous system. The correct positioning of neurons in the complex neuronal network determines in fact the input and output connections they establish and ultimately their functional role. Our current knowledge of the cellular and molecular mechanisms underlying neuron migration is mainly based on studies focused on migratory behaviors in laminated structures, e.g. the cortex, the hippocampus, or the cerebellum, where neurons move along radial and tangential migratory routes to ultimately reside in a specific neuronal layer (Reviewed in (Chédotal, 2010; Marín et al., 2010)). In contrast, less is known about migration processes guiding the formation of brain nuclei, which are often subdivided in smaller neuron-clusters of related neurons. It is not clear for example whether and how neurons of nearby nuclei can influence each other's migration, and which molecules guide the migration of neuron-subsets belonging to the same or to adjacent neuron-clusters. To address these fundamental questions, we focused our attention on the development of the dopaminergic system of the midbrain, an interesting example of brain structure formed by neuronal nuclei. The dopamine system receives afferent connections from several brain regions (Watabe-Uchida et al., 2012), mediates cognitive and motor behaviors, and is associated with multiple psychiatric and neurodegenerative disorders. Midbrain dopamine neurons (mDA neurons) are anatomically divided in three main neuron nuclei called substantia nigra compacta (SNc), ventral tegmental area (VTA), and retrorubral field (RRF). In addition, the substantia nigra reticulata (SNr), which resides at the ventro-lateral side of the SNc, is mainly composed by GABAergic neurons. Growing evidence demonstrates, however, that these nuclei may be further subdivided into smaller mDA and GABAergic neuron-subsets based on subset-specific molecular signatures (La Manno et al., 2016; Poulin et al., 2014). In particular, SNc may be subdivided in ventral and dorsal tiers (vSNc and dSNc), while SNr GABAergic neurons form at least two distinct neuronal populations positioned in the anterior and posterior SNr (Lahti et al., 2016). In the adult brain, SNc mDA neurons are strongly interconnected with the neighboring SNr GABAergic neurons: single-neuron tracing studies show that dendrites of SNc mDA neurons extend into the SNr (Fallon et al., 1978; Tepper et al., 1987), while SNr GABAergic neurons provide a local axon

collateral network that innervates both the SNr and the SNc (Mailly et al., 2003). In addition, circuit-tracing studies have demonstrated that SNr GABAergic neurons provide monosynaptic inputs onto SNc mDA neurons (Watabe-Uchida et al., 2012).

Very little is known about mDA and SNr GABAergic neuron migration. mDA neurons are born between embryonic day (E) 10.5 and E14.5 from mDA progenitors located in the ventral midbrain ventricular zone (Bayer et al., 1995; Bye et al., 2012). To reach their final destination in the marginal zone, mDA neurons undergo radial migration along the fibers of radial glia cells (Bodea et al., 2014; Shults et al., 1990). Then, SNc mDA neurons migrate tangentially, from the medial towards the lateral marginal zone, to ultimately develop the characteristic wing-like SNc structure. During tangential migration, SNc mDA neurons appear aligned to commissural axons which may function as migrating scaffolds (Kawano et al., 1995). At the same time, both anterior and posterior SNr GABAergic neurons are generated and undergo neuronal migration. In particular, GABAergic neurons of the anterior SNr are born around E9.5 from neural progenitors located in the ventricular zone of the caudal midbrain. From this position, they migrate following a rostro-lateral direction to ultimately occupy the SNr (Madrigal et al., 2016). Although mDA and SNr GABAergic neurons eventually occupy two adjacent territories and are functionally related, whether and how the migration of one population may influence the migration of the other is undetermined. Furthermore, based on loss-of-function mouse mutants where mDA neuron migration is impaired, only the extracellular matrix protein Reelin and its receptors have been implicated in the migration of a mDA neuron-subset, the intermediate SNc (Bodea et al., 2014; Kang et al., 2010; Nishikawa et al., 2003). However, the precise functional role of Reelin and its receptors is not clear yet.

Our study aims at understanding cellular and molecular processes that underlay the migration of different dopaminergic neuron-subtypes in relation to the migratory behavior of their neighboring GABAergic neurons using *in vivo* and *in vitro* approaches. Recently we have generated a new mouse model, called *Pitx3-ITC:ACTB-FlpE*, where SNc mDA neurons are labelled by Citrine expression and which distinguishes them from Citrine-negative VTA neurons both in embryonic and adult brains (Chapter 3). In this study, we analyze SNc mDA neuron migration using *the Pitx3-ITC:ACTB-FlpE* mouse model both in 2D and 3D. We then identify the axon guidance cue Netrin1 as a multi-functional key regulator of SNc mDA neuron migration. Our observations unveil that Netrin1 expressed by radial glia fibers steer the migration of one specific SNc mDA neuron-subset via the DCC receptor. In addition, Netrin1 expressed by longitudinal axons running across the ventral midbrain may guide SNr GABAergic neurons into the anterior midbrain where they generate the anterior SNr. SNr GABAergic neuron migration in the ventro-lateral part of the SNc determines the formation of the SNc wing-like structure present in postnatal and adult brains. Together, our findings unveil some of the principles of midbrain neuron migration based on neuron-axon and neuron-neuron interactions that orchestrate the development of both mDA neuron-subsets and adjacent brain nuclei.

Results

1. SNc mDA neuron migrate along three axes

We have recently developed a new mouse model where SNc mDA neurons are exclusively labelled by the fluorescent reporter Citrine, while VTA mDA neurons are Citrine-negative (Chapter 3). This mouse model, called *Pitx3-ITC:ACTB-FlpE*, allowed us to distinguish SNc mDA neurons and axons from VTA neurons, both in adult and embryonic brains (Chapter 3 and 4). In the midbrain, Citrine expression begins at E13.5 and continues throughout development towards adulthood. To determine the spatio-temporal features of SNc mDA neuron migration, midbrain coronal sections were analyzed by immunohistochemistry. The analysis was performed on *Pitx3-ITC:ACTB-FlpE* brains at three different developmental time points (E13.5, E16.5, and P0) (Figure 1A). Since in *Pitx3-ITC:ACTB-FlpE* mice not all SNc mDA neurons are labelled, leading and trailing processes of migrating SNc neurons could be visualized and used to determine the direction of movement. At E13.5 and E16.5, migrating SNc neurons were detected both in the medial and lateral intermediate zones, with leading and trailing processes oriented along the dorso-medial to ventro-lateral axis. In contrast, at P0 the medial mDA system was almost devoid of Citrine$^+$ neurons, indicating the SNc mDA neuron migration was complete. A similar analysis was performed on midbrain horizontal sections, both at E13.5 and P0, to examine the caudo-rostral migration of SNc mDA neurons (Figure 1B). Immunostaining for Citrine revealed that at E13.5, but not at P0, SNc mDA neurons were distributed along the developing dopamine system, from caudal to rostral levels, showing mDA neuronal processes oriented in a caudo-to-rostral direction.

Next, the migration of SNc mDA neurons was analyzed in 3D using 3DISCO (3-dimensional imaging of solvent cleared organs) clearing technology and light sheet imaging (Belle et al., 2014). This technique allowed us to visualize the entire dopamine system and the position of migrating Citrine$^+$ SNc mDA neurons. The analysis was performed on *Pitx3-ITC:ACTB-FlpE* brains at E13.5 and P0, time points representing a developing dopamine system and a system where mDA neuron migration is complete, respectively (Figure 2A-C). 3D reconstructions of the mDA system were analyzed by Imaris software to automatically detect all Citrine$^+$ mDA neurons and their spatial positions. Then, the mDA system was

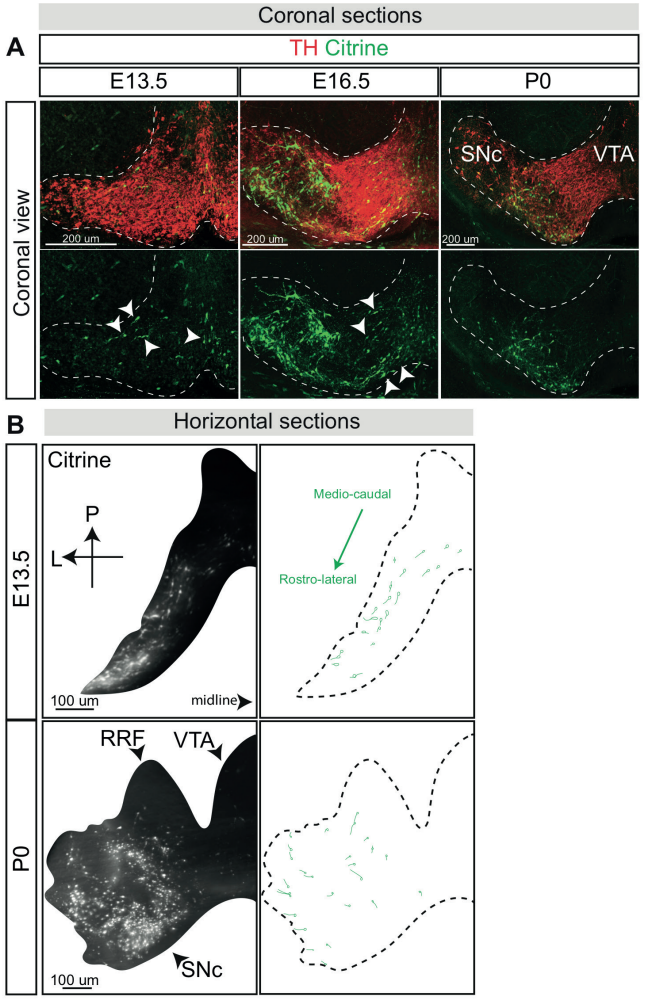

Figure 1

SNc mDA neuron migration in 2D

(A) Midbrain coronal sections of *Pitx3-ITC:ACTB-FlpE* brains at E13.5, E16.5, and P0. All mDA neurons are TH^+, while SNc mDA neurons are labelled by Citrine. Sparse labelling of SNc mDA neurons allows the visualization of leading and trailing processes. At E13.5 and E16.5, migrating processes of SNc mDA neurons are oriented in a medio-dorsal to ventro-lateral direction. Migrating SNc mDA neurons occupy both the medial and lateral intermediate zone. In contrast, at P0, SNc mDA neurons are confined to the lateral mDA system, indicating that at this age SNc mDA neuron migration is complete. (B) Horizontal sections of *Pitx3-ITC:ACTB-FlpE* mice at E13.5 and P0. TH immunostaining was used to define the borders of the mDA system (black). $Citrine^+$ SNc mDA neurons are shown in white. At E13.5, but not at P0, SNc mDA neurons are distributed all along the mDA system, from caudal to rostral regions. The direction of migrating processes shows that SNc mDA neurons migrate in a rostro-lateral direction.

divided in 8 Bins of equal thickness in caudo-rostral, medio-lateral, or dorso-ventral directions (Figure 2A-B). The number of $Citrine^+$ mDA neurons in each Bin was calculated and expressed as percentage of the total number of $Citrine^+$ neurons detected in the entire dopamine system (Figure 2C). Along the caudo-rostral axis, the percentage of SNc mDA neurons in the caudal Bins (Bin2 and Bin3) was higher at E13.5 as compared to P0, whereas in more rostral Bins (Bin6 and Bin7) cell counts were higher at P0 compared to E13.5 (Figure 2C). This indicates that SNc mDA neurons are migrating along the caudo-rostral axis from the caudal to the rostral midbrain. SNc mDA neurons were also migrating in the dorso-ventral and medio-lateral directions. The percentage of SNc mDA neurons in dorsal Bins (Bin4 and Bin5) was higher at E13.5 than at P0, while counts in ventral Bins (Bin7) was higher at P0 compared to E13.5. For medio-lateral migration, the percentage of $Citrine^+$ neurons in medial Bins (Bin1 and Bin2) was higher at E13.5 than P0, whereas the opposite was true in more lateral Bins (Bin4, Bin5, and Bin6) (Figure 2C).

In summary, we demonstrate by both 2D and 3D analyses that SNc mDA neuron migration occurs in three directions: dorso-ventral, medio-lateral, and caudo-rostral. These data for the first time show that neurons that are born in the ventricular zone of the caudal midbrain may migrate rostrally to generate the two fronto-lateral wing-like structures of the SNc.

2. Subdomain-specific expression of axon guidance molecules in the ventral midbrain

Although our results show that SNc mDA neuron migration occurs in three directions, very little is known about how this migration is mediated at the molecular level. To identify the underlying molecular mechanisms that guide SNc mDA neurons towards their final position, laser-capture microdissection was performed on the embryonic mDA system in combination with mass spectrometry to identify subdomain-specific proteins in the ventral midbrain at the time of SNc neuron migration (Figure 3A). The goal of this analysis was to identify axon guidance receptors expressed by migrating mDA neurons, and axon guidance cues expressed by the surrounding environment, since axon guidance molecules are likely candidates for controlling neuron migration. Three distinct areas were micro-dissected from the ventral dopaminergic midbrain: medial, ventro-lateral, and dorso-lateral regions. E16.5 *Pitx3-GFP* mouse brains (Zhao et al., 2004) expressing GFP in the entire mDA system were used to visualize the target regions for laser microdissection (Figure 3A). From the list of guidance molecules detected by mass spectrometry (Figure 3B), the axon guidance receptors PlxnA1, PlxnA4, and EphB1 were excluded from further analyses because of their expression patterns. PlxnA1 was found to be

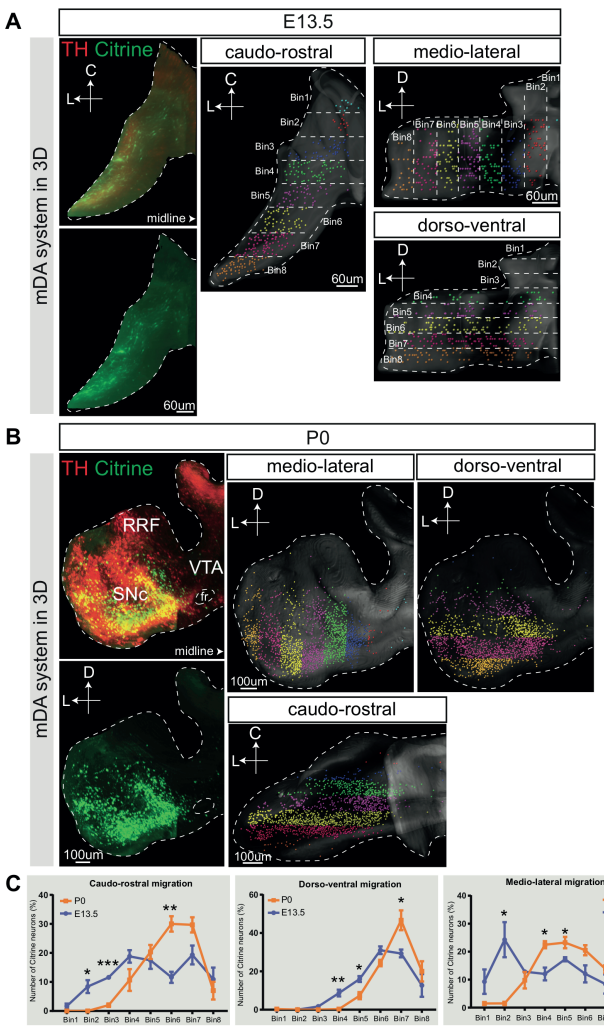

Figure 2

SNc mDA neuron migration in 3D

E13.5 and P0 *Pitx3-ITC:ACTB-FlpE* brains analyzed using 3DISCO (3-dimentional imaging of solvent cleared organs) clearing technology and light sheet imaging. (Left columns in A and B) TH immunostaing is used to delimit the mDA system (red). Citrine immunostaining labels SNc mDA neurons (green). (Middle and right columns in A and B) 3D reconstructions of the mDA system. Citrine^{+} mDA neurons are automatically detected and their spatial positions determined. The mDA system is divided in 8 Bins of equal thickness in caudo-rostral, medio-lateral, or dorso-ventral directions. (C) Quantification of the number of Citrine^{+} mDA neurons in each Bin expressed as percentage of the total number of Citrine^{+} neurons detected in the entire dopamine system. Three brains for each condition are analyzed. Results are shown as Mean ± SEM. Data were tested for significance by Student's *t*-test. *p<0.05, **p<0.01, ***p<0.001

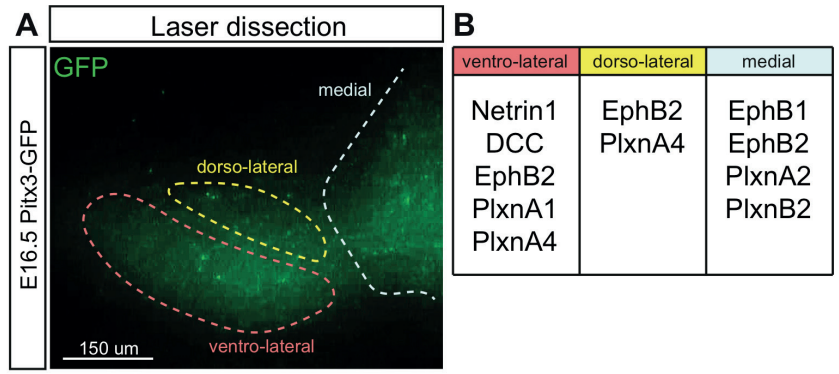

Figure 3

Laser-capture microdissection of three areas of the ventral midbrain

(A) Laser-capture microdissection was performed on E16.5 *Pitx3-GFP* midbrain sections. GFP fluorescence is shown in green. Three distinct areas were micro-dissected from the ventral midbrain: medial, ventro-lateral, and dorso-lateral regions. (B) Axon guidance molecules detected by mass spec analysis in the three midbrain areas.

expressed at low levels only by a few mDA neurons (Torre et al., 2010); PlxnA4 was reported to not be expressed in the midbrain by mDA neurons but rather by radial glia cells (Torre et al., 2010); while EphB1 expression was exclusively detected in neurons of the SNr (Richards et al., 2007). However, for PlxnB2 we detected an enrichment in medial mDA neurons by *in situ* hybridization on wild type E16.5 tissue sections (Suppl. Figure 1). In addition, X-Gal staining was performed on PlxnB2$^{LacZ/+}$ brain sections, which express the enzyme β-galactosidase downstream of the PlxnB2 promoter (Eucomm). Even in this case, an enrichment of X-Gal staining was observed in the medial compared to the lateral mDA system (Suppl. Figure 1). To understand whether PlxnB2 expression was required for mDA neuron migration, *PlxnB2-KO* brains were analyzed at E14.5 and P5. No mDA neuron migration defects were detected at both time points (Suppl. Figure 1), indicating that either PlxnB2 expression is not necessary for the correct migration of mDA neurons or that other molecules are functionally compensating for the absence of PlxnB2.

For the rest of the study, we focused on the axon guidance cue Netrin1 and its receptor DCC, which, from the screening, were both enriched in the ventro-lateral midbrain.

3. Lack of Netrin1 differentially affects distinct subsets of SNc mDA neurons

To determine whether Netrin1 expression is important for the correct migration of mDA neurons, a 3D analysis of the ventral midbrain was performed on E18.5 *Netrin1-KO* (Yung et al., 2015) and WT brains using the 3DISCO clearing technology and light sheet imaging. This method allowed us to visualize the entire mDA system in 3D to establish whether in *Netrin1-KO* brains the mDA system was altered. 3D reconstructions of the midbrain showed a strong change in mDA system morphology in *Netrin1-KO* brains compared to controls (Figure 4A). In particular, we observed an abnormal distribution of TH$^+$ neurons in the ventricular zone, a flattened VTA, a large number of TH$^+$ neurons in the reticular nucleus, and a population of mDA neurons positioned in a lateral territory which is normally occupied by the SNr (Figure 4A-B).

We next examined whether and how the migration of SNc mDA neurons was compromised in the absence of Netrin1. A 3D analysis was performed on the midbrain of E18.5 *Pitx3-ITC:ACTB-FlpE:Netrin1-KO* mice, to visualize Citrine$^+$ SNc mDA neurons in brains lacking Netrin1 expression. The results showed that the position of Citrine$^+$ neurons in *Netrin1-KO* brains was shifted laterally compared to WT brains (Figure 5A). To quantify this aberrant phenotype, the distance from the midline to the tissue edge was calculated and the area divided in three 3D Bins having equal thickness (Figure 5A). Then, the percentage of Citrine$^+$ neurons inside each Bin over the total number of Citrine$^+$ neurons was measured, and the difference between Netrin1 WT and KO Bins was calculated. The number of SNc mDA neurons decreased in medial Bin1 and Bin2 in *Netrin1-KO* brains compared to controls, whereas it was significantly increased in the most lateral Bin3 (Figure 5B). This indicates that loss of Netrin1 causes aberrant migration of SNc mDA neurons into more lateral territory.

To analysis this defect in more detail, *Pitx3-ITC:ACTB-FlpE:Netrin1-KO* brains were sectioned and immunostained for TH and Citrine. At the level of the anterior SNc, the two migration defects observed in the 3D reconstruction were confirmed: (1) a population of TH$^+$/Citrine$^+$ neurons shifted into more lateral territory that was normally occupied by SNr GABAergic neurons, and (2) a population of TH$^+$/Citrine$^-$ neurons that was aberrantly positioned in the dorsal reticular nucleus (Figure 5C-E). In order to determine whether this latter population constituted SNc or VTA mDA neurons, TH$^+$ neurons in the reticular nucleus were immunostained for Sox6 and Otx2, markers for SNc and VTA neurons, respectively (Panman et al., 2014). The majority of the dorsally mislocalized neurons was Sox6$^+$ and did not express Otx2 (Figure 5D-E). This, indicates that TH$^+$ neurons in the reticular nucleus are SNc mDA neurons. Altogether, our data show that, in absence of Netrin1, two different SNc mDA

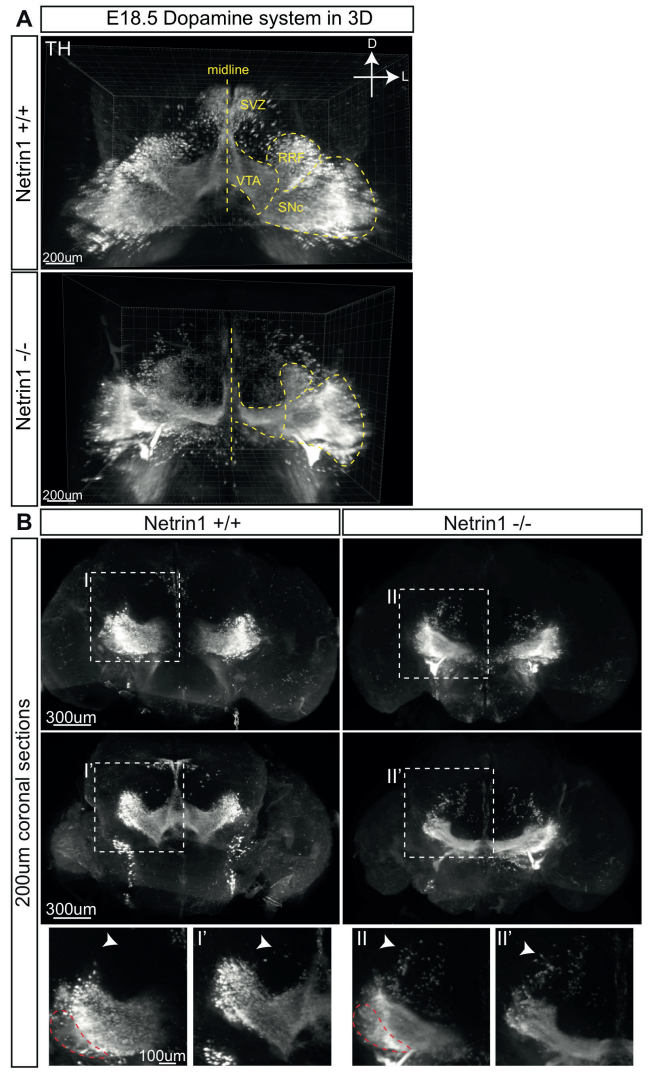

Figure 4

3D reconstruction of the mDA system in *Netrin1-KO* and control brains

(A) Frontal view of the mDA system in 3D. TH immunostaining is shown in white. Control (top) and *Netrin1-KO* (bottom) brains are compared. (B) 200um coronal sections from the brains shown in (A). In the *Netrin1-KO* brains as compared to controls, several defects are detected: an abnormal distribution of TH$^+$ neurons in the ventricular zone, a flattened VTA, a high number of TH$^+$ neurons in the reticular nucleus (white arrows), and a population of mDA neurons positioned in a lateral territory that is normally occupied by the SNr (red dotted lines).

neuron subsets become mislocalized: a population of Citrine$^-$ SNc mDA neurons is dispersed in the dorsal reticular nucleus, whereas Citrine$^+$ SNc mDA neurons shift more laterally into the SNr.

4. Netrin1 expressed by radial glia fibers guides SNc mDA neurons via DCC

To understand why lack of Netrin1 caused the aberrant migration of a subset of SNc mDA neurons into the reticular nucleus, Netrin1 expression patterns were investigated, both by *in situ* hybridization and immunohistochemistry. The expression of Netrin1 mRNA was analyzed at several developmental time points during mDA system development (E12.5, E14.5, and E16.5). At E12.5, Netrin1 mRNA was confined to the ventricular zone, which is the location of radial glia cells and mDA progenitors (Figure 6A). At E14.5 and E16.5, Netrin1 mRNA was also expressed by differentiated mDA neurons (Figure 6A). Surprisingly, at E12.5 Netrin1 protein was detected beyond the ventricular zone, in contrast to the expression shown by *in situ* hybridization (Figure 6B-D, Figure 10, Suppl. Figure 2). Netrin1 was co-expressed with the brain lipid binding protein (BLBP), a marker for radial glia cells, both at the level of cell bodies and radial fibers (Figure 6C). In addition, Netrin1 was detected in L1CAM$^+$ contralateral axons which cross the midline at the ventral midbrain, and by L1CAM$^+$ longitudinal axons in the cerebral peduncle (Figure 6B, Figure 10, Suppl. Figure 2). Although Netrin1 mRNA was strongly expressed by mDA neurons (Figure 6A), Netrin1 protein was not detected in mDA cell bodies (Figure 10C). Specificity of the anti-Netrin1 antibody was confirmed on E12.5 *Netrin1-KO* tissue sections (Figure 6B). The analysis of migrating mDA neurons revealed that at E12.5 the processes of radially migrating mDA neurons were aligned to Netrin1$^+$ radial glia fibers, indicating that Netrin1 may provide guidance for this neuron-subset (Figure 6D). To assess whether migrating mDA neurons are responsive to Netrin1 guidance, stripe assays were performed by plating dissociated E13.5 mDA neurons on a carpet of Netrin1 stripes. *Pitx3-GFP* embryos were used to visualize the ventral midbrain during dissection. We found that 80% of GFP$^+$ neurons were attracted by Netrin1 stripes, while they were evenly distributed on control stripes (Figure 6E). These results indicate that mDA neurons can respond to Netrin1.

Next, we asked whether Netrin1 expressed by radial glia fibers was required *in vivo* for the radial migration of mDA neurons, and whether the aberrant position of Citrine$^-$ SNc neurons in the reticular nucleus of *Netrin1-KO* brains was caused by lack of Netrin1 in radial glia fibers. To assess this hypothesis, E18.5 conditional KO *Shh-Cre:Netrin1$^{fl/fl}$* mice were analyzed by immunohistochemistry. In the ventral midbrain of these mice, the *Shh* promoter drives Cre expression in the floor plate and part of the basal plate both in radial glia cells and mDA progenitors

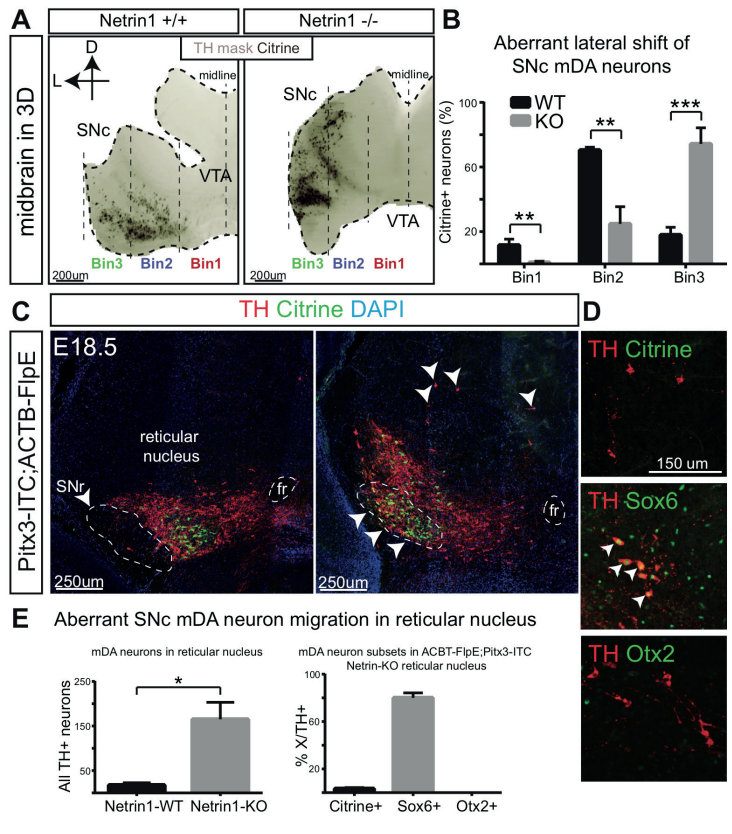

Figure 5

Altered migration of two SNc mDA populations in absence of Netrin1

Analysis of E18.5 *Pitx3-ITC:ACTB-FlpE:Netrin1-KO* and control mice in 3D (A, B) and in coronal sections (C-E). (A) Frontal view of half mDA system, with the midline on the right. TH immunostaining was used to determine the edges of the mDA system. Citrine$^+$ SNc mDA neurons are shown in black. The mDA system is divided by dotted lines in three 3D Bins having equal thickness. The percentage of Citrine$^+$ neurons in each Bin over the total amount of Citrine$^+$ neurons is measured both in *Netrin1-WT* and *KO* brains, and shown in (B). Citrine$^+$ neurons in *Netrin1-KO* brains are shifted more laterally compared to WT brains. Three brains for each condition are analyzed. Results are shown as Mean ± SEM. Data were tested for significance by Student's *t*-test. **p<0.01, ***p<0.001 (C) Immunostaining for TH and Citrine. Two migration defects are detected in absence of Netrin1: (1) a population of TH$^+$/Citrine$^+$ neurons is shifted laterally, and (2) a population of TH$^+$/Citrine$^-$ neurons that is aberrantly positioned in the reticular nucleus. (D) Immunostaining for Sox6, Otx2, TH, and Citrine on mDA neurons aberrantly positioned in the reticular nucleus of *Netrin1-KO* brains. The majority of the dorsally mislocalized neurons is Sox6$^+$, and does not express Otx2. (E) Quantification of the total number of mDA neurons mislocalized in the reticular nucleus of *Netrin1-KO* brains compared to controls (left). Quantification of TH$^+$ neurons mislocalized in the reticular nucleus of *Netrin1-KO* brains expressing Citrine, Sox6, or Otx2. Results are shown as percentage of mDA neurons positive for Citrine, Sox6, or Otx2 over the total amount of TH$^+$ neurons detected in the reticular nucleus. Three brains for each condition are analyzed. Results are shown as Mean ± SEM. Data were tested for significance by Student's *t*-test. *p<0.05

from E10.5 (Achim et al., 2012; Tang et al., 2009). *In situ* hybridization for Netrin1 at E13.5 on *Shh-Cre:Netrin1$^{fl/fl}$* and control brains showed that Netrin1 mRNA was conditionally ablated from the basal plate and floor plate of the ventral midbrain, and from mDA neurons (Figure 7A). *Shh-Cre:Netrin1$^{fl/fl}$* brains showed a population of TH$^+$ mDA neurons aberrantly positioned in the reticular nucleus, similarly to *Netrin1-KO* brains (Figure 7B). Netrin1 mRNA was detected in the dopamine system both at E14.5 and E16.5 (Figure 6A). Therefore, to exclude the possibility that the aberrant phenotype observed in E18.5 *Shh-Cre:Netrin1$^{fl/fl}$* brains was caused by lack of Netrin1 expression in the mDA neurons, Netrin1 was selectively removed from mDA neurons by crossing *Pitx3-Cre* and *Netrin1$^{fl/fl}$* mice. *Pitx3-Cre:Netrin1$^{fl/fl}$* mice express Cre in all mDA neurons from E13.5. No mDA neurons were detected in the reticular nucleus in these mice (Figure 7C). This suggests that radial glia fibers are the source of Netrin1 that guides the radial migration of a subset of SNc neurons.

DCC is a well characterized Netrin1 receptor, involved in mediating Netrin1 attraction both in axons and migrating neurons. DCC is expressed by migrating mDA neurons as shown by us and others (Chapter 4) (Xu et al., 2010), and *DCC-KO* brains display aberrantly positioned mDA neurons in the reticular nucleus, as observed in *Netrin1-KO* brains (Xu et al., 2010). Together, these observations suggested that DCC may be required in a SNc neuron-subset during radial migration to respond to Netrin1$^+$ radial glia fibers. The analysis of *Pitx3-Cre:DCC$^{fl/fl}$* brains, where DCC expression was conditionally ablated from all mDA neurons (Figure 8D in Chapter 4), indeed showed a subset of mDA neurons was abnormally positioned in the reticular nucleus (Figure 7D).

In conclusion, we have identified a subset of SNc neurons which migrate radially along Netrin1$^+$ radial glia fibers. Netrin1 functions as an attractant for migrating mDA neurons, and the conditional ablation of Netrin1 from radial glia fibers causes the aberrant migration of a mDA neuron-subset into the reticular nucleus. DCC expressed by mDA neurons mediates Netrin1-induced attraction to radial glia fibers, and the conditional removal of DCC expression from mDA neurons causes the abnormal positioning of mDA neurons in the reticular nucleus.

5. Aberrant migration of SNc mDA neurons and GABAergic neurons in the absence of Netrin1

Netrin1-KO brains showed two distinct migration defects: Citrine$^-$ SNc mDA neurons were aberrantly positioned in the reticular nucleus, whereas Citrine$^+$ SNc mDA neurons were shifted laterally into a region normally identified as SNr. While the first population requires Netrin1 expression by radial glia fibers, lack of Netrin1 expression from radial glia did not cause aberrant migration of Citrine$^+$ SNc mDA neurons into the SNr (Figure 7E).

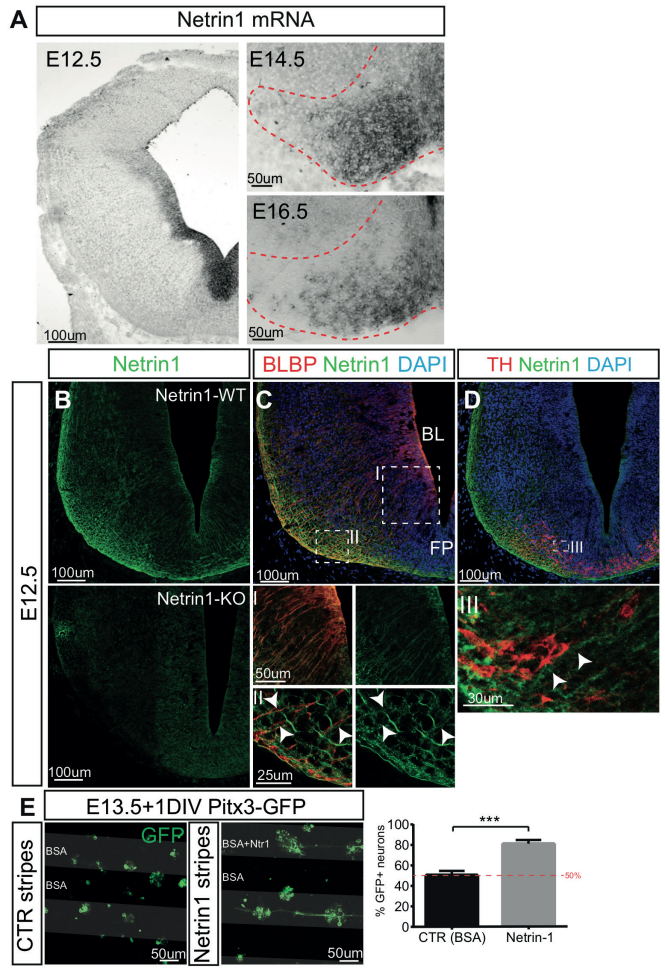

Figure 6

Netrin1 is expressed by radial glia fibers and *in vitro* functions as adhesive substrate for migrating mDA neurons

(A) *In situ* hybridization for Netrin1 mRNA on coronal sections at E12.5, E14.5, and E16.5. mDA system is defined by red dotted lines. Netrin1 mRNA is expressed by cells located in the ventricular zone at E12.5 and at later time points. Netrin1 mRNA is detected in the mDA system from E14.5 and during all embryonic development. (B) Immunostaining for Netrin1 in *WT* (top) and *Netrin1-KO* midbrain coronal sections. Netrin1 immunostaining is not detected in *Netrin1-KO* brains. (C) Netrin1 protein is expressed by BLBP$^+$ radial glia cells. The protein is detected both in cell bodies and fibers of radial glia cells (high mac at the bottom). (D) mDA neurons migrate along Netrin1$^+$ radial glia fibers. (E) E13.5 GFP$^+$ mDA neurons dissociated from *Pitx3-GFP* midbrains are plated on alternate stripes containing Netrin1 or control BSA. Results are quantified as percentage of GFP$^+$ neurons on Netrin1 stripes over the total amount of counted GFP$^+$ neurons. Three independent experiments are analyzed. Results are shown as Mean ± S.D. Data were tested for significance by Student's *t*-test. ***p<0.001

To investigate the cellular and molecular events that cause the lateral shift of Citrine$^+$ SNc mDA neurons in *Netrin1-KO* brains, we first asked whether mDA neurons were intermingled with GABAergic neurons of the anterior SNr. To visualize both neuronal populations, immunohistochemical analyses were performed on E18.5 *Netrin1-KO* and control brains for TH and Six3, markers for mDA neurons and GABAergic neurons of the anterior SNr, respectively (Conte et al., 2005; Lahti et al., 2016). In wild type brains, Six3$^+$ GABAergic neurons were grouped in a compact nucleus positioned ventro-lateral of the SNc. Six3$^+$ and TH$^+$ neurons were divided in two distinct and adjacent territories (Figure 8A). In *Netrin1-KO* brains, the lateral shift of mDA neurons was associated with a decreased number of GABAergic neurons in the SNr. mDA neurons and GABAergic neurons were not intermingled, but instead occupied two distinct territories (Figure 8A). Next, immunohistochemistry for DARPP32 was performed to label striatal projections. While DARPP32$^+$ striatal axons were projecting into the ventro-lateral SNr in control brains, they accumulated at the lateral edge of the midbrain in absence of Netrin1 (Figure 8B).

Next, *Pitx3-ITC:ACTB-FlpE:Netrin-KO* brains were analyzed to determine the position of Citrine$^+$ SNc mDA neurons in brains lacking Netrin1. Immunohistochemistry was performed on two coronal sections of the anterior dopamine system, where both the anterior SNc and SNr could be seen. When Netrin1 was lacking, Citrine$^+$ SNc mDA neurons were aberrantly positioned in the territory that was normally occupied by Six3$^+$ GABAergic neurons (Figure 8C). Six3$^+$ neurons were not forming a compact nucleus in the ventro-lateral SN, but were divided in smaller neuron-clusters often positioned at the lateral edge of the midbrain (Figure 8C) or, in some cases, located inside the SNc (Figure 8D). Furthermore, it is important to note that although Citrine$^+$ and Six3$^+$ neurons were aberrantly positioned in *Netrin1-KO* brains, these cells were never intermingled (Figure 8C-D). These observations suggest that these two populations may repel each other.

6. Migration of Six3$^+$ GABAergic neurons into the SNr is required for the correct development of the SNc

To dissect the mechanisms underlying the altered migration of SNc mDA and SNr GABAergic neurons in *Netrin1-KO* brains, it is important to understand how these neuronal populations migrate normally. Therefore, SNc mDA neuron and GABAergic neuron migration were studied in the rostral midbrain at critical developmental time points (E14.5, E15.5, and E16.5) (Figure 9A). At E14.5, Six3$^+$ GABAergic neurons were not detected in the anterior ventro-lateral midbrain, and mDA neurons were positioned at the edge of the ventral midbrain close to the pial surface. At E15.5, the first Six3$^+$ GABAergic neurons were

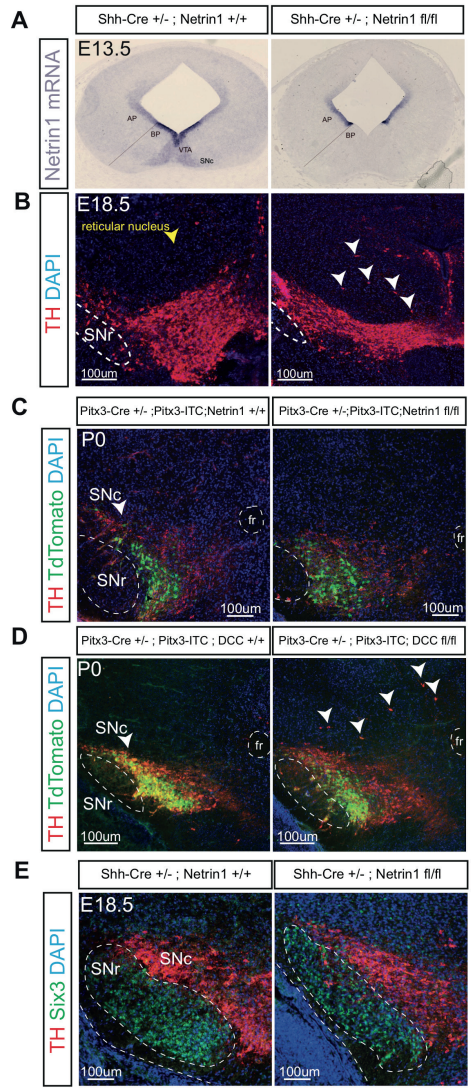

Figure 7

Netrin1$^+$ radial glia fibers guide mDA neuron radial migration via DCC *in vivo*

(A) Immunohistochemistry for TH on midbrain coronal sections in *Shh-Cre:Netrin1$^{fl/fl}$* and control. Loss of Netrin1 from radial glia cells and mDA neurons results in mislocalization of mDA neurons in the reticular nucleus. (B) Immunohistochemistry for TH and Citrine on midbrain coronal sections in *Pitx3-Cre:Netrin1$^{fl/fl}$* and control. Lack of Netrin1 expression from mDA neurons does not perturb mDA neuron migration. (C) Immunohistochemistry for TH and Citrine on midbrain coronal sections in *Pitx3-Cre:DCC$^{fl/fl}$* and control. The conditional removal of DCC from mDA neurons results in altered migration of mDA neurons in the reticular nucleus. (D) Immunohistochemistry for TH and Six3 on midbrain coronal sections in *Shh-Cre:Netrin1$^{fl/fl}$* and control. Loss of Netrin1 from mDA neurons and radial glia cells does not cause altered migration of Six3$^+$ GABAergic neurons.

detected ventro-laterally of the migrating SNc mDA neurons. One day later, at E16.5, the anterior SNr was more clearly defined, with many Six3$^+$ GABAergic neurons occupying the ventro-lateral part of the SNc. At this time point, SNc mDA neurons were no longer located next to the pial surface, but instead were positioned more dorsally (Figure 9A).

We then compared *Netrin1-KO* and control brains before and after GABAergic neuron migration (Figure 9B-C). At E13.5, the distribution of TH$^+$ and Six3$^+$ neurons in wild type and KO brains was comparable with mDA neurons located next to the pial surface. However, the mDA system appeared more flattened in *Netrin1-KO* brains compared to controls (Figure 9B). In contrast, a clear defect was detected between *Netrin1-KO* and control brains at E16.5. E16.5 wild type brains showed a compact cluster of Six3$^+$ GABAergic neurons forming the SNr. In contrast, lack of Netrin1 expression caused aberrant migration of both TH$^+$ and Six3$^+$ neurons. mDA neurons were shifted laterally, whereas the anterior population of GABAergic neurons was divided in small clusters, some flattened next to the pial surface and some located inside the SNc. Intriguingly, GABAergic and mDA neurons were occupying separate territories and did never mingle (Figure 9C).

Since SNc mDA neurons and SNr GABAergic neurons normally occupy two adjacent territories and both showed migration defects in *Netrin1-KO* brains, we hypothesized that the migration of SNc and SNr neurons was interdependent, i.e. altered migration of one population may affect the other. To assess whether mDA neurons influence Six3$^+$ GABAergic neuron migration, we performed an *in vivo* genetic ablation study. *DTA* mice, which conditionally express the subunit A of the diphtheria toxin, were crossed with *Pitx3-Cre* mice to ablate the mDA system from E13.5 onwards. E18.5 *Pitx3-Cre:DTA* mice displayed a complete loss of mDA neurons, whereas the position of Six3$^+$ GABAergic neurons of the SNr was unaffected (Figure 9D). Thus, the migration of Six3$^+$ GABAergic neurons of the anterior SNr does not require mDA neurons. On the other hand, migration of GABAergic neurons in the ventro-lateral side of the SNc may push mDA neurons, which are initially attached to the pial surface, more dorsally. To assess whether GABAergic neuron migration could influence the migration of SNc mDA neurons, *in vitro* slice cultures were used as a model for Six3$^+$ GABAergic neuron ablation. It has been described that Six3$^+$ GABAergic neurons originate in the caudal midbrain and migrate along the anterior-posterior axis towards the anterior SNr (Madrigal et al., 2016). Therefore, coronal slices were generated from *Pitx3-GFP* brains at E14.5. At this time point, mDA neurons are attached to the pial surface, whereas GABAergic neurons are still migrating from the caudal midbrain and are excluded from slices containing the rostral mDA system. Brain slices were fixed at 3 or 4 days *in vitro,* which corresponds to E17.5/E18.5 *in vivo*. After fixation, brain slices containing a low number of Six3$^+$ neurons were selected for analysis to

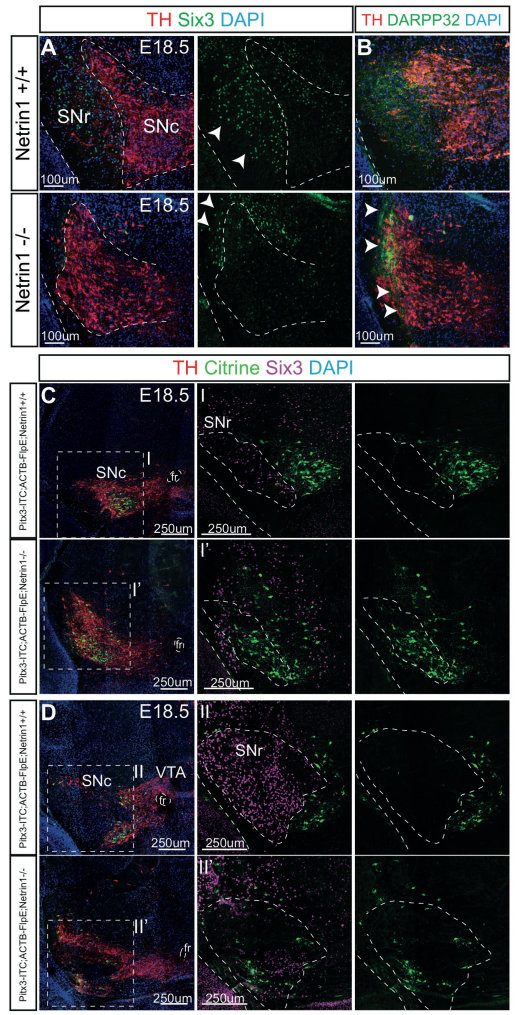

Figure 8

In Netrin1-KO brains, both Citrine+ SNc mDA neurons and Six3+ GABAergic neurons show aberrant migration

(A) Immunohistochemistry for TH and Six3 on coronal sections of *Netrin1-KO* and control midbrains. In WT brains, Six3$^+$ GABAergic neurons form a compact nucleus in the ventro-lateral side of the SNc. In *Netrin1-KO* brains, the lateral shift of mDA neurons is associated with a decreased number of GABAergic neurons aberrantly located in a small lateral region. (B) Immunohistochemistry for DARPP32$^+$ striatal projections. DARPP32$^+$ striatal axons project into the ventro-lateral SNr of control brains. In *Netrin1-KO* brains, they accumulate at the lateral edge of the midbrain. (C, D) Immunohistochemistry for TH, Citrine, and Six3 in *Pitx3-ITC:ACTB-FlpE:Netrin-KO* brains. Coronal sections from two levels of the anterior dopamine system are shown. Lack of Netrin1 determines Citrine$^+$ SNc mDA neurons mislocalization in the territory that is normally occupied by Six$^+$ GABAergic neurons. Six3$^+$ neurons do not form a compact nucleus in the ventro-lateral SN. They are instead divided in smaller neuron-clusters at the lateral edge of the midbrain.

assess the behavior of migrating mDA neurons in the absence of GABAergic neurons. This analysis showed that lack of Six3$^+$ GABAergic neurons prevented the formation of SNc wing-like structures. TH$^+$ neurons remained attached to the pial surface as observed in E14.5 brains, indicating that GABAergic neuron migration into the ventro-lateral side of the developing SNc is required for the development of the SNc (Figure 9E). Furthermore, these data suggest that migrating Six3$^+$ GABAergic neurons might repel mDA neurons to generate a region devoid of mDA neurons that will become the SNr.

7. Axonal expression of Netrin1 may guide Six3$^+$ GABAergic neuron migration

We observed that the formation of the SNc wing-like structure relies on the correct migration of Six3$^+$ GABAergic neurons. Thus, lack of Netrin1 might induce aberrant Six3$^+$ GABAergic neuron migration and, as a consequence, SNc mDA neurons remain partially attached to the pial surface of the midbrain. These events may result, at E18.5, in the lateral shift of SNc mDA neurons that is observed in *Netrin1-KO* brains. To understand which source of Netrin1 is important for Six3$^+$ GABAergic neuron migration, we performed immunohistochemical analyses to detect Netrin1 expression at several developmental time points (Figure 10A-C). In the midbrain of E12.5 embryos, both coronal and sagittal brain sections showed that Netrin1 was strongly expressed by L1CAM$^+$ longitudinal axons running in the cerebral peduncle (Figure 10A-B). Netrin1 was detected in the cerebral peduncle even at later developmental time points (E13.5, E14.5, and E16.5), when Six3$^+$ GABAergic neurons are migrating longitudinally from the caudal midbrain to the SNr (Figure 10C). These longitudinal Netrin1$^+$/L1CAM$^+$ axons may function as guidance scaffolds for SNr GABAergic neurons migrating from the posterior to the anterior midbrain.

We then evaluated whether migrating GABAergic neurons of the anterior SNr were responsive to Netrin1 guidance by plating E16.5 GABAergic neurons from the anterior SNr on a carpet of Netrin1 stripes. *Vgat-Cre:TdTomato* brains, which express TdTomato in all GABAergic neurons (Vong et al., 2011), were used to visualize and dissect GABAergic neurons from the anterior SNr (Figure 11A). 71% of TdTomato$^+$ neurons were attracted by Netrin1 stripes, while they were evenly distributed in controls (Figure 11B). This indicates that GABAergic neurons of the anterior SNr respond to the attractant cue Netrin1.

It has been shown that the adhesive effects induced by Netrin1 are often mediated by the axon guidance receptor DCC expressed by the growth cone of growing axons or migrating neurons (Junge et al., 2016; Shekarabi et al., 2005). To determine whether DCC receptor was mediating Netrin1-induced Six3$^+$ GABAergic neuron migration, *Pitx3-ITC:ACTB-FlpE:DCC-KO* brains were

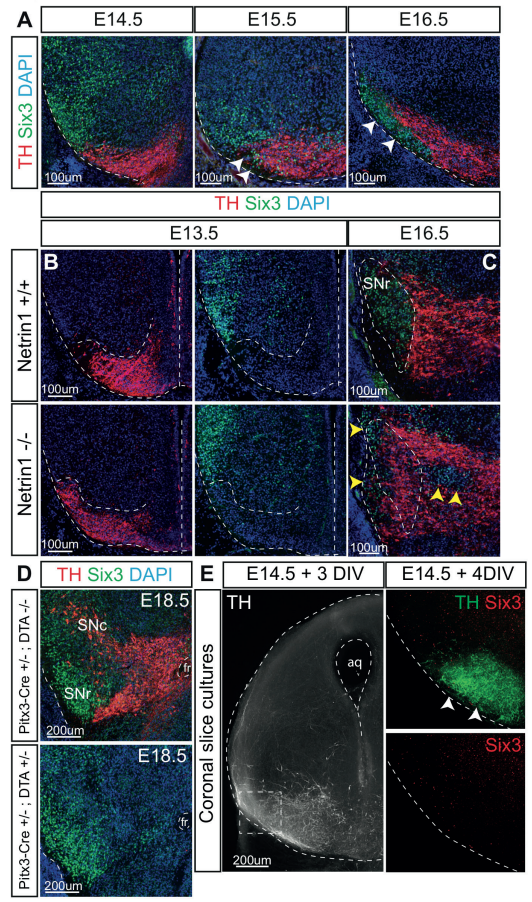

Figure 9

Migration of Six+ GABAergic neurons is required for the development of the SNc wing-like structure

(A) Immunohistochemistry at E14.5, E15.5, and E16.5 for TH and Six3, markers for mDA and SNr GABAergic neurons, respectively. The first migrating Six3$^+$ GABAergic neurons appear in the SNr at E15.5. At E16.5, the dimension of the Six3$^+$ neuron cluster increases and SNc mDA neurons are no longer located next to the pial surface. (B, C) Immunohistochemistry for TH and Six3 in *Netrin1-KO* and control brains at E13.5 (B) and E16.5 (C). At E13.5 the distribution of TH$^+$ and Six3$^+$ neurons in WT and KO brains is comparable. mDA neurons are next to the pial surface. At E16.5, mDA neurons are shifted laterally. In addition, Six3$^+$ GABAergic neurons are divided in small clusters, some flattened next to the pial surface and some located inside the mDA system. (D) Immunohistochemistry for TH and Six3 on coronal sections of E18.5 *Pitx3-Cre:DTA* brains and controls. mDA neurons are absent in *Pitx3-Cre:DTA* brains, while the migration of Six$^+$ GABAergic neurons is unaffected. (E) Midbrain slice cultures as a model of Six$^+$ GABAergic neuron ablation. Midbrain slices are obtained from E14.5 brains and cultured for 3 or 4 DIV. Immunohistochemistry for TH and Six3 is shown. In absence of Six$^+$ GABAergic neurons, mDA neurons remain attached to the pial surface.

analyzed to visualize both SNc mDA neurons and Six3$^+$ GABAergic neurons in brains lacking DCC expression. Surprisingly, we did not find migration defects in both neuronal populations, indicating that DCC expression is not required for the correct migration of GABAergic and mDA neurons of the SNr and SNc, respectively (Figure 11C).

In conclusion, Netrin1$^+$ longitudinal axons may provide a guidance scaffold for Six3$^+$ GABAergic neurons throughout their migration from the caudal midbrain towards the SNr. GABAergic neurons from the anterior SNr respond to Netrin1, which acts as an attractant guidance cue. DCC receptor does not mediate Netrin1-induced attraction.

8. Netrin1$^+$/L1CAM$^+$ longitudinal axons do not emerge from the spinal cord

To determine the origin of Netrin1$^+$/L1CAM$^+$ longitudinal axons, 3DISCO analysis for TH and L1CAM on an entire E13.5 embryo allowed the visualization of all L1CAM$^+$ axonal tracts present in the central nervous system. L1CAM expression was particularly high in spinal axons that extended rostrally out of the spinal cord to run across the ventral midbrain, in close proximity to the mesencephalic flexure and mDA neurons (Figure 12A). These observations were in accordance with previous reports that identify a group of commissural neurons in the rat spinal cord which are GABAergic and express L1CAM on their axons. The projections of these neurons grow rostrally out of the spinal cord into the medulla and then into the midbrain (Tran et al., 2004). To determine whether spinal axons extend longitudinally into the cerebral peduncle of the midbrain, *HoxB1-Cre* mice were crossed with *TdTomato* reporter mice. From E10.5 onwards, *HoxB1-Cre* mice express Cre in the entire spinal cord and in the hindbrain (rhombomere 3 and 4), but not in more rostral regions of the brain (Arenkiel et al., 2003). In *HoxB1-Cre:TdTomato* mice, all Cre$^+$ cells express TdTomato both in cell bodies and axons. The analysis of *HoxB1-Cre:TdTomato* mice revealed, however, that spinal cord TdTomato$^+$ axons run across the midbrain but they do not grow in the peduncular tract (Figure 12B). We concluded, therefore, that Netrin1$^+$ peduncular axons do not emerge from the spinal cord. Further studies are required to establish the brain origin of Netrin1$^+$ longitudinal axons elongating into the midbrain peduncular tract.

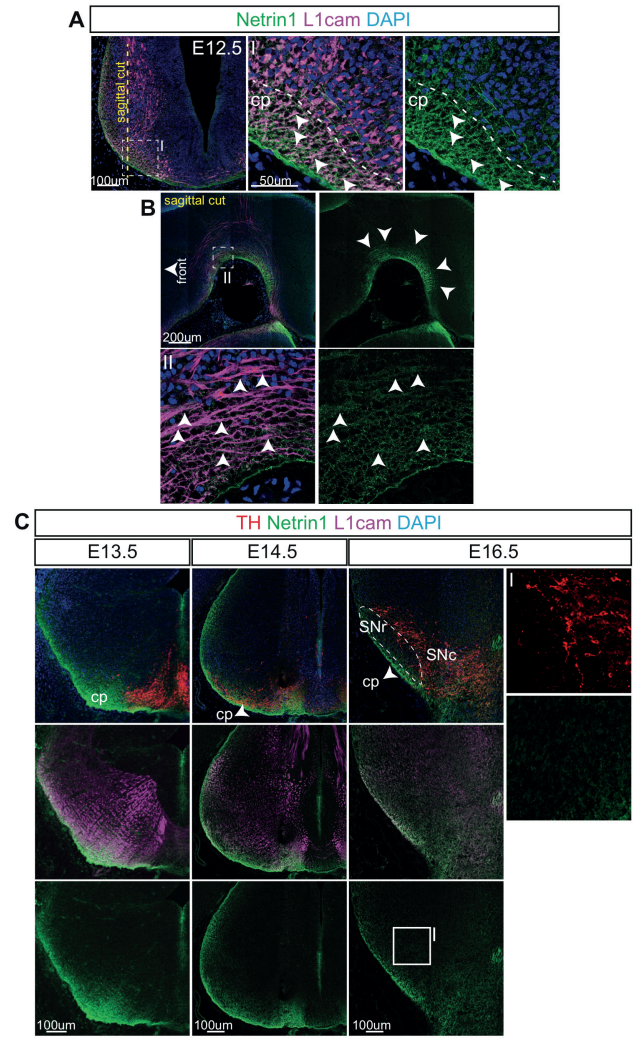

Figure 10
Netrin1 is expressed by peduncular axons during SNc and SNr development

(A, B) Immunohistochemistry for L1CAM and Netrin1 on E12.5 coronal (A) and sagittal (B) sections. Netrin1 is expressed by L1CAM$^+$ axons running in the cerebral peduncle. (C) Immunohistochemistry for TH, Netrin1, and L1CAM on midbrain coronal sections at E13.4, E14.5, and E16.5. Netrin1 is expressed by L1CAM$^+$ peduncular axons during the migration of SNr GABAergic neurons. mDA neurons do not show Netrin1 protein expression in cell bodies (high mag on the right).

Discussion

SNc mDA neurons migrate in three spatial directions

Previous attempts to characterize the migratory behavior of mDA neurons relied on the analyses of midbrain coronal sections, often at intermediate levels of the dopamine system. From these experiments, mDA neuron migration was described as a process of two phases: (1) a first phase of radial migration of SNc and VTA mDA neurons from the ventricular zone, through the intermediate zone, to the mantel zone (Bodea et al., 2014; Shults et al., 1990); and (2) tangential migration of SNc mDA neurons from the medial to lateral midbrain (Bodea et al., 2014; Kawano et al., 1995). However, the dopamine system is a complex structure that extends in 3-dimensions, with the neurogenic ventricular zone positioned more medio-caudally than the SNc wing-like structures, which protrude towards the rostro-lateral edges of the midbrain. Our 3D analysis shows that SNc mDA neurons migrate in three spatial directions (Figure 2). From the ventricular zone located in the medio-caudo-dorsal midbrain, SNc mDA neurons follow a ventral-lateral-rostral migratory route. These observations are corroborated by the analysis of migrating processes of SNc mDA neurons (Figure 1). In horizontal brain sections, the orientation of leading processes of SNc neurons is positioned caudo-rostrally.

Two recent studies have analyzed the radial migration of SNc and VTA mDA neurons to understand their distribution in the intermediate zone. Panman et al. used specific nuclear markers to distinguish SNc and VTA neurons and concluded that SNc and VTA neurons occupy distinct territories during radial migration. SNc mDA neurons migrate through the medial intermediate zone, while VTA mDA neurons are positioned more laterally (Panman et al., 2014). In contrast, Bodea et al. exploited the specific spatiotemporal expression pattern of Sonic hedgehog (Shh) by mDA progenitors to perform fate mapping of SNc and VTA mDA neurons. Labelling of these mDA populations did not reveal subset-specific radial migration. In the intermediate zone, SNc and VTA mDA neurons were intermingled (Bodea et al., 2014). Our study shows that radially migrating SNc mDA neurons are not confined to the medial intermediate zone. Instead they are dispersed throughout the intermediate zone, most likely intermingled with radially migrating VTA mDA neurons, as suggested by Bodea at al. (Figure 1A).

Migratory behavior of distinct SNc mDA neuron subsets

Radial migration of both VTA and SNc mDA neurons occurs from the neurogenic ventricular zone to the mantle zone, which is in close proximity to the pial surface of the ventral midbrain. During radial migration, mDA neurons are aligned to radial glia fibers (Kawano et al., 1995). These structures connect the ventricular zone to the pial surface and function as scaffolds for migrating mDA

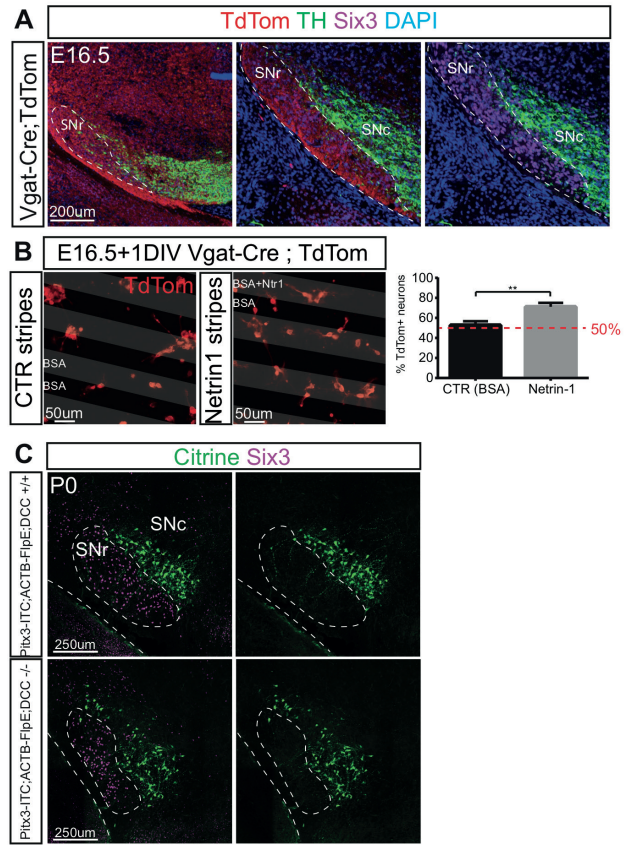

Figure 11

Anterior SNr GABAergic neurons are attracted by Netrin1 *in vitro*

(A) Immunohistochemistry for TdTomato, TH, and Six3 on E16.5 coronal sections of *Vgat-Cre:TdTomato* brains. TdTomato$^+$ neurons are Six3$^+$ and reside in the SNr. (B) E16.5 TdTomato$^+$ SNr GABAergic neurons dissociated from the anterior SNr of *Vgat-Cre:TdTomato* brains are plated on alternate stripes containing Netrin1 or control BSA. Results are quantified as percentage of TdTomato$^+$ neurons on Netrin1 stripes over the total amount of counted TdTomato$^+$ neurons. Three independent experiments are analyzed. Results are shown as Mean ± S.D. Data were tested for significance by Student's *t*-test. **p<0.01. (C) Immunohistochemistry for Citrine and Six3, markers for SNc mDA and SNr GABAergic neurons respectively, on coronal midbrain sections of *Pitx3-ITC:ACTB-Flp:DCC-KO* and control brains. Lack of DCC does not alter Six3$^+$ GABAergic neuron migration.

neurons. Although the physical interaction between SNc mDA neurons and radial glia fibers has been described a long time ago, the molecular mechanisms that mediate this interaction remain largely unknown. Recent results obtained by single-cell RNAseq on the embryonic ventral midbrain show that several axon guidance cues, e.g. Slits and Ephrins, are expressed by radial glia cells ((La Manno et al., 2016) and reviewed by us (Brignani and Pasterkamp, 2017)). These molecules may be responsible for both the development of radial glia cells and mDA neuron migration. However, none of these cues has been functionally implicated in the radial migration of mDA neurons.

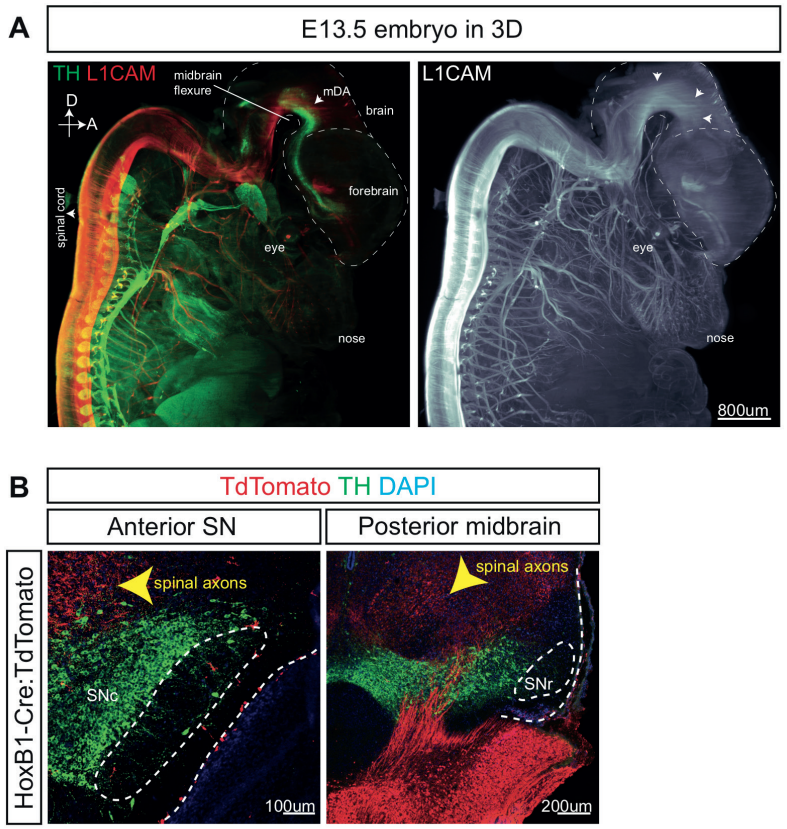

Figure 12

Netrin1^{+} peduncular axons do not emerge from the spinal cord

(A) 3D analysis of E13.5 wild type embryo stained for TH and L1CAM. An axonal bundle positive for L1CAM emerges from the spinal cord and extends across the midbrain, in close proximity to the mesencephalic flexure and mDA neurons. (B) Midbrain coronal sections of E18.5 *HoxB1-Cre:TdTomato* brains. In *HoxB1-Cre:TdTomato* mice, TdTomato is expressed by the entire spinal cord and by hindbrain (rhombomere 3 and 4) (Arenkiel et al., 2003). In the midbrain, TdTomato^{+} axons do not grow in the cerebral peduncle.

In our study, we identify the receptor DCC and its ligand Netrin1 as interesting candidate molecules to mediate the radial migration of mDA neuron-subsets. Both proteins were detected by laser micro-dissection and mass spec analysis to be expressed in the ventral midbrain during dopamine system development. Furthermore, earlier studies showed that both *Netrin1* and *DCC-KO* brains have ectopically positioned mDA neurons in the reticular nucleus at P0, when mDA neuron migration has been completed (Li et al., 2014; Xu et al., 2010). Although migration defects described in *Netrin1* and *DCC-KO* mice were similar, how Netrin1-DCC signaling mediates mDA neuron migration was unknown. We combined *in vivo* and *in vitro* experiments to demonstrate that Netrin1 is expressed by radial glia fibers, and functions as an attractant for a subset of radially migrating Sox6^{+} Citrine^{-} SNc mDA neurons. The activity of the DCC receptor expressed by SNc mDA neurons mediates Netrin1 attraction. In conclusion, we identify DCC-Netrin1 signaling as a molecular mechanism regulating the interaction between migrating SNc mDA neurons and radial glia fibers. Further studies are needed to determine which molecules guide the radial migration of other mDA neuron-subsets.

Pitx3-ITC:ACTB-FlpE:Netrin1-KO brains exhibit another prominent defect in mDA neuron migration, that was not described previously. At E18.5*, Netrin1-KO* brains do not show the typical wing-like structure of Citrine^{+} SNc mDA neurons. In contrast, Citrine^{+} SNc neurons are shifted in the ventro-lateral territory that is normally occupied by the GABAergic neurons of the anterior SNr (Figure 8). Further analyses demonstrate that the aberrant migration of Citrine^{+} SNc neurons is a consequence of the altered migration of the neighboring SNr GABAergic neurons. Migration of GABAergic neurons towards the SNr may induce the dorsal migration of SNc mDA neurons. During this phase, GABAergic neurons might repel SNc mDA neurons dorsally, to generate the SNr. Interestingly, we observed that although the morphology of SNc and SNr nuclei is altered in *Netrin1-KO* brains, SNc mDA neurons and SNr GABAergic neurons never intermingled (Figure 8). This suggests that one of the two neuronal populations (or both) might repel the other one. Together, these results demonstrate that the development of a specific neuronal population may rely on the correct formation of adjacent nuclei, and that the migration of a neuronal population may influence the migration of another one.

Netrin1-positive axons may guide GABAergic neurons towards the SNr

How is the correct migration of SNr GABAergic neurons achieved? And what is the role played by Netrin1? GABAergic neurons of the anterior SNr are generated at the ventricular zone of the posterior midbrain. From this region, they migrate radially towards the pial surface and longitudinally from the posterior to the anterior midbrain. Ultimately, these cells settle in the ventro-

lateral part of the SNc, forming the SNr nucleus (Madrigal et al., 2016). Our data unveil that, during longitudinal GABAergic neuron migration, Netrin1 is expressed by L1CAM$^+$ longitudinal axons of the cerebral peduncle from E12.5 to E16.5. This indicates that Netrin1 may act as a short-range guidance cue for migrating GABAergic neurons *in vivo*. When Netrin1 is provided as a short-range guidance cue *in vitro* in stripe assays, GABAergic neurons preferentially migrate on Netrin1$^+$ stripes. Thus, GABAergic neurons respond to Netrin1, which functions as a short-range attractant cue. In summary, our findings indicate that developing GABAergic neurons may use Netrin1$^+$ longitudinal axons as guidance scaffolds to migrate along the A-P axis. Therefore, lack of Netrin1 from longitudinal axons may cause the altered migration of SNr GABAergic neurons, which prevents the correct formation of the SNr. This determines in turn the aberrant positioning of Citrine$^+$ SNc mDA neurons, that do not migrate dorsally but remain attached to the pial surface, as observed in *Netrin1-KO* brains. Further studies are necessary to demonstrate whether the conditional ablation of Netrin1 from peduncular axons prevents both GABAergic neuron migration and the formation of the SNc wing-like structure. Furthermore, since SNc mDA neurons and GABAergic neurons establish connections with each other, it would be interesting to understand how the aberrant migration of these neurons affects the development of local SN neural networks.

The origin of peduncular axons

L1CAM$^+$/Netrin1$^+$ peduncular axons may function as guidance scaffold for SNr GABAergic neurons that undergo longitudinal migration along the A-P axis. However, the origin of these projections is still unclear. The 3D analysis performed on E13.5 wild type embryos suggested that L1CAM$^+$/Netrin1$^+$ peduncular axons could emerge from the spinal cord. However, *HoxB1-Cre:TdTomato* mice, that express TdTomato in the entire spinal cord and in the hindbrain (rhombomere 3 and 4), do not display TdTomato$^+$ axons in the peduncular tract. Therefore, L1CAM$^+$/Netrin1$^+$ peduncular axons do not emerge from the spinal cord, but from other brain regions. It has been shown, for example, that a subset of cortical neurons residing in layer V projects its axons from the cortex to the spinal cord crossing the internal capsule and the cerebral peduncle (Molyneaux et al., 2007; Welniarz et al., 2016). Although it has been demonstrated that Layer V cortical neurons are born between E12.5 and E14.5 (Molyneaux et al., 2007), it is not known when, during development, corticospinal projections reach the ventral midbrain. More efforts are needed to understand whether developing corticospinal axons travel across the midbrain in the cerebral peduncle during SNr GABAergic neuron migration (E14.5-E16.5). If this hypothesis is correct, cortex-specific Cre mouse lines may be used to conditionally ablate Netrin1 from peduncular axons and determine whether Netrin1 is required for mDA system development.

Migration of distinct midbrain GABAergic neuron-subsets

Migration of GABAergic neurons influences the positioning of SNc mDA neurons, but, interestingly, not *vice versa*. *In vivo* ablation of mDA neurons from E13.5 midbrains does not alter GABAergic neuron migration into the SNr, showing that the dopamine system is not involved in the development of its adjacent SNr nucleus. In addition to GABAergic neurons of the anterior SNr, the ventral midbrain hosts other GABAergic neuron populations associated with dopaminergic nuclei (Reviewed in (Morello and Partanen, 2015)). In particular, a scattered population of GABAergic neurons intermingles with mDA neurons. Recently, it has been shown that the migration of this GABAergic neuron-subset relies on mDA neurons in the ventral midbrain (Vasudevan et al., 2012). Pitx3-deficient *aphakia* mice, which selectively loose SNc mDA neurons during early developmental stages, display a significant reduction of GABAergic neurons intermingled with mDA neurons (Vasudevan et al., 2012). Furthermore, *in vitro* experiments show that this GABAergic neuron-subset is attracted by explants dissected from the ventral midbrain. The attraction is lost when the explants are isolated from the ventral midbrain of *aphakia* mice, indicating that the dopamine system may attract GABAergic neurons that are ultimately intermingled with mDA neurons (Vasudevan et al., 2012). It is therefore interesting to conclude that the ventral midbrain contains different GABAergic populations which display different migratory behaviors. The migration of GABAergic neurons from the posterior midbrain into the anterior SNr is mDA neuron-independent. In contrast, GABAergic neurons intermingled with mDA neurons require mDA neurons to migrate to their final position.

Netrin1 is a short-range chemoattractant with multiple roles in the development of midbrain neuron nuclei

Netrin1 has long been considered a prototypical example of a chemoattractant that, after being secreted, diffuses in the environment creating a long-range gradient. Extracellular gradients established by Netrin1 diffusion have been described to guide migrating neurons and elongating axons during the development of the central nervous system. In addition to this long-range activity, evidence is accumulating that Netrin1 also acts as a short-range guidance cue. In the spinal cord, for example, it was initially thought that Netrin1 secreted by floor plate cells was forming a gradient necessary to attract spinal commissural axons towards the midline (Kennedy et al., 1994). However, two very recent studies show that, both in the spinal cord and in the hindbrain, Netrin1 promotes ventrally directed axon outgrowth not by acting as a soluble diffusible molecule, but rather as a local adhesive substrate (Dominici et al., 2017; Varadarajan et al., 2017). To limit the range of Netrin1 diffusion, the secreted Netrin1 molecule may be bound to the cell membrane or the extracellular matrix (ECM) (Manitt and Kennedy, 2002; Manitt et al., 2001). In particular, Netrin1 can bind both

the ECM protein collagen-IV and heparin (Kappler et al., 2000; Yebra et al., 2003). In our study, we detect Netrin1 protein in close association with both midbrain radial glia fibers and longitudinal axons running in the cerebral peduncle. This suggest that Netrin1 is not creating a widespread extracellular gradient *in vivo*. In contrast, it is more likely that Netrin1 acts locally as a short-range guidance cue. In addition, we observe *in vitro* that both mDA neurons and SNr GABAergic neurons (at different developmental stages) show a preference for Netrin1 rather than for control stripes, indicating that Netrin1 functions as an adhesive substrate for these migrating neurons. Combining our *in vitro* and *in vivo* results, we conclude that in the midbrain Netrin1 expressed by longitudinal axons and radial glia fibers functions as a molecular scaffold for different populations of migrating neurons. More efforts are needed to establish how Netrin1 diffusion is limited in the midbrain *in vivo*, for example whether Netrin1 binds to neuronal/axonal membranes and/or to the ECM.

Conclusions

We characterize in detail the migratory behavior of SNc mDA neurons in the 3-dimensional dopamine system. We show that these neurons migrate along the three axes to ultimately generate the typical SNc wing-like structures present in postnatal and adult brains. In addition, we identify two distinct SNc mDA neuron-subsets that rely on different molecular mechanisms for their migration. The first population (Citrine^{-}) migrates along radial glia fibers. Netrin1/DCC signaling mediates this process. In contrast, the development of the second SNc mDA neuron-subset (Citrine^{+}) requires the correct migration of GABAergic neurons into the SNr. These observations demonstrate that the formation of a neuron-cluster (the SNc) can rely on the development of an adjacent nucleus (the SNr). Finally, we provide evidence that the migration of Citrine^{+} SNc mDA neurons needs Netrin1 in an indirect manner. Netrin1 expressed by the peduncular axons guides migrating SNr GABAergic neurons towards their final destination in the SNr. This determines in turn the dorsal migration of Citrine^{+} neurons and the generation of the SNc wing-like structure.

Material and methods

Mouse lines

All animal use and care were in accordance with institutional guidelines. The morning on which a vaginal plug was detected was considered embryonic day 0.5 (E0.5). *Pitx3-ITC* mice were generated by us and described in Chapter 3 of this thesis. *ACTB-FlpE* (Rodríguez et al., 2000), *DTA*, and *TdTomato* reporter mice were obtained from The Jackson Laboratories. *Pitx3-Cre* mice were a kind gift of Marten Smidt (University of Amsterdam) (Smidt et al., 2012). *Pitx3-GFP* mice were a kind gift from Meng Li (MRC Clinical Science Center) and provided by Marten Smidt (Zhao et al., 2004). *DCC$^{fl/fl}$* mice were kindly provided by Cecilia Flores (McGill University) (Manitt et al., 2013). *Netrin1-KO* and *Netrin1$^{fl/fl}$* mice were kindly provided by Lisa Goodrich (Harvard Medical School) (Yung et al., 2015). *Vgat-Cre* mice from Jackson Laboratories were provided by Corette Wierenga (Utrecht University) (Vong et al., 2011). *PlexinB2-KO* brains (Eucomm) were kindly sent by Roland Friedel (Icahn School of Medicine at Mount Sinai). *Shh-Cre:Netrin1$^{fl/fl}$* brains were a kind gift from Alain Chedotal (Institute de la Vision). *HoxB1-Cre* mice were a kind gift from Mario Capecchi (University of Utha) and were provided by Rüdiger Klein (Max Planck Institute).

Immunohistochemistry

Embryonic brains were isolated and fixed overnight at 4^{o}C in 4% PFA. Brains were cryoprotected in 30% sucrose in PBS, frozen and cryopreserved at -80^{o}C. 20 µl brain sections were prepared at the cryostat. For Netrin1 staining, antigen retrieval was performed with Na-Citrate pH8, with brain sections left in the microwave for 7 minutes at 180W. Sections were washed in PBS and blocked with blocking solution (0.4% Tryton X-100, 1% BSA, in PBS) for 1h at RT. Then, they were incubated with primary antibodies in blocking solution at 4^{o}C overnight. The next day, they were washed in PBS and incubated with secondary antibodies in blocking solution at RT for 1h. They were washed and counterstained with DAPI (4',6'-diamidino-2-phenylindole; 0.1 mg/ml in PBS; Invitrogen). Mounting was performed with FluorSave reagent (Merck Millipore). Staining was visualized on a Zeiss Axioskop A1 epi fluorescent microscope or by confocal laser-scanning microscopy (LSM 880, Zeiss).

Primary Ab.	Species	Company	Catalog Number	Concentration
TH	rabbit	Millipore	AB152	1:1000
TH	sheep	Millipore	AB1542	1:500
GFP	rabbit	Life technologies	A11122	1:500
GFP	chicken	Abcam	ab13970	1:500
Otx2	goat	R&D	AF1979	1:500
TdTomato	rabbit	Rockland	600-401-379	1:500
Sox6	rabbit	Abcam	Ab3045	1:500
Netrin1	goat	R&D	AF1109-SP	1:500
BLBP	rabbit	Abcam	Ab32423	1:500
Six3	rabbit	Rockland	600-401-A26	1:1000
DARPP	rat	R&D	MAB4230	1:1000
L1CAM	rat	Millipore	MAB5272	1:1000

In situ hybridization

Timed-pregnant females were sacrificed by means of cervical dislocation to collect embryonic brains, which were directly frozen. 16 µm sections were cut on a cryostat, air-dried for 2h and frozen at -80°C. Nonradioactive in situ hybridization was performed according to (Pasterkamp et al., 2007). cDNA was made from whole mouse brain RNA using a one-step RT-PCR kit (Qiagen), according to supplied protocol and using the following primers:

PlexinB2:
5'- ATCTGCTGTAGGCGGAAGGC -3'
5'- CTTCAACTGTGACACCATC -3'

Netrin1:
5'- GATGTGCCAAAGGCTACCAG -3'
5'- TTCTTGCACTTGCCCTTCTTC -3'

cDNA was cloned into pGEM-T Easy (Promega) and transcribed using either SP6 or T7 RNA polymerase (Roche) and digoxigenin-labeled nucleotide mix (Roche) to produce digoxigenin-labeled cRNA probes. Digoxigenin was detected using anti-digoxigenin FAB fragments conjugated to alkaline phosphatase (Roche; 1:5000) and stained with NBT/BCIP (Roche). Sections were mounted using FluorSave reagent (Merck Millipore) and visualized on a Zeiss Axioscope 2.

X-Gal staining

PlexinB2-KO and *WT* brains were isolated and fixed in 4% PFA for 4h and washed in PBS. Brains were sectioned with the vibratome to make 50um coronal sections. The reaction solution (4mM $K_3Fe(CN)_6$, 4mM $K_4Fe(CN)_6$, 2mM MgCl, 2mg/ul X-Gal) was prepared and filtered through 0.80 um filter. Sections were incubated in reaction solution at 37°C up to 2 days protected from light, and then they were washed in PBS. Next, immunostaining for TH was performed: sections were incubated in blocking buffer (0.5% Triton-X-100, 1% BSA, in PBS) for 1h at RT, and incubated in blocking buffer and primary antibody (rabbit anti-TH 1:1000, Millipore) ON at 4°C. The next day, they were washed extensively in PBS, and incubated in blocking buffer and secondary antibody (Alexa 568, Invitrogen) for 2h at RT. After washes in PBS, sections were mounted on microscope slides with FluorSave reagent (Merck Millipore). Images were acquired with the microscope Zeiss Axioscope 2.

3D-imaging of solvent cleared organs (3DISCO)

Pitx3-ITC:ACTB-FlpE, *Netrin1-KO*, and *Pitx3-ITC:ACTB-FlpE:Netrin1-KO* brains were isolated, fixed in 4% PFA at 4°C ON and washed in PBS. The clearing procedure was performed according to (Belle et al., 2014). Briefly, brains were immerged in blocking buffer (0.2% Gelatin, 0.5% Triton-X-100 and 0.01% thimerosal in PBS) at RT for 24h.
Next, brains were incubated for 7 days at 37°C in blocking buffer with 0.1% saponin and primary antibodies. Samples were extensively washed in blocking buffer. They were then incubated at 37°C ON in blocking buffer with saponin 0.1% and secondary antibodies (Alexa 568 and Alexa 647, Invitrogen). The blocking solution with secondary antibodies was filtered with a 0.20um filter before use. The next day, samples were washed extensively with blocking buffer. For tissue clearing, samples were subsequently incubated in 50% Tetrahydrofurane (THF, sigma), 80% THF, 100% THF, 100% dichloromethane (DCM, sigma), and 100% Dibenzylether (DBE, sigma). Z-stack images of entire brains were acquired with a light-sheet microscope (LSM 2, LaVision Biotech) and 3D reconstructions were made with Imaris software (Bitplane). For quantifications of migrating SNc neurons (Figure 2) or SNc neurons in *Netrin1-KO* brains (Figure 5), TH staining was used to manually draw a mask of the dopamine system. Then, $Citrine^+$ neurons were automatically detected by the Imaris software. For migrating SNc neurons (Figure 2), the dopamine system was divided in 8 Bins of equal thickness in the caudo-rostra, medio-lateral, or dorso-ventral directions. For SNc neurons in *Netrin1-KO* brains (Figure 5), the dopamine system was divided in 3 Bins of equal thickness in the medio-lateral direction. Midline and pial suface of the midbrain were used as references to establish the dimension of the Bins. The number of $Citrine^+$ mDA neurons in each Bin was counted and expressed as percentage of the

total number of Citrine$^+$ neurons detected in the entire dopamine system. Three brains were analyzed for each condition and statistical evaluations were done with GraphPad Prism 7 (Student *t*-test). Values are expressed as mean ± SEM.

Primary Ab.	Species	Company	Catalog Number	Concentration
TH	rabbit	Millipore	AB152	1:1000
TH	sheep	Millipore	AB1542	1:1000
GFP	rabbit	Life technologies	A11122	1:1000
L1CAM	rat	Millipore	MAB5272	1:1000

Laser capture microdissection

Fresh frozen sections of E16.5 Pitx3-GFP mouse brains were cut coronally (16 µm) and mounted on MembraneSlides 1.0 PEN (Zeiss). Sections were dried within the cryostat chamber to prevent protein degradation and stored at -80^{o}C until use. Before the laser dissection procedure, sections were air-dried. Laser capture microdissection was performed on a PALM laser microscope system (Zeiss). Dissected tissue was collected in lysis buffer (20mM Tris pH7.5, 150mM NaCl, 10% glycerol, 1% NP-40) containing protease inhibitor cocktail (Complete; Roche). After the procedure, LDS sample buffer (NuPAGE) and 2-mercaptoethanol was added and samples were stored at -80^{o}C. Samples were subjected to SDS-PAGE and stained using GelCode Blue Stain reagent (Thermo Scientific). Gels were sent for mass spectrometry analysis at the Erasmus Proteomics Center (Rotterdam).

Dissociation of mDA neurons or GABAergic neurons and stripe assay

Brains were isolated from E13.5 *Pitx3-GFP* or E16.5 *Vgat-Cre:TdTomato* mice. 300um coronal sections were obtained using the tissue chopper (McIllwain). To visualize GFP$^+$ or TdTomato$^+$ neurons under the dissection microscope, we added a stereo microscope fluorescent adapter (Nightsea) equipped with LED light and barrier filter. The region of interest was dissected from the midbrain and divided in small pieces. From *Vgat-Cer:TdTomato* brains, only the anterior SNr was isolated. Tissue was collected in Krebs solution (0.7% NaCl, 0.04% KCl, 0.02% KH_2PO_4, 0.2% $NaHCO_3$, 0.25% glucose and 0.001% phenol red) and dissociated by incubation with 0.25% trypsin in Krebs/EDTA for 15 min at 37°C. The reaction was stopped by adding 2mg soybean trypsin inhibitor. Next, the tissue was triturated with a pipette p1000 in Krebs solution containing 2mg soybean trypsin inhibitor and 20µg/ml DNAseI. Dissociated cells were resuspended in culture medium (Neurobasal medium (NB; Gibco, Invitrogen) containing 2mM L-glutamine (PAA), 1x penicillin/streptomycin (pen/strep, PAA), and B-27 supplement (Gibco, Invitrogen)).

The modified stripe assay was performed as in (Yamagishi et al., 2011). Briefly, alternating stripes (BSA or 20ug/ml Netrin1 (R&D, 1109-N1/CF)) were applied to petri dishes. Sonicated fluorescent beads (ThermoFisher, F8812) were added to identify the stripes. After stripes printing, BSA was applied to the entire surface. 35.000 neurons were plated on top of the stripes in 150ul of culture medium. Neurons were fixed after 24h with 4%PFA and sucrose 15% for 20min at RT and washed with PBS. To visualize the neurons, immunostaining was performed by blocking with blocking buffer (1% BSA and 0.1% Triton-X-100 in PBS) for 1h at RT. Neurons were incubated in primary antibodies (rabbit anti-GFP 1:500, LifeTechnologies; rabbit anti-TdTomato 1:500, Rockland) ON at 4^{o}C in blocking solution. Neurons were washed and incubated with secondary antibodies (Alexa 488, Invitrogen) for 1h at RT. Neurons on positive or negative stripes were counted. Values are expressed as Mean ± S.D. GraphPad Prism 7 was used to perform the statistical analysis (Student's *t*-test).

Midbrain slice cultures

E14.5 embryonic brains were isolated and 300um coronal slices were obtain with a tissue chopper (McIllwain). These slices were cultured on Millicell cell culture inserts (PTFE, 0.4 µm, Millipore) for two, three, or four days in 1.6ml culture medium (Basal Medium Eagle (Sigma) supplemented with cHBSS, glucose, glutamine and penicillin/streptomycin), as described previously (Polleux and Ghosh, 2002). Slices were then fixed in 4% PFA for 1h RT and washed in PBS. Immunostaining was performed by blocking the slices in blocking buffer (1% BSA, 0.5% Triton-X-100, in PBS) for 3h RT. The tissue was incubated in blocking buffer with primary antibodies (rabbit or sheep anti-TH 1:500, Millipore; rabbit anti-Six3 1:500, Abcam) ON at 4^{o}C. Next, slices were washed extensively in PBS, and incubated in blocking buffer with secondary antibodies for 2h RT. After, they were washed in PBS, mounted on microscope slides with ProLong Gold (Life Technologies), and visualized using the confocal laser-scanning microscopy (LSM 880, Zeiss).

Acknowledgements

We thank all the members of the Pasterkamp laboratory for discussions and suggestions, and Peter Burbach for the critical reading of the manuscript. Special thanks to Christian van der Meer, Leo Halewijn, and Mark Broekhoven who helped with the maintenance of mouse colonies. We acknowledge Marten Smidt, Cecilia Flores, Lisa Goodrich, Corette Wierenga, and Rüdiger Klein for providing us with mouse lines. Many thanks to Roland Friedel for sharing mouse tissues.
Work on axon guidance and the developing dopamine system was financially supported by the Netherlands Organization for Scientific Research (ALW-

VICI), the People Program (Marie Curie Actions) of the European Union's Seventh Framework Program (FP7) 2007–2013 under REA grant agreement number 289581 (NPlast), the UU Strategic Theme "Dynamics of Youth", and Stichting ParkinsonFonds.

References

Achim, K., Peltopuro, P., Lahti, L., Li, J., Salminen, M., and Partanen, J. (2012). Distinct developmental origins and regulatory mechanisms for GABAergic neurons associated with dopaminergic nuclei in the ventral mesodiencephalic region. Development *139*.

Arenkiel, B.R., Gaufo, G.O., and Capecchi, M.R. (2003). Hoxb1 neural crest preferentially form glia of the PNS. Dev. Dyn. *227*, 379–386.

Bayer, S.A., Wills, K. V, Triarhou, L.C., and Ghetti, B. (1995). Time of neuron origin and gradients of neurogenesis in midbrain dopaminergic neurons in the mouse. Exp. Brain Res. *105*, 191–199.

Belle, M., Godefroy, D., Dominici, C., Heitz-Marchaland, C., Zelina, P., Hellal, F., Bradke, F., and Chédotal, A. (2014). A Simple Method for 3D Analysis of Immunolabeled Axonal Tracts in a Transparent Nervous System.

Bodea, G.O., Spille, J.-H., Abe, P., Andersson, A.S., Acker-Palmer, A., Stumm, R., Kubitscheck, U., and Blaess, S. (2014). Reelin and CXCL12 regulate distinct migratory behaviors during the development of the dopaminergic system. Development *141*, 661–673.

Brignani, S., and Pasterkamp, R.J. (2017). Neuronal Subset-Specific Migration and Axonal Wiring Mechanisms in the Developing Midbrain Dopamine System. Front. Neuroanat. *11*, 55.

Bye, C.R., Thompson, L.H., and Parish, C.L. (2012). Birth dating of midbrain dopamine neurons identifies A9 enriched tissue for transplantation into parkinsonian mice. Exp. Neurol. *236*, 58–68.

Chédotal, A. (2010). Should I stay or should I go? Becoming a granule cell. Trends Neurosci. *33*, 163–172.

Conte, I., Morcillo, J., and Bovolenta, P. (2005). Comparative analysis of *Six3* and *Six6* distribution in the developing and adult mouse brain. Dev. Dyn. *234*, 718–725.

Dominici, C., Moreno-Bravo, J.A., Puiggros, S.R., Rappeneau, Q., Rama, N., Vieugue, P., Bernet, A., Mehlen, P., and Chédotal, A. (2017). Floor-plate-derived Netrin1 is dispensable for commissural axon guidance. Nature.

Fallon, J.H., Riley, J.N., and Moore, R.Y. (1978). Substantia nigra dopamine neurons: separate populations project to neostriatum and allocortex. Neurosci. Lett. *7*, 157–162.

Junge, H.J., Yung, A.R., Goodrich, L. V., and Chen, Z. (2016). Netrin1/DCC signaling promotes neuronal migration in the dorsal spinal cord. Neural Dev. *11*, 19.

Kang, W.-Y., Kim, S.-S., Cho, S.-K., Kim, S., Suh-Kim, H., Lee, Y.-D., Ballif, B., Arnaud, L., Arthur, W., Guris, D., et al. (2010). Migratory defect of mesencephalic dopaminergic neurons in developing reeler mice. Anat. Cell Biol. *43*, 241.

Kappler, J., Franken, S., Junghans, U., Hoffmann, R., Linke, T., Müller, H.W., and Koch, K.-W. (2000). Glycosaminoglycan-Binding Properties and Secondary Structure of the C-Terminus of Netrin1. Biochem. Biophys. Res. Commun. *271*, 287–291.

Kawano, H., Ohyama, K., Kawamura, K., and Nagatsu, I. (1995). Migration of dopaminergic neurons in the embryonic mesencephalon of mice. Dev. Brain Res. *86*, 101–113.

Kennedy, T.E., Serafini, T., de la Torre, J.R., and Tessier-Lavigne, M. (1994). Netrins are diffusible chemotropic factors for commissural axons in the embryonic spinal cord. Cell *78*, 425–435.

Lahti, L., Haugas, M., Tikker, L., Airavaara, M., Voutilainen, M.H., Anttila, J., Kumar, S., Inkinen, C., Salminen, M., and Partanen, J. (2016). Differentiation and molecular heterogeneity of inhibitory and excitatory neurons associated with midbrain dopaminergic nuclei. Development *143*.

Li, J., Duarte, T., Kocabas, A., Works, M., McConnell, S.K., and Hynes, M.A. (2014). Evidence for topographic guidance of dopaminergic axons by differential Netrin1 expression in the striatum. Mol. Cell. Neurosci. *61*, 85–96.

Madrigal, M.P., Moreno-Bravo, J.A., Martínez-López, J.E., Martínez, S., and Puelles, E. (2016). Mesencephalic origin of the rostral Substantia nigra pars reticulata. Brain Struct. Funct. *221*, 1403–1412.

Mailly, P., Charpier, S., Menetrey, A., and Deniau, J.-M. (2003). Three-dimensional organization of the recurrent axon collateral network of the substantia nigra pars reticulata neurons in the rat. J. Neurosci. *23*, 5247–5257.

Manitt, C., and Kennedy, T.E. (2002). Where the rubber meets the road: netrin expression and function in developing and adult nervous systems. Prog. Brain Res. *137*, 425–442.

Manitt, C., Colicos, M.A., Thompson, K.M., Rousselle, E., Peterson, A.C., and Kennedy, T.E. (2001). Widespread expression of Netrin1 by neurons and oligodendrocytes in the adult mammalian spinal cord. J. Neurosci. *21*, 3911–3922.

Manitt, C., Eng, C., Pokinko, M., Ryan, R.T., Torres-Berrío, A., Lopez, J.P., Yogendran, S. V, Daubaras, M.J.J., Grant, A., Schmidt, E.R.E., et al. (2013). dcc orchestrates the development of the prefrontal cortex during adolescence and is altered in psychiatric patients. Transl. Psychiatry *3*, e338.

La Manno, G., Gyllborg, D., Codeluppi, S., Nishimura, K., Salto, C., Zeisel, A., Borm, L.E., Stott, S.R.W., Toledo, E.M., Villaescusa, J.C., et al. (2016). Molecular Diversity of Midbrain Development in Mouse, Human, and Stem Cells. Cell *167*, 566–580.e19.

Marín, O., Valiente, M., Ge, X., and Tsai, L.-H. (2010). Guiding neuronal cell migrations. Cold Spring Harb. Perspect. Biol. *2*, a001834.

Molyneaux, B.J., Arlotta, P., Menezes, J.R.L., and Macklis, J.D. (2007). Neuronal subtype specification in the cerebral cortex. Nat. Rev. Neurosci. *8*, 427–437.

Morello, F., and Partanen, J. (2015). Diversity and development of local inhibitory and excitatory neurons associated with dopaminergic nuclei. FEBS Lett. *589*, 3693–3701.

Nishikawa, S., Goto, S., Yamada, K., Hamasaki, T., and Ushio, Y. (2003). Lack of Reelin causes malpositioning of nigral dopaminergic neurons: Evidence from comparison of normal andRelnrl mutant mice. J. Comp. Neurol. *461*, 166–173.

Panman, L., Papathanou, M., Laguna, A., Oosterveen, T., Volakakis, N., Acampora, D., Kurtsdotter, I., Yoshitake, T., Kehr, J., Joodmardi, E., et al. (2014). Sox6 and Otx2 Control the Specification of Substantia Nigra and Ventral Tegmental Area Dopamine Neurons. Cell Rep. *8*, 1018–1025.

Pasterkamp, R.J., Kolk, S.M., Hellemons, A.J., and Kolodkin, A.L. (2007). Expression patterns of semaphorin7A and plexinC1 during rat neural development suggest roles in axon guidance and neuronal migration. BMC Dev. Biol. *7*, 98.

Polleux, F., and Ghosh, A. (2002). The Slice Overlay Assay: A Versatile Tool to Study the Influence of Extracellular Signals on Neuronal Development. Sci. Signal. *2002*.

Poulin, J.-F., Zou, J., Drouin-Ouellet, J., Kim, K.-Y.A., Cicchetti, F., and Awatramani, R.B. (2014). Defining Midbrain Dopaminergic Neuron Diversity by Single-Cell Gene Expression Profiling. Cell Rep. *9*, 930–943.

Richards, A.B., Scheel, T.A., Wang, K., Henkemeyer, M., and Kromer, L.F. (2007). EphB1 null mice exhibit neuronal loss in substantia nigra pars reticulata and spontaneous locomotor hyperactivity. Eur. J. Neurosci. *25*, 2619–2628.

Rodríguez, C.I., Buchholz, F., Galloway, J., Sequerra, R., Kasper, J., Ayala, R., Stewart, A.F., and Dymecki, S.M. (2000). High-efficiency deleter mice show that FLPe is an alternative to Cre-loxP. Nat. Genet. *25*, 139–140.

Shekarabi, M., Moore, S.W., Tritsch, N.X., Morris, S.J., Bouchard, J.-F., and Kennedy, T.E. (2005). Deleted in colorectal cancer binding Netrin1 mediates cell substrate adhesion and recruits Cdc42, Rac1, Pak1, and N-WASP into an intracellular signaling complex that promotes growth cone expansion. J. Neurosci. *25*, 3132–3141.

Shults, C.W., Hashimoto, R., Brady, R.M., and Gage, F.H. (1990). Dopaminergic cells align along radial glia in the developing mesencephalon of the rat. Neuroscience *38*, 427–436.

Smidt, M.P., von Oerthel, L., Hoekstra, E.J., Schellevis, R.D., and Hoekman, M.F.M. (2012). Spatial and Temporal Lineage Analysis of a Pitx3-Driven Cre-Recombinase Knock-In Mouse Model. PLoS One *7*, e42641.

Tang, M., Miyamoto, Y., Huang, E.J., Ishibashi, M., Rowitch, D.H., McMahon, A.P., Sommer, L., Boussadia, O., and Kemler, R. (2009). Multiple roles of beta-catenin in controlling the neurogenic niche for midbrain dopamine neurons. Development *136*, 2027–2038.

Tepper, J.M., Sawyer, S.F., and Groves, P.M. (1987). Electrophysiologically identified nigral dopaminergic neurons intracellularly labeled with HRP: light-microscopic analysis. J. Neurosci. *7*, 2794–2806.

Torre, E.R., Gutekunst, C.-A., and Gross, R.E. (2010). Expression by midbrain dopamine neurons of Sema3A and 3F receptors is associated with chemorepulsion in vitro but a mild in vivo phenotype. Mol. Cell. Neurosci. *44*, 135–153.

Tran, T.S., Cohen-Cory, S., and Phelps, P.E. (2004). Embryonic GABAergic spinal commissural neurons project rostrally to mesencephalic targets. J. Comp. Neurol. *475*, 327–339.

Varadarajan, S.G., Kong, J.H., Phan, K.D., Kao, T.-J., Panaitof, S.C., Cardin, J., Eltzschig, H., Kania, A., Novitch, B.G., and Butler, S.J. (2017). Netrin1 Produced by Neural Progenitors, Not Floor Plate Cells, Is Required for Axon Guidance in the Spinal Cord. Neuron.

Vasudevan, A., Won, C., Li, S., Erdelyi, F., Szabo, G., and Kim, K.-S. (2012). Dopaminergic neurons modulate GABA neuron migration in the embryonic midbrain. Development *139*, 3136–3141.

Vong, L., Ye, C., Yang, Z., Choi, B., Chua, S., and Lowell, B.B. (2011). Leptin Action on GABAergic Neurons Prevents Obesity and Reduces Inhibitory Tone to POMC Neurons. Neuron *71*, 142–154.

Watabe-Uchida, M., Zhu, L., Ogawa, S.K., Vamanrao, A., Uchida, N., Bäckman, C.M., Malik, N., Zhang, Y., Shan, L., Grinberg, A., et al. (2012). Whole-brain mapping of direct inputs to midbrain dopamine neurons. Neuron *74*, 858–873.

Welniarz, Q., Dusart, I., and Roze, E. (2016). The corticospinal tract: Evolution, development, and human disorders. Dev. Neurobiol.

Xu, B., Goldman, J.S., Rymar, V.V., Forget, C., Lo, P.S., Bull, S.J., Vereker, E., Barker, P.A., Trudeau, L.E., Sadikot, A.F., et al. (2010). Critical Roles for the Netrin Receptor Deleted in Colorectal Cancer in Dopaminergic Neuronal Precursor Migration, Axon Guidance, and Axon Arborization. Neuroscience *169*, 932–949.

Yamagishi, S., Hampel, F., Hata, K., del Toro, D., Schwark, M., Kvachnina, E., Bastmeyer, M., Yamashita, T., Tarabykin, V., Klein, R., et al. (2011). FLRT2 and FLRT3 act as repulsive guidance cues for Unc5-positive neurons. EMBO J. *30*, 2920–2933.

Yebra, M., Montgomery, A.M.P., Diaferia, G.R., Kaido, T., Silletti, S., Perez, B., Just, M.L., Hildbrand, S., Hurford, R., Florkiewicz, E., et al. (2003). Recognition of the neural chemoattractant Netrin1 by integrins alpha6beta4 and alpha3beta1 regulates epithelial cell adhesion and migration. Dev. Cell *5*, 695–707.

Yung, A.R., Nishitani, A.M., and Goodrich, L. V (2015). Phenotypic analysis of mice completely lacking netrin 1. Development *142*, 3686–3691.

Zhao, S., Maxwell, S., Jimenez-Beristain, A., Vives, J., Kuehner, E., Zhao, J., O'Brien, C., de Felipe, C., Semina, E., and Li, M. (2004). Generation of embryonic stem cells and transgenic mice expressing green fluorescence protein in midbrain dopaminergic neurons. Eur. J. Neurosci. *19*, 1133–1140.

Supplemental information

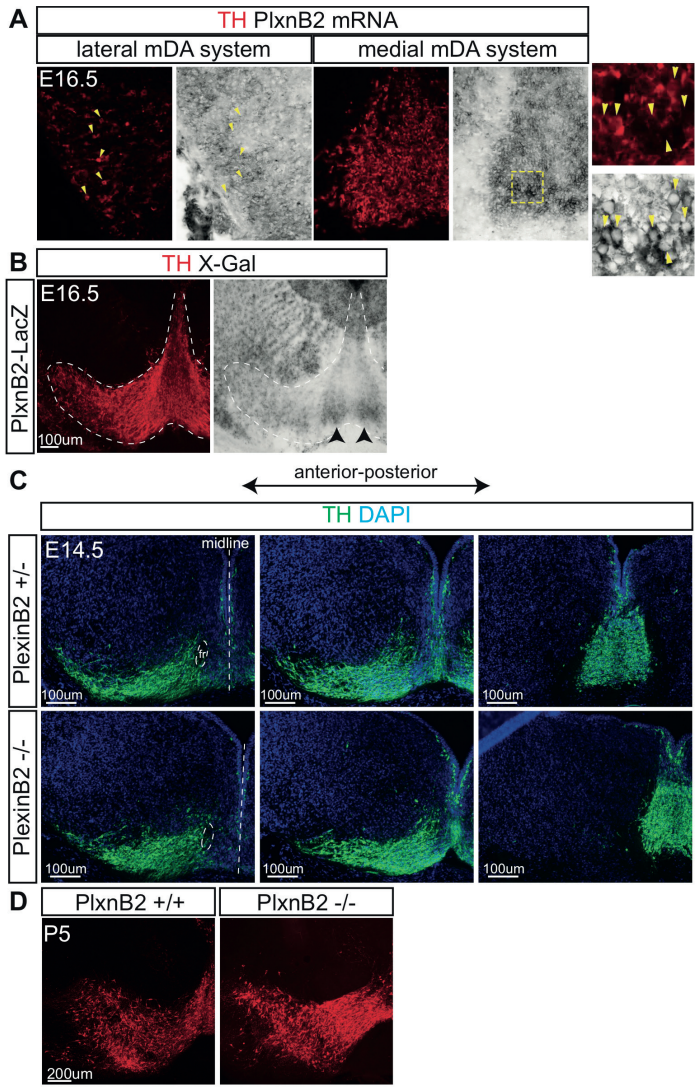

Suppl. Figure 1

PlxnB2 expressed by medial mDA neurons is not required for mDA neuron migration

(A) *In situ* hybridization for PlxnB2 on E16.5 coronal sections. PlxnB2 mRNA is enriched in medial mDA neurons. (B) X-Gal staining on E16.5 PlxnB2$^{+/LacZ}$ brains. X-Gal staining is stronger in the medial mDA system. (C, D) Coronal sections of the mDA system of *PlxnB2-KO* and control brains at E14.5 (C) and P5 (D).

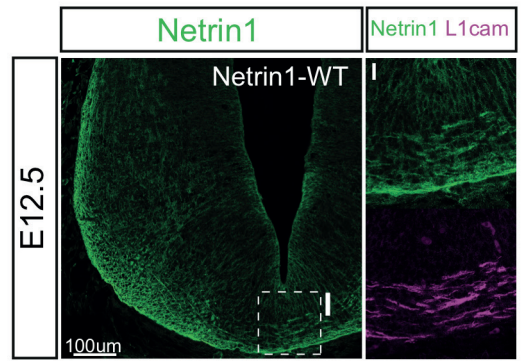

Suppl. Figure 2

Netrin1 is expressed by midbrain commissural axons

Immunostaining for Netrin1 and L1CAM on E12.5 midbrain coronal sections. Netrin1 and L1CAM are co-expressed by commissural axons that cross the ventral midbrain.

Chapter 6

General Discussion

A few sections are adapted from: *Brignani S and Pasterkamp RJ (2017) Neuronal Subset-Specific Migration and Axonal Wiring Mechanisms in the Developing Midbrain Dopamine System. Front. Neuroanat. 11:55.doi: 10.3389/fnana.2017.00055*

The mDA system is composed of heterogeneous mDA neuron subsets, which are defined by distinct molecular profiles (La Manno et al., 2016; Poulin et al., 2014) and by specific connections with different brain areas (Aransay et al., 2015; Gasbarri et al., 1996; Ikemoto, 2007; Khan et al., 2017; Lammel et al., 2008; Matsuda et al., 2009; Poulin et al., 2014; Stamatakis et al., 2013). To comprehend the cellular and molecular mechanisms underlying the formation of mDA subset-specific connections, the development of mDA neuron subsets needs to be characterized. In this thesis, we have developed new *in vivo* and *in vitro* approaches to distinguish mDA neuron subsets, with the aim to study their migration and axon guidance. The application of these new tools allowed to understand the ontogeny of subset-specific mDA neuron migration and axonal projections, and led to the identification of molecular pathways involved in mDA system wiring. The "General discussion" of this thesis aims at discussing our findings to shed light on general and fundamental biological principles of brain development, that may also generally apply to the subset-specific development of other neuronal systems.

1. Visualization of neuronal subsets *in vivo*

Studies focused on understanding neural network wiring often rely on the visualization of seemingly homogeneous neuronal populations, to determine how these neurons develop in space and time, and to define how they change after manipulation. However, genetic tools to selectively label mDA neuron subsets *in vivo* were lacking, and the mDA system was often studied as a whole. This was strongly limiting our comprehension of how different mDA neuron subsets can establish precise connections with distinct brain areas to acquire different and specific functions. In Chapter 3 of this thesis, we design a new genetic approach to visualize mDA neuron subsets based on the expression of different fluorescent proteins in distinct mDA neuron clusters. *In vivo* florescent labelling of mDA neuron subsets allows to study migration and axon guidance of each neuronal subset individually and to isolate mDA subsets to determine their precise molecular profile. In addition, this approach enables the analysis of structural alterations of mDA neuron subsets in mice lacking axon guidance genes involved in mDA system wiring, to specifically link the function of axon guidance genes to mDA neuronal cell types.

To differentially label mDA neuron subsets *in vivo*, the activity of single gene promoters cannot be exploited to induce the expression of fluorescent reporters in specific mDA populations. In fact, no promoters are known to be active only in single and homogeneous mDA neuron clusters. Our new genetic strategy, called "Pitx3-ITC", relies on the simultaneous activation of multiple promoters in a single mouse. This, in turn, induces the expression of different fluorescent proteins in specific mDA neuron clusters, such as SNc and VTA mDA neurons or in even smaller neuron subsets. This new genetic approach may be applied in other neuronal systems that, similar to the mDA system, are characterized by a high level of molecular and functional heterogeneity.

The initial characterization of *Pitx3-ITC* transgenic mice revealed an unexpected pattern of ITC expression. The Pitx3-ITC construct, designed to label the entire mDA system, is expressed by SNc mDA neurons *in vivo*. In contrast, Pitx3-ITC is not active in VTA mDA neurons, which are therefore not labelled by any fluorescent protein. This expression pattern is observed in all three *Pitx3-ITC* founder mouse lines that we obtained, indicating that, most likely, the Pitx3-ITC BAC construct lacks regulatory elements important for driving gene expression in VTA mDA neurons. In order to obtain a *Pitx3-ITC* mouse line which expresses ITC in all mDA neurons, we are now generating new *Pitx3-ITC* mice applying a knock-in approach. It has been shown that both *Pitx3-Cre* and *Pitx3-GFP* mouse lines generated using a knock-in strategy express Cre and GFP, respectively, in all mDA neurons (Smidt et al., 2012; Zhao et al., 2004). In these mouse lines, all the required regulatory elements are in the correct position to induce the proper activity of the *Pitx3* promoter and, in turn, the expression of Cre and GFP in all mDA neurons. In combination with the new knock-in *Pitx3-ITC* mouse line, mDA subset-specific Cre or Flp mouse lines are being generated or are already available. Examples of gene promoters which can be used to target VTA mDA neurons or VTA mDA neuron subsets are the following: the promoters *Grp* or *Adcyap1* are markers of VTA mDA neurons innervating the nucleus accumbens of the ventral striatum (Ekstrand et al., 2014); the promoter *Slc32a1* is active in a small subset of VTA mDA neurons which may project to the lateral habenula (Stamatakis et al., 2013); and the promoter *Cck* labels all VTA mDA neurons. The Sox6 promoter may be used to specifically label all SNc mDA neurons (Panman et al., 2014).

Although the ITC expression pattern is not as expected, *Pitx3-ITC* mice represent a valuable tool that opens new opportunities to study SNc mDA neuron development *in vivo*. In *Pitx3-ITC* mice, SNc mDA neurons together with their axons and dendrites can be distinguished from other mDA neuron subsets. This means that the ontogeny of SNc mDA neurons can now be analyzed in detail, and that structural changes in the nigrostriatal pathway in mice lacking axon guidance genes can be detected. Furthermore, since *Pitx3-ITC* mice show sparse labelling of SNc mDA neurons, the anatomical structure of single SNc mDA neurons can be visualized. During mDA neuron migration, for example, migrating processes (leading and trailing processes) of single SNc neurons are detected and the direction of migration can therefore be determined.

2. Single neuron labelling

Different mDA neuron-subtypes establish connections with distinct pre- and post-synaptic partners. Developing mDA-axon subsets navigate towards distinct target brain regions, they innervate specific target sub-domains, and arborize to different extents. It has been shown, for example, that in the adult striatum individual SNc mDA axons form widely spread and highly dense axonal bushes, that may establish connections with approximately 75.000 striatal neurons (Matsuda et al., 2009). At the post-synaptic level, mDA neurons can have dendritic fields that differ in position and extension in relation to the afferent connections they receive. The cellular and molecular processes underlying the development of these different features are largely undetermined, mainly due to the lack of genetic tools useful to visualize neuronal processes at single-cell resolution during development. These aspects of neuron development are difficult to study when a large population of neurons is labelled.

In our attempt to generate Cre and Flp mouse lines to selectively target SNc and VTA mDA neurons, we developed transgenic lines that allow labelling of individual SNc and VTA mDA neurons (Chapter 3). Single-cell labelling enables the visualization of axons and dendrites of single mDA neurons, allowing us to detect for example the extensive nigrostriatal axonal bushes in the dorsal striatum, as already described by Matsuda et al. (2009). These mouse lines offer the opportunity to study the mechanisms that shape subset-specific dendritic patterning and the generation of the extensive axonal bushes in the striatum during development. The visualization of neuronal processes at a single-cell resolution allows us to study whether and how neuronal morphology changes in mice lacking the expression of axon guidance molecules, to ultimately determine the functional role of these molecules in mDA neuron development. In Chapter 4 of this thesis, we provide evidence indicating that Netrin1, expressed by striatal neurons, induces nigrostriatal axon branching in the dorsal striatum *in vivo*. In this study, a large portion of SNc mDA neurons were selectively labelled in mice lacking Netrin1 expression. These mice showed that, in absence of Netrin1, nigrostriatal axons successfully innervate the dorsal striatum but that their axonal branching is strongly reduced. It would now be interesting to evaluate the altered nigrostriatal axon branching in *Netrin1*-KO mice at the single-cell level, by crossing *Netrin1*-KO mice with our new mouse lines enabling the visualization of individual SNc mDA neurons. This approach would allow us to study in detail the development of single nigrostriatal fibers in the striatum *in vivo* and to understand how their branching process is altered in absence of Netrin1.

3. mDA system development relies on pre-existing scaffolds

In this thesis, the development of mDA neuron subsets has been studied from different perspectives: SNc mDA neuron migration is analyzed in Chapter 5; and mDA subset-specific axon growth and guidance are examined in Chapter 2 and 4. In the latter chapters, we focus on (1) the mesohabenular pathway established between VTA mDA neurons and the lateral subnucleus of the habenula, and (2) the nigrostriatal and mesolimbic pathways, that connect SNc and VTA mDA neurons to the dorsal and ventral striatum, respectively. In all these studies we first determine the ontogeny of the system, and then analyze the cellular and molecular mechanisms responsible for its wiring. It is very interesting to note that, in all these different contexts (i.e. neuron migration and subset-specific axon navigation), our findings show that the development of the mDA system relies on pre-existing cellular scaffolds.

SNc and VTA mDA neurons are born in the floor plate of the midbrain ventricular zone, and from there migrate to their final destination in the marginal zone. As described in Chapter 5, SNc mDA neuron migration follows three directions: dorso-ventral, medio-lateral, and caudo-rostral. In contrast, the leading and trailing processes of VTA mDA neurons are almost exclusively oriented radially, strongly indicating that VTA mDA neurons mainly migrate radially (Bodea et al., 2014). To migrate in the dorso-ventral direction, mDA neurons undergo a first phase of radial migration. During this phase, both SNc and VTA mDA neurons have leading and trailing processes oriented radially, aligned with the fibers of radial glia cells, as demonstrated by us and others (Bodea et al., 2014; Shults et al., 1990). Radial glia fibers function as scaffolds for radially migrating mDA neurons, similarly to their role in the developing cortex (Marín et al., 2010). Radial glia fibers provide physical support to migrating neurons and, most importantly, they provide a migratory direction to follow. During the second phase of mDA neuron migration, SNc mDA neurons migrate in the medio-lateral and caudo-rostral directions. It has been proposed that during medio-lateral migration the leading processes of SNc mDA neurons follow commissural axons, presumably axons originating from neurons located in the lateral midbrain (Kawano et al., 1995). However, strong functional evidence supporting this hypothesis is lacking. In this thesis, we have shown that SNc mDA neurons migrate also along the anterior-posterior axis. It is not known, however, if during this phase of caudo-rostral migration SNc mDA neurons rely on pre-existing guidance scaffolds.

A migratory behavior that requires pre-existing scaffolds is adopted by a subset of migrating SNr GABAergic neurons. As shown by Madrigal et al. (2016), GABAergic neurons of the anterior SNr migrate from the posterior to the anterior midbrain to form a neuron cluster positioned at the ventro-lateral side

of the SNc wing-like structure. In Chapter 5, we provide evidence indicating that migrating anterior-SNr GABAergic neurons may be guided in a caudo-rostral direction by pre-existing longitudinal axons of the cerebral peduncle. Like radial glia fibers, axons of the cerebral peduncle may function as guidance scaffolds for these migrating neurons.

Pre-existing guidance scaffolds are important not only for neuron migration, they are crucial also for mDA axon development, for example for axons of the mesohabenular pathway. The habenula is positioned in the dorso-medial diencephalon and is composed of two main subdomains: the lateral (LHb) and the medial habenula (MHb). Efferent habenular axons fasciculate together to form the fasciculus retroflexus (FR), which has an outer sheath of LHb axons surrounding a core of MHb axons (Bianco and Wilson, 2009). VTA mDA axons projecting to the LHb are confined to the sheath domain of the FR. In Chapter 2 of this thesis, we demonstrate that the physical interaction between VTA mDA axons and axons of the FR-sheath is required for the correct development of the system, and limbic-system associated membrane protein (LAMP) is an important mediator of this process. Loss of FR axons completely prevents growth of mDA axons towards the habenula, indicating that habenular axons provide guidance to elongating mesohabenular projections. These findings show that the LHb determines its own dopaminergic afferents by projecting axons towards the VTA. mDA axons are collected and guided by habenular axons of FR-sheath, relying on a mechanism of reciprocal axon-axon interactions.

In addition to the mesohabenular pathway, our results and those of others strongly suggest that also VTA mDA axons elongating towards the striatum may rely on pre-existing axonal scaffolds. *DCC* and *Netrin1* KO mice show that a subset of mDA axons leaves the MFB turning ventrally at the level of the caudal hypothalamus, an important intermediate target for developing mDA axons. These axons form an aberrant bundle that crosses the ventral midline (Chapter 4 and (Li et al., 2014; Xu et al., 2010). Using the *Pitx3-ITC* mouse model, nigrostriatal axons were labelled in *Netrin1-KO* brains demonstrating that the aberrant TH^+ axon bundle observed in the caudal hypothalamus is not composed of SNc mDA axons. This strongly suggests that the absence of *Netrin1* and *DCC* causes the misrouting of VTA mDA axons that normally grow towards the forebrain. Interestingly, this phenotype is not detected in mice in which *DCC* is conditionally ablated from mDA neurons from E13.5 onwards (Chapter 4). This observation indicates that DCC expression may be required cell-autonomously for the development of other (non-dopaminergic) longitudinal axons. In *DCC* KO brains, the formation of the aberrant TH^+ axon bundle may be the consequence of the misrouting of these non-dopaminergic longitudinal axons that normally function as scaffolds for mDA axons. Similar to radial glia fibers for migrating mDA neurons, pre-existing axon bundles may act as guidance scaffolds for different mDA axon subsets.

Because of these mechanisms of neuron-fiber and axon-axon interactions, migrating mDA neurons and elongating mDA axons do not randomly explore the surrounding environment to ultimately find their final position or target brain area. In contrast, they are guided in a more orderly and efficient way by pre-existing brain structures. However, this efficiency may come at a cost: the development of the mDA system may become more vulnerable. When the development of guiding scaffolds is perturbed, mDA system wiring may be compromised. It is possible that disorders characterized by defects in the mDA system may originally be caused by alterations in non-dopaminergic structures that play a role in supporting the developing mDA system. Further efforts are needed to understand the function of pre-existing cellular scaffolds in mDA system development and their role in diseases.

4. Development of dopaminergic axon-subtypes

During development, mDA axons navigate from the midbrain to the forebrain in a tight axonal bundle, the MFB. In Chapter 4 of this thesis, we have studied the mechanisms of elongation and guidance of dopaminergic axon-subsets. Two different transgenic mouse lines were used to selectively visualize SNc mDA axons and VTA mDA axons and to determine their ontogeny. Our results show that, during development, SNc and VTA mDA projections are located in the dorsal and ventral MFB, respectively, rather than being distributed throughout the bundle. When they arrive at their striatal target, nigrostriatal projections invade and innervate the dorsal striatum, whereas mesolimbic projections specifically target the ventral striatum, without forming mis-targeted collaterals in non-specific striatal compartments. The topographic organization of mDA axon-subsets in the MFB may be therefore very important for the correct development of subset-specific connections in the striatum. Nigrostriatal and mesolimbic axon segregation may act as a sorting mechanism: the location of an axon in the MFB may determine its final position in the striatum. Alterations of mDA axon-subset segregation in the MFB might therefore determine an aberrant innervation of the target.

Mechanisms of pre-target axon sorting have already been described in other neuronal systems, such as the visual and olfactory systems (Imai et al., 2009; Plas et al., 2005). Here, sensory neurons are connected to their respective targets maintaining their neighbor-neighbor relationships in the target field, in order to represent the detected sensory information as a topographic map in the brain. The formation of these maps does not solely depend on axon-target interaction. Topographic order emerges already in axon bundles, through a process called pre-target axon sorting. This mechanism allows elongating axons, which are at first intermingled, to segregate in axon-subsets, to acquire a specific spatial order

before reaching the target. Pre-target axon sorting is established by axon guidance cue and receptor pairs that show graded expression in elongating axons.
How is the segregation of axon-subsets achieved in the mDA system? Does it rely on the mechanism of pre-target axon sorting observed in the visual and olfactory systems? According to our data, in the MFB nigrostriatal and mesolimbic axons are segregated in two distinct axon-subsets throughout all their navigation to the striatum. In contrast to visual and olfactory axons, the two mDA axon-subsets are not intermingled during the first phase of their development. In addition, our results show that SNc mDA axons invade the striatum earlier than VTA mDA axons. This observation suggests that the navigation of nigrostriatal projections towards the striatum starts before that of mesolimbic projections. This hypothesis is in line with birth-dating of mDA neuron-subsets. It has been shown that the majority of SNc mDA neurons is born before VTA mDA neurons (Bayer et al., 1995; Bye et al., 2012), indicating that SNc mDA axons are most likely generated earlier than VTA mDA axons. Therefore, early-born SNc mDA axons may form a first axon tract directed towards the forebrain, that is then followed by late-born VTA mDA axons. If this hypothesis is true, nigrostriatal projections may provide guidance to VTA mDA axons by expressing specific guidance cues. To understand whether SNc mDA axons are required by VTA mDA axons during their navigation towards the striatum, SNc mDA projections could be ablated or mis-routed from very early developmental stages, to then determine whether the elongation of VTA mDA axons is perturbed. However, these approaches are difficult to implement because of lack of genetic tools. Cre or Flp mouse lines are not available to selectively ablate SNc mDA axons, or to conditionally knock-out axon guidance genes from mDA neuron-subsets. Furthermore, none of the genetically modified mouse lines described in literature displays clear nigrostriatal axon mis-routing. To comprehend whether developing VTA mDA projections rely on pre-existing nigrostriatal axons, it is therefore necessary to generate new genetic tools to specifically target mDA neuron-subtypes. The ability to manipulate and alter the development of mDA axon-subsets will also allow to determine whether the segregation of mDA axon in the MFB is important for the formation of subset-specific connections in the striatum.

5. Netrin1 is a master regulator of mDA system development

In addition to studying the fundamental mechanisms that drive mDA system wiring at a cellular level, in this thesis we have extensively investigated the molecular mechanisms that orchestrate mDA system development. We have identified molecular pathways involved in both mDA neuron subset migration and mDA axon subset guidance. Our findings clearly show that Netrin1 is a master regulator of mDA system development. Netrin1 acts during several stages of mDA system wiring: (1) Netrin1 is important for VTA mDA axon entry of the lateral habenula (Chapter 2); (2) it functions as a branching promoter for SNc mDA axons in the dorsal striatum (Chapter 4); and (3) it is essential during SNc mDA and SNr GABAergic neuron migration (Chapter 5).
(1) As discussed in the previous section, mesohabenular axons are guided towards the lateral habenula by following FR-sheath projections that function as a scaffold. Once VTA mDA axons arrive at the edge of the lateral habenular, the innervation of the lateral nucleus is mediated by Netrin1/DCC signaling. Netrin1 is expressed by the lateral habenula, but not by the medial nucleus, and is a potent attractant for the DCC^{+} mDA axons that are approaching the lateral nucleus. In both *Netrin1* and *DCC* KO mice, mDA axons no longer innervate the lateral habenula, but instead stall at its ventral border.
(2) Netrin1 is expressed by striatal neurons and, according to our findings, induces SNc mDA axon branching in the dorsal striatum. In *Netrin1* KO mice, nigrostriatal axons can invade the striatal compartment but the level of nigrostriatal innervation is strongly reduced as compared to control brains. These observations are in line with *in vitro* experiments showing that the administration of Netrin1 to dissociated mDA neurons induces mDA axon branching (Xu et al., 2010). In contrast to the mesohabenular system, Netrin1-induced SNc mDA axon branching is not mediated by the receptor DCC. When *DCC* is conditionally removed from mDA axons from E13.5 onwards, *in vivo* nigrostriatal branching appears normal. This suggests that other receptors mediate Netrin1 activity in this context.
However, our findings are in contrast with a developmental model recently proposed by (Li et al., 2014), which supports a different functional role of Netrin1 in the mDA axon innervation of the striatum. According to this study, different levels of Netrin1 expression in the striatum function as topographic guidance for developing mDA axons: low expression levels of Netrin1 in the dorso-medial striatum act as an attractant for elongating SNc mDA axons; while high expression levels of Netrin1 in the ventro-lateral striatum attracts developing VTA mDA axons (Li et al., 2014). In line with these observations, the study argues that SNc mDA axons do not innervate the dorso-medial striatum in *Netrin1-KO* mice, but rather accumulate in the ventro-lateral striatum (Li et al., 2014). Our results did not reveal an accumulation of SNc mDA axons in the ventral striatum, as discussed by Li et al. A significant decrease of nigrostriatal axons was observed in the dorsal striatum, but the overall pattern of SNc axon innervation was preserved in *Netrin1-KO* brains. The accumulation of mDA axons in the ventral striatum described by Li et al. might be caused by an increase of VTA mDA axon innervation or branching.
(3) In Chapter 5, we demonstrate that Netrin1 is expressed by both radial glia fibers and peduncular axons, and is important for the migration of SNc

mDA neuron subsets. The expression pattern of Netrin1 protein appears in close association with both midbrain radial glia fibers and peduncular axons suggesting that Netrin1 is not creating a widespread extracellular gradient *in vivo*. According to our results, it is more likely that Netrin1 functions as a short-range guidance cue. To limit its diffusion, the secreted Netrin1 protein may be bound to the cell membrane or the extracellular matrix (Kappler et al., 2000; Manitt and Kennedy, 2002; Manitt et al., 2001).

In the midbrain, we show that Netrin1 expression in radial glia fibers is important for the radial migration of a subset of SNc mDA neurons (Citrine^{-}/Sox6^{+}). When Netrin1 is conditionally ablated from radial glia cells *in vivo*, a group of SNc mDA neurons is no longer aligned to radial glia fibers but is instead aberrantly positioned in the dorsal reticular nucleus. In addition, dissociated mDA neurons *in vitro* preferentially migrate on Netrin1 stripes rather than on a control protein. DCC is cell-autonomously required by this subset of mDA neurons. Loss of DCC from mDA neurons *in vivo* causes a similar phenotype, with a subset of mDA neurons positioned in the reticular nucleus. Together, these data show that Netrin1 is required for the radial migration of a mDA neuron subset, but not for the radial migration of all mDA neurons, that in contrast relies on the activity of other molecules. Single-cell RNAseq data of the developing ventral midbrain, reviewed by us in (Brignani and Pasterkamp, 2017), demonstrates that radial glia cells express several axon guidance cues (e.g. Slits, Eph/Ephrins, and Semaphorins) (La Manno et al., 2016). These molecules might play a role in the development of the radial glia fibers, but also in guiding the radial migration of different mDA neuron subsets. Further *in vitro* and *in vivo* analyses should unveil whether they are functionally implicated in this process. To select the molecules that may elicit an attractive or repulsive response in migrating mDA neurons, *in vitro* stripe assays may be performed by plating dissociated mDA neurons on a carpet of stripes of the candidate molecule. Then, the selected genes may be further tested *in vivo* by analyzing KO mice lacking the guidance gene of interest, to determine whether the gene is required for the correct migration of mDA neurons. In addition, *Pitx3-ITC;ACTB-FlpE* and *CCK-Cre;TdTom* mouse lines can be crossed with the KO mice of interest to label SNc or VTA mDA neurons, and to understand whether the candidate gene is involved in the migration of specific mDA neuron subsets.

In Chapter 5, we show that Netrin1 is also indirectly required for the migration of another SNc mDA neuron subset (Citrine^{+}/Sox6^{+}). Our data suggests that Netrin1 expressed by peduncular axons may guide the caudo-rostral migration of anterior SNc GABAergic neurons. In *Netrin1* KO brains, the migration of this GABAergic neuron population is altered, with fewer GABAergic neurons positioned at the ventro-lateral side of the SNc. As a consequence, SNc mDA neurons remain attached to the pial surface of the ventral midbrain, and do not form the characteristic wing-like structure present in postnatal and adult brains. In this context, the DCC receptor is not required, neither for SNc mDA neurons nor for SNr GABAergic neuron migration. In E18.5 *DCC-KO* brains, when neuron migration is complete, both neuronal populations are located at the correct position.

In conclusion, we provide extensive evidence supporting the fundamental role of Netrin1 in mDA system development. The effects of Netrin1 are mediated by DCC receptor in some but not all of the studied developmental processes. This indicates that distinct mDA neuron subsets express different Netrin1 receptors at specific developmental phases, demonstrating again the highly heterogeneous nature of mDA neurons. We have shown in Chapter 4, for example, that Netrin1-induced SNc mDA axon branching in the dorsal striatum is not mediated by DCC expressed by mDA axons. This therefore suggests that other Netrin1 receptors are needed by mDA neurons to accurately respond to Netrin1 in the dorsal striatum. The mRNA of both Neogenin and DsCAM, two molecules identified as Netrin1 receptors (Ly et al., 2008; Xu et al., 2014), has been detected in mDA neurons during development (van den Heuvel et al., 2013; La Manno et al., 2016). However, nothing is known about their roles in mDA axon guidance and whether they may be functionally involved in the Netrin1-induced nigrostriatal branching. To evaluate this latter hypothesis, both *in vitro* and *in vivo* experiments may be performed. For example, knockdown of Neogenin or DsCAM mRNA may be conducted on dissociated SNc mDA neurons to test whether Netrin1 induces nigrostriatal axon branching *in vitro* upon receptors ablation. In addition, *Neogenin*-KO and *DsCAM*-KO mouse brains can be analyzed to determine whether lack of the two receptors may cause a reduction of nigrostriatal axon branching in the striatum *in vivo*.

6. Future directions

Because of their important functional roles and their implication in disease, mDA neurons have been studied extensively. Several studies have recently focused on dissecting the molecular programs that dictate the formation of mDA connectivity. Approaches such as single cell omics have begun to provide insight into the different neuronal subsets that comprise the mDA system. Despite recent progress, many questions remain. For example, in the adult brain, mDA neurons receive afferents from many different brain areas, but the developmental programs involved in establishing mDA afferent connectivity remain largely unidentified. Furthermore, while many cues are now known to affect mDA axons, the structure and development of mDA dendrites remains largely unexplored. Technological advances such as light-sheet microscopy and single-cell omics approaches will help to provide insight into these and other questions. More studies focused on understanding the heterogeneity of

mDA neurons are needed for several reasons: (1) SNc mDA neurons are more prone to degeneration in Parkinson's disease than VTA neurons (Albin et al., 1989). The identification of molecular profiles that correlate with different mDA neuron subsets may increase our understanding of why certain neurons are more vulnerable than others. (2) Understanding the molecular features of different mDA subsets may improve the generation and the characterization of iPSC-derived mDA neurons subsets. This will help to obtain better *in vitro* models of human mDA cell-types and more specific mDA neurons to transplant into Parkinson's disease patients. (3) New genetic markers selective for mDA subsets can be used to generate Cre or Flp mouse lines to target mDA neuron subsets. These new mouse lines would allow the expression of fluorescent reporter proteins for the visualization of mDA neuronal subsets, to conditionally knock-out genes and study their functions, and to perform optogenetic analyses on molecularly homogeneous mDA neurons.

A better understanding of mDA system development is also essential from a clinical perspective. mDA neurons of the VTA have been implicated in disorders such as drug addiction, depression, and schizophrenia (reviewed in (Morales and Pickel, 2012; Walsh and Han, 2014)), and evidence indicates that developmental and/or adult structural changes of neuronal networks may in part underline the pathogenesis of these disorders (Robinson and Kolb, 2004). In particular for drug addiction-behaviors, it has been shown that the expression of axon guidance genes changes in the mDA system after long-term exposure to drugs. Further, drug-induced behaviors can be altered upon genetic manipulation of axon guidance genes (Auger et al., 2013; Flores et al., 2005; Pokinko et al., 2015; Sieber et al., 2004). Moreover, genome-wide association studies and gene expression profiling have linked axon guidance proteins to Parkinson's disease (reviewed in (Van Battum et al., 2015)). Due to their roles in mDA system development, changes in the expression or function of axon guidance genes may lead to defects in the formation or maintenance of mDA neuron connectivity and function. Although axon guidance events are crucial for the correct development of mDA nigrostriatal and mesocorticolimbic pathways, their precise role during the pathogenesis of mDA system-related diseases is largely unknown. To date, only the repulsive guidance molecule member a (RGMa) has been functionally linked to Parkinson's disease. In Parkinson's disease patients, RGMa is upregulated in SNc mDA neurons (Bossers et al., 2009). In addition, it has been recently shown that RGMa overexpression in mDA neurons of adult mice results in a selective degeneration of SNc mDA neurons and in a progressive movement disorder (Korecka et al., 2017). Further studies on the role of axon guidance molecules during the development and plasticity of mDA networks are required to better understand their potential contribution to diseases. Understanding how the dopamine system develops will also aid the development of more effective cell-replacement strategies in Parkinson's disease patients. The molecular ingredients required to build a functional nigrostriatal pathway could be applied to improve the integration of transplanted mDA neurons into the degenerating dopamine system.

References

Albin, R.L., Young, A.B., and Penney, J.B. (1989). The functional anatomy of basal ganglia disorders. Trends Neurosci. *12*, 366–375.

Aransay, A., Rodríguez-López, C., García-Amado, M., Clascá, F., and Prensa, L. (2015). Long-range projection neurons of the mouse ventral tegmental area: a single-cell axon tracing analysis. Front. Neuroanat. *9*, 59.

Auger, M.L., Schmidt, E.R.E., Manitt, C., Dal-Bo, G., Pasterkamp, R.J., and Flores, C. (2013). unc5c haploinsufficient phenotype: striking similarities with the dcc haploinsufficiency model. Eur. J. Neurosci. *38*, 2853–2863.

Van Battum, E.Y., Brignani, S., and Pasterkamp, R.J. (2015). Axon guidance proteins in neurological disorders. Lancet Neurol. *14*.

Bayer, S.A., Wills, K. V, Triarhou, L.C., and Ghetti, B. (1995). Time of neuron origin and gradients of neurogenesis in midbrain dopaminergic neurons in the mouse. Exp. Brain Res. *105*, 191–199.

Bianco, I.H., and Wilson, S.W. (2009). The habenular nuclei: a conserved asymmetric relay station in the vertebrate brain. Philos. Trans. R. Soc. B Biol. Sci. *364*, 1005–1020.

Bodea, G.O., Spille, J.-H., Abe, P., Andersson, A.S., Acker-Palmer, A., Stumm, R., Kubitscheck, U., and Blaess, S. (2014). Reelin and CXCL12 regulate distinct migratory behaviors during the development of the dopaminergic system. Development *141*, 661–673.

Bossers, K., Meerhoff, G., Balesar, R., van Dongen, J.W., Kruse, C.G., Swaab, D.F., and Verhaagen, J. (2009). Analysis of gene expression in Parkinson's disease: possible involvement of neurotrophic support and axon guidance in dopaminergic cell death. Brain Pathol. *19*, 91–107.

Brignani, S., and Pasterkamp, R.J. (2017). Neuronal Subset-Specific Migration and Axonal Wiring Mechanisms in the Developing Midbrain Dopamine System. Front. Neuroanat. *11*, 55.

Bye, C.R., Thompson, L.H., and Parish, C.L. (2012). Birth dating of midbrain dopamine neurons identifies A9 enriched tissue for transplantation into parkinsonian mice. Exp. Neurol. *236*, 58–68.

Ekstrand, M.I., Nectow, A.R., Knight, Z.A., Latcha, K.N., Pomeranz, L.E., and Friedman, J.M. (2014). Molecular profiling of neurons based on connectivity. Cell *157*, 1230–1242.

Flores, C., Manitt, C., Rodaros, D., Thompson, K.M., Rajabi, H., Luk, K.C., Tritsch, N.X., Sadikot, A.F., Stewart, J., and Kennedy, T.E. (2005). Netrin receptor deficient mice exhibit functional reorganization of dopaminergic systems and do not sensitize to amphetamine. Mol. Psychiatry *10*, 606–612.

Gasbarri, A., Packard, M.G., Sulli, A., Pacitti, C., Innocenzi, R., and Perciavalle, V. (1996). The projections of the retrorubral field A8 to the hippocampal formation in the rat. Exp. Brain Res. *112*, 244–252.

Gerfen, C.R., Paletzki, R., and Heintz, N. (2013). GENSAT BAC Cre-Recombinase Driver Lines to Study the Functional Organization of Cerebral Cortical and Basal Ganglia Circuits. Neuron *80*, 1368–1383.

Harris, J.A., Hirokawa, K.E., Sorensen, S.A., Gu, H., Mills, M., Ng, L.L., Bohn, P., Mortrud, M., Ouellette, B., Kidney, J., et al. (2014). Anatomical characterization of Cre driver mice for neural circuit mapping and manipulation. Front. Neural Circuits *8*, 76.

van den Heuvel, D.M.A., Hellemons, A.J.C.G.M., and Pasterkamp, R.J. (2013). Spatiotemporal expression of repulsive guidance molecules (RGMs) and their receptor neogenin in the mouse brain. PLoS One *8*, e55828.

Ikemoto, S. (2007). Dopamine reward circuitry: Two projection systems from the ventral midbrain to the nucleus accumbens–olfactory tubercle complex. Brain Res. Rev. *56*, 27–78.

Imai, T., Yamazaki, T., Kobayakawa, R., Kobayakawa, K., Abe, T., Suzuki, M., and Sakano, H. (2009). Pre-target axon sorting establishes the neural map topography. Science *325*, 585–590.

Kappler, J., Franken, S., Junghans, U., Hoffmann, R., Linke, T., Müller, H.W., and Koch, K.-W. (2000). Glycosaminoglycan-Binding Properties and Secondary Structure of the C-Terminus of Netrin1. Biochem. Biophys. Res. Commun. *271*, 287–291.

Kawano, H., Ohyama, K., Kawamura, K., and Nagatsu, I. (1995). Migration of dopaminergic neurons in the embryonic mesencephalon of mice. Dev. Brain Res. *86*, 101–113.

Khan, S., Stott, S.R.W., Chabrat, A., Truckenbrodt, A.M., Spencer-Dene, B., Nave, K.-A., Guillemot, F., Levesque, M., and Ang, S.-L. (2017). Survival of a Novel Subset of Midbrain Dopaminergic Neurons Projecting to the Lateral Septum Is Dependent on NeuroD Proteins. J. Neurosci. *37*.

Korecka, J.A., Moloney, E.B., Eggers, R., Hobo, B., Scheffer, S., Ras-Verloop, N., Pasterkamp, R.J., Swaab, D.F., Smit, A.B., van Kesteren, R.E., et al. (2017). Repulsive Guidance Molecule a (RGMa) Induces Neuropathological and Behavioral Changes That Closely Resemble Parkinson's Disease. J. Neurosci. *37*, 9361–9379.

Lammel, S., Hetzel, A., Häckel, O., Jones, I., Liss, B., and Roeper, J. (2008). Unique properties of mesoprefrontal neurons within a dual mesocorticolimbic dopamine system. Neuron *57*, 760–773.

Li, J., Duarte, T., Kocabas, A., Works, M., McConnell, S.K., and Hynes, M.A. (2014). Evidence for topographic guidance of dopaminergic axons by differential Netrin1 expression in the striatum. Mol. Cell. Neurosci. *61*, 85–96.

Ly, A., Nikolaev, A., Suresh, G., Zheng, Y., Tessier-Lavigne, M., and Stein, E. (2008). DSCAM Is a Netrin Receptor that Collaborates with DCC in Mediating Turning Responses to Netrin1. Cell *133*, 1241–1254.

Madrigal, M.P., Moreno-Bravo, J.A., Martínez-López, J.E., Martínez, S., and Puelles, E. (2016). Mesencephalic origin of the rostral Substantia nigra pars reticulata. Brain Struct. Funct. *221*, 1403–1412.

Manitt, C., and Kennedy, T.E. (2002). Where the rubber meets the road: netrin expression and function in developing and adult nervous systems. Prog. Brain Res. *137*, 425–442.

Manitt, C., Colicos, M.A., Thompson, K.M., Rousselle, E., Peterson, A.C., and Kennedy, T.E. (2001). Widespread expression of Netrin1 by neurons and oligodendrocytes in the adult mammalian spinal cord. J. Neurosci. *21*, 3911–3922.

La Manno, G., Gyllborg, D., Codeluppi, S., Nishimura, K., Salto, C., Zeisel, A., Borm, L.E., Stott, S.R.W., Toledo, E.M., Villaescusa, J.C., et al. (2016). Molecular Diversity of Midbrain Development in Mouse, Human, and Stem Cells. Cell *167*, 566–580.e19.

Marín, O., Valiente, M., Ge, X., and Tsai, L.-H. (2010). Guiding neuronal cell migrations. Cold Spring Harb. Perspect. Biol. *2*, a001834.

Matsuda, W., Furuta, T., Nakamura, K.C., Hioki, H., Fujiyama, F., Arai, R., and Kaneko, T. (2009). Single nigrostriatal dopaminergic neurons form widely spread and highly dense axonal arborizations in the neostriatum. J. Neurosci. *29*, 444–453.

Morales, M., and Pickel, V.M. (2012). Insights to drug addiction derived from ultrastructural views of the mesocorticolimbic system. Ann. N. Y. Acad. Sci. *1248*, 71–88.

Panman, L., Papathanou, M., Laguna, A., Oosterveen, T., Volakakis, N., Acampora, D., Kurtsdotter, I., Yoshitake, T., Kehr, J., Joodmardi, E., et al. (2014). Sox6 and Otx2 Control the Specification of Substantia Nigra and Ventral Tegmental Area Dopamine Neurons. Cell Rep. *8*, 1018–1025.

Plas, D.T., Lopez, J.E., and Crair, M.C. (2005). Pretarget sorting of retinocollicular axons in the mouse. J. Comp. Neurol. *491*, 305–319.

Pokinko, M., Moquin, L., Torres-Berrío, A., Gratton, A., and Flores, C. (2015). Resilience to amphetamine in mouse models of Netrin1 haploinsufficiency: role of mesocortical dopamine. Psychopharmacology (Berl). *232*, 3719–3729.

Poulin, J.-F., Zou, J., Drouin-Ouellet, J., Kim, K.-Y.A., Cicchetti, F., and Awatramani, R.B. (2014). Defining Midbrain Dopaminergic Neuron Diversity by Single-Cell Gene Expression Profiling. Cell Rep. *9*, 930–943.

Robinson, T.E., and Kolb, B. (2004). Structural plasticity associated with exposure to drugs of abuse. Neuropharmacology *47*, 33–46.

Shults, C.W., Hashimoto, R., Brady, R.M., and Gage, F.H. (1990). Dopaminergic cells align along radial glia in the developing mesencephalon of the rat. Neuroscience *38*, 427–436.

Sieber, B.-A., Kuzmin, A., Canals, J.M., Danielsson, A., Paratcha, G., Arenas, E., Alberch, J., Ögren, S.O., and Ibáñez, C.F. (2004). Disruption of EphA/ephrin-A signaling in the nigrostriatal system reduces dopaminergic innervation and dissociates behavioral responses to amphetamine and cocaine. Mol. Cell. Neurosci. *26*, 418–428.

Smidt, M.P., von Oerthel, L., Hoekstra, E.J., Schellevis, R.D., and Hoekman, M.F.M. (2012). Spatial and Temporal Lineage Analysis of a Pitx3-Driven Cre-Recombinase Knock-In Mouse Model. PLoS One *7*, e42641.

Stamatakis, A.M., Jennings, J.H., Ung, R.L., Blair, G.A., Weinberg, R.J., Neve, R.L., Boyce, F., Mattis, J., Ramakrishnan, C., Deisseroth, K., et al. (2013). A Unique Population of Ventral Tegmental Area Neurons Inhibits the Lateral Habenula to Promote Reward. Neuron *80*, 1039–1053.

Walsh, J.J., and Han, M.H. (2014). The heterogeneity of ventral tegmental area neurons: Projection functions in a mood-related context. Neuroscience *282*, 101–108.

Xu, B., Goldman, J.S., Rymar, V.V., Forget, C., Lo, P.S., Bull, S.J., Vereker, E., Barker, P.A., Trudeau, L.E., Sadikot, A.F., et al. (2010). Critical Roles for the Netrin Receptor Deleted in Colorectal Cancer in Dopaminergic Neuronal Precursor Migration, Axon Guidance, and Axon Arborization. Neuroscience *169*, 932–949.

Xu, K., Wu, Z., Renier, N., Antipenko, A., Tzvetkova-Robev, D., Xu, Y., Minchenko, M., Nardi-Dei, V., Rajashankar, K.R., Himanen, J., et al. (2014). Neural migration. Structures of Netrin1 bound to two receptors provide insight into its axon guidance mechanism. Science *344*, 1275–1279.

Zhao, S., Maxwell, S., Jimenez-Beristain, A., Vives, J., Kuehner, E., Zhao, J., O'Brien, C., de Felipe, C., Semina, E., and Li, M. (2004). Generation of embryonic stem cells and transgenic mice expressing green fluorescence protein in midbrain dopaminergic neurons. Eur. J. Neurosci. *19*, 1133–1140.

Addendum

Samenvatting in het Nederlands

Curriculum Vitae

List of Publications

Acknowledgments

Samenvatting in het Nederlands

In dit proefschrift bestuderen we de ontwikkeling van dopaminerge neuronen in de ventrale middenhersenen. Deze neuronen vormen samen het dopaminesysteem dat een fundamentele functionele rol speelt bij verschillende cognitieve en motorische gedragingen. Veranderingen in het functioneren van het dopaminesysteem kunnen ten grondslag liggen aan ernstige ziekten, zoals de ziekte van Parkinson, schizofrenie, verslaving en depressie.

Het dopaminesysteem wordt reeds lange tijd op basis van anatomische kenmerken onderverdeeld in drie hoofdkernen: substantia nigra pars compacta (SNc), ventraal tegmentum (VTA) en het retrorubrale veld (RRF). Het wordt echter duidelijk dat neuronen binnen het anatomisch gedefinieerde dopaminesysteem niet homogeen zijn. Er bestaan meerdere afzonderlijke middenbrein dopaminerge (mDA) neuronale deelverzamelingen binnen en over de grenzen van de SNc, VTA en RRF. Onderzoekers hebben bijvoorbeeld subgroepen van dopaminerge neuronen geïdentificeerd die verschillen wat betreft expressie van moleculaire markers, afferente inputs en de hersengebieden die ze innerveren. Om te begrijpen hoe deze verschillen ontstaan worden de oorsprong van en moleculaire programma's in mDA neuronale subsets intensief bestudeerd. Het is aannemelijk, en deels bekend, dat verschillende mDA neuronen specifieke moleculaire signalen tot expressie brengen die subset-specifieke differentiatie, migratie en axon-sturing mogelijk maken.

Dit proefschrift is gericht op het ontrafelen van cellulaire en moleculaire processen die de ontwikkeling van mDA neuronale subsets aansturen. Daarvoor wordt een combinatie van cellulaire, moleculaire en genetische benaderingen gebruikt.

In **hoofdstuk 2** bestuderen we de ontwikkeling van een deelverzameling van VTA mDA neuronen die de laterale habenula innerveert. We tonen aan dat de habenula de eigen afferente innervatie bepaalt door ontwikkeling van projecties die VTA mDA axonen naar de laterale habenula leiden. Een mechanisme van axon-axon interactie werkt in samenspel met lokale expressie van Netrin1 door de laterale habenula, die de binnenkomst van mDA axonen mogelijk maakt.

In **hoofdstuk 3** presenteren we een nieuwe genetische strategie om mDA neuronale subsets *in vivo* te onderscheiden, in zowel embryonale als volwassen muizenbreinen. Deze aanpak, Pitx3-ITC genaamd, is gebaseerd op de expressie van verschillende fluorescente eiwitten in afzonderlijke mDA neuronale subsets in een enkele muis. De karakterisatie van verschillende muislijnen toont aan dat *Pitx3-ITC* muizen selectieve labeling van SNc mDA neuronen mogelijk maken. Daarnaast hebben wij *Nrp2-FlpO* en *Gucy2C-Cre* muislijnen gegenereerd die, in combinatie met *Pitx3-ITC* muizen, afzonderlijke mDA neuronen kunnen labelen. Deze muislijnen maken visualisatie van dendrieten en axonale projecties van enkelvoudige mDA neuronen mogelijk.

In **hoofdstuk 4** bestuderen we de ontogenie van nigrostriatale en mesocorticolimbische axonale projecties. Om deze twee mDA routes *in vivo* te onderscheiden gebruiken wij twee transgene muismodellen die respectievelijk SNc en VTA neuronen labelen. In het tweede deel van dit hoofdstuk analyseren we de rol van het axon-sturende eiwit Netrin1 tijdens de ontwikkeling van SNc mDA axonen. We tonen aan dat Netrin1 de vertakking van SNc mDA axonen in het dorsale striatum induceert.

In het eerste deel van **hoofdstuk 5** analyseren we de migratie van SNc mDA neuronen in 2D en 3D, en concluderen dat SNc mDA neuronen in drie ruimtelijke richtingen migreren, nl., langs de caudo-rostrale, medio-laterale en dorso-ventrale assen. Vervolgens onderzoeken we de cellulaire en moleculaire mechanismen die de migratie van verschillende SNc mDA neuronale subsets reguleren. Onze studie onthult nieuwe mechanismen van mDA neuron migratie, gebaseerd op interactie tussen verschillende neuronale populaties in de middenhersenen en tussen neuronale cellichamen en axonen. Bovendien identificeren we Netrin1 als een belangrijke regulator van deze processen.

Dit proefschrift onthult ontwikkelingsmechanismen die de migratie en axon-sturing van mDA neuronale subsets reguleren. Deze principes zijn mogelijk niet alleen van toepassing op het dopaminesysteem in de middenhersenen, maar ook op vele andere neuronale clusters in het zich ontwikkelende brein. Daarnaast biedt dit proefschrift nieuwe genetische hulpmiddelen die in toekomstige studies gebruikt kunnen worden om de ontwikkeling van het dopaminesysteem beter te begrijpen.

Curriculum vitae

I was born on the 8th of August 1986 in Manerbio, Italy. After my high school studies at the Liceo Scientifico Leonardo in Brescia, I moved to the beautiful city of Bologna for the next five years. From the University of Bologna, I received the BSc in Biotechnology in 2008 and the MSc in Molecular Biotechnology in 2011. As part of my training, I completed in 2008 an internship at the Department of Biology (University of Bologna) in the group of Prof. Antonio Contestabile. Later in 2010-2011, I did an internship at the University of Milan under the supervision of Prof. Elena Cattaneo and Prof. Luciano Conti. From 2005 to 2011, I was also a student of the Collegio Superiore, the School of Excellence of the University of Bologna. In 2012 I started my PhD at the Department of Translational Neuroscience at the UMC Utrecht in the Netherlands. All my PhD studies were supervised by Prof. Jeroen Pasterkamp. From 2013 to 2016 I was a PhD candidate of the European Marie Curie initial training network (ITN) "NPlast". The results of my PhD studies are presented in this dissertation. I am now continuing my postdoctoral research in the laboratory of Prof. Rüdiger Klein at the Max Planck Institute of Neurobiology in Munich, Germany.

List of publications

S. Brignani and R.J. Pasterkamp, Neuronal subset-specific migration and axonal wiring mechanisms in the developing midbrain dopamine system. *Frontiers in Neuroanatomy* (2017) Jul. Review

E.Y. Van Battum*, **S. Brignani***, R.J. Pasterkamp, Axon guidance proteins in neurological disorders. *Lancet Neurology* (2015) May;14(5):532-46. Review

E.R.E. Schmidt, **S. Brignani**, Y.Adolfs, S. Lemstra, J. Demmers, M. Vidaki, A.L. Donahoo, K Lilleväli, E. Vasar, L.J. Richards, D. Karagogeos, S.M. Kolk, R.J. Pasterkamp, Subdomain-mediated axon-axon signaling and chemoattraction cooperate to regulate afferent innervation of the lateral habenula. *Neuron* (2014) Jul;16;83(2):372-87

S. Eleuteri, B. Monti, **S. Brignani**, A. Contestabile, Chronic dietary administration of valproic acid protects neurons of the rat nucleus basalis magnocellularis from ibotenic acid neurotoxicity. *Neurotox Res.* (2009) Feb;15(2):127-32

* Co-first authorship

Acknowledgments

My most important thanks go to my supervisor, Jeroen. I am very grateful for his constant support throughout all these years, especially for his dedication and time spent in our innumerable and never-ending discussions. He has been always available for me and his support was fundamental to increase my self-confidence. Working with him taught me that there is no hierarchy in scientific discussions. I want to thank him also for giving me the opportunity to attend conferences all around the world, to meet other researchers and discuss with them. I will always remember the moments of enthusiasm and happiness shared between us after a new discovery.

I want to thank my co-supervisor, Peter, for his always-positive and always-constructive attitude. His warm words after my seminars were always very rewarding. I want to thank him also for the advices during the last phase of my PhD and for his critical reading of my thesis.

I am grateful to all the members of my Doctoral Committee, prof. dr. Casper Hoogenraad, prof. Freek Hoebeek, prof. dr. Joost Verhaagen, prof. dr. Louk Vanderschuren, and prof. dr. Rick Dijkhuizen for evaluating my thesis.

Many thanks to all the people of the Department of Translational Neuroscience at the UMC Utrecht and in particular to my big group of research with all the colleagues who accompanied my journey from the early to the late days: Andreia, Anita, Anna, Anna, Bart, Christiaan, Divya, Danielle, Eljo, Emma, Ewoud, Ewout, Francesca, Giuliano, Kati, Ketharini, Leo, Lieke, Lill Eva, Marieke, Marina, Mark, Mark, Mateja, Max, Oliver, Pavol, Renata, Sandra, Susan, Suzanne, Vamshi, Youri. All these people were able to create a strong network full of stimuli, support, reciprocal help, and friendship. I was very lacky to be part of this group with these people, and I will always think of them with a mixture of nostalgia and gratitude.

This thesis benefited enormously from all the intensive discussions, ideas, suggestions, and technical support provided by many fundamental people that I want to sincerely thank.

Big thanks to Divya, who was my close companion during many scientific adventures. Thanks to her ideas and work the ITC project proceeded forward and continued after my departure. I want to thank her for sharing technical knowledge and for being supportive during the hard times. Thanks for all the fun we had together.

Many thanks to Ewoud, who was my first teacher in the lab. I want to thank him especially for sharing with me his genuine scientific passion, his ideas, and all his technical knowledge. I will remember the excitement we shared during the last phases of the Habenula project, and the intense discussions for planning the future of the ITC project. During the first two years of my PhD, he was always available and I am grateful to him.

Anna came in the lab as a master student and soon we became an efficient Italian-duo-team. We shared many moments of frustration and excitement, and I want to thank her for her dedication and her important contributions to the ITC project.

I want to thank Youri for setting up the microscope facility, for sharing his technical knowledge, and for his fundamental contributions to the ITC project. Without him and his work, the 3D imaging and analysis would not be in this thesis.

I am thankful to Eljo, who started the 3D imaging. Thanks to her advices during the years spent together in the lab.

Thanks to the mater students who contributed to ITC project: Anna, Erik, Maaike, and Stephanie. Thanks to their work, their ideas, their questions and doubts.

I am very grateful to all the people who took care of the many mouse lines important in the ITC project. These people were crucial for the success of the entire work. Many thanks to Christiaan, Leo, Youri, Mark, Marjolein, and all the animal care takers.

During my PhD, I was very lucky to meet people happy to share with me their scientific enthusiasm and to provide important advices. Thanks to these colleagues and friends, I could keep my mental health during the frustrating phases and to fully enjoy the moments of scientific success.

My biggest words of thanks go to Mark. With his broad scientific knowledge and his creativity, he was (and is) a constant source of new ideas and new projects. His sincere passion for understanding how nature works has been a strong stimulus for me and my work.

Many thanks to Francesca and Giuliano, my two Italian friends in the lab. Francesca was the very first friend I found in the Netherlands. She was an example of strength and endurance to me. I want to thank especially her generosity, her support and help inside and outside the lab. Thanks to Giuliano for sharing so many ideas and solutions, and for being always available for discussions and relaxing moments.

Big thanks go to my Vriendinnen in the lab: Ketharini, Renata, Suzanne, Mateja and Yujie. These girls were able to create the warmest and funniest environment in the lab. Without this positive atmosphere in my everyday life, I doubt I could survive the hard times. Thanks to Ketharini, to her gentle smile,

her constant optimism, and her natural empathy. Thanks to Renata, who was there from the beginning with her strength and determination. Thanks to my Dutchy friend and conference-buddy Suzanne, for being always so hilarious, full of spirit, and with an open smile. Thanks to Mateja, to her kindness and generosity during the last months of my PhD. She should have arrived earlier. And thanks to the gentle Yujie, who created a very warm atmosphere in the office.

I want to thank my old friends at home and all the new friends that I met during these years abroad, thanks for all the adventures we shared. Thanks to Nico, Francy, Chiara and Monica, Giampaolo and Alessio, thanks to the friends in the Netherlands, in Umbria and the new friends in Germany.

A big thank to my wide family, my aunts, uncles, cousins, and my grandmother for being always so warm when I come back home.

I feel deep gratitude to my family. Thanks to my parents, Laura and Antonio, for being the nest where I can always come back. Thanks to my sister Lidia, my most precious friend and confident. Thanks to my big bro Marco, who brings the music!

My last thanks go to Ivano, who wants to explore and understand the world with me. Thanks for the intense happiness.